TIME DEPENDENT STUDIES OF FOAM STABILITY USING IMAGE ANALYSIS, ELECTRICAL RESISTIVITY AND ULTRASOUND

by

Daiva Daugelaite

A thesis submitted to the Faculty of Graduate Studies of
The University of Manitoba
In partial fulfillment of the requirements of the degree of

DOCTOR OF PHILOSOPHY

Department of Food Science
University of Manitoba
Winnipeg, Manitoba

I hereby declare that I am the sole author of this thesis.
I authorize the University of Manitoba to lend this thesis to other institutions or individuals for the purpose of scholarly research.

Daiva Daugelaite

I further authorize the University of Manitoba to reproduce this thesis by photocopying or by other means, in total or in part, at the request of other institutions or individuals for the purpose of scholarly research.

Daiva Daugelaite

The University of Manitoba requires the signature of all persons using or photocopying this thesis. Please sign below and give address and date.

ACKNOWLEDGEMENTS

I would like to thank many individuals that helped me through the preparation of this dissertation. I would like to than my advisor Dr. Martin Scanlon, for critically looking at research facts and papers. Your knowledge, experience and discipline helped me overcome challenges during the research program. I would like to than Dr. John Page for his positiveness, always being willing to answer questions and explain physics concepts. Also I want to thank the entire physic lab, especially Anatoliy Strybulevich, who helped in difficult moments. Special thanks to Valentin Leroy, for your input to my research work, kindness and encouragement. I also want to thank Dr.Harry Sapirstein for advice and support and for serving as a committee member.

I am very greatfull for financial support received through Dr. Martin Scanlon's NSERC grant over all the program years, UMSU and UMGSA for providing travel grants. Thank you John Thoroski and to Innovatech Egg Products, for supplying eggs for the research.

I want to thank all food science students – I have wonderful memories of hanging out and going on trips with you! My office mates, Silvi, Arshala, Filiz and Marta, who always had stories to share and laugh. I hope to see everyone in the future.

I want also to thank my tennis team mates, especially Eewei, Souk and Sean for support and balance through out tough last program years. Special thanks to overseas lithuanian friends, Viktoria, Asta, Egis, for being so far but yet supportive.

Most importantly, I would like to thank my family for encouragement, always being there. I could not have done it without you.

If you can keep your head when all about you
Are losing theirs and blaming it on you;
If you can trust yourself when all men doubt you,
But make allowance for their doubting too;
If you can wait and not be tired by waiting,
Or, being lied about, don't deal in lies,
Or, being hated, don't give way to hating,
And yet don't look too good, nor talk too wise;

If you can dream - and not make dreams your master;
If you can think - and not make thoughts your aim;
If you can meet with triumph and disaster
And treat those two imposters just the same;
If you can bear to hear the truth you've spoken
Twisted by knaves to make a trap for fools,
Or watch the things you gave your life to broken,
And stoop and build 'em up with wornout tools;

If you can make one heap of all your winnings
And risk it on one turn of pitch-and-toss,
And lose, and start again at your beginnings
And never breath a word about your loss;
If you can force your heart and nerve and sinew
To serve your turn long after they are gone,
And so hold on when there is nothing in you
Except the Will which says to them: "Hold on";

If you can talk with crowds and keep your virtue,
Or walk with kings - nor lose the common touch;
If neither foes nor loving friends can hurt you;
If all men count with you, but none too much;
If you can fill the unforgiving minute
With sixty seconds' worth of distance run -
Yours is the Earth and everything that's in it,
And - which is more - you'll be a Man my son!

Rudyard Kipling
Poem ``If```

TABLE OF CONTENT

ACKNOWLEDGEMENTS iv
LIST OF FIGURES x
LIST OF TABLES xxi
NOTATIONS xxii
ABSTRACT xxvii
CHAPTER 1 INTRODUCTION 1
1.2 Objective statement 4
CHAPTER 2. LITERATURE REVIEW 7
2.1 Introduction 7
2.1.1 History of food foams 8
2.1.1.1 Different origins of food foams 8
2.1.1.2 Liquid foams 10
2.1.1.3 Solid foams 10
2.2 Foams 11
2.2.1 Influence of components on foam structure and stability 11
2.2.2 Surfactant foams 12
2.2.2.1 Low Molecular Weight 12
2.2.2.2 High Molecular Weight 13
2.2.2.3 Protein foams 14
2.2.2.3.1 General 14
2.2.2.3.2 Egg white proteins 15
2.2.2.3.3 Sucrose and sodium chloride impact on egg white foam formation 18
2.2.3 Foam making ways 19
2.2.3.1 Foam making techniques 19
2.2.3.1.1 Whipping 20
2.2.3.1.2 Shaking 20
2.2.3.1.3 Bubbling method 21
2.2.3.1.4 Nucleation 22
2.2.3.2 Influence of techniques used on foam structure 23
2.2.4 Foam structure 23
2.2.4.1 Bubble size distribution 25
2.2.5 Foam properties 28
2.2.5.1 Rheology of the foam 28

2.2.5.1.1 Yield stress 28
2.2.5.1.2 Small and large strain 30
2.2.5.2 Surface tension 33
2.2.6 Foam stability 35
2.2.6.1 Drainage 37
2.2.6.1.1 Drainage in egg white foams 38
2.2.6.1.2 Free drainage 39
2.2.6.2. Disproportionation 45
2.2.6.3 Coalescence 48
2.2.6.4 Ostwald ripening 49
2.2.6.5 Bubble size distribution evolution during aging 50
2.3 Techniques 51
2.3.1 Application of ultrasound to study foam aging processes 51
2.3.1.1 Wave propagation in different media 51
2.3.1.2 Principles of measurements 52
2.3.1.2.1 Transmission (Low frequency) 52
2.3.1.2.1.1 Velocity measurements 53
2.3.1.2.1.2 Attenuation coefficient 55
2.3.1.2.1.3 Signal analysis: Fast Fourier transform 56
2.3.1.2.2 Reflection technique 57
2.3.1.2.2.1 Acoustic impedance measurements 58
2.3.1.3 Ultrasonic studies on low void fraction bubbly media 60
2.3.1.4 Ultrasonic studies on high void fraction-foams 63
2.3.2 Electrical measurement techniques 66
2.3.2.1 Conductance of solutions 66
2.3.2.1.1 Ohm's law for electrolytes 67
2.3.2.1.1.1 Liquid content and electrical conductivity relation in foam 70
2.3.2.1.1.2 Foam structure (tortuosity, bubble size) effect on conductivity 72
2.3.2.1.1.3 Foam dynamic property measurements by using electrical conductivity 74
2.3.2.1.2 Non-conducting foam property assessment by using capacitance measurements 78
2.3.3 Foam imaging principles 79
2.3.3.1 Techniques 80
2.3.3.1.1 2D imaging techniques – Microscopy 80

2.3.3.1.2 Challenges encountered using optical microscopy technique for 2D foam imaging 82
2.3.3.1.3 3D imaging techniques 83
CHAPTER 3. MATERIALS AND METHODS 87
3.1 Foam sample preparation 87
3.2 Density measurements 89
3.3 Ultrasound measurements 90
3.4 Foam resistivity measurements 92
3.4.1 Foam resistivity measurement technique 92
3.4.2 Electrical properties of foam 96
3.4.3 Current meter-converter design 97
3.4.4 Electrical conductivity cell calibration 98
3.5 Egg white and *Gillette* foam surface 2D digital image technique 99
CHAPTER 4. IMAGE ANALYSIS 103
4.1 Introduction 103
4.2 Results and discussion 105
4.3 Conclusions 120
CHAPTER 5. ACQUISITION OF ULTRASONIC PARAMETERS IN HIGH VOID FRACTION FOAMS 121
CHAPTER 6. TIME-DEPENDENT ULTRASOUND MEASUREMENTS IN HIGH VOID FRACTION FOAMS 132
6.1 Experimental results and interpretation 132
6.2 Interpretation of velocity results according to foam compressibility 137
6.3 Interpretation of the results according to a second effective medium approach 140
6.4 Application of Foldy model to interpret the results for high void fraction foams 149
6.4.1 The Foldy model 149
6.4.2 Data acquisition for the Foldy model 152
6.4.2.1 Properties of egg white foam matrix 152
6.4.2.2 Properties of Gillette foam matrix 154
6.4.2.3 Bubble properties 155
6.4.3 Comparison of Foldy model predictions with experiment 156
6.5 Interpretation of $\alpha\lambda/f$ 161
6.5.1 Comparison of Foldy model to theoretical monodispersed and polydispersed egg white foams 165
6.6 Conclusion 175

CHAPTER 7. EGG WHITE FOAM RESISTIVITY RESULTS AND DISCUSSION 176
7.1 Introduction 176
7.1 Egg white foam resistivity measurement results 176
7.2 Egg white foam conductivity and liquid fraction results 181
7.3 Estimation of liquid fraction in aging egg white foams from resistivity measurements 183
7.4 Egg white foam liquid fraction changes during aging 183
7.5 Immobility of egg white foams 191
7.6 Conclusion 193
CHAPTER 8. GENERAL DISCUSSION 195
CHAPTER 9. CONTRIBUTIONS TO KNOWLEDGE AND SUGGESTIONS FOR FUTURE WORK 201
9.1 Bubble size evolution in aging egg white and *Gillette* foams 201
9.2 Liquid drainage in egg white foams 202
9.3 Low intensity (40kHz) ultrasound study on high void fraction foam aging process 202
REFERENCES 206
APPENDIX 224
A. DSC STUDY ON ANGEL FOOD CAKE BATTER AND ITS COMPONENTS 225
A.1. Introduction 225
A.2 Literature review 225
A.2.1 DSC basic principles 225
A.2.1.1 Endotherms of wheat flour 226
A.2.1. 2 Endothems of wheat flour starch 227
A.2.1.3 Endotherms of wheat proteins 227
A.2.1.4 Egg white protein endotherms 229
A.2.1.5 Sugar effect on starch and protein endotherms 229
A.3 Materials and methods 230
A.4 Results and discussion 232
A.5 General difficulties encountered 238
A.6 Conclusions 238

LIST OF FIGURES

Figure. 2.1. Version of bubbly juice at pH 4.6; sun ripened berry fruits lightly covered in virgin olive oil and lime. Cold beet root bubbles.....9

Figure 2.2. Examples of foam structures made by: a) blowing gas, b) blowing gas (turbulent flow), c) sparging, d) blending, e) shaking, f) nucleation of gas (beer froth).....22

Figure 2.3. Structure of the foam a) polyhedral foam and b) wet foam.....24

Figure 2.4. a) Polyhedral foam structure elements. 1 – Plateau triangle; 2 – Plateau border; b) Four linear Plateau borders meeting in a node (vertex).....25

Figure 2.5. The principle diagram of conducting system.....68

Figure 2.6. Cross section view of wet (a) and polyhedral (b) foams to illustrate tortuosity.....72

Figure 2.7. Foam microconductivity measurement apparatus 75

Figure 2.8. a) Electrical resistance technique developed by Barigou *et al*. (2001) to measure foam drainage. The column has 5 electrodes and is made of Perspex glass. Dimensions are given in mm. b) Electrode configuration.....76

Figure 2.9. Set up diagram for assessing foam properties by using capacitance measurements...78

Figure 2.10. Individual bubble in a liquid (Van der Net *et al.*, 2007). B_o, B_i- the outer and the inner boundary of illuminated bubble. D_o-diameter of the outer illuminated bubble.....83

Figure 3.1. Ultrasound experiment set-up a).....91

Figure 3.1. Ultrasound experiment set-up: b) sample holder.....91

Figure 3.2. Transmitted waveform through a foam sample at a central frequency of 40 kHz 92

Figure 3.3. Electrical resistivity technique for measuring foam aging.....94

Figure 3.4. Design of the cell for electrical resistivity measurements. Dimensions given in millimeters.....95

Figure 3.5. Electrical circuit diagram representing a foam.....97

Figure 3.6. Electrical circuit scheme of current meter-converter for a single ring.....98

Figure 3.7. Measured and standard conductivity of KCl and NaCl solutions. Solid line represents Linear fit to measured conductivity. Symbols represent: ■ - measured conductivity of KCl, ▫ - measured conductivity of NaCl. Slope for KCl=1.006. Slope for NaCl=1.031.....99

Figure 3.8. Foam (φ = 0.78) image at 0 s aging time.....100

Figure 3.9. Photo processing steps for the image shown in Figure 3.8. a) After using *Bandpass* filter, b) After applying *Threshold* function, c) After applying *Invert* function, d) After selecting *Analyze particles* and choosing to show as a mask *ellipses*.....102
Figure 4.1. Images of aging egg white foam of 0.65 void fraction. Image dimensions 532 μm x 450 μm.....104
Figure 4.2. Images of aging egg white foam of 0.78 void fraction. Image dimensions 532 μm x 450 μm.....105
Figure 4.3. Bubble radii distribution in 0.65 void fraction egg white foam at 0 min of aging....106
Figure 4.4. Bubble radii distribution in 0.65 void fraction egg white foam at 21 min of aging..107
Figure 4.5. Bubble radii distribution in 0.65 void fraction egg white foam at 41.5 min of aging.....107
Figure 4.6. Bubble radii distribution in 0.78 void fraction egg white foam at 0 min of aging....108
Figure 4.7. Bubble radii distribution in 0.78 void fraction egg white foam at 22 min of aging..108
Figure 4.8. Bubble radii distribution in 0.78 void fraction egg white foam at 42 min of aging..109
Figure 4.9. Photographs of aging *Gillette* foam of 0.90 void fraction (ρ = 0.084 g/cm^3). Image dimensions 532 μmx450 μm.....111
Figure 4.10. Photographs of aging *Gillette* foam of void fraction 0.93 (ρ = 0.064 g/cm^3). Image dimensions 532 μmx450 μm.....112
Figure 4.11. Bubble radii distribution in 0.064 g/cm^3 density *Gillette* foamy at 0 min of aging.....113
Figure 4.12. Bubble radii distribution in 0.064 g/cm^3 density *Gillette* foamy at 30 min of aging.....113
Figure 4.13. Bubble radii distribution in 0.064 g/cm^3 density *Gillette* foamy at 60 min of aging.....114
Figure 4.14. Bubble radii distribution in 0.064 g/cm^3 density *Gillette* foamy at 90 min of aging.....114
Figure 4.15. Bubble radii distribution in 0.064 g/cm^3 density *Gillette* foamy at 120 min of aging.....115
Figure 4.16. Bubble radii distribution in 0.084 g/cm^3 density *Gillette* foamy at 0 min of aging.....115

Figure 4.17. Bubble radii distribution in 0.084 g/cm^3 density *Gillette* foamy at 30 min of aging.....116
Figure 4.18. Bubble radii distribution in 0.084 g/cm^3 density *Gillette* foamy at 60 min of aging.....116
Figure 4.19. Bubble radii distribution in 0.084 g/cm^3 density *Gillette* foamy at 90 min of aging.....117
Figure 4.20. Bubble radii distribution in 0.084 g/cm^3 density *Gillette* foamy at 120 min of aging.....117
Figure 4.21. Average bubble radius versus egg white foam aging time determined by image analysis. Symbols represents these two void fractions: −□− $\varphi = 0.68$, -○- $\varphi = 0.78$. The solid line represents a fitted power law expression to $\varphi = 0.78$ void fraction data points, which is $R = 8.3+3.3 \cdot t^{0.34}$ (t-aging time). Error bars represent standard deviation of 3 replicates. The broad dashed line represents a slope of 0.5.....119
Figure 4.22. Average bubble radius versus *Gillette* foam aging time determined by image analysis. Symbols represent these void fractions: −□− $\varphi = 0.90$, -○- $\varphi = 0.93$, −■− data from Durian *et al.* (1991). The broad dashed line represents a slope of 0.5, while our data and that of Durian *et al.* (1991) have a slope that is 0.4. The broad dashed line represents a slope of 0.5, while our data and that of Durian *et al.* (1991) have a slope that is 0.4. Error bars represent standard deviation of 3 replicates.....120
Figure 5.1. Amplitude versus transit time for a filtered signal (-----) and an unfiltered signal (line).....123
Figure 5.2. Signal transmitted through the 0.65 void fraction foam sample of 1mm thickness at 0 min of aging time. The central frequency and bandwidth were 30 kHz and 10 kHz.....124
Figure 5.3. Transit time of first maximum as a function of foam sample thickness at 0 min of aging time.....125
Figure 5.4. Amplitude of first minimum as a function of sample thickness at 0 min of aging time.....125
Figure 5.5. Waveform of the filtered signal of 0.65 void fraction foam, 2.5 mm thickness. Solid line represents signal at 0 min of aging, ----- represents signal after 43 min of aging.....126

Figure 5.6. Filtered reference signal (-----) and truncated signal (line).....127
Figure 5.7. The phase as a function of frequency of the ultrasonic signal (0 min of aging, 0.65 void fraction egg white foam). 128
Figure 5.8. The amplitude as a function of frequency of the ultrasonic signal (0 min of aging, 0.65 void fraction egg white foam).....128
Figure 5.9. $\alpha \cdot L$ plotted versus thickness in order to estimate the offset in attenuation coefficient, at 37 kHz, at 6min of aging (0.65 void fraction egg white foam).....130
Figure 5.10. Phase velocity versus aging time for 0.78 void fraction foam at 20 kHz. Symbols represent uncorrected phase velocity for different thicknesses: −□− 1 mm, -○−2 mm, −△− 2.5 mm; corrected phase velocity for different thicknesses: −■− 1 mm, −●− 2 mm, −▲− 2.5 mm.....131
Figure 5.11. Attenuation coefficient versus aging time for 0.78 void fraction foam at 20 kHz for different thicknesses. Symbols represent uncorrected attenuation coefficient for different thicknesses: -□- 1 mm, -○− 2 mm, −△− 2.5 mm; corrected attenuation coefficient for different thicknesses:−■− 1 mm, —●— 2 mm, −▲− 2.5 mm.....131
Figure 6.1. Phase velocity versus aging time of 0.65 void fraction egg white foam. The symbols represent these frequencies: ■ 20kHz, ● 25 kHz, ▲ 30 kHz, ▼ 40 kHz.....134
Figure 6.2. Phase velocity versus aging time of 0.78 void fraction egg white foam. The symbols represent these frequencies: ■ 20 kHz, ● 25 kHz, ▲ 30 kHz, ▼ 40 kHz.....134
Figure 6.3. Attenuation versus aging time of 0.65 void fraction egg white foam. The symbols represent these frequencies: ■ 20 kHz, ● 25 kHz, ▲ 30 kHz, ▼ 40 kHz.....135
Figure 6.4. Attenuation versus aging time of 0.78 void fraction egg white foam. The symbols represent these frequencies: ■ 20 kHz, ● 25 kHz, ▲ 30 kHz, ▼ 40 kHz.....135
Figure 6.5. Phase velocity versus aging time for *Gillette* foamy. The closed symbols represent $\varphi = 0.93$ ($\rho = 0.064$ g/cm^3) *Gillette* foamy: ■ 25 kHz, ● 30 kHz, ▲ 37 kHz, ▼ 40 kHz. Open symbols represent $\varphi = 0.90$ ($\rho = 0.084$ g/cm^3) *Gillette* foamy: □ 25 kHz, ○ 30 kHz, △ 37 kHz, ▽ 40 kHz.....136

Figure 6.6. Attenuation versus aging time for *Gillette* foamy. The closed symbols represent $\varphi = 0.93$; $\rho = 0.064$ g/cm^3 *Gillette* foamy: ■ 25 kHz, ● 30 kHz, ▲ 37 kHz, ▼ 40 kHz. Open symbols represent $\varphi = 0.90$; $\rho = 0.084$ g/cm^3 *Gillette* foamy: ▫ 25 kHz, ○ 30 kHz, △ 37 kHz, ▽ 40 kHz.....136

Figure 6.7. Simulated (according to Formula 7.4) Wood's velocity in egg white (·····) and Gillette (——) foam. Measured experimental values of egg white (at 37 kHz) (■) and *Gillette* (at 40 kHz frequency) (▲) foams, Where $\chi_{liq} = 3.5 \cdot 10^{-10}$ Pa, $\chi_{gas} = 1 \cdot 10^{-5}$ Pa, $\rho_{eggliq} = 1.226$ g/cm^3, $\rho_{Gilletliq} = 1$ g/cm^3. For the egg white foam of void fraction $\varphi = 0.65$, $v_{EggWood} = 18.9$ m/s, and for $\varphi = 0.78$, $v_{EggWood} = 22$ m/s. For *Gillette* foamy $\varphi = 0.90$, $v_{GillWood} = 35$ m/s and $\varphi = 0.93$, $v_{GillWood} = 39$m/s.....138

Figure 6.8. $\alpha\lambda/f$ versus aging time for 0.65 void fraction foam. The symbols represents these frequencies: ■ 20 kHz, ● 25 kHz, ▲ 30 kHz, ▼ 40 kHz. Error bars represent standard deviation.....142

Figure 6.9. $\alpha\lambda/f$ versus aging time for 0.78 void fraction foam. The symbols represents these frequencies: ■ 20kHz, ● 25 kHz, ▲ 30 kHz, ▼ 40 kHz. Error bars represent standard deviation.....143

Figure 6.10. $\alpha\lambda/f$ versus aging time for *Gillette* foamy ($\varphi = 0.90$; $\rho = 0.084$ g/cm^3). The symbols represent: ■ 25 kHz, ● 30 kHz, ▲ 37 kHz, ▼ 40 kHz. Error bars represent standard deviation.....143

Figure 6.11. $\alpha\lambda/f$ versus aging time for *Gillette* foamy ($\varphi = 0.93$; $\rho = 0.064$ g/cm^3). The symbols represent: ■ 25 kHz, ● 30 kHz, ▲ 37 kHz, ▼ 40 kHz. Error bars represent standard deviation.....144

Figure 6.12. $\alpha\lambda/f$ (averaged $\alpha\lambda/f$ value of four frequencies: 20 kHz, 25 kHz, 30 kHz and 40 kHz) and r^2 (from image analysis) versus aging time for 0.78 void fraction egg white foam. Symbols represent: △ $\alpha\lambda/f$; ■ r^2. Error bars represent standard deviation.....144

Figure 6.13. $\alpha\lambda/f$ (averaged $\alpha\lambda/f$ value of four frequencies: 20 kHz, 25 kHz, 30 kHz and 40 kHz) and r^2 (from image analysis) versus aging time for 0.65 void fraction egg white foam. Symbols represent: △ $\alpha\lambda/f$; ■ r^2. Error bars represent standard deviation.....145

Figure 6.14. $\alpha\lambda/f$ (averaged $\alpha\lambda/f$ value of four frequencies: 20 kHz, 25 kHz, 37 kHz and 40 kHz) and r^2 (from image analysis) versus aging time for void fraction *Gillette* foam ($\varphi = 0.90$; $\rho = 0.084$ g/cm^3). Symbols represent: △ is $\alpha\lambda/f$; ■ is r^2. Error bars represent standard deviation.....145

Figure 6.15. $\alpha\lambda/f$ (averaged $\alpha\lambda/f$ value of four frequencies: 20 kHz, 25 kHz, 30 kHz and 40 kHz) and r^2 (from image analysis) versus aging time for void fraction *Gillette* foam ($\varphi = 0.93$; $\rho = 0.064$ g/cm^3). Symbols represent: △ is $\alpha\lambda/f$; ■ is r^2. Error bars represent standard deviation.....146

Figure 6.16. Damping constant contributions for 10 μm radii bubble distribution ($\sigma_{st} = 0.1$) if the matrix is water liquid. The symbols represent: □ radiation, ○ thermal, △ viscous, ▼ total damping.....147

Figure 6.17. Damping constant (δ) contributions for 10 μm radii bubble distribution ($\sigma_{st} = 0.1$) if the matrix is egg white liquid. The symbols represent: □ radiation, ○ thermal, △ viscous, ▼ total damping.....148

Figure 6.18. G′ (■) and G″(△) of egg white versus frequency. Linear fit of G′ (——) and G″ (·····) through data obtained from rheological and ultrasound measurements.....153

Figure 6.19. G′ (■) and G″ (▫) of egg white liquid versus frequency. G′ (▲) and G″ (△) of *Gillette* liquid versus frequency. (Linear fit of G′ and G″(- - - ·) through the egg white and *Gillette* liquid data obtained from rheological and ultrasound measurements). Solid line represents G″of water.....155

Figure 6.20. Experimental results and prediction of modified Foldy's models for phase velocity in the 0.78 void fraction egg white foam. Three aging times, for experimental data: ■ 0 min, ● 22 min, ▲ 34 min; Foldy 1 model prediction: ▫ 0 min, ○ 22 min, △ 34 min; Foldy 2 model: ■ 0 min, ● 22 min, ▲ 34 min. For comparison $v_w = 22$ m/s.....157

Figure 6.21. Experimental results and prediction of modified Foldy's models for phase velocity in the 0.65 void fraction egg white foam. Three aging times, for experimental data: —■— 0 min, —●— 22 min, —▲— 42 min; Foldy 1 model prediction: ▫ 0 min, ○ 22 min, △ 42 min; Foldy 2 model: ■ 0 min, • 22 min, ▲ 42 min. For comparison v_w = 17.66 m/s.....158

Figure 6.22 Experimental results and prediction of modified Foldy's models for phase velocity in the lower density *Gillette* foam (φ = 0.93; ρ = 0.064 g/cm^3). Four aging times: —■— 0 min, —●— 30 min, —▲— 60 min, -▼- 90 min. Foldy 1 model prediction: ▫ 0 min, ○ 30 min, △ 60 min, ▽ 90 min; Foldy 2 model: ■ 0 min, • 30 min, ▲ 60 min, ▼ 90 min. $v_{GillWood}$ = 39 m/s.....158

Figure 6.23. Experimental results and prediction of modified Foldy's model for phase velocity in the higher density *Gillette* foam (φ = 0.90; ρ = 0.084 g/cm^3). Four aging times: —■— 0 min, —●— 30 min, —▲— 60 min, -▼- 90 min. Foldy 1 model prediction: ▫ 0 min, ○ 30 min, △ 60 min, ▽ 90 min; Foldy 2 model: ■ 0 min, • 30 min, ▲ 60 min, ▼ 90 min. $v_{GillWood}$ = 35 m/s.....159

Figure 6.24. Results and prediction of modified Foldy's models for attenuation coefficient in the 0.78 void fraction egg white foam. Three aging times, for experimental data: —■— 0 min, —●— 22 min, —▲— 34 min; Foldy 1 model prediction: ▫ 0 min, ○ 22 min, △ 34 min; Foldy 2 model: ▪ 0 min, • 22 min, ▲ 34 min.....159

Figure 6.25. Results and prediction of modified Foldy's models for attenuation coefficient in the 0.65 void fraction egg white foam. Three aging times, for experimental data: —■— 0min, —●— 22 min, —▲— 42 min; Foldy 1 model prediction: ▫ 0 min, ○ 22 min, △ 42 min; Foldy 2 model ■ 0 min, • 22 min, ▲ 42 min.....160

Figure 6.26. Results and prediction of modified Foldy's models for attenuation coefficient in the (φ = 0.93; ρ = 0.064 g/cm^3) *Gillette* foam. Four aging times: —■— 0 min, —●— 30 min, —▲— 60 min, -▼- 90 min. Foldy 1 model prediction: ▫ 0 min, ○ 30 min, △ 60 min, ▽ 90 min; Foldy 2 model: ■ 0 min, • 30 min, ▲ 60 min, ▼ 90 min.....160

Figure 6.27. Results and prediction of modified Foldy's models for attenuation coefficient in the (φ = 0.90; ρ = 0.084 g/cm^3) *Gillette* foam. Four aging times: 0 min, 30min, 60 min, 90 min. Foldy 1 model prediction: 0 min, 30 min, 60 min, 90 min; Foldy 2 model: 0 min, 30 min, 60 min, 90 min.....161

Figure 6.28. Foldy's prediction and experimental result of $\alpha\lambda/f$ versus frequency for 0.78 void fraction egg white foam. Three aging times, for experimental data: 20 kHz, 25 kHz, 30 kHz, 40 kHz (only for 0 min); Foldy 1 model prediction: 20 kHz, 25 kHz, 30 kHz, 40 kHz; Foldy 2 model 20 kHz, 25 kHz, 30 kHz, 40 kHz. Error bars represent standard deviation.....163

Figure 6.29. Foldy's prediction and experimental result of $\alpha\lambda/f$ versus frequency for 0.65 void fraction egg white foam. Three aging times, for experimental data: 20 kHz, 25 kHz, 30 kHz, 40 kHz (only for 0 min); Foldy 1 model prediction: 20 kHz, 25 kHz, 30 kHz, 40 kHz; Foldy 2 model 20 kHz, 25 kHz, 30 kHz, 40 kHz. Error bars represent standard deviation.....163

Figure 6.30. Foldy's prediction and experimental result of $\alpha\lambda/f$ versus frequency for 0.93 void fraction *Gillette* foam. Four aging times, for experimental data: 25 kHz, 30 kHz, 37 kHz, 40 kHz; Foldy 1 model prediction: 25 kHz, 30 kHz, 37 kHz, 40 kHz; Foldy 2 model 25 kHz, 30 kHz, 37 kHz, 40 kHz. Error bars represent standard deviation.....164

Figure 6.31. Foldy's prediction and experimental result of $\alpha\lambda/f$ versus frequency for 0.90 void fraction *Gillette* foam. Four aging times, for experimental data: 25 kHz, 30 kHz, 37 kHz, 40 kHz; Foldy 1 model prediction: 25 kHz, 30 kHz, 37 kHz, 40 kHz; Foldy 2 model 25 kHz, 30 kHz, 37 kHz, 40 kHz. Error bars represent standard deviation.....164

Figure 6.32. Theoretical monodispersed bubble distribution where the symbols represent radius (μ_r) and standard deviation or width σ_{st}) of the bubble distribution are: —— μ_r = 5 μm, σ_{st} = 0.15; - - - · μ_r = 15 μm, σ_{st} = 0.05; ····· μ_r = 25 μm, σ_{st} = 0.05; -·-·- μ_r = 50 μm, σ_{st} = 0.015.....165

Figure 6.33. Foldy 1 prediction of $\alpha\lambda/f$ versus frequency for an almost monodisperse distribution of bubbles in egg white and water media: • μ_r =5 μm, ▲ μ_r = 15 μm, ▼ μ_r = 25 μm, ■ μ_r = 50 μm; for egg white media: ○ μ_r =5 μm, △ μ_r = 15 μm, ▽ μ_r = 25 μm, □ μ_r = 50 μm.....167

Figure 6.34. Simulation of $\alpha\lambda/f$ versus r for water media based on Foldy 1 model. The symbols represent: ··□··· 1 kHz, ··○·· 10 kHz, ··△·· 20 kHz, ···▽·· 30 kHz, ··◇·· 40 kHz, ··◁·· 50 kHz. Solid line represents fit $\alpha\lambda/f=r^2/20$.....168

Figure 6.35. Simulation of $\alpha\lambda/f$ versus r for egg white media based on Foldy 1. The symbols represent: ··□··· 1 kHz, ··○·· 10 kHz, ··△·· 20 kHz, ···▽·· 30 kHz, ··◇·· 40 kHz, ··◁·· 50 kHz. Solid line represents fit $\alpha\lambda/f=10+r^2/20$, dashed line represents fit $\alpha\lambda/f=r^2/10$.....169

Figure 6.36. $\alpha\lambda/f$ (averaged over four frequencies) versus $\langle r\rangle$ (mean radius) for egg white and *Gillette* foams. The symbols represent: □ *Gillette* foam with 0.93 void fraction, solid line represents best power law fit, $\alpha\lambda/f = 0.09\cdot r^{2.04}$; ($\chi^2_{red}$= 0.87, R–Squared = 0.98), dashed line (- - -) represents forced r^2 power law fit, $\alpha\lambda/f = 0.104\cdot r^2$, ($\chi^2_{red}$= 0.68, R–Squared = 0.98).

·△· *Gillette* with 0.90 void fraction, solid grey line represents best power law, $\alpha\lambda/f = 0.059\cdot r^{2.12}$, ($\chi^2_{red}$= 0.013, R-Squared = 0.999); Dotted grey line (·····) represents forced r^2 power law fit $\alpha\lambda/f = 0.086\cdot r^2$, ($\chi^2_{red}$= 0.078, R–Squared = 0.99). ■ egg white foam with 0.78 void fraction, solid line represents best power law fit, $\alpha\lambda/f = 0.018\cdot r^{2.75}$; ($\chi^2_{red}$= 0.91, R–Squared is 0.94), black dashed line represents r^2 forced fit $\alpha\lambda/f = 0.19\cdot r^2$, ($\chi^2_{red}$= 2.17, R-Squared = 0.88). ▲ egg white foam with 0.65 void fraction, solid grey line represents simple power law fit, $\alpha\lambda/f = 0.22\cdot r^{1.94}$, ($\chi^2_{red}$= 9.1, R–Squared = 0.95), dashed grey line represents forced to r^2 fit,

$\alpha\lambda/f = 0.18 \cdot r^2$, ($\chi^2_{red}$= 6.22, R–Squared = 0.96). Error bars represent standard deviation.....171

Figure 6.37. $\alpha\lambda/f$ versus $\langle r \rangle$ (mean radius) for egg white foams, replotted to show fits to a power law with a constant offset (solid lines). The symbols represent:

■ egg white foam with 0.78 void fraction: solid line represents the best fit to a power law plus a constant, $\alpha\lambda/f = 30.7+0.00016 \cdot r^{4.1}$, ($\chi^2_{red}$= 0.49, R–Squared = 0.97). The dashed line represents the best fit to a simple power law (no offset) from Figure 7.38.

▲ egg white foam with 0.65 void fraction, solid grey line represents best fit to a power law plus a constant, $\alpha\lambda/f = 54.6+2.32 \cdot 10^{-5} \cdot r^{4.5}$. ($\chi^2_{red}$= 0.89, R–Squared is 0.99). The dotted line is the fit to a simple power law (no offset) from Figure 7.38. Error bars represent standard deviation.....172

Figure 7.1. Resistivity versus aging time for foams of 4 void fractions (φ) at different foam heights (H): φ = 0.60: H = 0.05 m (■), H = 0.035 m (●), H = 0.075 m (▲); φ = 0.65: H = 0.05 m (□), H = 0.035 m (◇), H = 0.075 m (△); φ = 0.78: H = 0.05 m (⊟), H = 0.035 m (⊕), H = 0.075 m (⊞); φ = 0.81: H = 0.05 m (⊠), H = 0.035 m (⊗), H = 0.075 m (⊠). In Figure 4.1 a), the horizontal line of low resistivity represents the resistivity value of the egg white and sugar mixture without air. Figure 4.1 b) is the magnified early foam aging stage results that are displayed in Figure 4.1 a).....178

Figure 7.2. Theoretical and measured (•) relative conductivity versus liquid fraction. There is linear dependence between ε and σ up till ε = 0.6. Symbols represent: theoretical relative conductivity (equation 2.84) (–○–), theoretical relative conductivity with tortuosity model (equation 2.85) (–△–). Linear fit (represents the line through experimental points in the figure) resulting in this ε and σ_r relationship: $\sigma_r = \varepsilon \cdot 0.8894-0.09028$. Error bars represent standard deviation of 3 replications of ε and σ_r (In Figure 4.2 some error bars are smaller than the symbol).....181

Figure 7.3. Foam (φ = 0.60) normalized liquid fraction ($\varepsilon/\varepsilon_o$) versus aging time at different foam heights (H). An arrow indicates an increase of the foam height (H) from the bottom to the top. Symbols represent these foams heights: H = 0.05 m (□), H = 0.015 m (◇), H = 0.035 m (▽), H = 0.065 m (–◇–), H = 0.075 m (△).....188

Figure 7.4. Foam (φ = 0.65) normalized liquid fraction ($\varepsilon/\varepsilon_o$) versus aging time at different foam heights (H). An arrow indicates increase of the foam height from the bottom to the top. Symbols represent these foams heights: H = 0.05 m (□), H = 0.015 m (○), H = 0.035 m (▽), H = 0.065 m (◇), H = 0.075 m (△).....188

Figure 7.5. Foam (φ = 0.78) normalized liquid fraction ($\varepsilon/\varepsilon_o$) versus aging time at different foam heights (H). An arrow indicates increase of the foam height from the bottom to the top. Symbols represent these foams heights: H = 0.05 m (□), H = 0.015 m (○), H = 0.035 m (▽), H = 0.065 m (◇), H = 0.075 m (△).....189

Figure 7.6. Foam (φ = 0.81) normalized liquid fraction ($\varepsilon/\varepsilon_o$) versus aging time at different foam heights (H). An arrow indicates increase of the foam height from the bottom to the top. Symbols represent these foams heights: H = 0.05 m (□), H = 0.015 m (○), H = 0.035 m (▽), H = 0.075 m (△).....189

Figure 7.7. Foam normalized liquid fraction ($\varepsilon/\varepsilon_o$) versus aging time at a foam heights of H = 0.035 m. Symbols represent different void fractions (φ):0.60 (□), 0.65(○), 0.78(△), 0.81(▽).....190

Figure 7.8. Foam normalized liquid fraction ($\varepsilon/\varepsilon_o$) versus aging time at a foam heights of H=0.075m. Symbols represent different void fractions (φ): 0.60 (⊟), 0.65(⊕), 0.78(⊞), 0.81(⊛).....190

Figure A.4.1. Effect of sugar on denaturation of egg white proteins. Thermal effects of sugar and egg white liquid were prepared in these proportions (w.b.): a) 0:1, b) 0.5:1, c) 1:1.....234

Figure A.4.2. Denaturation temperatures of egg white proteins over different sugar ratio in egg white liquid (w.b.). Symbols represent: ■ is conalbumin, ● is ovalbumin.....235

Figure A.4.3. Effect of sugar on denaturation of soft wheat flour components. Flour, water and sugar mixture was prepared in these proportions (w.b.) a) 1:3:0, b) 1:6:1, c) 1:2:1, d) 1:0.89:1.....237

Figure A.4.4. Thermogram of a) egg white and flour mixture in a ratio of (w.b) 0.83:0.26, b) angel food cake batter, sugar, egg white and flour in a ratio (w.b): 0.83:0.83:0.26.....237

LIST OF TABLES

Table 2.1. Physical and chemical properties of egg white.....16
Table 2.2. Inorganic elements in egg white.....66
Table 3.1. Measured density and calculated void fraction of egg white and sugar foam.....88
Table 6.1. Liquid egg white and sugar foam matrix* parameters.....154
Table 6.2. *Gillette* (Sensitive) foam matrix* (without air) parameters.....154
Table A.3.1. List of experiments used for DSC analyses.....232

NOTATIONS

a_r	radius of the inner electrode	(m)
A	signal amplitude	(V)
A_{off}	offset in transit time	(s)
A_{sam}	sample signal amplitude	(V)
A_{ref}	reference single amplitude	(V)
A_r	area	(m^2)
A_0	the signal amplitude at the leading edge of the sample	(V)
A_P	Plateau border cross sectional area	(m^2)
A_1	pre-exponential factor	
$b(t,t_0)$	scaling factor	
b_c	correction factor	
b_r	radius of the cell	(m)
B	slope	
c_g	geometrical constant	
c_j	concentration of ions	(mol/L)
C	capacitance	(F)
C_c	cell constant (C_0=0.413)	
Ca	Capillary number	
d	distance	(m)
D	bubble diameter	(m)
D_f	gas diffusivity through films	(m^2/s)
D_{eff}	the effective diffusion coefficient	(m^2/s)
D_o	diameter of the outer illuminated bubble	(m)
D_{th}	gas thermal diffusivity	(m^2/s)
$\mathbf{E}$	electric field strength	(V/m)
f	frequency	(Hz)
F	force	(N)
F_f	Faraday constant	(C/mol)
F_b, F_g	buoyancy and gravity force	(N)
$\tilde{F}_{max}$	dimensionless mean contribution of a single bubble to the yield stress	
$f_s(r)$	observed bubble size distribution	
$F(r)$	true (corrected) bubble size distribution	
$f(r_j)$	normal probability density function	
$f(r_j')$	log-normal probability density function	
$f(V_j)$	population density by bubble size in volume units	(m^{-3})
$f(\varepsilon)$	a function of ε	
g	acceleration due to gravity	(m/s^2)
G_c	conductance	(S)
$\mathbf{G}$	pressure gradient	(Pa/m)
G	(complex) shear modulus	(Pa)
G', G''	storage, loss shear modulus	(Pa)
G_0	static shear modulus	(Pa)
h	height of one ring of the cell	(m)
h_l	accumulated liquid height	(m)

H	initial foam height	(m)
He	solubility of the gas	(mol/(m^3·Pa))
i	current density	(A/m^2)
j	the order number for sorted bubbles in ascending sizes	
j'	imaginary part of resistance	
I	current	(A)
I_s	scattering intensity	(1/cm)
k	the wave number	(1/m)
$\mathbf{k}$	wave vector	
k_f	prefactor for aqueous foams	
k', k''	real and imaginary part of wave vector	
$k_0^{'}$	number of classes (bins)	
k_o	wave vector in the matrix	
K	permeability constant for the diffusing gas	((m^2·s)/kg)
K_v	volume rate of gas transfer	
K_x	permeability dimensionless constant	
L	length	(m)
L	the sample thickness	(m)
L_ε	effective length between electrodes at liquid fraction ε	(m)
L_{el}	length of the path between electrodes	(m)
L_p	the Plateau border length	(m)
L_v	total Plateau border length per unit volume of network	(m/L)
m	exponent	
M	dimensionless number	
n	empirical parameter	
N	the total number of bubbles	
n'_{total}	total number of observed bubbles	
n_{tot}	total number of bubbles per unit volume	
n_j	number of individual bubbles	
P_a	atmospheric pressure	(Pa)
P_c	capillary pressure	(Pa)
P_r, P_s	reference, sample pressure wave amplitude	(V)
r	bubble mean radius	(m)
r_i	initial bubble radius	(m)
r_j	midpoint of the j^{th} class in the histogram of bubble sizes	(m)
r_{32}	surface-volume mean radius (Sauter mean radius)	(m)
r_o	orifice radius	(m)
r_P	curvature of Plateau border	(m)
r_f	function of impedance	
R	resistance	(Ohm)
R_f	reflectance coefficient	
R_g	universal gas constant	(J/(K·mol)
q	scattering vector	
S_f	film area	(m^2)
S_0/V_0	surface area of spherical bubbles per unit volume of the foam	
t	time	(s)

t_c	coarsening time	(s)
t_i	initial disproportionation time	(s)
t_f	function of impedance	
t_0	time scale	(s)
t_{sam}	transit time in sample	(s)
t_{ref}	transit time in reference	(s)
t_{trans}	transit time	(s)
T	transmission coefficient	
T_a	absolute temperature	(K)
$tan\ \delta^{o}$	phase shift	(degrees)
u_j	mobility of ions in solution	(m^2/(s·V)
U	work	(J)
v	velocity	(m/s; mm/μs)
v_j	velocity of ions in solution	(cm/hr)
v_d	drainage velocity	(m/s)
v_g	group velocity	(m/s; mm/μs)
v_m	ideal gas molar volume	(m^3/mol)
v_p	phase velocity	(m/s; mm/μs)
v_w	Woods velocity	(m/s; mm/μs)
V	voltage	(V)
V_j	j bubble volume	(m^3)
V_{foam}	volume of the foam	(m^3)
V_{liq}	volume of the initial foaming liquid	(m^3)
V_L	velocity of the sound	(m/s
w	bubble size distribution width	(m; μm)
w_o	bubble diameter	(m)
x_c	bubble mean size of normal distribution	(m)
x_g	geometric mean of bubble size	(m)
Y	admittance	(Ohm)
z	measurement location at the foam height	(m)
z_j	ion charge number	
z_0	length scale	(m)
Z	acoustic impedance of the sample	((N·s)/m^3)
Z_0	acoustic impedance of the reference material	((N·s)/m^3)
Z_i	impedance	(Ohms)

Greek letters

α	attenuation coefficient	(m^{-1}, mm^{-1})
α_d	dissociation constant	
$\alpha_s(t,t_0)$	scaling factor	
β	longitudinal (elasticity) modulus	(N/m^2; Pa)
ß	coefficient described in the polytrophic index of gas	
β_c	constant (for dry foams~10)	

γ	surface tension	(N/m)
$\dot{\gamma}$	shear rate	(1/s)
Γ	Gibb's elasticity	(N/m)
$\Delta\Phi$	phase difference	(rad)
ΔP_r	pressure change	(Pa)
Δp_d	driving pressure	(Pa)
Δp	acoustic excess pressure	(Pa)
ΔV	bin size representing bubble volume	(m^3)
Υ	ratio of specific heat capacity for air	
δ	dimensionless damping constant	
δ^{rad}	radial damping constant	
δ^{ther}	thermal damping constant	
δ^{visc}	viscous damping constant	
δ^{total}	total damping constant: $\delta^{total}=\delta^{rad}+\delta^{ther}+\delta^{visc}$	
δ_ε	geometrical constant	
δ_a, δ_v	geometrical constants used to describe Plateau Border section and node shape	
δ_f	film thickness	(m)
δ_P	Plateau border width	(m)
$\delta\rho^2$	contrast	
δ^o	phase	(degrees)
ε	liquid fraction	
ε_c	liquid fraction of randomly packed bubbles	
η	bulk viscosity	(Pa·s)
η_s	shear viscosity	(g/(cm·s)
η_v	variable	
θ	scattering angle	(degrees)
λ	wavelength	(m)
μ_r	the mean of bubble size of log-normal distribution	(m)
ξ	empirical parameter	
ξ_F	Fourier coefficient	
ξ'	particle velocity	(m/s)
ξ	tortuosity	
Π	disjoining pressure	(Pa)
Π_{vDw}	attractive van der Waals force	(N/m^2)
Π_{DL}	repulsive force	(N/m^2)
Π_{SR}	short repulsive force	(N/m^2)
ρ	density of the foam	(kg/m^3)
ρ_{eff}	effective density	(kg/m^3)
ρ_l	density of liquid	(kg/m^3)
ρ_r	resistivity	(Ohm/s)
ρ_0	density of foaming liquid with no air in it	(kg/m^3)
$\rho(t)$	density of the foam at different whipping time	(kg/m^3)
σ	conductivity	(S/m)
σ_r	relative conductivity	

σ_f	foam conductivity	(S/m)
σ_g	standard deviation of log-normal distribution	
σ_{st}	standard deviation of normal distribution	
σ_{liq}	liquid conductivity	(S/m)
τ_I	relaxation time	(s)
τ_y	yield stress	(Pa)
Φ	phase	(degrees)
φ	void fraction	
χ	adiabatic compressibility	(1/Pa)
χ_{eff}	effective compressibility	(1/Pa)
χ_l	compressibility of liquid	(1/Pa)
χ^2_{red}	Reduced Chi-Squared	
ω	angular frequency	(1/s)
ω_n	angular frequency of n component	(1/s)
ω_p	probability of rupture event per time and unit surface	(s/m^2)
ω_M	Minnaert frequency	(Hz)
ω_o	resonance frequency	(Hz)
ψ	exponent	

Abbreviations

DWS	diffusive wave spectroscopy
FFT	Fast Fourier transform
HMW	high molecular weight
LMW	low molecular weight
SMW	small molecular weight

ABSTRACT

The production of highly aerated foods remains a challenge that requires skill to obtain desired appearance and texture. Since foams are fragile and inherently unstable, evaluation of structure changes with time requires a delicate approach. Non-invasive but informative evaluation of changes in aerated food properties is a desired goal to be achieved in this thesis.

I studied the aging of egg white foams of different void fraction using two noninvasive techniques - ultrasonic spectroscopy and electrical resistivity - with a view to understanding aging mechanisms that would affect the quality of the final product. To help in interpretation of the results, a commercial high void fraction foam, *Gillette* (Sensitive), was also analyzed. As a support technique for ultrasound results I used image analysis in order quantitatively evaluate the size of bubbles in the foams. Large increases in attenuation were observed with increasing aging time and frequency. Results were modeled using an effective medium theory originated by Foldy (1945) in order to understand the factors governing foam lifetime and texture. From electrical resistance measurements, liquid fraction changes in an egg white foam column were evaluated quantitatively and qualitatively by using a generalized free drainage model. Although egg-white foams were more prone to changes due to drainage, I observed that for all foams the ultrasonic scaling parameter $\alpha\lambda/f$ was proportional to the square of average bubble size (indicative of a diffusively driven aging process due to disproportionation of bubbles). Slopes of $\alpha\lambda/f$ versus aging time were $6\cdot10^{-8}$ and $11\cdot10^{-8}$ for egg white foams of void fraction 0.65 and 0.78, respectively, indicating that disproportionation progressed approximately twice as fast in the high void fraction foam. The slopes of $\alpha\lambda/f$ versus aging time were similar for both *Gillette* foam void fractions (0.93 and 0.91) at a value of $1.5\cdot10^{-8}$ s^{-1}, attributable to a lower solubility of isobutane compared to air. By combining ultrasound and electrical resistivity, this thesis has

provided novel insights into understanding instability processes occurring in foams. Potentially, ultrasound techniques could be used instead of imaging for foam aging studies, since non-invasive and non-destructive measurements of attenuation and phase velocity permit interrogation of opaque foam structures.

CHAPTER 1 INTRODUCTION

Due to a unique texture perception, foamy foods are distinct from non-aerated food products. Foamy structured products are very popular beyond food science as well. Some drugs produced with a foamy structure have better bioavailability and activity; therefore, foams are used also in the pharmaceutical industry (Zhang *et al*., 2010; Wu *et al*., 2011). Solid foams are used widely in industry due to foam`s ability to achieve different mechanical properties, from flexibility to strength, in both cases with reduced weight due to the lower density of foams (Ibeh and Bubacz, 2008; Squeo and Quadrini, 2010). Food or non-food foams have the same structure and properties. In order to produce liquid food foams, scientists and cooks strive to incorporate the maximum amount of air into the foaming liquid and obtain relatively small bubbles, since this is the key to obtaining stable foams (Allen *et al*., 2006; Campbell, 2008). Dairy foams, such as whipped cream, consist of bubbles stabilized by fat (Eisner *et al*., 2007; Campbell, 2008), while in egg white foams, bubbles are stabilized by creating viscoelastic films once the partially denatured protein is exposed to the air-water interface (Raikos *et al*., 2007). Egg white foams are generally complex systems, consisting of several foaming protein components, where some lower the surface tension and others act as stabilizing agents (Kokini and van Aken, 2006). As a result of this complexity, the temperature and pH of the foaming solution have a big influence on foaming capacity and foam stability (Johnson and Zabik, 1981a, 1981b; Patino *et al*., 1995; Magdassi *et al.,* 1996; Martin *et al.,* 2002; Kralova and Sjöblom, 2009; Langevin, 2009; Allen *et al*., 2006). Synthetic foam stability is affected less by such factors, since the foam is often obtained by aerating a liquid with a single, low molecular weight surface active component (Garrett and Gratton, 1995; Bezelgues *et al.,* 2008). Therefore, in attempting to understand foam

creation and foam stability in food products, it is useful to look at more simple foam systems in order to understand more complicated food ones.

A classical angel food cake recipe is a good food example to illustrate the challenges and struggles one might face in the kitchen and in a large scale baking facility in making a foam. The challenge consists in the unstable liquid foam nature that leads to drainage, disproportionation and coalescence at room temperature or in the initial stages of baking (20-60 ^{0}C) (Mizukoshi, 1983). In cake batter that is not optimally aerated, drainage processes that will potentially cause a failure in baking a cake manufacture can occur. Because of high sugar content in the batter, the necessary amount of water for protein denaturation and starch gelatinization is reduced. As a result, starch does not fully gelatinize, because high temperatures are needed in this limited amount of water system. In this case, following baking the cake structure is not fully solidified and the baked product has an impaired uneven texture or even significant reduction of volume due to cake collapse (Pyler, 1988). Therefore it is important to understand instability mechanisms and evaluate quantitatively the foams required for cake making, in order to advance and initiate new bakery foam formulation and making technologies.

Foam structure and stability is highly dependent on the amount of air in the foam. Indeed, volume fraction of air distinctively separates foams into two categories in terms of rheological properties: wet foams and dry foams (Heller and Kuntamukkula, 1987; Weaire and Hutzler, 1999). Wet foams with spherical bubbles are more prone to instability due to drainage, whereas in dry foams greater amounts of gas migrate from one neighbouring smaller bubble to another bigger bubble through the very thin, separating films. The latter effect, known as disproportionation, enables bubble radius to grow with time and the growth rate is described as time dependent (Durian *et al*., 1991). These changes in bubble size distribution strongly impact

foam rheological behaviour (Cohen-Addad *et al.*, 1998; Weaire and Hutzler, 1999), namely in a dry aging foam, the foam`s shear modulus scales with frequency in a power law manner (Cohen-Addad *et al.*, 1998).

Because of the time dependent changes in the structure and properties of foams, any industry producing or developing new foam formulations is in need of non-invasive and non-destructive tools. Low frequency ultrasound as a technique has been used for more than a decade in scientist labs to investigate low void fraction aerated materials, such as dough, bubbly gels and gas-liquid-solid systems (Povey, 1989; Elmehdi, 2001; Cents *et al.*, 2004; Bellido, 2007; Cobus *et al.*, 2007; Fan, 2007; Strybulevych *et al*., 2007; Leroy, *et al*., 2008). By measuring the phase velocity and attenuation of propagating ultrasound waves and applying effective medium theory, valuable information on dough rheological properties can be obtained (Elmehdi, 2001; Bellido, 2007). These properties are impacted by the properties of the matrix and bubble size distribution. Investigations of very high void fraction foam aging processes are fewer. Studies of 92% gas synthetic *Gillette* foam by using low frequency (37-84 kHz) ultrasound gave insight on changes in foam structural properties: the attenuation increased due to bubble radius growth as the foam coarsened and phase velocity was reduced due to decreasing elasticity of the foam (Mujica and Fauve, 2002). Experimental phase velocity and attenuation results combined with image analysis results of bubble size led to a quantitative evaluation of the foam aging process in the *Gillette* foam (Mujica and Fauve, 2002).

To investigate highly aerated food and non-food foam structure and stability, it is necessary to integrate ultrasound experiment results with the available physics theory of wave propagation in this complex foam medium. Applying other commonly used techniques, such as imaging and electrical conductivity techniques (Yianatos *et al*., 1985; Phelan *et al*., 1996; Weaire

and Hutzler, 1999; Barigou *et al*., 2001; Feitosa *et al*., 2005) as support tools to obtain additional information on foam aging process will lead to better understanding of foam instability processes. In addition, new knowledge can be obtained to determine which factors and conditions govern foam stability processes.

1.2 Objective statement

In this thesis highly aerated food foams and non-food foams were studied. Cake batter structure and stability is related to the properties of the egg white foam from which the cake is made. Food foams very often are a good base for aerated baked products, such as meringues, soufflés, and angel food cakes, as the aerated structure gives to the product porosity, high volume and soft texture. Non-food foams are very common in different industry areas, like metallurgy, pharmacy and others. In this research I used *Gillette* foam, a very well studied foam, as a guide to give some insight into the behaviour of more complex food foams. The structure and stability of any aerated food product are related to the properties of the foam from which the product is made. The void fraction and bubble sizes of the foam determine the product volume and porosity. However, foams are unstable and rheological properties change with time. Those structure changes are even more accelerated when the temperature rises to 60 C, as occurs in the first stage of baking. Addition of flour, in order to make a cake batter, slows down foam structure degradation, but does not stop it fully. Specifically, the change in bubble size distribution and void fraction affects the rheology of the system. Instability in a foam arises due to diffusively driven bubble disproportionation, coalescence between bubbles, and liquid drainage. As for very dry foams, like highly aerated egg white and *Gillette* foams, the disproportionation process is the dominant mode and liquid drainage has a minor effect on foam stability. Therefore, the first

objective of this research is to use ultrasound as a method of detection of structural changes arising from disproportionation that occur during foam aging at room temperature.

The second objective is to use an electrical resistivity measurement technique to follow liquid drainage in egg white foams. Liquid drainage occurs in the foam due to gravity and capillary effects. However, rising temperature in the oven reduces aerated product viscosity and therefore accelerates liquid flow downwards (Mizukoshi, 1983). However the addition of flour reduces liquid drainage. Nevertheless, during the product baking process, liquid drainage is accelerated and is only stopped fully at the thermal transition temperature of the aerated product components.

Since ultrasound measured parameters are affected by the changing bubble size in aging foam, it is important to determine those changes by techniques capable of sizing bubbles. Microscope imaging of aging foam is a conventional but reliable tool to obtain bubble sizes, and image analysis will quantify these sizes and allow determination of bubble growth rate that leads to an evaluation of the disproportionation process in the foam. Therefore, the third objective is to evaluate quantitatively bubble size changes due to aging in different void fraction foams by using an imaging technique coupled with image analysis.

Research objectives are as follows:

1. *Characterize disproportionation in egg white and non-food foams by ultrasound:*

   Apply existing fundamental theories of ultrasound wave propagation in aerated materials to ultrasound and image measurement results in order to evaluate the foam aging process quantitatively and the parameters affecting the instability process. From measured ultrasonic parameters (velocity and attenuation), the rate of disproportionation in different void fraction and type foams will be determined. To analyse and understand the

mechanisms governing ultrasound wave propagation in high void fraction egg white and *Gillette* aging foams, a foam model with theoretical monodispered bubble size distribution will be compared to experimental results. The ultrasound results on egg white and *Gillette* foams will be interpreted by using long wavelength theory (Wood`s approximation) and a modified effective medium theory originated by Foldy (1945).

2. *Characterize liquid drainage in egg white foam by using electrical conductivity measurements:*

   Changes in conductivity will be monitored as a function of time thus giving information on dynamic foam properties as liquid content changes with time at different heights in the foam (the rate of foam drainage). By using a generalized two boundary liquid drainage model, parameters affecting liquid foam drainage regime will be determined.

3. *Characterize food and non food foam structure and structural changes during aging by using image analysis:*

   Microscope imaging technique will be used as an additional technique to validate ultrasound measurements and as a reliable tool to determine bubble size distributions in aging food and non-food foams. Image analysis itself will provide information on foam instability governing mechanisms. The scaling of the bubble mean radius squared with aging time determines if disproportionation or liquid drainage is the dominant instability process in the foam. As well, quantification of the bubble size distribution in aging foams will serve for application of theoretical models of ultrasound wave propagation in aerated viscoelastic media.

CHAPTER 2. LITERATURE REVIEW

2.1 Introduction

With newly arising interest for natural, healthy and good quality products, interest in foams as a novel application is not only happening in the food industry, but also in cosmetics, metallurgy, drugs and the building industry. For many years floating foams have been used to separate minerals from extracted ore, foams are used for fire fighting, and foams are used as drilling liquids in oil production (Höhler and Cohen-Addad, 2005). With changing public perception of environmentally friendly living styles, foams made from renewable materials, called biofoams, find application in thermal insulation of homes (Banik and Sain, 2008).

Foamy foods or aerated food applications are very common, since the foam nature dramatically influences the perception of texture and flavour (Campbell, 1999, 2008; Kokini and van Aken, 2006). Foods such as bread, fluffy cakes, mousses, whipped creams, ice creams, cappuccino coffee milk froths are met everyday in our lives. Some of the foams, no matter what their appearance and wonderful taste are very unstable, the lifetime of which may be a couple of minutes. Foam stability is important for the shelf life of the product, as well as for some food processing operations such as mixing and kneading.

With a rapidly growing demand of new foam applications there is a need to develop new, advanced, non-intrusive techniques able to determine quality and foam life time. Foam research history is quite old - dating back to Joseph Plateau in 1873, who defined for the first time foam's polyhedral structure. Fundamental techniques of rheology, light scattering and electrical resistivity have been used to precisely characterise foam structure and properties for many years.

New techniques, such as ultrasound, are beginning to appear as promising non-invasive and non-destructive tools.

A pioneering step was taken a decade ago to develop a new non-invasive ultrasonic technique to characterize low void fraction bubbly liquids by the scientists Povey and McClements (Povey and McClements , 1989; McClements, 1995). This was continued by Leroy *et al*. (2008). A big step was taken by Mujica and Fauve (2002) by using ultrasound to investigate very high void fraction *Gillette* foams. It is important to mention that the previously studied Gillette foams have a continuous medium whose viscosity is similar to water. As we will see in our ultrasound research on egg white foams, the properties of the continuous medium are as important as the void fraction and bubble size distribution. Though ultrasonic studies on foams are difficult, some physicists are attracted to this challenge, and real applications of ultrasound for analysing foam properties in the food industry are still in the works.

2.1.1 History of food foams

2.1.1.1 Different origins of food foams

Culinary art of foams is as colourful as our world, with different cultures and traditions, and dating back even to the days of ancient Egypt (Campbell 2008). The oldest and most common aerated food product is our daily bread, whose spongy structure is created due to natural fermentation of sugars by yeast and, as a result of it, the CO_2 that is produced aerates the dough.

Dairy foams such as whipped cream, ice cream and other highly aerated, sweet foams are related to a technology revolution at the beginning of the 19th century. Egg foams have been made since the early 17th century, and have been very common until the present time since many dessert foods are egg-foam based. Examples of products that require whisking eggs are soufflés (originated in France), meringues, mousses, zabaglione (Italy), angel and sponge cakes

(America), and Pavlova (New Zealand). The distinct foaming capacity of hen eggs to incorporate 7 to 8 times as much air as their volume fraction in egg whites made them popular all around the world. However, mass production of foamy foods was limited until the 19th century, when technology improvements allowed the large scale whipping processes that require big mechanical work inputs (Campbell and Mougeot, 1999; Campbell, 2008).

New ingredients for stabilizing this inherently unstable structure allow the creation of new foamy products. An important factor to be mentioned is the skill or science that comes into play for making new products (Campbell, 2008). The merger of science and traditional kitchen skills aroused the molecular gastronomy trend, and spurred a scientific discipline in many universities (Barham *et al.,* 2010), with spectacular food flavours, textures and shapes. This new food philosophy approach was taken by one the best restaurants in the world, "*El Bulli"* and spectacular food creations are available not only in the scientific lab, but also in the public eye. One of the examples of such dishes is shown in Figure 2.1, created by "*El Bulli*" chefs, described in their own words as "the food is entrapped into gigantic bubbles and the explosion of them gives the full flavour sensation" (Arboleya *et al.,* 2008).

Figure. 2.1. Version of bubbly juice at pH 4.6; sun ripened berry fruits lightly covered in virgin olive oil and lime. Photograph from Jose Luis Lopez de Zubiria (Arboleya *et al.,* 2008).

2.1.1.2 Liquid foams

Unbaked food foams such as whipped cream, zabaglione, ice cream, dairy desserts, soft doughs, confectionary, marshmallow, cappuccino foam are liquid foams and their lifetime is relatively short (Campbell, 1999). Typically the air content by volume in wet foam is around 50 % and the bubble size is a critical parameter since it influences the texture, mouth feel, and stability of the product (Balerin *et al*., 2007). Surfactants play a big role in this case as they stabilize foam structure for a specific period of time, which determines the product shelf life. Other natural stability-enhancing compounds in foamy foods are proteins (zabaglione, egg foams), fat crystals (whipped cream, puff pastry) and ice crystals (ice cream, frozen desserts) (Campbell, 1999).

2.1.1.3 Solid foams

Baked, solid food foams such as breads, puddings, muffins, doughnuts and dumplings are often produced from chemically leavened or fermented dough. Alternatively, gas is mechanically whipped into a batter, such as cakes and meringues. In both cases, all of these product structures are stabilized by the baking process (Campbell, 1999; Schramm, 2005). Bread dough is aerated by CO_2 produced by yeast as a result of sugar fermentation. Low density, very light texture baked products are usually obtained because of high air content created from an egg white foam base. Examples are angel food cake, puddings, muffins, meringues, Madeira cake, pound and sponge cakes (Campbell, 1999).

Egg white foam based cake structure, for example angel food cake, is stabilized during the baking process. The quality of such cakes depends on the thermal expansion of gas in the egg white foam based batter and on thermal setting of the protein-starch network. This results in products having high volume, low density and soft crumb (Bennion and Bamford, 1973; Pyler,

1988; Sahi and Alava, 2003). In this literature review the challenging points in making angel food cake will be addressed: foam stability and structure, and the importance of ingredients in the overall foam making process.

2.2 Foams

2.2.1 Influence of components on foam structure and stability

In order to make a stable foam, the requirement for the foaming liquids is that there is a good adsorption at the air-water interface. This can be achieved by low molecular weight surfactants, like sodium dodecyl sulphate (SDS) or high molecular weight and complex structured proteins or polysaccharides (Allen *et al*., 2006; Saint-Jalmes, 2006). To name a few, suitable proteins for creating foams are ovalbumin, bovine or human albumin, gliadin, gluten, soy isolate, casein, whey, modified fish proteins, sunflower concentrate and many others (Halling, 1981; Allen *et al*., 2006). A specific grade of surfactants derived from various microorganisms are biosurfactants. Newly extracted from the fungus *Trichoderma reesei* is the protein hydrophobin HFBII that shows unusual foam stability for 4 months even at a very low hydrophobin concentration of 0.1wt%. As this protein is present in mushrooms it is possible to use it in liquid food foam stabilization (Cox *et al*., 2009).

A noticeable difference between low molecular weight surfactant molecules and protein molecules is that there are time-dependent changes in the conformation of protein molecules. As a result, there are longer adsorption times for proteins at the surface air-water interface and changes due to protein coagulation during the foam formation process (Halling, 1981; Kralova and Sjöblom, 2009). During the foam making process, native protein structure is changed and after reaching the highest foam volume, volume starts decreasing. The reason for this volume

decrease is protein denaturation because of excessive agitation or beating and the altered protein migrates back into the protein bulk solution as solid particles. This phenomenon is not observed in the foam making process with surfactants (Halling, 1981).

2.2.2 Surfactant foams

2.2.2.1 Low Molecular Weight

In the food industry, it is important to control the product stability and rheological properties and therefore different type of stabilizers, either low or high molecular weight surfactants, are used. Low molecular weight surfactants usually are of lipidic origin, such as monoglycerides. In general, in the food industry low-molecular mass surfactants consist of lecithins, glycolipids, saponins, fatty alcohols, trans, saturated and unsaturated fatty acids. Insoluble in water surfactants that form so-called crystal lamellae form double layers of monomer molecules which diffuse slowly at the air-liquid interface and participate in foaming and stabilize the foam. Examples of such food grade surfactants are lecithins and lysolecithins, sodium stearoyl lactylate (SSL) and mono- and di-glycerides. Stable foams with small bubble size are obtained using these surfactants because of their ability to form a viscoelastic surfactant layer around the bubble (Garrett and Gratton, 1995; Shrestsha *et al*., 2006; Bezelgues *et al.*, 2008). A good food surfactant lowers the surface tension of water from 72 mN/m to 30 mN/m (Garrett *et al*., 1995; Cohen-Addad *et al.*, 1998). Non-food surfactants, like *Gillette* foamy, lower the liquid surface tension to 30 mN/m (Rouyer *et al*., 2005). Low molecular weight surfactants are extremely mobile at the air-water interface and can very quickly reduce the surface tension (Kralova and Sjöblom, 2009).

2.2.2.2 High Molecular Weight

High molecular weight surfactant category consists of proteins and heterogeneous protein-LMW surfactant complexes. The latter type of complex surfactants are where protein interacts with a small molecular weight surfactant through an opposite charge on the protein, as for example the complex formed from Tween 20 (polyoxyethylene sorbitan monolaurate) and β-lactoglobulin (Coke *et al.,* 1990; Bos and Vliet, 2001). This type of surfactant system stabilizes the whole bubble structure and its rheological properties very well: surfactants at the air-water interface make the protein film more flexible and movable, therefore the films are more ready to respond to deformations (Bos and Vliet, 2001). Changes in pH have a big influence on protein-type stabilized systems because the overall protein charge is altered. The ratio of electrostatically bound surfactant to protein is expressed through their molar concentrations at specific pH levels and plotted versus the unbound surfactant concentration as a cationic or anionic binding isotherm (Magdassi *et al.,* 1996; Liu *et al*., 2005; Kralova and Sjöblom, 2009; Langevin, 2009). Therefore, as the pH of the system changes, protein charge is shifted and the bound surfactant concentration may be increased or decreased according to the binding isotherm (Magdassi *et al.*, 1996; Patino *et al*., 2008). Surfactant concentration in a protein solution matters a lot in complex formation and foam stabilization, as it can have an opposite, destabilizing effect (Coke *et al.*, 1990; Liu *et al*., 2005; Kralova and Sjöblom, 2009). Increasing, for example, Tween 20 concentration allows competitive displacement of protein to occur at the air-water interface, resulting in overall foam instability (Coke *et al.,* 1990; Wilde *et al*., 2004).

Overall surfactant foams and protein foam stabilization mechanisms are different. In the case of the low molecular weight surfactant SDS, foam film stability is maintained through electrostatic repulsive interactions of electrical double layers (Coke *et al*., 1990; German and

Philips, 1994; Walstra, 1996; Saint-Jalmes *et al*., 2005). In the case of protein foams, stability is governed by the aggregates of insoluble denatured proteins that are entrapped in the films and thus slow liquid drainage (Walstra, 2003; Eisner *et al.,* 2005; Saint-Jalmes *et al.*, 2005).

2.2.2.3 Protein foams

2.2.2.3.1 General

Examples of good foaming agents successfully used in the food industry are modified natural proteins of soy, gelatine, casein, egg white, whey, whey protein isolate (WPI), lactoglobulins, lyzosyme, wheat proteins (gluten, gliadin and glutenin) (Mita *et al.*, 1978; Narchi *et al*., 2007; Patino *et al.*, 2008; Kralova and Sjöblom, 2009). Many naturally occurring proteins are too hydrophobic or too hydrophilic for good foaming properties, and so chemical or enzymatic modification of them makes them more surface active. For many proteins the rule applies that near the protein's isoelectric point the stability of the formed foam is significantly improved (German and Phillips, 1994).

Protein film stability and elasticity vary due to the fact that proteins consist of different amino acids so that different intermolecular interactions occur, including hydrogen bonding, electrostatic interactions, disulfide bonding, and van der Waals interactions (German and Phillips, 1994; Kralova and Sjöblom, 2009). Globular proteins like β-lactoglobulin, ovalbumin and lysozyme form more stable films than β-casein, because the globular structure is more viscoelastic, thereby promoting stability at the bubble interface (Allen *et al*., 2006; Foegeding *et al*., 2006).

From olden times, hen eggs are very well known foaming ingredients. Further on in the literature review the properties of egg white from hen eggs will be discussed. Because of egg white and egg yolk (Kamat *et al.*, 1973), a highly nutritious composition and an abundant variety

of proteins with various gelling and foaming properties has been available. Currently there are 78 hen egg white proteins discovered (Mann, 2007). Egg whites can be whipped up to eight times their volume and therefore form very high void fraction foams and foamy products, as for example in the production of soufflés (Campbell, 2008).

2.2.2.3.2 Egg white proteins

Egg white proteins first of all are macromolecules, which are easily able to change conformational structure once they adsorb at the air-water interface. This process is enabled by amphiphilic group exposure at the air-water interface, and as a result of the reduction in surface tension, stable films are created (Nakamura, 1963, 1964; Du *et al.,* 2002a). Proteins not only create, but as well stabilize, the new created surfaces and this function depends on the type of the protein, its molecular weight, its isoelectric point, the pH of the environment, the degree of glycosylation and phosphorylation and the sulphydryl/disulphide bond number (Patino *et al*., 1995; Mine, 2002; Damodaran, 2005; Raikos *et al*., 2007).

Food protein solutions usually are a mixture of different types of proteins whose groups can interact between each other and impact the stability of the dispersed structure. The major egg white proteins are ovalbumin, conalbumin, ovomucoid, ovomucin, lysozyme, globulin G_2, globulin G_3 and avidin (Table 2.1).

Table 2.1. Physical and chemical properties of egg white (Stevens, 1991; Li-Chan *et al*., 1995; Alleoni, 2006).

Protein	Egg white (%, dry weight)	IP	Molecular weight (Da)	T_d (^oC)	Characteristics
Ovalbumin	54.0	4.5	44,500	84.0	Phosphoglycoprotein
Conalbumin	12.0	6.1	77,700	61.0	Binds metallic ions
Ovomucoid	11.0	4.1	28,000	77.0	Inhibits trypsin
Ovomucin	3.5	4.5-5.0	$5.5 \cdot 10^6$-$8.3 \cdot 10^6$	-	Sialoprotein; viscous
Lysozyme	3.4	10.7	14,300	75.0	Lyses some bacteria
Globulin G_2	4.0	5.5	49,000	92.5	-
Globulin G_3	4.0	5.8	49,000	-	-
Ovoinhibitor	1.5	5.1	49,000	-	Inhibits serine proteases
Ovoglycoprotein	1.0	3.9	24,400	-	Sialoprotein
Ovoflavoprotein	0.8	4.0	32,000	-	Binds riboflavin
Ovomacroglobulin	0.5	4.5	$7.69 \cdot 10^5$		Strongly antigenic
Cystatine	0.05	5.1	12,700	-	Inhibits thiol proteases
Avidin	0.05	10.0	68,300	85	Binds biotine

IP-isoelectric point, T_d-denaturation temperature in water or buffer.

The main egg white protein ovalbumin is separated into three fractions, each of which has a different phosphorus content. Ovalbumin in the molecule has 4 free sulphydryl groups and one disulphide group. Ovalbumin structure changes to s-ovalbumin with different covalent bonding upon storing egg whites for a long time and, as a result, this protein is more heat stable (Donovan and Mapes, 1976). The altered s-ovalbumin structure results in a higher denaturation temperature, while ovalbumin denatures at 84 ^{0}C. Temperature changes during storage and pH have an impact on s-ovalbumin formation too.

Ovalbumin alone is able to form a foam suitable to make an angel food cake after longer whipping time, although the cake has tougher structure (Johnson and Zabik, 1981a). Cake made from foam made without ovalbumin, only using ovomucin and ovoglobulin, collapses during baking, and that means that ovalbumin is necessary to support the structure during baking (Johnson and Zabik, 1981a). Increased ovomucin amount reduces the baked cake volume.

However, higher volume cakes were baked from egg whites with increased amount of ovomucin and lysozyme protein solution. This can be explained from the formation of a complex structure from lysozyme and ovomucin. On the other hand, in the absence of ovomucin, the foaming properties of the positively charged lysozyme improve, and that may be due to interaction with negatively charged ovomucoid or ovalbumin protein parts (Johnson and Zabik, 1981a). In egg white, three globulins are present: G_1, G_2 and G_3, where the G_1 globulin was later identified as lysozyme (Kaminski, 1956). Globulins, by reducing surface tension, can increase foaminess even in the presence of ovomucin and lysozyme. A totally opposite result is achieved with lysozyme being in the protein mixture: the foam volume is reduced, but the cake volume is increased (Johnson and Zabik, 1981a; 1981b).

Beating or whipping egg whites for a long time denatures proteins - ovomucin becomes insoluble, having little water holding capacity and the film around the bubble loses its elasticity (Nakamura and Sato, 1964; Raikos *et al*., 2007). However, protein ability to open its conformational structure or in other words, to denature, is necessary to form a viscoelastic film. Ovomucoid has a very high heat resistance and mechanical whipping does not cause protein denaturation (Johnson and Zabik, 1981b). This property, resistance to denaturation, in other words, the unfolding of the structure of the protein, results in poor foaminess. As an example, proteins like lysozyme having a higher number of disulphide bonds, show lack of foaminess due to a stable tertiary structure. Conalbumin is observed to have smaller foamability and has an effect of reducing the cake tenderness. Scanning electron micrographs (SEM) revealed that both lysozyme and conalbumin foam films looked inflexible and rigid and thick (Johnson and Zabik, 1981a, 1981b). In contrast, ovalbumin films examined with SEM looked very thin. Ovalbumin having fewer disulphide bonds shows better foaming power, therefore it suggests that disulphide

reactions influence foaming of the protein and a higher number of bonds impacts negatively on protein foamability.

Globulins increase viscosity and reduce surface tension during foam formation and as well minimize drainage effects in the foam (Alleoni, 2006). Large volume cake can be obtained from foams containing globulins and ovalbumin (Johnson and Zabik, 1981a, 1981b).

In summary, lysozyme, conalbumin, ovomucoid and ovomucin have lower foaming power, while globulins and ovalbumin have higher foaming power. In addition, ovomucin has the highest viscosity of all egg white proteins. Ovomucoid reduces the surface tension the most while ovalbumin reduces it the least. In angel cake making, globulins and ovalbumin are important in the foam making stage because they have the highest foaming capacity; ovomucin stabilizes the foam because it is able to quickly unfold at the air-water interface. Ovalbumin contributes to cake structure setting during baking as its denaturation temperature is the highest. The rest of the egg white proteins does not have a specific function but rather acts as a medium to create foam (MacDonnell *et al.*, 1955).

2.2.2.3.3 Sucrose and sodium chloride impact on egg white foam formation

Salts like sodium chloride change the physicochemical properties of egg white by changing the ionic strength of the protein-NaCl solution and the extent of interaction between different protein groups (German and Phillips, 1994; Damodaran, 2005). Sodium chloride enhances protein adsorption at the air-water interface during the foaming process; therefore a large volume foam can be created (Raikos *et al.*, 2007). Apparently, sodium chloride also increases protein stability to heat denaturation (Raikos *et al.*, 2007).

Sugar increases the viscosity of the egg white protein solution and reduces the degree that proteins unfold at the air–water surface, therefore the foaminess is reduced, especially during the

first foaming stage (Patino *et al*., 1995; Raikos *et al.*, 2007). On the other hand, sucrose increases viscosity and this contributes to the foam stability because the viscosity of the liquid in the foam film lamella viscosity increases and this slows the liquid drainage process. Sucrose however, can increase adsorption of some of the proteins at the air-water interface too. Foaminess of ovalbumin, which is a major part of egg white, is decreased because hydrogen bonds between sugar and ovalbumin molecules are formed, which decreases protein surface activity and adsorption at the air-water interface (Poole *et al*., 1987; Patino *et al*., 1995; Foegeding *et al*., 2006; Raikos *et al.*, 2007). Once the ovalbumin and sugar complex is formed, instead of adsorbing at the air-water interface ovalbumin stays in the foaming solution (Raikos *et al*., 2007).

2.2.3 Foam making ways

Foams are two phase systems created by dispersing air or other gases into the liquid phase. The new surface area is created against an increased surface energy component that is attempting to be minimized. Because proteins and surface active agents are able to lower surface tension at the air-water interface, some of them are able to stabilize the whole dispersed system (foam structure). A good foaming protein is considered one that rapidly diffuses to the air-water interface, changes its orientation and forms a viscous film around the air bubble (Murray, 2007; German and Phillips, 1994).

2.2.3.1 Foam making techniques

The method that is used to make foam largely affects the foam structure and stability. Using different foam making methods can cause the bubble sizes in protein foams to vary from 1 μm to 10 mm (Halling, 1981). Foam making ways can be classified into four groups: the air is incorporated into the liquid by whipping, shaking or bubbling methods or by nucleation (Weaire

and Hutzler, 1999). Different foaming methods require different protein concentration to obtain the same volume of the foam. For foam production, protein concentration can be smaller in gas sparging and shaking techniques compared to whipping (Bos *et al*., 2003).

2.2.3.1.1 Whipping

Whipping is perhaps the most common way of producing foamed foods; although, bubble size in a formed foam varies a lot (Figure 2.4). A new surface is created by using whipping action that causes shearing of the multiphase liquid. The whipping process involves creating and at the same time disrupting a new air-liquid interface (Bos *et al*., 2003).

During foam formation, the pressure inside the bubble, as it is getting smaller, increases, as a result of an overall increase of surface area around newly formed bubbles (see section 2.2.5.2). In some cases during whipping, the surfactant or protein can not move to the interface, so the concentration of surface active component around the bubbles can be different. As well, during whipping, bubbles are continuously broken down and new ones formed (German and Phillips, 1994; Lau and Dickinson, 2004).

Efficiency of foam production by whipping depends on the geometry of the mixing blades, the volume and the speed of the mixer. As well as for other foaming methods, rheological and surface properties of the liquid have a major impact on foaming efficiency (Prins, 1988). For example, it is necessary to vary the whipping time for those egg whites whose structure has been altered by homogenization, aging or removal of some components in order to incorporate the highest amount of air into the foam (MacDonnell *et al.*, 1955).

2.2.3.1.2 Shaking

Foam making by shaking is performed by shaking a container with a foaming liquid at a certain frequency and amplitude. The amount of air incorporated into the liquid depends on the

liquid viscosity, surface tension and origin of the foaming agent. The pressure difference inside the container and the atmosphere has a big impact on the foam bubble size too (German and Phillips, 1994).

2.2.3.1.3 Bubbling method

The bubbling method, or sparging, is used in ice cream and mousse making processes. Afterwards, in the ice cream making process, for further bubble size reduction, a whipping action is used. During this process the air is injected through an orifice or plate with holes (Prins, 1988) into the viscous liquid so that a gas bubble of radius (r) leaves the orifice end when the gravity force (F_g), the force holding the bubble to the orifice, is equal to the buoyancy force (F_b). The gas bubble formation process can be expressed by the formula (Prins, 1988; Pugh, 1996):

$$\mathrm{r} = \sqrt[3]{\frac{3\gamma r_o}{2\rho_l g}} \tag{2.1}$$

where r_o - orifice radius, g - acceleration due to gravity, ρ_l - liquid density, γ - surface tension. Buoyancy force is $F_b = (4/3)\pi r^3 g\rho_l$. Orifice size and surface tension of the liquid are critical because they determine the formed bubble size.

Bubbling or sparging allows controlling of air bubble formation and the formed bubbles are more uniform, so it is possible to produce a monodisperse wet foam (Ganan-Calvo *et al*., 2004). However, this method has dynamic limitations: using poor foaming agents at a slow bubbling rate, too little foam is formed. This method is useful to test foamability of different solutions. On the small foam production scale, instead of an orifice, a nozzle can be used and as the gas is blowing through the foaming liquid, a stream of micro bubbles is produced (Ganan-Calvo *et al.*, 2004).

The bubbling method is used to test the foamability of solutions because it only requires a small amount of foam solution (Prins, 2006). Foaming capacity can be expressed as the interfacial area that can be created by the foaming agent and expressed by overrun:

$$Overrun = \frac{V_{foam} - V_{liq}}{V_{liq}} \cdot 100 \quad (2.2)$$

where V_{foam} is volume of the foam and V_{liq} is volume of the initial foaming liquid.

2.2.3.1.4 Nucleation

Foaming by nucleation of gas bubbles occurs in a supersaturated liquid, for example, on the surface of a glass of beer or champagne (Weaire and Hutzler, 1999). Nucleation does not start on its own – a particle, dust or scratch on the glass of beer or champagne serves as a bubble nucleation trigger in the drink supersaturated with CO_2 (Bamforth, 2004). Shaving foam is produced by a nucleation process, where a pressurized container contains foaming liquid and gas.

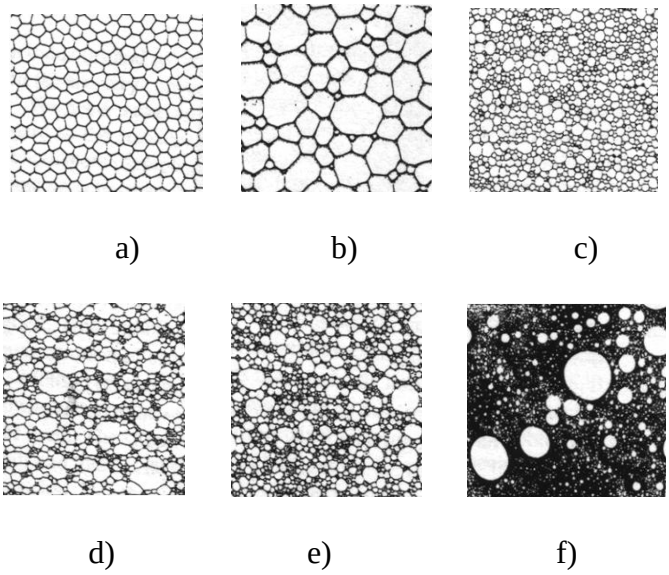

Figure 2.2. Examples of foam structures made by: a) blowing gas, b) blowing gas (turbulent flow), c) sparging, d) blending, e) shaking, f) nucleation of gas (beer froth). (Taken from Weaire and Hutzler, 1999).

2.2.3.2 Influence of techniques used on foam structure

Foam structure depends on the techniques used that influence the hydrodynamic conditions and surface properties of the bubbles. Different methods and techniques may produce foams with different bubble size distributions. Even the same foaming technique, but changed parameters such as air injection rate may result in different foam structure. As an example, blowing gas through a thin nozzle at a constant low rate may produce monodispersed foam. If the flow rate is increased and even varied during the aeration process – foam with polydispersed bubbles is produced (Weaire and Hutzler, 1999). By using whipping, beating or shaking techniques one produces polydisperse foams, where the bubble size distribution is usually characterized by a log-normal distribution (Weaire and Hutzler, 1999). If bubble nucleation sites are uniform and small, the bubbles formed through the nucleation process are relatively monodispersed.

2.2.4 Foam structure

Any liquid foam structure is described by two parameters: void fraction (φ) or liquid fraction (ε) and bubble size distribution (Spencer, 2006).

$$\varphi = 1 - \frac{\rho(t)}{\rho_0} \tag{2.3}$$

$$\varepsilon = 1 - \varphi \tag{2.4}$$

where φ is bubble void fraction, $\rho(t)$ is density of the foam at different whipping time, ρ_0 is density of foaming liquid with no air in it.

If the foam is not a runny liquid, as for dough where it has a stiff hard texture, instead of void fraction the term porosity is used. As was addressed before (Figure 2.2), the foam making method determines the achieved void fraction and bubble size distribution. Foams made by a whipping foaming solution usually produce a polydispersed bubble distribution (Weaire and

Hutzler, 1999). Monodispersed foams (Figure 2.4, a)) can be produced by blowing gas into the nozzle in the solution at a relatively slow rate (Wilde, 1996).

Low void fraction foams are different in their structure and stability as compared to high void fraction (Figure 2.3).

To define a foam as wet usually means that the bubbles in this foam are spherical and do not touch each other (Weaire and Hutzler, 1999) and this structure exists in the foam if the air content does not increase beyond 65 %.

a)

b)

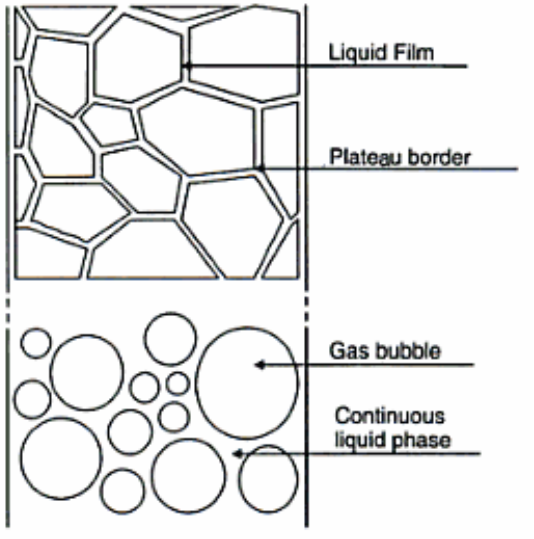

Figure 2.3 Structure of the foam a) polyhedral foam and b) wet foam, (Taken from Prins (2006))

Foams are dry when a large air amount is dispersed in liquid, so that a polyhedral foam is obtained (Figure 2.3 a)), and where the bubbles are close to each other, so that the geometrical shape of the individual bubbles is more like a dodecahedron. The liquid film separating two bubbles in the spherical or polyhedral foam is called a lamella. In polyhedral foam those lamellae are essentially flat, while in a spherical foam the lamellae are rounded. A good example of a solid foam with spherical bubbles is ice cream, where bubble size varies between 20 μm and 60 μm (Chang and Hartel, 2002).

Beyond the limit of 65 % air fraction, bubbles in the foam start touching each other and the higher the air content, the flatter the bubble walls are. At this point, foam structure is characterised as polyhedral and the border where two films meet is called a Plateau border.

Dry, polyhedral foam elements and rules governing their structural organization were first defined by Plateau, and they are as follows. A Plateau border (also known as a channel) is formed when three lamellae (and not more than that) intersect forming a triangle at an angle of 120 degrees (Figure 2.4a-1). Along the length of the lamella this triangle has the geometry shown in Figure 2.4a-2. Four Plateau borders meet at one point called a node (vertex) (Goldfarb *et al*., 1997), as shown in Figure 2.4b.

a)

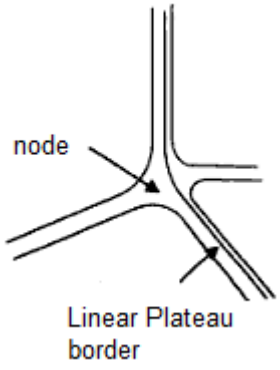

b)

Figure 2.4. a) Polyhedral foam structure elements. 1 – Plateau triangle; 2 – Plateau border; b) Four linear Plateau borders meeting in a node (vertex) (Taken from Goldfarb *et al*., 1997).

The network of channels called Plateau borders are connected at vertices, whose shape and size varies depending on the void fraction and bubble size (Weaire and Hutzler, 1999). Beer foam is a good example of polyhedral foam (May *et al*., 1996).

2.2.4.1 Bubble size distribution

In order to better understand foam structure evolution it is useful to visualize bubble size distribution in one way or another graphically. Bubble or crystal size studies have been done in

rocks of volcanic origin (magma and lava), metals and other media (Bisperink, *et al*., 1992; Gaonach *et al*., 1996; Proussevitch *et al*., 2007). It was observed that size distributions of bubbles were not well characterized by using normal statistical functions. Therefore, size distributions were instead characterized by logarithmic statistical family functions (log-normal, logistic and Weibull) that fit the observed bubble size distribution the best (Proussevitch *et al*., 2007).

The usual way of representing image data as a population density diagram is by sorting the bubble sizes or volumes into size ranges and plotting as a frequency against bubble size (volume or radii) histogram. It is useful to present data as a distribution density or as a frequency distribution. The former is obtained by dividing the population by the number of bubbles and the latter in addition by taking the bubble percentage of each bubble size:

$$f(V_j) = \frac{1}{n'_{total}} \frac{n_j}{\Delta V} \tag{2.5}$$

where $f(V_j)$ is population density by bubble size in volume units, V_j is bubble volume of bubble j bin size, n'_{total} is the total number of observed bubbles, ΔV is the bin size representing bubble volume, n_j is number of individual bubble in size class (bin) j.

If the observed distribution consists of multiple peaks or modes, it is impossible to accurately define the distribution by using logarithmic functions, since it monotonically decreases. Therefore, a solution is transformation of the observed distribution to logarithmic scale and treating it as a linear analog of the logarithmic distribution. For example, all observed bubble volumes are converted to their logarithm and the results replotted by choosing equal bin sizes in log units. The transformation of a distribution density function into its logarithm isn't straightforward. As an example, transformation of the distribution density of a normal function

($f(r_j)$) in linear form into logarithm form ($f(r_j^{'})$) is done in the following way (Proussevitch *et al.*, 2007):

$$f(r_j) = \frac{1}{\sigma_{st}\sqrt{2\pi}} exp\left[-\frac{(r_j - x_c)^2}{2\sigma_{st}^2}\right] \qquad (2.6) \qquad \Rightarrow f(r_j') = \frac{1}{\sigma_g r_j \sqrt{2\pi}} exp\left[-\frac{1}{2\sigma_g^2} ln^2\left(\frac{r_j}{\mu_r}\right)\right] \qquad (2.7)$$

where x_c – bubble mean size of normal distribution, μ_r - bubble mean size of log-normal distribution, σ_{st} and σ_g are the standard deviations of the normal and log-normal distribution, r_j - midpoint of the j^{th} class in the histogram of bubble sizes, $f(r_j)$ – normal probability density function of x_c. The details of linear function conversion into its logarithm are given in the work of Proussevitch *et al.* (2007).

Most of the time, bubble size is estimated from 2D images and because of view limitations small bubbles can be missed (De Vries, 1972). Bubble size distribution estimated from a 2D view will be different from the bulk, and hence correction of the statistical distribution is proposed (De Vries, 1972):

$$F(r) = \left[\int_0^\infty \frac{f_s(r)dr}{r}\right]^{-1} \frac{f_s(r)}{r} \qquad (2.8)$$

where $F(r)$ is the corrected bubble size distribution in foam bulk and $f_s(r)$ is observed bubble size distribution obtained from experiments (De Vries, 1972; Cheng and Lemlich, 1983).

Spencer (2006) whipped foams from egg white products and sugar up to 0.81 void fraction. He obtained bubble size distributions from microscope image analysis and statistically characterized foams by using a two parameter log-normal function (Formula 2.7):

From log-normal distribution scale, bubble size mean (μ_r) and standard deviation (σ_g) is converted to geometric mean (x_c) and standard deviation (σ_{st}) in normal distributed scale by using these equations:

$$x_c = \exp(\mu_r) \qquad (2.9)$$

$$\sigma_{st} = \exp(\sigma_g) \tag{2.10}$$

2.2.5 Foam properties

2.2.5.1 Rheology of the foam

Foams from a rheological point of view are interesting to study because of their dual liquid-solid like nature, which depends on void fraction, bubble size distribution and the applied stress magnitude (Weaire and Hutzler, 1999; Höhler and Cohen-Addad, 2005). Rheological properties of the bulk foam reflect the inner structure (bubble size distribution) and the amount of air in the foam. Foam physical changes, drainage and disproportionation that are typical foam aging phenomena, affect the rheological behaviour of foams.

Foams in terms of physics models are considered as complex fluids and their structure can be viewed as a disordered packing of small soft units (Höhler and Cohen-Addad, 2005). One of the models – the soft glassy material model - is applied for foams, since foams show slow mechanical relaxation behaviour, a behaviour common to complex fluid properties such as viscoelasticity (solid, liquid like), jamming and yield stress.

2.2.5.1.1 Yield stress

The foam rheological behaviour transition from solid to liquid like occurs when a certain value of stress called the yield stress is reached. Prior to the yield stress, at low applied stress, the solid-like behaviour of a foam arises due to bubble jamming and resistance of the bubble structure (Heller and Kuntamukkula, 1987; Höhler and Cohen-Addad, 2005). After the shear stress exceeds the yield value, foam viscosity depends on the magnitude of the shear rate. The yield stress (τ_y) of the foam is therefore a parameter that describes foam mechanical properties and it strongly depends on the foam liquid fraction (ε). For monodispersed systems the foam-like

behaviour starts at a void fraction of 0.64 (Rouyer *et al*., 2005). A higher void fraction of 0.74 is required for a polydispersed system of bubbles (Princen and Kiss, 1986). For polydispersed foams it was found that as the surface mean volume radius (r_{32}) increases, the yield stress decreases. Marze *et al*. (2009) gave an expression for the yield stress as a function of liquid fraction:

$$\tau_y = k_f \left(\frac{\gamma}{\mathrm{r}}\right)(\varepsilon_c - \varepsilon)^2 \tag{2.11}$$

For aqueous foams, the prefactor k_f = 0.53 (Mason *et al*., 1996), and the liquid fraction of randomly packed bubbles ε_c = 0.36, γ is surface tension, r is bubble mean radius.

Princen (1985) gives the yield stress expression in another form for the void fraction range between 0.74-1:

$$\tau_y = 1.28\frac{\gamma}{\mathrm{r}_{32}}\varphi^{1/3}\tilde{\mathrm{F}}_{\max}(\varphi) \tag{2.12}$$

where γ is surface tension, r_{32} is surface mean volume radius, φ is void fraction, $\tilde{F}_{max}$ is dimensionless mean contribution of a single bubble to the yield stress. For monodispersed foams $\tilde{F}_{max}$ can be derived from 2D analysis. For polydispersed foam, Princen (1985) determined $\tilde{F}_{max}$ experimentally, using concentric-cylinder geometry and recording τ_y as void fraction increased ($\varphi > 0.75$), where constant γ and r were known.

The bubble size, r_{32} (also called the Sauter mean bubble radius) is the surface mean volume radius of the bubble in the spherical and equal volume state. The value of r_{32} is obtained from the bubble size distribution histogram (Princen and Kiss, 1986):

$$\mathrm{r}_{32} = \frac{\sum_j n_j r_j^3}{\sum_j n_j r_j^2} = \frac{3V_0}{S_0} \tag{2.13}$$

where n_j is the number of bubbles in the bin of size j, r_j is mean bubble radius in the bin, and S_0/V_0 is surface area of spherical bubbles per unit volume of the foam.

The yield stress for egg white or whey protein isolate foams can be easily measured by using a vane rheometer (Pernell *et al.*, 2000) as well as in oscillatory tests. In the cake making process, yield stress is important information in baking and confectionary because it characterizes the foam and batter rheological properties. It is necessary to obtain a foam with optimum rheological properties as these properties contribute to the overall foam stability (Pernell *et al*., 2000).

2.2.5.1.2 Small and large strain

Foam properties and stability can be determined by using small and large strain rheological tests. Oscillatory frequency sweep test on the foam is performed in the linear range by applying small amplitude controlled shear stress or strain in a sinusoidal manner and recording the response (Cohen-Addad *et al*., 1998). The magnitude of applied stress varies from foam to foam since it must be assured that the applied stress does not destroy or change the foam structure irreversibly (Höhler and Cohen-Addad, 2005). Therefore, prior experiments are performed to determine the linear range of shear stress and shear strain.

The loss (G'') and storage (G') shear modulus characterise foam behaviour as an elastic or viscous material. A complex modulus (G) relates shear and storage modulus as a function of frequency (ω) through the equations (Höhler and Cohen-Addad, 2005):

$$G(\omega)=G'(\omega)+iG''(\omega) \tag{2.14}$$

$$\tan\delta = G''/G' \tag{2.15}$$

where $\tan\delta$ is the phase shift, measured in degrees, i^2=-1.

It is established that high void fraction foams possess elastic material properties (G' is greater than G''), while lower void fraction foams behave as viscous materials (G'' is greater than G' values). The distinction between viscous and elastic behaviour of the foam occurs at a

critical void fraction (see yield stress section). At this critical void fraction, the round bubble spheres start touching each other and become closely packed as the void fraction increases further (Gopal and Durian, 2003).

A lot of work has been done on very dry ($\varphi = 0.93$) *Gillette* foams (Höhler and Cohen-Addad, 2005). In the small strain regime, an almost linear response was observed for both moduli *G'* and *G"* as a function of frequency. An increase of *G'* was noticed only at the higher shear frequencies, and it was also noticeable that *G"* increases proportional to $\omega^{1/2}$ at a higher frequency range from 1Hz to10 Hz. If low frequency oscillatory experiments show that the *G'* response exhibits a plateau region, then the lowest value of *G'* corresponds to the foam's static shear modulus (G_0), so that the foam response to an applied shear stress is an elastic strain. Based on a 2D model for dry polydispersed and monodispersed foams (Höhler and Cohen-Addad, 2005), G_0 is proportional to interfacial tension (γ) and Sauter mean bubble radius (r_{32}) when the void fraction is close to 1:

$$G_0 = 0.51\gamma / r_{32} \qquad \text{when} \quad \varphi \approx 1 \tag{2.16}$$

The elastic behaviour of the foam is highly dependent on the void fraction, or to be more precise, on bubble packing, and it vanishes after the void fraction is reduced to $\varphi_c \cong 0.64$ for monodisperse bubbles. Therefore, G_0 in foams determined at low frequencies from *G'* measurements varies as $\varphi(\varphi - \varphi_c)$ (Saint-Jalmes and Durian, 1999). Princen and Kiss (1986) from experimental results developed a more accurate estimating relation for G_0:

$$G_0 = 1.769\frac{\gamma}{r_{32}}\varphi^{1/3}(\varphi - 0.712) \tag{2.17}$$

Studies done on casein and surfactant (SDS) foams ($\varepsilon = 0.15$) showed that *G'* is almost independent of foaming liquid origin and the gas used at low strains. However, *G"* showed some variation in response to applied strain for casein and surfactant foams, the origin of which is

unclear (Marze *et al*., 2005). Rheological studies done on casein foam aging made with two different gasses (N_2 and C_2F_6) showed variation in response of *G'* and *G"* to applied stress at constant frequency and stress. The gas and the chemical composition of the lamellae sets the different rate of coarsening and drainage (Marze *et al*., 2005).

Rheological tests show a *G'* decrease as the foam undergoes softening with aging time. This is the result of increasing air bubble size and decrease of overall surface area. Foam aging causes a decrease of *G"* and yield stress too. Experimental curves of flowing foams fit to the empirical Herschel-Buckley model:

$$\tau=\tau_y+\xi\dot{\gamma}^n \tag{2.18}$$

where ξ and n are empirical parameters, $\dot{\gamma}$ - shear rate. Theoretically *n* values were predicted to be around 2/3, while experimentally, *n* values are in the 0.25-1 range (Gopal and Durian, 1999; Princen and Kiss, 1986). Experiments done on egg white foams showed a shear thinning behaviour as shear rate increases (Spencer, 2006).

Rheology can be used to investigate foam structure changes with time, though it is complicated because aging in foams involves interrelated disproportionation and drainage mechanisms. In addition, there is a clear distinction between wet and dry foams, as wet foams consist of two components, gas and liquid, that have to be looked at separately (Chavez-Montez *et al*., 2006). The measured values of the foam viscosity are higher than the viscosity of the foam continuous media (Höhler and Cohen-Addad, 2005).

From experiments done on *Gillette* foam (void fraction of 0.93) (Cohen-Addad *et al.*, 1998) and its evolution with time, where coarsening was the dominant aging mechanism, it was established that the complex shear modulus (*G*) can be scaled on one arbitrary chosen reference line with a particular chosen aging time:

$$G(\omega, t) = b(t, t_0)G(\omega\, \alpha_s(t, t_0), t_0) \quad (2.19)$$

where the scaling factor $b(t,t_0)$ has to be determined based on the disproportionation rate and is related to the static shear modulus as $b(t,t_0) \propto G_0(t)/G_0(t_0)$. A common factor $\alpha_s(t,t_0)$ governs the increase of all the mechanical relaxation times (τ_I) with foam age and is related through relationship $\tau_I(t)/\tau_I(t_0)) \propto \alpha_s(t,t_0)$.

From the relation 2.19 it was determined that plotting the scaling factor $b(t,t_0)$ versus aging times, the shear modulus is inversely proportional to the square root of aging time (Princen and Kiss, 1986; Cohen-Addad *et al*., 1998).

Extensive studies on aging egg white foams (Spencer, 2006) showed that slopes of the scaling factor varied depending on the initial void fraction of the foam, therefore indicating domination of one of the aging mechanisms: drainage or disproportionation. From small strain frequency sweeps, data were obtained and later scaled onto a single curve to give slopes for egg white foams between +1 and -0.5. In the first case the drainage process is dominating for egg foams mixed for a shorter time, while in the second case, for egg foams mixed for longer times disproportionation dominates. For angel food cake batters, the slopes varied from 0.36 to -0.38. This reduction of drainage and disproportionation effects with time is due to flour addition into the foam mixture which increases the batter viscosity (Spencer, 2006).

2.2.5.2 Surface tension

Surface tension is important in describing intrinsic liquid properties: if surface tension did not exist - all liquids would be gases. Surface tension (γ) can be defined as a surface energy per unit area and it is a liquid as well as a solid material property (Weaire and Hutzler, 1999). In the foam making process a new surface is created because there is a large energy input and the energy required is proportional to the surface tension. Therefore, surface tension can be looked at

as the work (U) required in order to create new surface area (A_r). Surface tension is proportional to the force (F) per unit length (L) (Weaire and Hutzler, 1999):

$$U=\gamma A_r \tag{2.20}$$

$$\gamma=F/L \tag{2.21}$$

Practically, surface tension can be measured by using the Wilhelmy plate method (Wu *et al*., 1999).

The lamella that surrounds the air bubble is exposed to pressure and surface tension at the gas liquid interface. For a spherical bubble the law, of Laplace describes the pressure difference, which sets diffusion of gas from samller bubbles to the lager ones:

$$\Delta P_r = 2\gamma / r \tag{2.22}$$

Creating a new surface as in the foam making case, the surfactants and proteins adsorb at the air liquid interface, and therefore the overall system energy is decreased. Minimization of surface tension is important because it allows creation of a new interface as well as its stabilization. Liquid surface tension will change if surface active compounds are present, with surface tension reduction capacity limited by the surfactant concentration in the foaming liquid.

A certain amount of surfactant incorporated into the liquid minimizes surface tension at the air-liquid interface once the surfactant monolayer is formed, with hydrophilic parts directed into the liquid and the hydrophobic ends being in the air (Kralova and Sjöblom, 2009). Gibbs elasticity can be described as the rate of change of surface tension (Weaire and Hutzler, 1999; Georgieva *et al*., 2009):

$$\Gamma = d\gamma / d \log A_r \tag{2.23}$$

where Γ – Gibb's elasticity, A_r – surface area, γ – surface tension. In the case, when the surface expansion is fast and there is no time for protiens to adsorb, Gibbs elasticity is proportional to the surface tension and protein concentration. Due to film thinning, surface tension increases and the surfactant's role is to restore equilibrium and prevent film breakage. Surfactants can stabilize thinning of films to some degree, but afterwards due to drainage effects in the film, surfactant concentration changes and breakage of the film occurs (Weaire and Hutzler, 1999).

As the surfactant concentration reaches the critical micelle concentration (CMC), surfactant molecules do not adsorb at the air-water interface, but start instead to form surfactant micelles in the bulk liquid (Joseph, 1997; Kralova and Sjöblom, 2009). It is important to mention that LMW surfactants adsorb quicker than proteins and the adsorption process depends on the surfactant concentration. Thus, surface tension of the liquid is always correlated to foaminess (Saint-Jalmes, 2005).

2.2.6 Foam stability

The majority of aqueous (liquid) foams are not stable over time and instability arises due to gravitational drainage, disproportionation and coalescence. Disproportionation or coarsening in foam manifests because of pressure differences between smaller and larger bubbles. In very dry foams, like *Gillette* foamy, bubbles usually only disproportionate and almost no liquid drains out. However, in the food industry these foam examples are rare and disproportionation is intermixed with liquid drainage. Disproportionation can enhance liquid drainage: as a result of bubblegrowth, the Plateau border thickness increases and that contributes to faster liquid flow (rate) which occurs due to gravity (Saint-Jalmes, 2006; Saint-Jalmes and Durian, 1999; Saint-Jalmes and Langevin, 2002; Saint-Jalmes *et al*., 2000).

Foam coalescence, disproportionation and liquid drainage are all related processes in the foam collapse event (Barik and Roy, 2009). In order to minimize free energy that has been used to create new bubble surface, the two phases air and liquid tend to separate. Liquid starts moving from the lamellae to the Plateau borders and thus thinning of the films occurs. This lamella thinning finally causes rupture of the film separating two bubbles, creating a new large bubble. Due to disproportionation gas slowly diffuses from smaller bubbles to the larger ones, as a result causing overall bubble size increase in the foam. Due to gravity force the liquid from Plateau borders starts moving down and liquid drainage occurs in the foam. The drainage rate for different foams varies, and it strongly depends on the viscosity of the continuous phase. It is important to mention that the foam-making method determines the bubble size distribution and void fraction; as a result it has an impact on foam stability (Halling, 1981; Koehler *et al*., 1998; Saint-Jalmes and Durian, 1999; Koehler *et al*., 2000; Saint-Jalmes *et al*., 2000; Hilgenfeldt *et al*., 2001; Saint-Jalmes and Langevin, 2002; Koehler *et al*., 2004a, 2004b; Maurdev *et al*., 2006; Saint-Jalmes, 2006).

Foam stability can be measured as the time required to drain out a certain amount of liquid from the foam or the rate of foam volume decreases with time (Alleoni, 2006; Raikos *et al*., 2007). However, evaluation of foam stability only by measuring drained liquid is not very rigorous. Bubble size distribution and lamella thickness are important parameters that have to be determined in order to evaluate different foams completely. There is a lack of techniques that would evaluate these foam instability events quantitatively (German and Phillips, 1994).

Just as attractive electrostatic forces are important to elastic film formation, because they contribute to protein foam film stability by enhancing rigidity and viscosity, and while electrostatic repulsion forces work towards separation of the films, electrostatic attraction and

repulsion phenomena can also destabilize the foam. The pH of foaming solutions is usually such that it is away from the protein's pI (isoelectric point is the pH at which carries no net electrical charge), of the protein, but pI has a big influence on protein foam stability. Protein foam stability can be enhanced if the proteins are soluble at the isoelectric point and the greatest strength of the film is produced (Halling, 1981; Zhu and Damodaran, 1994; Zayas, 1997; Hammershøj *et al*., 1999; Davis *et al*., 2004). The lamellae formed around the bubble are thicker and therefore more stable at the pI, because electrostatic attractive forces are the highest and repulsion is the lowest. The ability to stabilise foams varies widely with different proteins but most importantly, soluble proteins can create a stable foam structure. Fresh egg white isoelectric point varies slightly due to the presence of different types of proteins and is around pH 7-8 (Kinsela and Whitehead, 1987).

The film thickness of the foam is another factor to be considered that impacts foam stability. Thick films are relatively more stable, and in addition, if the foaming protein liquid viscosity is high enough, the foam stability with small bubbles size can be further improved because the film thins at a slower rate. Secondly, film stability can be enhanced if hydrophilic particles are added prior to the foaming procedure, so that when the foam is formed particles are located in the films separating two bubbles. Particles as well can be formed during the whipping process if proteins are used as the foaming agent, since mechanical treatments create denatured protein particles (Walstra, 2003).

2.2.6.1 Drainage

Liquid drainage in the foam that occurs solely due to gravity and capillary force is defined as free drainage. In foam physics there is the artificially created situation when the foaming liquid is poured at a certain rate on the top of the foam or a precise amount foaming liquid is injected only once (Koehler *et al*., 2000). In the first case, drainage is called forced

drainage and in the second case pulsed drainage (Koehler *et al.*, 2000). The liquid distribution that moves downwards within the foam height during free, forced and pulsed drainage is different. However, since for my research (as for food foams) only free drainage is relevant, this drainage mechanism will be discussed in detail.

2.2.6.1.1 Drainage in egg white foams

Studies done on egg white foam drainage show that drained out liquid contain proteins and in addition, some of the protein structures are altered (MacDonnell *et al.,* 1955). Qualitative and quantitative analysis of the liquid drained out of the foam shows that the composition of the proteins is different than it is in fresh egg white (MacDonnell *et al.,* 1955). A very small amount of coagulated ovomucin and lysozyme was found in drained-out liquid from egg white foam, which means that ovomucin is contributing to the foam stability and is the slowest draining. Lysozyme enzymatic activity has changed in drained egg white liquid as well (MacDonnell *et al.,* 1955). Ovalbumin structure does not change to a big extent. In the drained liquid, globulins and ovomucoid were found as well in lower amounts than in the original egg white (Cunningham, 1976). Conalbumin is drained out of the foam more extensively than lysozyme. Globulin fractions G_1 and G_2 were not found in the drained liquid, suggesting that these proteins remain in the foam structure.

It is important to mention that ovalbumin is extremely sensitive to overbeating as compared with other foaming proteins (Hiling, 1981). Long whipping times of ovalbumin result in decreased viscosity and increased drainage rates. This can be explained if one remembers to look at ovalbumin as a biological material that contains the native, non-modified structure, because similar coagulation effects have not been found in foams made from dried egg white (Hiling, 1981).

Collected drained-out liquid of egg white foam has a lower viscosity, increased pH level (from pH 9 to pH 9.3) and the whipping time to create a new foam from the drained-out liquid is longer (Cunningham, 1976). In addition, chromatograms of the proteins show that repeated whipping of drained out egg white liquid changed protein structure to some extent. Cake made from foam drained liquid had a lower volume and a coarser structure (Cunningham, 1976).

2.2.6.1.2 Free drainage

As one of the foam instability events, drainage occurs due to gravity and capillarity effects that lead to foam collapse. With time, the draining liquid flows from the top layers of the foam, making it drier and drier, while the bottom of the foam is getting wetter and eventually the liquid starts accumulating at the container bottom. The amount of the accumulated liquid can be evaluated quantitatively from the relationship (Hilgenfeldt *et al*., 2001):

$$h_l(t) = H\varepsilon_0 - \int_H^0 \varepsilon(z,t)dz \tag{2.24}$$

where h_l is the accumulated liquid height, H is initial foam height, ε_0 is liquid fraction at time t=0, ε is liquid fraction at time t, z is measurement location at the foam height, t is aging time.

To understand and evaluate foam instability quantitatively on a macroscopic scale, the drainage phenomenon is usually analyzed using the Plateau border concept. The liquid in the foam is located in the Plateau borders and liquid films, so the higher the void fraction, the more liquid resides in the Plateau borders. When void fraction reduces, the flat film feature is lost and most of the liquid remains in the films (Lemlich, 1978a).

The drainage process from the physics point of view is analyzed in terms of two different regimes that are discussed further. Plateau border surface viscoelasticity, which depends on the surfactant used in the foaming liquid, sets the drainage regime in the foam. Changing the origin of surfactant and concentration changes surface elasticity, therefore a transition from rigid to

mobile surfaces can be achieved. Plateau border surfaces can be rigid (immobile) or mobile, moving with the fluid flow. In the first case, when the surfaces are immobile, the liquid flow is proportional to the cross section of the Plateau border and strong viscous dissipations occur due to liquid bulk viscosity at Plateau borders. This liquid flow is known also as Poiseuille-like flow (Koehler *et al*., 2004a; Saint-Jalmes, 2006). In the second case, when the Plateau border surfaces are mobile, viscous dissipations are less in the Plateau borders, but higher in the nodes. Therefore, this regime is also known as the node-dominated regime, where the velocity of liquid flow is constant at all cross sections of the Plateau border and is described as plug flow (Saint-Jalmes, 2006).

In the foam the liquid flows downwards due to gravity through the Plateau borders, while capillarity effects make the flat films wetter and balance out gravity driven drainage. The capillary effect is a micro scale phenomenon during which a liquid in thin tubes, porous materials and foams tends to move "upwards" against the gravity force. Capillary effects in foams manifest through liquid flow to the drier foam region from the wetter part of the foam. Capillary pressures in dry and wet foams are different: the radius (r_P) of the Plateau Border is bigger in the wetter foam, and therefore capillary pressure is lower. The film thinning driving pressure Δp_d is the net result of suction due to capillary pressure (γ/r_p) in the adjacent Plateau border channels and the disjoining pressure Π in the films (Bhakta and Ruckenstein, 1997):

$$\Delta p_d = \gamma/r_p - \Pi \tag{2.25}$$

Π is computed as the sum of attractive van der Waals force (Π_{vDw}) and repulsive force (Π_{DL}) arising from interaction of the two double layers and as well short range repulsive force (Π_{SR}):

$$\Pi = \Pi_{vDw} + \Pi_{DL} + \Pi_{SR} \tag{2.26}$$

The latter interaction (Π_{SR}) is common for long chain non-ionic surfactants and polymers, such as proteins adsorbed on the surface molecules. Therefore, positive (Π) results in repulsive forces and it opposes film thinning, while negative (Π) forces increase the driving pressure (Δp_d) which as a result accelerates film thinning. Overall, capillary effects causing film thinning contribute to gravity driven liquid drainage and these effects balance out drainage resulting in steady state flow of liquid (Saint-Jalmes, 2006). It is important to mention that because of capillarity effects, not all liquid drains out of the foam.

However, the situation in the foam with a fixed liquid fraction consisting of small bubbles can be different than in a foam with large ones. The Plateau Border radius (r_P) determines the Capillary number and the Capillary number dictates the velocity (v_d) of the liquid flow ($Ca = \eta v_d / \gamma$, η is bulk viscosity). For example, capillary pressure and suction (P_c >100 Pa) will be high in a foam with a liquid fraction of 0.01 and bubble size of 1 mm (Saint-Jalmes, 2006). When bubbles in the foam are very small and films very thin, almost no liquid drainage occurs in the films, in comparison to in the Plateau borders. Film contribution to drainage can not be negligible if the Plateau border surfaces are mobile and films are the thickness of $10^{-2} \cdot L_P$, (where L_P is a typical Plateau border length). However, it is rare that films in high void fraction foams can ever be this thick and the film drainage contribution to the drainage process is really small (Koehler *et al.*, 2004a 2004b; Saint-Jalmes, 2006). What is important about film drainage is that once the films starts to drain, film stability is reduced, therefore coalescence and gas diffusion to neighbouring bubbles can occur (Koehler *et al.*, 2004; Saint-Jalmes, 2006).

For the rigid surfaces, bulk viscosity (η) of the foaming liquid is the dominant factor in the drainage process. However, liquid flow coupling occurs between the flow inside the Plateau borders and at the surface, causing surface shear (Saint-Jalmes, 2006). The cause of shear at the

Plateau border surfaces is produced by the border's triangular shape: the speed of liquid flow at the corners is zero, therefore shear originates at the triangular surface of the Plateau border (Koehler *et al*., 2000; Saint-Jalmes and Langevin, 2002). The liquid flow through the Plateau border channels causes surfactant concentration fluctuations at the channel surface. Liquid flow pushes surfactants downwards, from the channel top to the bottom, and if adsorption time at the Plateau border surface is long, it creates a downward gradient in surfactant concentration. This could happen if the adsorption time of the surfactant is long enough, however in most cases surfactant molecule adsorption time is short (Koehler *et al*., 2000).

The relation between surface shear viscosity (η_s) and bulk viscosity (η) dissipation effects gives a number (*M*), from which two drainage regimes can be determined:

$$M = \frac{\eta r_P}{\eta_s} \tag{2.27}$$

where r_P is the radius of curvature of the Plateau border ($r_P \sim D\varepsilon^{1/2}$, where D is the bubble diameter) (Leonard and Lemlich, 1965; Koehler *et al.*, 2004a, 2004b; Saint-Jalmes, 2006) When $M<1$ the regime is Poiseuille like, if $M>1$ the flow regime is node dominated. So different regimes can be obtained by varying bubble size and foaming liquid origin (Saint-Jalmes, 2006). For the foams made with a constant liquid fraction of either SDS or protein solution it was determined that drainage velocity was proportional to liquid fraction change over time: $v_d \sim \varepsilon^{1/2}$ (for SDS foams) and $v_d \sim \varepsilon$ (for protein foams) respectively (Saint-Jalmes, 2006).

Drainage in the foams is to some extent related to the experimental conditions, such as the size and shape of the container (Saint-Jalmes, 2006). Foam height (*H*) must also be considered taking into account the foam liquid fraction, capillary suction and bubble size distribution. Drainage will start occurring only when the capillary forces are overcome. This results in a time delay where no apparent drainage occurs. It could be the situation that for small

heights of a foam with small bubble size and small liquid fraction, no liquid drains out, as for example *Gillette* foamy (Saint-Jalmes, 2006). Therefore, from real experimental results one can separate free drainage into three stages: first, when no liquid leaks out - liquid hold-up has to build up in order to overcome capillary forces; second: the liquid starts accumulating at the bottom of the foam; third: the drainage reaches steady state (Koehler *et al.*, 2000; Hilgenfeldt *et al.* 2001). During the free drainage stage the liquid fraction varies with aging time within a foam at different heights and it follows the power law:

$$\varepsilon(z) = t^{\psi} \tag{2.28}$$

The exponent ψ depends on the parameter χ_p in equation 2.30 as it defines the characteristic time and length scales. Parameter ψ is the exponent in equation 2.28, which takes into account a number of parameters (geometry elements (L_P), density (ρ), bulk viscosity (η), surface tension (γ), and permeability constant (K_x) that controls the drainage regime type in a foam through the following 2.30 and 2.32 equations:

$$\chi_p = \frac{z}{z_0}\sqrt{\frac{t_0}{t}} \tag{2.29}$$

where z =0, the height at the top of the foam, and t_0 and z_0 are the typical time and length scales given by:

$$t_0 = \frac{C_o \gamma \eta}{2K_x(\rho g)^2 L_P^3} \tag{2.30}$$

$$L_P \sim \frac{D}{3} \tag{2.31}$$

where C_o - constant (C_o = 0.413), γ - surface tension, ρ - density of the foam, L_P - is the Plateau border length, D - the bubble diameter, g - acceleration due to gravity, η - viscosity, K_x – permeability dimensionless constant, which depends on the drainage regime (for rigid

surfaces K_1 is 0.0063 and for mobile surfaces (determined by the geometry of the node wall and the flow field inside the nodes) $K_{1/2}$ is 0.003).

$$z_0 = \frac{C_0 \gamma}{2\rho g L_P} \tag{2.32}$$

For rigid surfaces, which correspond to protein or LMW surfactant foams:

$\varepsilon \sim t^{-2/3}$ for $\chi_P < 1$, $\varepsilon \sim t^{-1}$ for $\chi_P > 1$ (2.33)

For mobile surfaces, which correspond to foams made of SMW surfactant foams:

$\varepsilon \sim t^{-1}$ for $\chi_P < 1$, $\varepsilon \sim t^{-2}$ for $\chi_P > 1$ (2.34)

The liquid drainage model is based on porous media and is using Darcy's law (Saint-Jalmes, 2006). However Darcy's law is restricted, because during drainage the channel cross-section and flow condition changes (Verbist *et al.,* 1996). The flowing liquid velocity *v* is related to the pressure gradient (***G***), which includes gravitational forces and capillarity pressure. Pressure gradient is expressed through permeability (K) and liquid viscosity (η): $\boldsymbol{G} = \eta v_d / K$. Permeability depends on the liquid fraction (ε) because the change of bubble size is related to the liquid fraction. The foam drainage equation is derived from Darcy's law (Saint-Jalmes, 2006):

$$\frac{\partial \varepsilon}{\partial t} + \nabla \cdot (\varepsilon v_d) = 0 \tag{2.35}$$

The variation in the liquid fraction $\varepsilon(r,t)$ in the foam during aging time t is described by this equation (operators act as spatial coordinates) (Koehler *et al*., 2000):

$$\frac{\partial \varepsilon}{\partial t} + \nabla \cdot \left(\frac{\rho_l g}{\eta} \varepsilon K(\varepsilon) \right) - \nabla \cdot \left(\frac{\gamma \sqrt{\delta K}(\varepsilon)}{2 \eta L \sqrt{\varepsilon}} \nabla \varepsilon \right) = 0 \tag{2.36}$$

In the case of a freely draining foam when there is no capillary effect, with the liquid flow only in Plateau borders, the relationship between velocity of the freely draining liquid in the foam and bubble radius can be described by the simple power law relationship (Saint-Jalmes, 2006):

$$v_d = \frac{\rho_l g K_x \mathrm{r}^2}{\eta} \varepsilon^m \tag{2.37}$$

where ε is liquid fraction, K_x is permeability constant, which varies depending on whether the drainage regime is channel dominant or node dominant; m is an exponent, which is 1 if drainage regime is channel dominant and if node dominant, it is 0.5; η is viscosity; r is bubble mean radius; ρ_l is density of the liquid; g is acceleration due to gravity .

Strong capillary forces influence liquid drainage because liquid can flow from the wetter to drier liquid regions. Then the, liquid drainage velocity is given by:

$$v_d = \frac{K_x r_P r^2}{\eta} \left(\rho_l g - \partial z \frac{\gamma}{r_P} \right) \varepsilon^{\chi} \tag{2.38}$$

where γ is surface tension, r_P is curvature of the Plateau border, K_x is permeability dimensionless constant, r is bubble mean radius (Britan *et al.,* 2009). In equation 2.39 $\rho_l g$ represents gravity driven drainage and γ / r_p represents capillary pressure.

2.2.6.2. Disproportionation

Once the foam with high void fraction is made, it faces destabilization from a number of coarsening mechanisms: gas transport between bubbles leads to disproportionation while film rupture can lead to coalescence. The lamella that surrounds the air bubble is exposed to overpressure which depends to interfacial tension and bubble radius (Formula 2.22). This formula, known as the law of Laplace, shows that if interfacial tension is a constant, pressure inside small bubbles is bigger than in an adjacent larger bubble. Due to this fact, gas from small bubbles tends to migrate to bigger ones and so called disproportionation of the bubbles occurs (Gandolfo and Rosano, 1997; Britan *et al.,* 2009). The gas from smaller bubbles diffuses into the larger ones by dissolving into the film liquid and desorbs in the larger bubbles

and that leads to a gradual bubble growth (Weaire and Hutzler, 1999). Gas diffusion rate through the lamella is proportional to the rate of diffusion across a plane:

$$K_v = K \cdot S_f \cdot \Delta P_r \tag{2.39}$$

where K is a gas permeability constant ($m^2 \cdot s \cdot kg^{-1}$), ΔP_r is pressure difference, S_f is film area, K_v is volume rate of gas transfer (m^3/s).

The same gas diffusion process is occurring in bubbly liquids where the bubble lamellae are thick and bubbles are well separated from each other. This process is called Ostwald ripening and is common for bubbly liquids where the gas fraction is low.

It is noticed that in the foam where disproportionation is the dominant aging process, bubble mean radius (r) increase depends on aging time (t) (Weaire and Hutzler, 1999):

$$r \sim (t - t_i)^{1/2} \tag{2.40}$$

where t_i is initial disproportionation time, t is aging time.

In a very dry foams, with very low ε, bubbles disproportionate and coalesce, so that bubble size increases and the foam overall undergoes the so called coarsening process. Coalescence process will be discussed in the next section (2.2.6.3).

The majority of coarsening studies have been done on one layer of foam bubbles (2D studies) and recently experiments were conducted on 3D foams. Based on 2D foam studies, it was determined that the hexagonal bubble, with six sides (n=6) remains stable, but when n<6, the bubble shrinks and if n>6 – the bubble expands. This is the principle of von Neumann's law. From experimental analysis and simulations it was determined that the bubble size scales as $t^{1/2}$, while the bubble area and number increases as t and t^{-1} (Jurine *et al.*, 2005). The results on 3D foams from multiple light scattering experiments show the same scaling law for 2D foams: the bubble radius is proportional to the time scale $t^{1/2}$ (Durian *et al*., 1991b).

Scaling of the 2D and 3D foam is not the same. 2D foam has been studied since Plateau's first experiments and scaling of the coarsening foam obeys von Neumann's law, which was discussed previously. Fewer experiments have been done on 3D foams because of the opaque nature of foam and studying by using light is challenging because of strong multiple light scattering (Durian *et al.*, 1991a). Therefore direct observations, as is feasible for 2D foams, are not possible for 3D foams. 3D foam imaging requires application of light transport theory, which implies that because of strong multiple scattering, light waves travel in the foam through a diffusion process (Durian *et al*., 1991a).

From light scattering experiments done on coarsening of polydispersed Gillette 3D foams, it was determined that after 20 min of aging, the mean bubble radius (initial r=15μm), scales with aging time as $t^{0.45}$ (Durian *et al*., 1991b). Coarsening mainly occurs in very dry foams while wet foams do not coarsen or coarsening occurs at longer aging times. Studies done on wet monodispersed foams show that once the bubble radius increases 10% beyond its initial size, 3D foam bubble size scaling is proportional to $t^{1/3}$ (Ganan-Calvo *et al.*, 2004; Marquez *et al*., 2004; Barik and Roy, 2009). Coarsening in wet foams is more similar to Ostwald ripening since the bubbles in the foam are perfectly spherical.

The coarsening time (t_c), which involves disproportionation and coalescence events can be defined by the relationship (Saint-Jalmes, 2006):

$$t_c = \frac{L_P^2}{2D_{eff}f(\varepsilon)} \tag{2.41}$$

where L_P is the length of Plateau Border, $f(\varepsilon)$ is a function of ε, and D_{eff} is the effective diffusion coefficient which depends on the properties of the gas and foaming liquid, as well as film thickness (Hilgenfeldt *et al*, 2001; Saint-Jalmes, 2006). The effective diffusion coefficient is given by:

$$D_{eff} = \frac{4\delta_a}{3\delta_v\beta_c}\frac{D_f He \gamma v_m}{\delta_f} \quad (2.42)$$

where: γ is surface tension, δ_f is film thickness, δ_a, δ_v is geometrical constants, used to describe Plateau Border section and node shape, v_m is ideal gas molar volume, D_f is gas diffusivity through the films, *He* is Henry's constant or solubility of the gas, β_c is constant (for dry foams ~10) (Saint-Jalmes, 2006). High solubility and diffusivity of the gases that are used to make foams accelerates the coarsening effect. But gases with low solubility can be used, for example C_2F_6 is much less soluble than CO_2 (Hilgenfeldt *et al.*, 2001). It is hard to determine the form of $f(\varepsilon)$ in Formula 2.41. Vera and Durian (2002) for a reliable set of experimental data proposed the scaling of $f(\varepsilon) \sim 1/\varepsilon^{1/2}$, while based on the same void fraction dry foam geometry $f(\varepsilon) = 1 - \sqrt{\varepsilon/\varepsilon_c}$ (ε_c=0.36) (Hutzler and Weaire, 1999) and Saint-Jalmes (2006) reports for monodispersed foams $f(\varepsilon)$ being equal to $\left(1 - \sqrt{\varepsilon/0.44}\right)^2$. Hilgenfeldt *et al.* (2001) have established a better description of the experimental results with the following approximation for ε:

$$\varepsilon(z) = \frac{\varepsilon_c}{\left(1 - \frac{\rho_l g L_P \sqrt{\varepsilon} z}{\sqrt{\delta_\varepsilon}\gamma}\right)^2} \quad (2.43)$$

where ε_c = 0.36, the liquid fraction for randomly packed bubbles; δ_ε is geometrical constant ($\delta_\varepsilon \approx 0.171$); L_P is the length of Plateau Border, z is measurement location in the foam.

2.2.6.3 Coalescence

The coalescence event occurs as a bubble lamella thins so much due to gravitational drainage that it immediately breaks down between two neighbouring bubbles (Monin *et al.*, 2000; Carrier and Colin, 2003; Saint–Jalmes, 2006). The second bubble size distribution peak is usually smaller and is shifted to larger bubble sizes. Coalescence is common not only in foams

but in emulsions as well (Weaire and Hutzler, 1999). Studying coalescence as a single foam destruction event requires carefully choosing a perfluorohexane saturated nitrogen gas mixture, whose diffusivity would be negligible and Ostwald ripening would be eliminated (Carrier and Colin, 2003). The coalescence rate depends on total foam cell area, film area and film drainage time. It was observed from experiments that coalescence occurs in the foam when the liquid fraction reaches 0.0005 to 0.0007 and it depends on the surfactant nature and its concentration, but not on bubble size (Carrier and Colin, 2003). A model quantifying the rupture rate has been developed from studies on concentrated emulsions and the number of rupture events per unit time is given by (Monin *et al*., 2000):

$$dN/dt = 2\pi r^2 N \omega_p \tag{2.44}$$

where N is the total number of bubbles, r is mean bubble radius, ω_p is probability of rupture event per unit time and unit surface.

2.2.6.4 Ostwald ripening

Ostwald ripening is common in bubbly liquids rather than in foams and the same law of Laplace (Formula 2.26) drives bubble growth. Differently from foams, in bubbly liquids gas bubbles are perfectly spherical and at a distance from each other, so there is no disproportionation or coalescence, but in fact Ostwald ripening is a slow process (Walstra, 2003). De Vries theory considers only two bubbles in a liquid situation (large and small) and estimates how fast gas from the smaller bubble diffuses into the larger bubble causing the smaller one to disappear over time (Walstra, 2003):

$$r^2(t) = \mathrm{r}_i^2 - \frac{R_g T_a D_f H e \gamma}{P_a \delta_f} t \tag{2.45}$$

where r_i is initial bubble mean radius, D_f is gas diffusion coefficient in water, P_a is atmospheric pressure, He is solubility of the gas, R_g is universal gas constant (8.315 J·K-1·mol^{-1}), δ_f is film thickness, T_a is absolute temperature.

2.2.6.5 Bubble size distribution evolution during aging

Changes in bubble size due to gas diffusion leads, as in the disproportionation process, to bubble size growth. Other foam instability mechanisms such as liquid drainage and coalescence impact the bubble size distribution as well. Bubble size distribution changes can also give insight on aging processes that are occurring in the foam. As an example, bimodal bubble size distribution can indicate the coalescence phenomenon in the foam (Lemlich, 1978a; Magrabi *et al*., 1999; Saint–Jalmes, 2006).

First time analysis of the evolving bubble radius in aging foam was approached by Lemlich (1978a). The assumption was made that drainage in the lamellae does not happen and the liquid fraction remains constant in the aging foam and is equal to the initial foam liquid fraction. Modelling of an aging foam of higher liquid content must consider the stronger drainage effects and the reduction of lamellae thickness (Magrabi *et al*., 1999). Saint–Jalmes (2006) presented in his work a detailed analysis of coupling of drainage and bubble coarsening. Film thinning causes shorter time and path for gas to diffuse into a neighbouring bubble, therefore this fact must be considered when modelling foam aging. The overall model is based on the assumption that gas diffusion occurs from the bubble which is smaller than the mean bubble size to the larger one. Gas diffuses first into the liquid of Plateau borders and then it diffuses into the larger bubbles that have a smaller Laplace pressure (Magrabi *et al.*, 1999).

2.3 Techniques

2.3.1 Application of ultrasound to study foam aging processes

2.3.1.1 Wave propagation in different media

A sound or acoustic wave is a pressure wave which propagates through the material as a sequential vibration of atoms or molecules. The velocity at which the wave propagates is determined by the elastic properties of the material, as well as its density. For example, in the case of a fluid, the velocity depends on the compressibility and density, and therefore reveals useful information about the mechanical properties of the medium. As the wave travels through the material, it loses energy due to various attenuation mechanisms, which also probe structural and dynamic mechanical properties. The sound pressure energy is lost because of three phenomena: reflection, scattering and adsorption. The sound wave is partially reflected at the interface of two different media (e.g., air and liquid). As the traveling sound wave strikes an inclusion in the medium (e.g., a bubble), the wave is scattered in all directions and, depending on the number of scatterers, the wave can travel in multiple trajectories. Absorption of the sound wave occurs via several dissipative mechanisms, such as viscous losses and thermal damping, with the result that mechanical wave energy is converted into heat (Leighton 1996, Povey, 1997).

Producing a sound requires doing mechanical work, such as blowing in a flute in the case of musical instruments or generating vibrational displacements in a piezoelectric transducer in the case of ultrasound instrumentation. Therefore sound propagation results in the transmission of mechanical energy through media, where sound energy losses depend on the elastic and viscous properties of the media. Ultrasound can be generated and detected using the same transducer which generates a sound wave by converting an applied voltage into a mechanical displacement of the transducer element, and detects a sound wave by working in reverse. If the received sound

energy is very low, it is necessary to use an amplifier, a device that increases the electrical signal detected by the receiving transducer. An important feature to mention about transducers is that they are usually working in a limited range of frequencies (Leighton, 1996).

Ultrasonic waves are very much similar to sound waves. An ultrasonic wave can be described as a wave traveling through a medium at a frequency higher than 20 kHz (Leighton, 1996). In ultrasonic spectroscopy measurements usually two types of waves are used: longitudinal and shear waves. A longitudinal wave is a wave in which the movement of particles is in the same direction as the wave travels. Applying a compression force perpendicular to the surface generates the particle motion. If the force is applied parallel to the surface, shear waves will be generated and particles will be displaced perpendicularly to the direction of the wave propagation. The velocity of these traveling waves is proportional to frequency (f) and wavelength (λ):

$$v_p = f\lambda = \omega/k \tag{2.46}$$

where angular frequency is $\omega = 2\pi f$; k - the wave number.

Another type of wave, called a Rayleigh wave, travels across the material surface. As an example, natural Rayleigh waves are produced during earth-quakes. In this case, the wave involves elliptically moving particles in the material. Plate or Lamb wave particle movement is also complex, and these waves can only penetrate into the solid material approximately less than a wavelength (Leighton, 1996).

2.3.1.2 Principles of measurements

2.3.1.2.1 Transmission (Low frequency)

A typical ultrasound transmission experimental set-up consists of a pulse generator, two ultrasonic transducers and an oscilloscope (for example, see Povey, 1997). Two

transducers are attached to the parallel sides of the sample. The pulse generator produces an electrical pulse, and the transducer converts the electrical pulse to an ultrasonic pulse. This initial pulse has its own frequency spectrum and amplitude and velocity of traveling wave that can be described by equation 2.48. The ultrasonic wave travels through the sample and is detected with a second transducer. The second transducer acts as a receiver and converts the ultrasonic wave to an electrical signal, which is displayed on the oscilloscope. The pulse created by the transducer is active for a finite period of time, usually called the pulse width. The pulse travels through the sample with a characteristic velocity, which is called the group velocity (v_g). This velocity (v_g) is equal to the distance (L) divided by the time (t) that the pulse travels ($v_g = L/t$), where the time is usually measured at the peak of the pulse. The pulse contains several sinusoidal oscillations. As for any sinusoidal wave, one cycle is accomplished when a moving particle in the sine wave reaches its initial spatial position. At a given frequency, the oscillations travel at a different velocity, called the phase velocity.

2.3.1.2.1.1 Velocity measurements

The traveling sound wave velocity in a material depends on the type of wave, material density and the elastic properties of the material through which the wave propagates (Povey, 1997). As the pulse is comprised of many different frequencies, its shape will change if each frequency component travels at a different phase velocity. However, if all the sinusoidal waves travel in the medium with the same phase velocity no matter which frequency they are, this medium is called non-dispersive and the pulse shape remains the same. The phase velocity (v_p) of a wave is defined as the rate which the phase of a given frequency component of the wave propagates:

$$v_p = \frac{\omega}{k} \tag{2.47}$$

where ω is the angular frequency ($\omega = 2\pi f$), $k = 2\pi/\lambda$, k is the wave number.

A different type of velocity is known as the group velocity. A sound wave is usually produced by sending a finite pulse, with a number of wave cycles. In dispersive media, the different frequency waves that make up the pulse will travel at their own velocities, which are frequency dependent. The summation of slower and faster traveling waves results in a pulse that travels at a single velocity, called the group velocity, which is different to that of the individual wave components. The group velocity (v_g) depends on the rate of change of frequency with wave vector, and is given by (Leighton, 1996; Page *et al*., 1997; Povey, 1997).

$$v_g = d\omega/dk \tag{2.48}$$

where k is the wave number, ω is radial frequency. Technically, in ultrasonic measurements broad-band transducers and wave generators are used, so that the recorded signal is comprised of many sinusoidal waves with different frequencies; from the measured pulse, it is possible also to extract the phase velocity at a specific frequency using Fourier analysis (section 2.3.1.2.1.3).

Sound measurements in highly attenuating media are a complicated task, because phase velocity and attenuation depend on each other. The phase velocity and attenuation are related to the real (k') and imaginary (k'') parts of the wave vector k:

$$k = k' + ik'' \tag{2.49}$$

$$k' = \frac{\omega}{v_p} \tag{2.50}$$

$$k'' = \alpha / 2 \tag{2.51}$$

where α is the attenuation coefficient (Neper m^{-1}); v_p is the phase velocity. As long as $\alpha << k'$, attenuation effects on sound propagation are minimal.

The velocity of a longitudinal wave traveling in homogenous liquids or gases depends on two important material properties. In this case, velocity is proportional to adiabatic compressibility (χ) and density (ρ) because there is no heat transfer or loss to surroundings:

$$v_p^2 = 1/\chi\rho \tag{2.52}$$

In solid materials with viscoelastic properties such as dough, yogurt and pastes, the longitudinal phase velocity of ultrasound waves is dependent on additional material properties (Povey, 1997). In this case, the longitudinal modulus (β) depends on both the compressibility and the shear modulus, as well as the material density:

$$v_p = \sqrt{\frac{\beta}{\rho}} \tag{2.53}$$

$$\beta = \chi^{-1} + 4G/3 \tag{2.54}$$

where ρ - material density, β - longitudinal modulus for a material exhibiting elastic properties, χ - the adiabatic compressibility and G - the shear modulus (Elmehdi *et al*., 2003; Povey, 1997). This equation is valid for materials with a low sound attenuation, where the imaginary part of the longitudinal modulus is negligible compared with the real part.

2.3.1.2.1.2 Attenuation coefficient

The attenuation coefficient represents the amount of lost energy per unit distance traveled, as measured from the change in signal amplitude between the incident and transmitted signals (Samari, 1994). For a longitudinal ultrasonic ballistic pulse, which travels coherently through a medium of thickness (L) in the forward direction without scattering, the change in signal amplitude is related to the attenuation coefficient (α) as (Elmehdi *et al*., 2003):

$$A = A_0 e^{-\alpha\frac{L}{2}} \tag{2.55}$$

where A is the signal amplitude, A_0 is the signal amplitude at the leading edge of the sample; L is the sample thickness. Here α is the intensity attenuation coefficient, which is twice the amplitude attenuation coefficient. Therefore signal amplitude reduction is exponentially dependent on material thickness. Most materials and food products attenuate sound, while scattering objects, especially air bubbles and inclusions, make sound scatter out of the forward direction, thereby reducing the wave energy that is transported ballistically through the sample.

Attenuation of the signal arises from two mechanisms: absorption (or dissipation) and scattering. Energy loss of the traveling sound wave due to absorption occurs because mechanical energy is converted into heat as the wave travels through viscous media. As well, heat flow occurs in the material between contractions and rarefactions of the sound wave; therefore energy is lost due to this thermal mechanism unless the conditions are strictly adiabatic or isothermal (Leighton, 1996).

In non-homogenous materials, sound wave energy is lost from the direct beam due to scattering from discontinuities of the material. Also, there can be enhanced viscous losses at the interfaces between the inclusions and the matrix material in which they are embedded. Usually, the higher the sound wave frequency, the higher the wave energy losses due to scattering; therefore, waves are more attenuated at higher frequencies and this mechanism shows a strong frequency dependence (Leighton, 1996).

2.3.1.2.1.3 Signal analysis: Fast Fourier transform

Fast Fourier transform (FFT) is a mathematical algorithm and is an important step in ultrasound waveform analysis that leads to extraction of information on phase and amplitude magnitude changes as a function of frequency. In other words, FFT transforms a function which is in the time domain (i.e., an ultrasonic signal waveform) into a function which is in the

frequency domain. Fourier analysis depends on the property of a time varying physical variable ξ_F, which can be expressed as the sum of cosine and sine, or complex exponential, functions of frequency (Povey, 1997). As sine and cosine of appropriate equally spaced frequencies are multiplied by a physical variable ξ_{Fn} and then added together, the original signal waveform is reconstructed:

$$\xi_F(t) = \sum_{n=1}^{\infty} \xi_{Fn}(\omega) \exp(i\omega_n t) \quad (2.56)$$

Equation (2.56) is a discrete approximation to an exact Fourier transform, which is obtained by replacing the sum in (2.56) by an integral. (The FFT is used because the digitized ultrasonic signals are recorded at discrete times, and so the frequencies are discrete, not continuous, variables as well.) A plot of Fourier coefficients $\xi_{Fn}(\omega)$ against frequency is called the Fourier transform of ξ_{Fn} and it allows us to express these coefficients as amplitude and phase as a function of frequency (Povey, 1997).

2.3.1.2.2 Reflection technique

Sound waves can be partially reflected from the interface of two different media, which are distinguished by having different physical properties, and therefore different acoustic impedances, as described in detail in section 2.3.1.2.2.1 (Leighton, 1996). The remaining sound energy is transmitted through the boundary into the second medium and both amplitude and phase of the transmitted and reflected waveform are changed (Fan, 2007). The reflection technique is implemented by using a pulse-echo reflectometer and is a very useful technique in obtaining information on sizes of particles, droplets and bubbles in materials (Povey, 1997).

2.3.1.2.2.1 Acoustic impedance measurements

Acoustic impedance can be described as an acoustic excess pressure relative to the particle velocity (Leighton, 1996). Acoustic impedance is given by:

$$Z = \Delta p/\xi' = \rho\omega/k \approx \rho v_p \qquad (2.57)$$

where Δp is acoustic excess pressure, ξ' is particle velocity, ρ - density, and v_p - wave velocity.

In the reflectance technique, the same transducer is used as a transmitter and as a receiver. In ultrasonic reflectance measurements a transducer is often attached to a plastic rod or plastic cell, whose acoustic impedance is well known (McClements and Fairley, 1991). When the signal is sent from the transducer, it travels through the rod to reach the sample (foam in my case) and is partially reflected. The wave pulse reflected from the foam sample can be characterized by a reflection coefficient (R_f) given by (Leroy *et al*., 2010):

$$R_f = \mathrm{r_f}\left(1 - \frac{t_f^2 exp\ (2ikL)}{1-\mathrm{r}_f^2 exp\ (2ikL)}\right) \qquad (2.58)$$

where L is the sample thickness, and r_f, and t_f are functions of impedance:

$$\mathrm{r}_f = \frac{Z-Z_0}{Z+Z_0} \qquad (2.59)$$

$$t_f^2 = \frac{4ZZ_0}{(Z+Z_0)^2} \qquad (2.60)$$

where Z_0 is the impedance of the plastic and is known, Z is impedance of the sample. In most cases t_f^2 can be neglected if the sample is thick enough and there are no multiple reflections; then $R_f = r_f$. The reflection coefficient (R_f) is defined as the ratio of reflected wave amplitude and incident wave amplitude, and depends on the impedance of the two materials (Equation 2.59) (Leroy *et al*., 2010).

If we measure the reflected signal from the plastic rod and air boundary, and the signal is fully reflected, the reflection coefficient (R_f) can be considered as $R_f = -1$. On the other hand, if the signal is fully transmitted and then absorbed, no signal is reflected, $R_f = 0$. In the intermediate case, the signal is partially reflected, enabling an unknown material's acoustic impedance to be determined.

The procedure for performing a reflectance experiment is as follows. The reference signal is obtained by measuring the signal reflecting from air or from water, whose acoustical impedance is known: $Z = \rho v$, ρ is density of air or water, v is velocity in air or water. When reflection from air is used to obtain the reference signal, the procedure is especially simple, since $R_f = -1$; in the subsequent discussion, I will consider only consider the analysis of data for this case. Afterwards the reflected signal from the sample is measured. From the recorded waveforms of the reflected signal, phase and amplitude can be extracted by an FFT technique using Formula 2.56. The ratio of reference pressure wave amplitude (P_r) and sample pressure wave amplitude (P_s) obtained from the FFT gives x:

$$x = \frac{FFT(P_s)}{FFT(P_r)} = -\frac{Z - Z_0}{Z + Z_0} \ , \tag{2.61}$$

from which the impedance of the sample of interest (Z) can be calculated:

$$Z = Z_0 \frac{1 - x}{1 + x} \tag{2.62}$$

From reflection measurements a transmission coefficient T can also be calculated, which is described as the ratio of transmitted wave and incidence wave amplitudes:

$$T = \frac{2Z}{Z + Z_0} \tag{2.63}$$

In general, the impedance of the material equals $Z = \rho v$ only when attenuation is small. If attenuation is big, acoustic impedance is a function of both the phase velocity and the attenuation. It is expressed through a complex expression:

$$Z = \frac{\rho v}{1 + i\frac{v\alpha}{2\omega}} \tag{2.64}$$

Equation (2.64) can be solved for the attenuation coefficient and phase velocity in terms of the real and imaginary parts of *Z*, yielding relationships 2.66 and 2.65 respectively:

$$v_p = \frac{1}{\rho \Re e\frac{1}{Z}} \tag{2.65}$$

$$\alpha = 2\omega\rho \times \Im m\left(\frac{1}{Z}\right) \tag{2.66}$$

2.3.1.3 Ultrasonic studies on low void fraction bubbly media

Ultrasound is used to investigate food properties such as concentration of solutions, emulsion droplet size, meat composition, gelation phenomena, lipid crystallinity and the size and concentration of air bubbles in very dilute systems (Saggin and Coupland, 2001; Cents *et al*., 2004; Wilson, 2005; Cobus *et al.,* 2007). Extensive studies have also been performed with ultrasonic techniques on bread dough (Elmehdi, 2001; Bellido, 2007; Fan, 2007). Using ultrasonic spectroscopy, the composition of aerated foods containing low concentrations of bubbles may be investigated and information on the bubble size distribution and concentration can be obtained (Silberman, 1957; Povey, 1997; Strybulevych *et al*., 2007).

Ultrasonic acoustic spectroscopy methods were thought by some to not be suitable for the analysis of aerated materials containing more than a very small amount of bubbles (>0.1%) because the signal is highly attenuated and it cannot be propagated far enough through the

sample to be detected (Kulmyrzaev *et al*., 2001). However, studies have shown that information about bubble characteristics in concentrated systems can be obtained if an ultrasonic wave is reflected from the surface of the sample, rather than transmitted through it (Fairley *et al*., 1991). Successful experiments have also been performed in transmission provided that the sample is thin enough (Elmehdi, 2001; Fan, 2007; Bellido, 2007).

Small amounts of air inclusions (bubbles) in water dramatically decrease sound wave propagation velocity at low frequencies; for example, 1% air in water decreases the sound velocity to approximately 120 m/s, and 53% of air in water decreases sound velocity to 22 m/s, in comparison to pure water where the velocity is 1500 m/s (Povey, 1997). Another phenomenon that greatly impacts sound wave propagation velocity in bubbly media is the resonance phenomenon, which was first studied by Minnaert in 1933 (e.g., see Povey, 1997). The resonance frequency of the bubble in water is now called the Minnaert frequency ω_M :

$$\omega_M = \sqrt{\frac{3\,\Upsilon P_a}{\rho r^2}} \tag{2.67}$$

where Υ - the ratio of the heat capacities of the gas in the bubble, P_a – atmospheric pressure, ρ - density of water (liquid), r - bubble mean radius. The effect of resonance on the phase velocity and attenuation has been observed experimentally in both monodisperse and polydisperse bubbly liquids and gels, which show large peaks in both quantities as a function of frequency (Leroy 2008, and references therein). As the size distribution is widened, making it more polydisperse, the resonance peaks become less sharp (Leighton, 1996).

Recent measurements of phase velocity and attenuation in bubbly gel samples (φ = 0.015-0.05) were carried out by Leroy *et al*. (2008). To explain the phase velocity and attenuation results close to bubble resonance, Leroy *et al*. (2008) used Foldy's original model

(Foldy, 1945), extended to include absorption as well as scattering (Prosperetti, 1977) and Foldy's model corrected by Henyey's approach (Henyey, 1999). Foldy's model is named after the scientist Leslie Foldy, who published a paper on multiple scattering of waves by randomly distributed collection of scatterers in 1945. Foldy's theory can be used to explain the phase velocity and attenuation results close to bubble resonance frequency for low void fraction bubbly media (Fan, 2007; Leroy *et al*., 2008). Foldy's theory takes the approach that the scattering from the bubbles can be treated independently, so that the effect of *n* bubbles is simply *n* times the effect of a single bubble; thus, the bubbles in the liquid are assumed not to interact with each other: the bubbles in the liquid are considered as individual, single cases. Once the frequency of the propagating waves approaches the Minnaert frequency, the bubble starts to resonate and large changes in the velocity and attenuation are predicted. Henyey (1999) attempted to correct Foldy's model by including the average effect of neighbouring bubbles on the scattering contribution to the attenuation and velocity; this correction was achieved by replacing the water medium around each bubble by the average effective medium. Good overall agreement between measured results and predictions of both Foldy's model and Foldy's model corrected by Henyey's approach were found for nearly monodisperse bubble size distributions (φ = 0.015) close to the resonance frequency (Leroy *et al*., 2008). In measurements of bubble gel samples (φ = 0.15) near the low frequency of 50 kHz, which was close to the resonance frequency, a significant change in phase velocity and attenuation magnitudes was found, meaning that the medium was dispersive. At higher frequencies, above the bubble resonance frequency (100-200 kHz), high attenuation was measured in the same sample, which agreed with Foldy's and Henyey's models. However, for the same 50 kHz frequencies, a discrepancy for phase velocity results and the model predictions exists, and this was not easy to explain (Leroy *et al*., 2008).

Nonetheless, Leroy *et al*, (2008) concluded that the Foldy model gives an "imperfect but satisfactory" description of the phase velocity and attenuation for bubble concentrations up to 1%.

Another important result obtained from ultrasonic measurements in monodisperse and polydisperse samples of 0.01 void fraction is that there is a clear difference in phase velocity and attenuation results for those two samples (Leroy *et al*., 2008). Measurements of phase velocity and attenuation are more complicated in gel samples of higher void fraction (φ = 0.05), due to higher order multiple scattering effects.

2.3.1.4 Ultrasonic studies on high void fraction-foams

As was mentioned earlier, sound waves in high void fraction foams are highly attenuated and the mechanism responsible for it is multiple scattering and dissipation of sound waves as they interact with the surfaces of different sized air bubbles. Very few studies have been done on real foams where the void fraction is higher than 0.50.

A study on heat transfer effects on sound propagation in high void fraction 0.95-0.99 foams and ready-made foams (*Gillette*) was presented by Goldfarb *et al*. (1992). In these studies an attempt was made to clarify the high attenuation mechanisms (thermal and viscous) that are dominant in the foams, taking into account the high void fraction foam structure elements: Plateau borders and channels. Measurement results at 5 kHz frequency can be described by the sound wave propagation model suggested by Goldfarb *et al.* (1992). The model suggests that as an acoustic wave travels through the foam with small bubbles, the pressure wave induces liquid flow in the foam Plateau borders and the sound energy is absorbed through this liquid flow. In the case of foam with large bubbles, thermal dissipation is the dominant attenuation mechanism.

Goldfarb *et al.* (1992) determined that the velocity in the foam is inversely proportional to the square root of the moisture content. However, the measured adiabatic velocity was 10-15% above the theoretical values. As an example, foam (φ = 0.95) with a bubble size of 0.44 mm had a measured velocity of 72 m/s, whereas the model predicted: 53 m/s. Results obtained from Gillette foam (φ = 0.95) measurements were 51 m/s, and the prediction gave 46.5 m/s. The discrepancy between measured results was attributed by Goldfarb *et al.* (1992) to insufficient foam structure details being incorporated into the physical model. The drier the foam, the less liquid moves through the Plateau Borders. As well, it was suggested that the less liquid there is in the structure, the less heat is transferred (less thermal dissipation) and thus the velocity would increase.

Mujica and Fauve (2002) studied a high void fraction *Gillette* foam as well. Their measured and predicted velocity values were also at odds: at 5 kHz frequency the measured initial velocity of the Gillette foam (ρ = 0.076) was 65 m/s and the calculated Woods effective sound velocity was v_W = 40 m/s. Mujica and Fauve (2002) examined sound wave propagation effects arising from aging of high void fraction *Gillette* foam. Since Gillette foams have essentially no drainage effects, characterization of bubble disproportionation phenomena in the foam was the primary goal. In their study both ultrasonic attenuation and phase velocity were measured at several frequencies: 5 kHz, 37 kHz, 63 kHz and 84 kHz. A simple scaling argument based on the Foldy-Prosperetti model, as well as Biot theory, were used in explaining the results. Biot theory models wave propagation in a porous medium having two continuous phases (fluid and solid). In their paper, Mujica and Fauve (2002) argued that viscous coupling between the gas and liquid in a foam ensures no relative displacement of the fluid and solid components,

allowing the Biot model to be applied despite the difference between the closed cell structure of a foam and the open cell assumption of the theory.

Phase velocity results showed a decrease from 65 m/s to 50 m/s (Mujica and Fauve, 2002) during four hours of aging, which is a reflection that Gillette foam softens as disproportionation occurs. Mujica and Fauve (2002) were able to explain these observations using their implementation of Biot theory, obtaining reasonable agreement with their experimental results In addition, a disproportionation effect on attenuation was evident, which was attributed the dependence of thermal losses on bubble size. It was determined that the ultrasonic parameter $\alpha\lambda/f$ obtained from measurements scaled linearly with time. From imaging measurements the mean bubble radius $\langle r \rangle$ for aging *Gillette* foam shows: $\langle r \rangle^2 \propto t$. Therefore the conclusion was made that $\alpha\lambda/f$ is proportional to $\langle r \rangle^2$: $\alpha\lambda/f \sim \langle r \rangle^2$. After a thorough analysis of dissipation effects it was determined that thermal effects are the dominant contribution in sound attenuation (Mujica and Fauve, 2002), supporting the observed scaling behaviour.

An interesting ultrasound study was done by Magrabi *et al.* (2001) on foam drainage effects. Low frequency sound waves of 3.4 kHz were used to follow liquid drainage in a tall (0.20 m) column filled with foam (φ = 0.95) made from generic aqueous-film-forming fire-fighting foam concentrate by using compressed air. The hydrophone and speaker were actually immersed in the foam and the sound velocity (v) was related to the liquid content (ε = 1 - φ) through the relation:

$$v = \sqrt{\frac{\Upsilon P_a}{\rho}\left(\frac{1}{\varepsilon(1-\varepsilon)}\right)} \tag{2.68}$$

where Υ is the ratio of the heat capacities at constant pressure and volume (representing the isentropic expansion of an ideal gas) and P_a is atmospheric pressure. The change of liquid

fraction in the foam was successfully determined from this type of ultrasonic experiment. Good agreement was found between liquid content measured with ultrasound and that determined directly by measuring the drained liquid mass.

2.3.2 Electrical measurement techniques

2.3.2.1 Conductance of solutions

Conductivity measurements of foams provide very useful information about stability, surface tension and foam viscosity (Weaire *et al*., 1995). Most of the time, synthetic foams (SDS, *Gillette* foamy) are naturally non-conductive. The solution usually is a surfactant type (ionic or nonionic) and consists of organic compounds that do not have enough ionic groups that can carry the electric charge. Therefore, strong electrolytes like KCl or NaCl are added, as for example, at a concentration of 0.04 M (Datye and Lemlich, 1983). Food foams, such as egg white foams, do not require the addition of salts, because egg white liquid contains enough ions (K^+, Na^+, Fe^{2+}, Mn^{2+}, Cl^-, H^+) for the electrical current to be conducted. In addition, egg proteins possess polar groups that participate in carrying electric charge. In Table 2.2 ion amounts that are present in egg white are given.

Table 2.2 Inorganic elements in egg white (Li-Chan *et al*., 1995)

Inorganic element	Egg White (mg/egg)
Na^+	53
Mg^{2+}	3
P	6
S	64
Cl^-	51
K^+	55
Ca^{2+}	4
Fe^{3+}	0.3
Total	**236.3**

2.3.2.1.1 Ohm's law for electrolytes

Salts, bases or acids in water dissociate into ions (cations and anions) and form electrolyte solutions. Free ions in a water solution once placed in an electrostatic field start moving parallel to the direction of electric field and the electric charge is carried between the two electrodes. As a result, the current passes through the electrolyte solution.

Dissociated ions, even though they may have the same charge, do not have the same ionic mobility and therefore do not equally conduct the current. Ion contribution to electric current depends on the individual ion charges, concentration, and how easily the ion moves in the solution under the influence of an electric field. Once, for example, sodium chloride is placed into a solvent (water), salt components dissociate into sodium and chloride ions due to interaction between solvent and solute molecules:

$$NaCl \rightarrow Na^{+} + Cl^{-} \tag{2.69}$$

The degree of dissociation (α_d) separates electrolytes into strong and weak, where in the case of strong electrolytes $\alpha_d = 1$, and in the case of weak electrolyte α_d is low.

The ability of an electrolyte solution to conduct current is described by conductivity. Electrical conductivity of the solution depends on the viscosity of liquid solution, temperature and the species of ions present. Ions in water solution move chaotically, in any direction. However, once an electric potential is applied, ions move in the direction of the electric field, and current is conducted. Positively charged ions will move in the opposite direction to the negative charged ions. If an alternating current is used, the ion motion is reversed as the applied electric potential (voltage) changes charge from positive to negative. The amount of current I transferred in the solution depends on the electric field strength $\boldsymbol{E}$ and the cross sectional area A_r perpendicular to the crossing current (Figure 2.5).

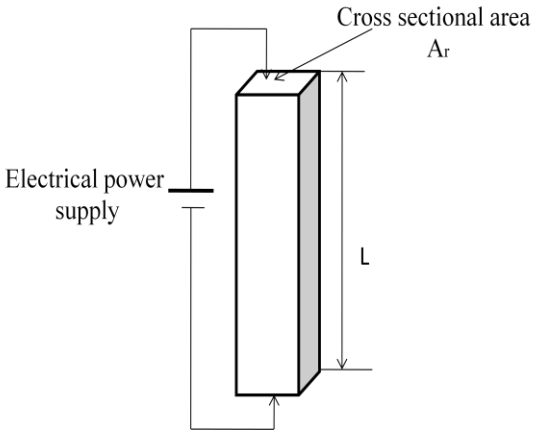

Figure 2.5. The principle diagram of conducting system. (Taken from Mortimer, 2008).

Universal Ohm's law states that flowing electrical current between selected points is proportional to potential difference and inversely proportional to resistance:

$$I = V/R \tag{2.70}$$

where R is the resistance of the conductor, V is potential applied across the conductor, I is the current, proportional to the amount of passed charge through the cross sectional area. Electrical conductance (G_c) is inversely proportional to resistance and measures how easily electrical charge flows along the electrical element (Bleaney and Bleaney, 1976):

$$G_c = 1/R \tag{2.71}$$

The current density, (i) is proportional to current passing through the area (A_r) and Ohms law for the rectangular conductive object (Figure 2.5) can be written (Mortimer, 2008):

$$i = \frac{I}{A_r} = \frac{V}{\mathrm{RA_r}} = \frac{\boldsymbol{E}L}{\rho_\mathrm{r}\mathrm{L}} = \frac{\boldsymbol{E}}{\rho_\mathrm{r}} = \sigma\boldsymbol{E} \tag{2.72}$$

where I is current, L is the length of the conductor, $\boldsymbol{E}$ is electric field strength ($\boldsymbol{E} = V/L$), σ is conductivity, ρ_r is resistivity. Electrical conductivity is a property of a material. Ohm's law for ionic solutions or a conductor that has a shape can be written:

$$R = \frac{L}{\sigma A_\mathrm{r}} \tag{2.73}$$

where: σ – conductivity, L - length, A_r - cross-sectional area. It is convenient in resistivity measurements to determine the cell constant C_c, which is the ratio of length to sample area (Silbey *et al*., 2004; Mortimer, 2008):

$$L/A_r = C_c \tag{2.74}$$

$$\sigma = C_c/R \tag{2.75}$$

Concentration of ions has a major effect on the number and mobility of ions. The mobility of ions u_j is the velocity v_j with which ions move in the solution under the influence of the electric field (Bawendi, 2005; Bagotsky, 2006; Mortimer, 2008):

$$u_j = v_j/\boldsymbol{E} \tag{2.76}$$

The solution conductivity (σ) containing different ions and concentrations will be the sum of all ion contributions in carrying the charge in the electrical field ($\boldsymbol{E}$) direction, where individual ion contribution depends on its charge number (z_j) and electric mobility (u_j). The conductivity of the electrolyte solution can be expressed as the sum of the total current which is the sum of each positive and negative ion moving in the electric field (Bawendi, 2005; Mortimer, 2008):

$$\sigma = F_f \sum_i z_j c_j u_j \tag{2.77}$$

where F_f - Faraday constant, z_j – charge of ions, c_j – concentration of ions, u_j – mobility of ions.

Conductivity, σ (S/cm or 1/(Ωm), is an intrinsic property of a conductive material, which quantitatively characterizes how much current can be transported in the material. Conductivity is the inverse measure of resistivity ($\rho_r = 1/\sigma$) and depends on the temperature, but not on the shape and size of the conductive material.

2.3.2.1.1.1 Liquid content and electrical conductivity relation in foam

The electrical conductivity of a two-phase air and liquid dispersion varies depending on the air content (Datye and Lemlich, 1983; Feitosa *et al*., 2005). Air is a non-conducting medium, so electrical current passes only through the liquid foam phase. In the very wet limit, air bubbles are perfectly spherical, while in the dry limit bubbles are compact, touching each other and are polyhedral in shape. In the first case, the Maxwell expression describes the relationship between liquid content (ε) and relative conductivity of the foam (σ_r):

$$\sigma_{\mathrm{r}} = \frac{\sigma_f}{\sigma_{liq}} = \left(\frac{2\varepsilon}{3-\varepsilon}\right) \tag{2.78}$$

where σ_f is conductivity of the foam and σ_{liq} is the conductivity of the liquid.

The Lemlich equation, on the other hand, describes the very dry foam limit where the liquid remains in Plateau borders (Feitosa *et al*., 2005):

$$\sigma_{\mathrm{r}} = \left(\frac{1}{3}\right)\varepsilon \tag{2.79}$$

On another hand a theoretical case when all the liquid phase remains in the surrounding films of the bubbles was derived by Agnihotri and Lemlich (1981) which relates liquid fraction to conductivity by the relationship:

$$\sigma_{\mathrm{r}} = \frac{\varepsilon}{1.4} \tag{2.80}$$

Lemlich's (1978b) expression assumes that the electric current passes through the network of Plateau borders and neglects the film contribution which is a good approximation in the very dry foam case. As the liquid content in the foam increases, the experimental conductivity starts deviating from relation (2.79) at 0.35 liquid fraction (Phelan *et al*., 1996). At this liquid fraction, the conductivity relation (2.79) based on the idealised Kelvin model (named after Lord Kelvin in 1887, where the idealized foam structure consists of a bytruncated cubic

honeycomb structure that preserves the most efficient foam) is no longer valid, since the assumption of negligible liquid fraction in film faces no longer holds. Phelan *et al*. (1996) showed that it is necessary to make a correction to Formula 2.79 to be applicable in reality. In Phelan's corrected formula, the Plateau border width (δ_P), length (L_P) and the total Plateau border length per unit volume of network (L_v) was taken into consideration:

$$\sigma_r = \frac{1}{3}\frac{L_v c_g \delta_P^2}{\left(1-1.27\frac{\delta_P}{L_P}\right)} \tag{2.81}$$

where $c_g = \left(\sqrt{3} - \frac{\pi}{2}\right)$ – a geometrical constant. The Plateau border cross sectional area (A_p) is:

$$A_p = c_g \delta_P^2 \tag{2.82}$$

Different expressions for the very dry and very wet limit arise from different foam structures. However, these equations do not cover the middle liquid fraction range of the foam. Feitosa *et al*. (2005), after conducting experiments with foams in this middle wetness range, and analysing previous experimental results, derived these relations:

$$\sigma_{\mathrm{r}} = \frac{2\varepsilon(1+12\varepsilon)}{6+29\varepsilon-9\varepsilon^2} \tag{2.83}$$

$$\varepsilon = \frac{3\sigma_{\mathrm{r}}(1+11\sigma_{\mathrm{r}})}{1+25\sigma_{\mathrm{r}}+10\sigma_{\mathrm{r}}} \tag{2.84}$$

Equations (2.83) and (2.84) cover all range of liquid fraction, from 0 to 1 and therefore liquid fraction in the foam can be deduced from the relative conductivity of the foam. However, these relationships (equation 2.83 and 2.84) confirm what was determined previously by Datye *et al.* (1983): foam relative conductivity depends solely on the void fraction but not on the surfactant used or foam bubble size polydispersity. Datye and Lemlich (1983) used non-ionic, ionic and anionic surfactant solutions with addition of KCl to increase foaming solution conductivity. However, Wilde (1996) addressed the fact that if in a foaming solution there are

charged species that are adsorbed at the air bubble, the relative conductivity of the foam is higher as the number of charged species is higher, and the conductivity of the foaming liquid is lower.

2.3.2.1.1.2 Foam structure (tortuosity, bubble size) effect on conductivity

Two foams that have very high and low liquid content will have different structure and therefore the passing current path will be of different length. The ratio of foam (σ_f) and liquid (σ_{liq}) conductivities is equal to the liquid fraction (ε) and tortuosity (ξ) ratio (Yianatos *et al*., 1985):

$$\frac{\sigma_f}{\sigma_{liq}} = \left(\frac{\varepsilon}{\xi}\right) \tag{2.85}$$

In Figure 2.6 two cases are presented that illustrate tortuosity in wet and polyhedral foams, where L_ε is the pathway around the bubbles and L_{el} is the length between two electrodes.

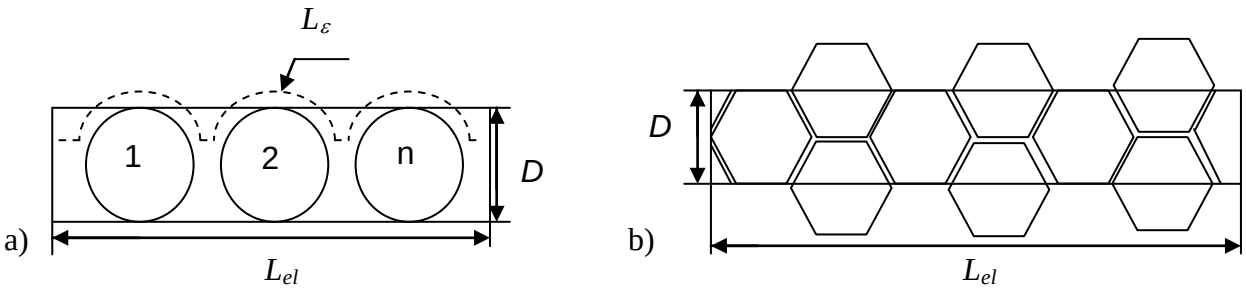

Figure 2.6. Cross section view of wet (a) and polyhedral (b) foams to illustrate tortuosity (Taken from Yianatos *et al*., 1985).

$$\xi = \frac{L_\varepsilon}{L_{el}} \tag{2.86}$$

Where σ_r is relative conductivity, L_ε is effective length between electrodes at liquid fraction ε; L_{el} is the length between two electrodes, cm.

Tortuosity (ξ) in most cases means that $L_\varepsilon > L_{el}$ and so ξ is higher than 1. Initially, the tortuosity model was developed to describe conductivity in porous media and statistical

calculations were done with non-conducting spherical glass beads, which were immersed in conducting liquid. Later a statistical model was applied for foams where non-conducting glass beads represented air bubbles as in the case of foams. Weissberg (1963) gave a simplified conductivity model for beads of the same or similar size, which randomly overlap:

$$\xi = 1 - 0.5\ln(1-\varepsilon) \tag{2.87}$$

Yianatos *et al*. (1985) has taken into consideration the geometrical structure and the expression of tortuosity in bubbly liquids (air fraction range: 0-0.3), where the bubbles are spherical, is:

$$\xi = 1 + 0.55\varepsilon \tag{2.88}$$

In the dry foam case (air fraction range: 0.60-0.95), where bubbles are polyhedral and ions move along the liquid channels, this relation holds for tortuosity (Yianatos *et al*., 1985):

$$\xi = 2.315\varepsilon \tag{2.89}$$

Formulas 2.88 and 2.89 are able to relate liquid conductivity and liquid fraction over a wide liquid fraction range from 0.05 till 1, while Formula 2.87 covers all liquid fraction range. Tortuosity (ξ) for the wet ($\varepsilon \rightarrow 1$) foams becomes infinity, while in most cases (with the more reliable test region where air fractions are 0.60-0.95, because tortuosity value calculations when $\varepsilon < 0.60$ is very sensitive to errors in gas fraction measurements) $L_\varepsilon > L_{el}$ (Formula 2.86) and ξ is higher than 1 (Achwal and Stepanek, 1975).

Datye and Lemlich (1983) conducted experiments showing that surfactant type and concentration had very little effect on the relative conductivity of the foam, and liquid composition out of the drained liquid foam was equal to the initial foaming liquid composition. They used cationic, anionic and non-ionic surfactant types, with KCl addition, to increase conductivity. The same researchers determined for two monodispersed very dry (ε = 0.005-0.05)

foams where void fraction was constant and bubble size for one foam was 3.13 mm and for the second 1.63 mm, that the conductivity of the two foams was different. This effect was not due to measurement errors, but as suggested, due to surface tension and the triangular curvature of the Plateau border. This means that by increasing bubble radius (r), the curvature of Plateau border decreases and the pressure (ΔP_r) in the triangular shape of the Plateau borders increases, and this causes higher liquid suction from the lamellae. As a result, the overall conductivity increases due to increased liquid and as well electric charge carrying ion flow in the Plateau borders (Datye and Lemlich, 1983). The overall effect on the monodispersed foam with smaller bubble size is that for a constant liquid fraction (ε) the relative conductivity (σ_r) is 8% lower than for the foam with larger bubbles (Datye and Lemlich, 1983).

2.3.2.1.1.3 Foam dynamic property measurements by using electrical conductivity

Electrical conductivity is applied widely for measuring foam instability. Foams made of liquid continuous phase are rarely stable: with time, the foam undergoes gravity driven liquid drainage and disproportionation (Weaire and Hutzler, 1999). Conductivity measurement is based on the main fact that foam relative conductivity (σ_r) linearly proportional to liquid fraction (ε) in the foam and linearity remains till $\varepsilon \sim 0.35$, as from this liquid fraction bubble size distribution in the foam changes to a more compact foam structure (Phelan *et al*., 1996). Free drainage is harder to analyze than forced (Saint-Jalmes and Langevin, 2002).

Foam conductivity measurements, depending on the design and amount of the foam can give information on differences in the interfacial characteristics of foaming liquids (surfactant, protein), as for example in the microconductivity case (Wright and Hemmant, 1987). A microconductivity apparatus is displayed in Figure 2.7. The distinct feature of microconductivity

measurements is small sample size (2 mL of foaming liquid) and the volume doubles up to 4.2 mL as the foam is made (Wright and Hemmant, 1987; Wilde, 1996).

Another design for electrical conductivity measurements is displayed in Figure 2.8. In this design the foam is produced by blowing the gas (Nitrogen) through the liquid. Nitrogen is less soluble than air and coarsening in the foam is slower. The big height of the column is necessary to initiate enough liquid drainage in the foam. The column itself can be a cylinder or rectangular shape, and the platinum electrodes will be attached to the walls of the columns. In the design of Barigou *et al*. (2001), steel rings served as the outer electrode and the inner rod as another. The electrode size, distance between them and positioning in the measurement vessel have a big impact on result accuracy. If the vessel and electrode shape are different, the electric field lines and the field strength are not uniform. This is especially a problem if the electrodes are thin because the electric field lines are denser at the electrode vicinity. As well the electrode width has to be bigger than the foam bubble size.

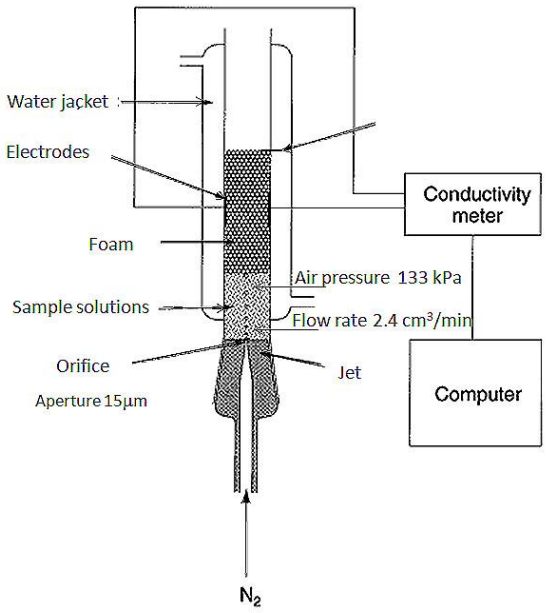

Figure 2.7. Foam microconductivity measurement apparatus. Taken from Wilde (1996).

In the case of using a hydrophilic (such as glass) measurement container, and depending on the apparatus design, the draining foam may form a liquid layer on the measurement container walls, and therefore measured resistance values will be lower. This potentially may happen when measuring the conductivity of very dry foam, when liquid fraction is 0.1 (Karapantsios and Papara, 2008). Barigou *et al*. (2001) proposed a different electrical principle for measurement of the foam, where the inner rod serves as one electrode and outer rings serve as a second electrode. This measurement design measures current flow through the foam only and restricts current flow through the formed liquid layer on the cell walls.

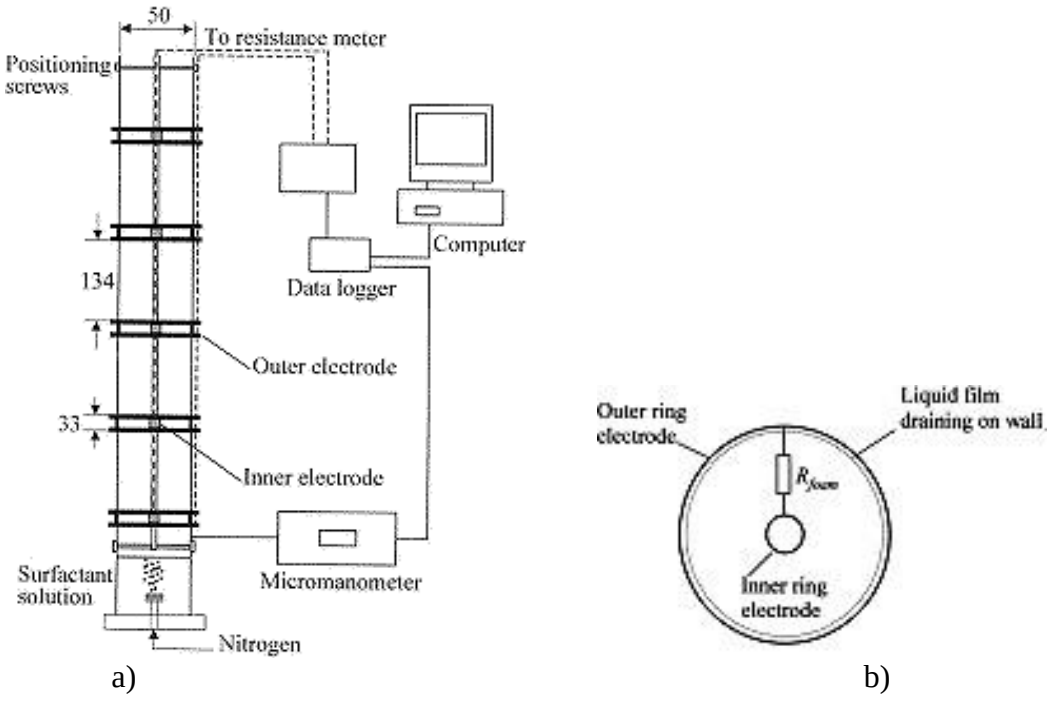

Figure 2.8 a) Electrical resistance technique developed by Barigou *et al*. (2001) to measure foam drainage. The column has 5 electrodes and is made of Perspex glass. Dimensions are given in mm. b) Electrode configuration.

An important parameter in electrical measurements of the foam is the excitation current amplitude and frequency, because depending on the chemical nature of the electrode, the active surface of the electrode may change and that will give spurious results. This effect is pronounced

when using electrodes of small dimension and the bubbles coalesce at the surface of the electrode; therefore this changes the electrode active surface. Electrode active surface refers to the area where the liquid foam films actually touch the electrode surface; therefore only through this contact will electric current pass. The chosen frequency needs to be high enough to reduce electrode polarization effect and as well minimize the capacitive property of the foam. Barigou *et al.* (2001) in their set up used 1 kHz alternating frequency. A lot of criticism has been expressed on the use of frequencies lower than 1 kHz because it is not possible at these frequencies to eliminate capacitive impedance fully from electrical resistivity measurements with stainless steel electrodes (Karapantsios and Papara, 2008). For stainless steel electrodes, in order to measure resistance of the foam and avoid capacitive effects, one should use 10-100 kHz frequency for water type foam systems (Karapantsios and Papara, 2008).

An important detail to mention in electrical foam measurements is electrode cross talk when electrodes are placed parallel to each other, even though they are electrically isolated. A good solution for this problem is to use a multiplexer. A multiplexer works by taking the reading of one ring and switching to the next one. Switching between the rings occurs in 1 millisecond, so it can be considered as almost simultaneous data reading of all rings. Alternatively, not using the multiplexer, the electrodes have to be separated far apart from each other and the voltage has to be applied separately. As well, the data has to be recorded using isolated channels on the data-logger (Barigou *et al*., 2001; Karapantsios and Papara, 2008).

Before performing electrical conductivity measurements the measurement container is calibrated to find the container or cell constant C_c (Formula 2.75). Barigou *et al.* (2001) used a γ-ray absorption technique to calibrate the liquid hold-up in the foam. The principle of calibration is based on the fact that γ-ray absorption in the foam depends on the proportion of liquid and air

in the system. In liquids γ-rays are attenuated more than in gas. A simpler way of obtaining the calibration constant is by measuring known concentrations of strong electrolyte (NaCl, KCl) solutions (Cheng and Lemlich, 1983). A different way of calibrating the device is by using precision resistors. From the calibration curve obtained based on precision resistors, the measured signal is converted into equivalent conductivity (Karapantsios and Papara, 2008).

2.3.2.1.2 Non-conducting foam property assessment by using capacitance measurements

First of all, the choice of using a capacitance technique is influenced by the electrical properties of the foam. Hutzler *et al.* (1995) have shown in their work on capacitance measurement techniques, that liquid drainage can be evaluated in non-conducting foams without the need for adding electrolytes to the foaming solution.

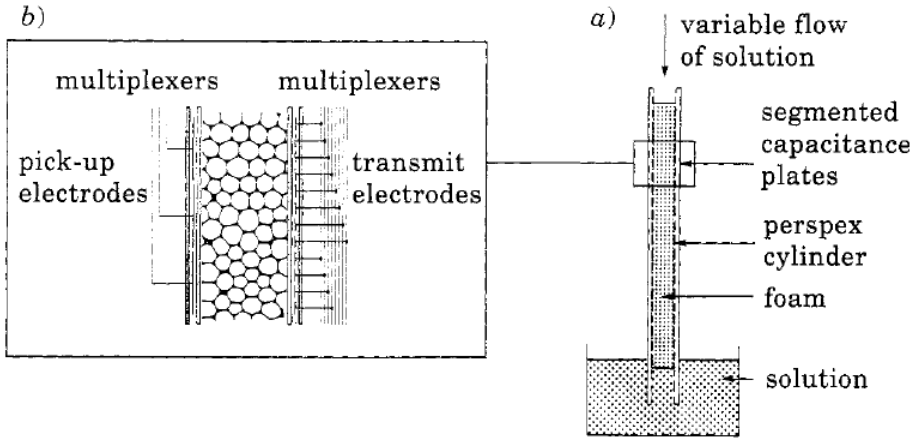

Figure 2.9. Set up diagram for assessing foam properties by using capacitance measurements. Taken from Hutzler *et al*. (1995).

In Figure 2.9 a simplistic capacitance measurement equipment set up is displayed. The measurement column was immersed into the pool of non-ionic solution and by blowing the gas through the thin nozzle located beneath the column, the foam was made with a bubble size of a few millimetres. The measurement column had 46 segmented capacitors and was 92 cm in

height. The signal going through the foam was measured by using a multiplexer within the kHz frequency range. Prior to the measurement the apparatus was calibrated. Based on the air content in the foam and the dielectric constant of both phases, it was possible to measure the changing density profile as a function of foam height over aging time. Good results were obtained on free, forced and pulsed foam drainage, therefore Hutzler *et al.* (1995) recommended the AC capacitance method for non-conducting foam investigations.

2.3.3 Foam imaging principles

In order to better understand the behaviour and structure of foam, visual observations are performed by using two or three dimensional techniques (Weaire and Hutzler, 1999, Pugh, 2005). Foam structure observations are difficult due to the opaque nature of foams, but such observations are very important, since they provide a fundamental parameter – the bubble size distribution. Therefore, scientists very often choose visual foam structure observations by using 2D optical techniques. A 2D technique relies on imaging the foam surface and thereafter processing, or analysing, sequentially taken photos in order to obtain the bubble radius distribution. Afterwards, from the 2D images an assumption is made about the whole three dimensional foam structure or structure changes during the aging process (Thomas *et al.,* 1998; Weaire and Hutzler, 1999; Van der Net *et al.*, 2007).

The 3D technique is more sophisticated, so it has been implemented very recently (Pugh, 2005). 3D foam structure can be obtained by using different optical and non-optical techniques (Thomas *et al.*, 1998 ; Weaire and Hutzler, 1999; Pugh, 2005). 2D and 3D imaging on foams provides different information on foam structure and instability processes. As was mentioned before, 2D and 3D imaging gives information on bubble size distributions and foam changing

structure during aging which can be used in analysing and modeling liquid drainage (Thomas *et al.,* 1998).

2.3.3.1 Techniques

2.3.3.1.1 2D imaging techniques – Microscopy

A 2D view of the foam can be obtained by using microscopy techniques: confocal microscopy (Weaire and Hutzler, 1999; Thomas *et al.,* 1998), scanning electron microscopy (SEM) (Chang and Hartel, 2002; Caillet *et al*., 2003), transmission electron microscopy (TEM) photonic microscopy (Caillet *et al*., 2003) and optical light microscopy (Chang and Hartel, 2002; Sahi and Alava, 2003) techniques. For different food products it is reported that different imaging techniques are used, as for example, for whipped cream, TEM and SEM are used more often, for imaging ice cream structure and other frozen foams – SEM (Caillet *et al*., 2003). SEM and optical light microscopy yielded the same results on bubble size distribution for ice cream and whipped cream (Chang and Hartel, 2002).

Confocal microscopy (Thomas *et al.,* 1998; Weaire and Hutzler, 1999) is the most commonly used technique in research with the purpose of reconstructing three dimensional images. By using a small depth of field; it is possible to determine 3D features of the foam which are in the focal plane. From a series of photos, a 3D view of the foam structure is obtained. The difficulties faced using this technique are associated with strong light reflection and refraction from foam bubbles. Therefore, the light source is placed behind the sample so that the lamellae become invisible and Plateau borders are dark shadows (Thomas *et al.,* 1998). Thomas *et al.* (1998) mention the difficulty in obtaining photos from film negatives with consistent quality. An algorithm is applied to make a series of photos that can be used in a skeletonization process. Elements of the foam structure, like Plateau borders, are then connected into one structure.

Light microscopy encounters several disadvantages over other techniques for imaging frozen samples, such as ice cream, which melt during preparation and during imaging (Chang and Hartel, 2002). The sample can be damaged as it is placed in a special capsule in order to perform electron microscopy imaging. Secondly, freeze drying in a sample can occur during preparation for cryo-SEM techniques and induce structural changes in the aerated structures. In light microscopy the sample is examined in the frozen natural product state and the pictures obtained are of very high resolution and magnification (Caillet *et al*., 2003). Photon microscopy, based on reflected light flux differences, also allows investigation of samples in a frozen state and is based on direct light reflection from the surface of an ice cream sample (Caillet *et al*., 2003).

In transmission imaging experiments the right sample thickness has to be chosen in order to have enough light passing through the sample so that good quality images can be obtained. Sample size has to be representative enough so that in the foam layer compressed between two glass slides more than one layer of bubbles is present. The investigated area is often less than 1 mm^2 and magnification varies from 78 to 100 times (Sahi and Alava, 2003; Spencer, 2006). An unavoidable problem in 2D foam imaging experiments is that it is necessary to squeeze the foam between two slides so that one layer of bubbles is obtained in a sample (Sahi and Alava, 2003). Sahi and Alava (2003) investigated the case where the bubbles were flattened between the two slides; therefore the squeezed bubble was considered as a circular flattened disc and from it the bubble volume and potential bubble radius calculated (Sahi and Alava, 2003). Up to 1 mm thickness (Spencer, 2006) of sample can be investigated if the foam is like egg white so that it is more light transparent, and therefore a number of bubbles remain in the foam layer between the two slides. The acquired 2D photos represent only the foam surface bubble size distribution and

in analysis the assumption is made that all bubbles are spherical. Several difficulties are faced in optical imaging analysis that will be discussed in the section 2.3.3.1.2.

2.3.3.1.2 Challenges encountered using optical microscopy technique for 2D foam imaging

Liquid foams, due to the presence of air bubbles, scatter, reflect and refract the rays of light that pass through the layer of foam. These phenomena depend on the foam structure, and explicitly on the void fraction. A number of physical and geometrical parameters impact the final imaging result, therefore it is important to discuss the major outcome and the way of interpreting the optical "illusion" we consider as the real bubble image (Van der Net *et al.*, 2007). A single bubble in a liquid acts as a diverging lens for rays of light. When the foam image is obtained by putting the sample in front of the light source, the black shadow rings often are understood in foam bubble imaging as bubbles themselves, however it is not true. The ring that we see in the foam image and assume that it is a true bubble size is formed due to reflection and multiple refractions when the rays of light cross the liquid (lamella) – gas boundary. The bubble itself acts as some sort of "shaped lens" for rays of light passing through it, so that the light waves are reflected or multiply refracted. In addition, bubbles are between two glass slides, which creates a second complication when the light passes through the glass-air boundary. As an example, in the single bubble case Van der Net *et al.* (2007) have shown that the actual bubble size can be calculated from a 2D bubble image.

In Figure 2.10 the theoretical case of a single bubble sandwiched between two glass slides is shown. The dark shadows indicate the area where no light can come through.

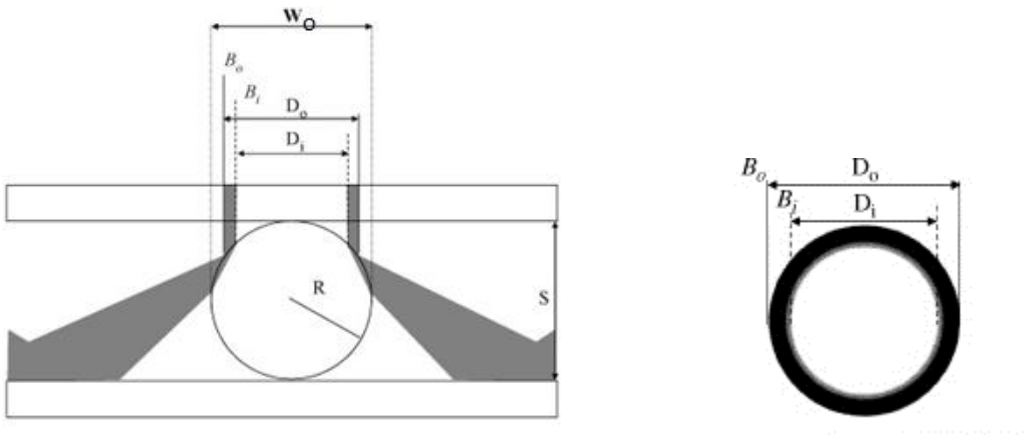

Figure 2.10 Individual bubble in a liquid (Van der Net *et al.*, 2007). B_o, B_i- the outer and the inner boundary of illuminated bubble. D_o-diameter of the outer illuminated bubble.

The simplified calculation of a single bubble radius in a liquid (Figure 2.11) is given by (Van der Net *et al.*, 2007):

$$r = \frac{W_o}{2} = 1.097 D_0 \tag{2.90}$$

where D_o - diameter of the outer illuminated bubble, w_o - bubble diameter.

2.3.3.1.3 3D imaging techniques

A number of 3D imaging techniques can be used to obtain three dimensional foam structures; to name a few are: magnetic resonance imaging (MRI) (Morris and Morris, 1965; Gonatas *et al*., 1995; Prause *et al*., 1995; Baldwin *et al*., 1996; Weaire and Hutzler, 1999; Stevenson *et al*., 2003; Baete *et al*., 2008), X-ray tomography (Lambert *et al.*, 2005; Von der Schulenburg *et al*., 2007), electrical resistance tomography (ERT) (Cilliers and Sadr-Kazemi, 1999), electrical capacitance tomography (ECT) (Bennett *et al.*, 2002), optical axial tomography (Monnereau and Vignes-Adler, 1998; Thomas *et al*., 1998; Monnereau *et al*., 2001) and neutron or X-ray scattering techniques (Thomas *et al.*, 1998; Weaire and Hutzler, 1999; Rami-Shojaei *et al*., 2009).

Tomography measurements are based on transmitting the X-ray signal through the foam sample at different angles and recording the passed signal at a number of points, so that the 3D view at the foam cross section is obtained (Cilliers and Sadr-Kazemi, 1999).

Electrical resistance tomography (ERT) is a non-invasive technique and is applied in industry for instant non-uniform 3D foam surface structure measurements (Cilliers and Sadr-Kazemi, 1999, Wang and Cilliers, 1999). The measurement principle relies on conductivity measurements made on the top layer of the foam, where the large bubbles show lower conductivity as a result of a lesser amount of Plateau borders. The pictures that are obtained pass through several processing steps and afterwards valuable information on bubble size distribution, bubble shape and specific surface area is obtained (Cilliers and Sadr-Kazemi, 1999). In addition, electrical capacitance tomography (ECT) measures the capacitance of the foam between the electrodes, and this method is suitable for non-conducting very dry open foams (Bennett *et al*., 2002).

For optical axial tomography the sample has to be a little transparent and a large depth of field optical system is used (Thomas *et al*., 1998). The thicker the sample, the more light that travels through the sample is attenuated; in particular, Plateau borders don't allow the light to pass through and they appear on the photograph as dark edges (Monnereau *et al*., 2001). Liquid foams refract the light, therefore it impacts the image quality so that light refraction has to be considered in the 3D image reconstruction algorithm. As well, liquid foams are not stable when compared with solid ones; therefore the structure derived from the taken measurements isn't precise (Thomas *et al*., 1998; Monnereau *et al*., 2001).

The small-angle neutron scattering (SANS) (Axelos and Bouè, 2003) technique uses a neutron beam transmission principle. Several difficulties are encountered using the SANS

method: 1) for wet foams, the scattered beam in the centre of the foam is combined with the transmitted beam, and therefore measurements are inaccurate; 2) estimation of the liquid fraction for dry foams by using transmission data was found to be unreliable. Despite difficulties in using this method, from the scattering intensity data, Porod's law (Formula 2.91) allows the average bubble size to be established accurately from specific area:

$$I_s = 2\pi\delta\rho^2 \left({}^{S_0}/_{V_0} \right) \left({}^{1}/_{q^4} \right) \tag{2.91}$$

where I_s – scattering intensity (1/cm), $\delta\rho^2$ - contrast, q-scattering vector (($q = 4\pi sin\theta)/\lambda$, λ - wavelength, 2θ - scattering angle), S_0/V_0 – area of spherical bubbles per unit volume of the foam, ($\frac{S_0}{V_0} = \frac{4\pi r^2}{({}^4/_3\pi r^3)\varphi} = \frac{3\varphi}{r}$, φ - void fraction, r - bubble radius).

Magnetic resonance imaging (MRI) is a well known non-invasive technique able to provide a foam 3D structure image by detecting the polarization density of nuclear (H^1) momentum at different positions in space (Gonatas *et al*., 1995). The method is suitable for following aging processes: drainage and coarsening of relatively wet food foams such as egg whites and beer, because MRI responds to the liquid content in the foam (Weaire and Hutzler, 1999). Therefore, any sample containing H^1 or polarized protons can be examined by using MRI (Prause *et al*., 1995). By using the MRI technique H^1 spectrum, signal intensity is measured in the foam and a 3D density distribution as a function of foam height can be obtained (Weaire and Hutzler, 1999). Also by using MRI, vertical slice images of the foam can be taken at different aging times and afterwards images are analyzed by manually fitting circles in each bubble (Gonatas *et al*., 1995). The histograms of bubble size distribution give an idea of the inner structure changes of the foam during aging time. Gonatas *et al*. (1995) weren't able to implement the 3rd axis in MRI scanning technique, unlike Prause *et al*. (1995) where a true 3D image was

obtained. The limitation of the MRI method is that it is suitable for wet liquid foams, which don't have polyhedral structure. However, wet foams drain quickly and that causes signal fluctuation or loss (Prause *et al*., 1995). In the set up of Gonatas *et al.* (1995) it took 10 min to scan wet foam, while to examine dry foam it took 3 min. In contrast, though, Prause *et al*. (1995) found that a scanning of 3D foam sample and averaging of the signal took 34 min.

In the X-ray tomography technique X-rays are propagated through the relatively small 1 cm^3 sample over a 180 degree angular setting and done also along all the sample height. To obtain one radiograph only 150 s was required and in total 900 frames were taken. Afterwards, from radiographs using attenuation information a 3D image was reconstructed. Besides structural information, from binary images the change of bubble volume can be determined, bubble lamellae thickness and liquid fraction in the foam at the same height during aging (Lambert *et al*., 2005; Von der Schulenburg *et al*., 2007).

CHAPTER 3. MATERIALS AND METHODS

3.1 Foam sample preparation

A typical formulation was chosen to make type angel food cake foams. The original recipe includes 83 g sugar, 83 g egg white, 23 g soft wheat flour, salt, and cream of tartar (Pyler, 1988; Spencer, 2006) was slightly modified. Flour was not added to the egg white foam to make the batter because it was out of my ultrasound and electrical resistivity research scope. Salt and cream of tartar were omitted as well, due to the reason that these ingredients are strong electrolytes and would have an impact on foam resistivity measurements.

For all experiments liquid egg whites (Innovatech, Winnipeg, MB) were used. Egg products were kept frozen at -20 ^{o}C in small 200ml containers until they were needed. Prior to each experiment two steps were taken to prepare frozen egg whites. Firstly, 12 hours was necessary to defrost the liquid egg whites at 4 ^{o}C. Before each experiment egg whites were allowed to sit in a room until they reached ambient temperature (22 ^{o}C). Secondly, the liquid egg whites were filtered through cheese cloth in order to remove non- homogenous egg white parts.

Powdered sugar (Rogers Sugar Ltd.) was bought in 1kg bags and used for the experiments.

A small scale domestic **Kitchen Aid** (Hobart Company, Model 4C, 200 Watts) mixer with 10 variable speed was used in our experiments. Two components, sugar and egg whites were poured in a steel bowl and blended at speed *1* for 5 min with stainless steel 3 wire whip in order to allow the sugar to dissolve as much as possible before incorporating the air. Afterwards, high speed mixing *6* was used to mix air into the egg whites and sugar mixture. Whipping times of the foam were chosen according to the void fractions reported in a thesis from this laboratory (Spencer, 2006). To investigate aging foam processes in the majority of experiments two whipping times were chosen: 180 s and 600 s. The foam whipped for 180 s has a void fraction of

0.65 and polydisperse bubble structure. A whipping time of 600 s whipping time corresponds to a void fraction of 0.78. Whipping the egg whites and sugar mixture for 600 seconds is the approximate time necessary to form a so called stiff peak in the foam (Burgett *et al.,* 2003).

Density measurements of egg white foams were repeated, because Spencer (2006) used to make egg white foam from cooled, 4 ^{o}C temperature egg whites. In our experiments we used egg whites at ambient (22 ^{o}C) temperature to make sure that made foam is the same ambient temperature, since stable temperature is critical in order to obtain reliable results from ultrasound measurements. Four high speed mixing times was chosen to obtain egg white foam with the void fractions of 0.60, 0.65, 0.78 and 0.81. By using Formula 2.3 the foam void fractions were calculated from the measured density values. In table 4.1 egg white foam densities and void fractions are given

Table 3.1. Measured density and calculated void fraction of egg white and sugar foam. The experiments were replicated three times.

Whipping time (s)	**Density (kg/m^3)**	**St. dev.**	**Void Fraction**	**St. dev.**
0	1224.7	1.2	0	
120	481.0	44.5	0.60	0.036
180	420.5	45.4	0.65	0.036
600	260.5	3.0	0.78	0.002
360*	227.1	7.7	0.81	0.006

*The single case, using fresh, not frozen egg whites in order to incorporate the highest amount of air in the foam. Freezing/thawing cycles and prolonged storage affect egg white conformational structure, therefore reduces egg white liquid viscosity (Wootton *et al.,* 1981) and foaming properties and foam stability (Wootton *et al.,* 1981).

The second type of foam used, but only in ultrasound experiments, was a non-food foam, prepared using *Gillette* Sensitive foamy shaving cream. Besides the basic ingredients (triethanolamine stearate with small amount, <1%, of sodium lauryl sulfate and polyethylene glycol lauryl ether and emulsified liquid hydrocarbon gases), in commercial *Gillette* Sensitive foam there are other high molecular weight polymers (Procter and Gamble, 2011), that are kept

in an aqueous solution under high pressure (Barik and Roy, 2009). To produce *Gillette* foam was relatively an easy task, however void fraction, and bubble size distribution was based on shaking duration and how energetically shaking was performed. To prepare this foam, the container was shaken for approximately 10 s, and then the foam was sprayed out into known volume container to assure that required density is achieved. For imaging and ultrasound experiments on *Gillette* foam, samples were prepared in two densities: 0.064 ±0.0036 g/cm^3 and 0.084±0.001 g/cm^3. The void fractions were 0.93±0.0036 and 0.90±0.001, respectively. Afterwards, exactly in the same manner as with the egg white foam, Gillette foam was placed on the top of the transducer and gently squeezed down.

3.2 Density measurements

For egg white foams, density measurements were performed in 60 mL glass containers (knowing that the density of the foam is equal to the weight and known volume ratio). Whipped foam was gently placed inside the container using a metal spatula. Measurements were done twice and the foam was placed in such a way that air gaps were not formed inside the container.

For density measurements of *Gillette* foam, the can was shaken and the foam was sprayed into a 120 mL volume glass container. A second spray of the *Gillette* foam was done onto the surface of the bottom transducer so that this material was analysed ultrasonically. The third spray, performed identically to the first one, was done to obtain a replicate measurement of foam density. Exactly the same procedure was followed when performing imaging experiments, except that the sample was sprayed on the microscope slide. More details on the microscope imaging sample preparation and set up is given in section 3.5.

3.3 Ultrasound measurements

Foam aging processes were monitored by using the ultrasound measurement set-up that is shown in Figure 3.1. Ultrasound measurements of foams were performed with two 40 kHz (**Panametric Inc.)** transducers. A thin layer of foam was immediately placed on the surface of the bottom transducer. The top transducer was placed on the top of the foam and gently squeezed so that the holder of the top transducer would just be touching the 3 micrometers. The thickness of the gap was manipulated by adjusting the micrometers. The gap between the plates was sealed with tape. Sealing prevented moisture evaporation from the foam and kept the experiment in constant conditions. Experiments were done in duplicates.

The top transducer was driven by the pulser **PUNDIT** 5058 PR (Manufacturer Olympus) and a pulse was propagated into the foam from the transmitting ultrasonic transducer. The foam samples were placed between two transducers, which were supported by transducer holders that controlled the parallelism of the transducer faces and allowed a particular sample thickness to be specified (Figure 3.1 b). The signal was detected by the lower transducer and amplified by the receiver (**Panametrics,** Manufacturer Olympus NDT, Waltham, Massachusetts, USA). From there, the signal was displayed right away on the digital oscilloscope (**Tektronix TDS 5052,** National Instruments, Austin, Texas, USA). The data were transferred onto the computer by using the **TDSWAVE** program (comes along with the Tektronix TDS oscilloscope) written in C language. Monitoring of foam sample aging with time was enabled by using a program, **Fan1,** written in Matlab by Yuanzhong Fan. More details about this program are given in the thesis (Fan, 2007). Before every experiment with foams, a reference signal was recorded. An example of a recorded waveform for a foam sample is given in Figure 3.2.

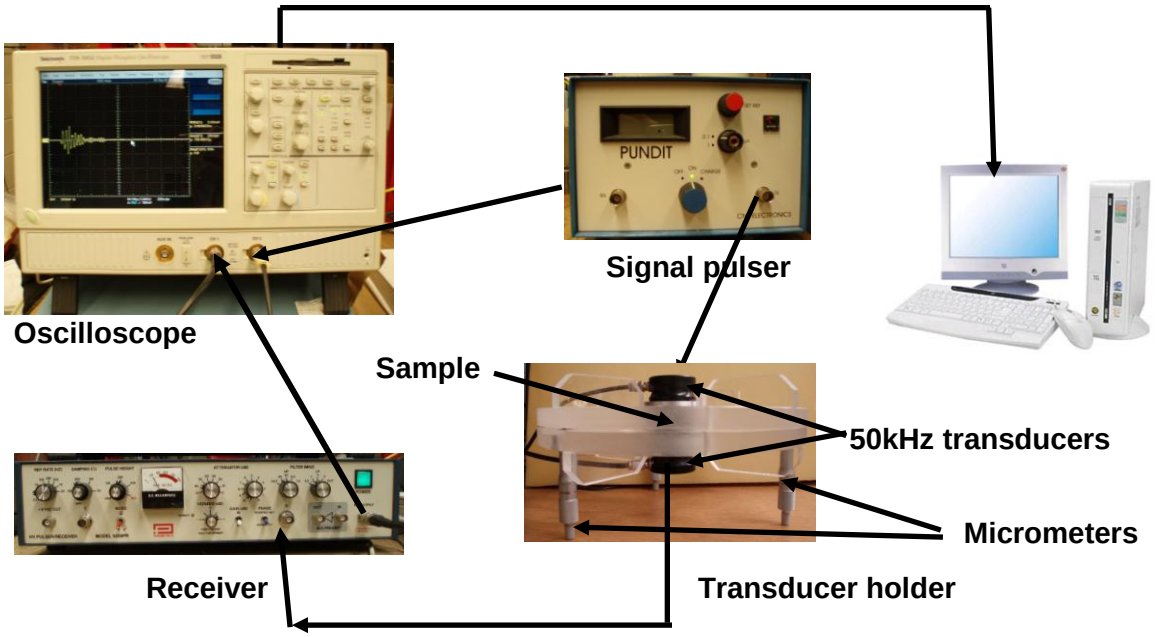

Figure 3.1 Ultrasound experiment set-up a).

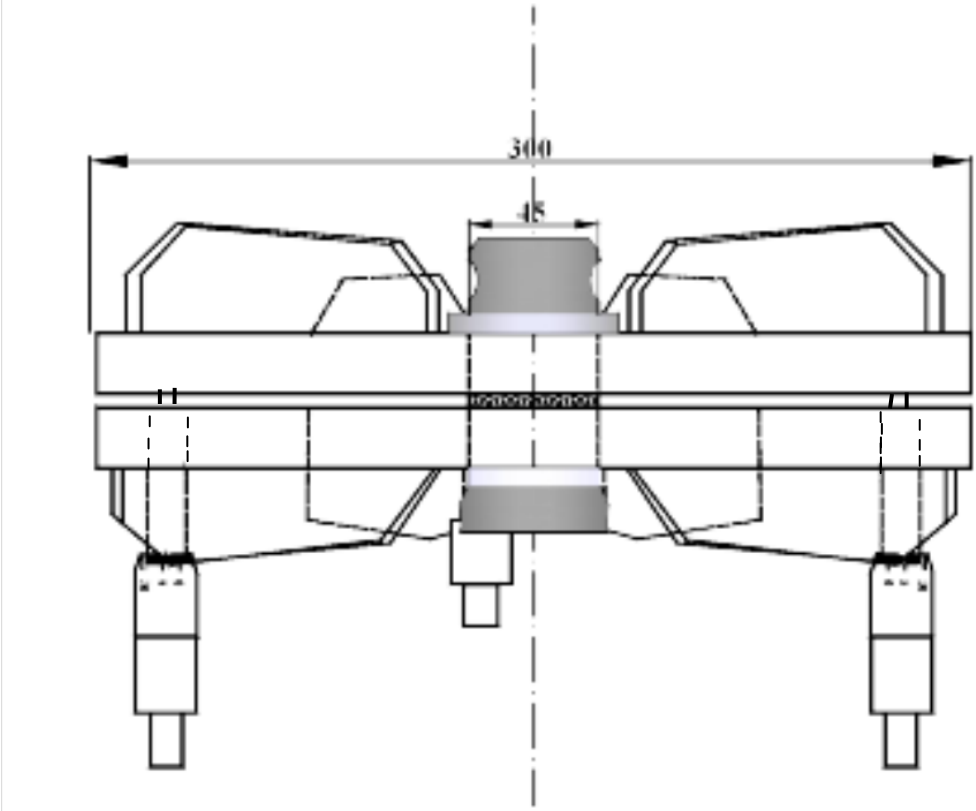

Figure 3.1 Ultrasound experiment set-up: b) sample holder.

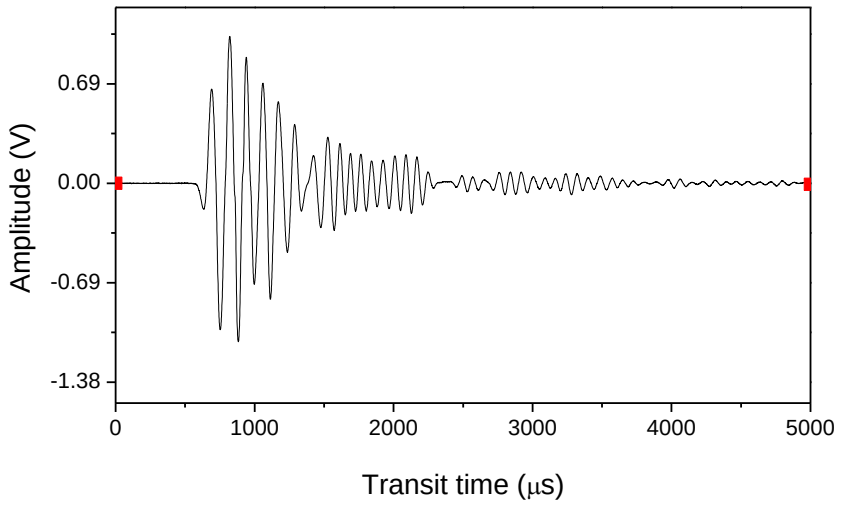

Figure 3.2. Transmitted waveform through a foam sample at a central frequency of 40 kHz.

3.4 Foam resistivity measurements

3.4.1 Foam resistivity measurement technique

Electrical resistivity measurements were performed only with egg white foams. Based on the apparatus of Barigou *et al*., (2001) for this purpose, a 7 cm diameter and 15 cm height cylinder was made for electrical conductometry measurements. Kurt Hildebrand designed and Richard Hamel (Physics and Astronomy Department, University of Manitoba) builded the electrical measurement circuit for the resistivity measurement set-up. The cylinder was made by firmly stacking together 15 steel and 15 polyoxymethylene (**Delrin**) plastic rings. Plastic and steel rings were alternated along the height of the cylinder, thereby separating the steel rings physically and electrically. The structure was tightened up from the bottom to the top by using 4 steel rods. To avoid leakage, the rings were sealed with silicone gel. In Figure 3.4 a sketch of the cylinder with the physical dimensions is shown.

The steel rings worked as outer electrodes and the plastic rings acted as electrical insulators. The central rod acted as an inner electrode, and was positioned in the cylinder's geometrical centre. The rod thickness was chosen after conducting preliminary experiments using KCl and NaCl electrolyte solutions with different thickness rods. As the shape of the electrode determines the orientation of electric field lines, the rod thickness has to be considered too. For an inner rod that is very thin (1 mm), electric field lines around it are too dense and the measured resistance of the salt solutions was higher than theoretical. After an analysis of measured results and theoretical calculations the decision was made to use a 6.4 mm thickness rod.

A steel spatula and spoon was used to load whipped egg white foam samples inside the cylinder in less than 5 min. The top of the cylinder was covered with plastic film to avoid moisture evaporation from the foam. Afterwards, 15 electrical wires were connected to the tabs attached to the outer rings. The inner rod and outer rings were connected to the current meter-converter, which was hooked up to a data logger (Figure 3.3). In our measurements a multiplexer principle was used. During a given scan, the multiplexer takes one of the 15 data output lines and switching between the lines occurs within a millisecond. Therefore it is possible to have accurate simultaneous monitoring of all the rings even in fast draining foams. Each data point that was recorded consisted of a number of scans and therefore assured accurate measurements by averaging over a number of scans. For the selected AC frequency, a scan rate of 20 kHz was chosen. The electrical signal from the data logger was acquired by using the LabVIEW program (National Instruments, Austin, Texas, USA).

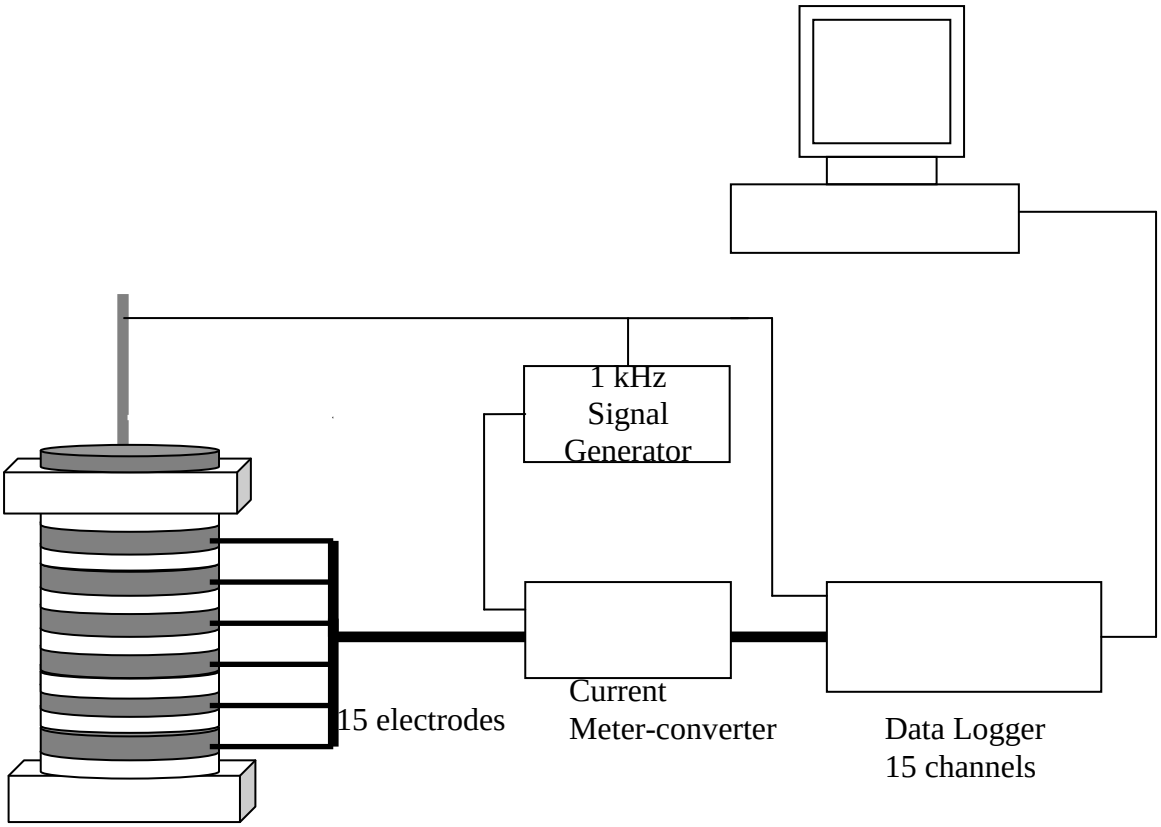

Figure 3.3. Electrical resistivity technique for measuring foam aging.

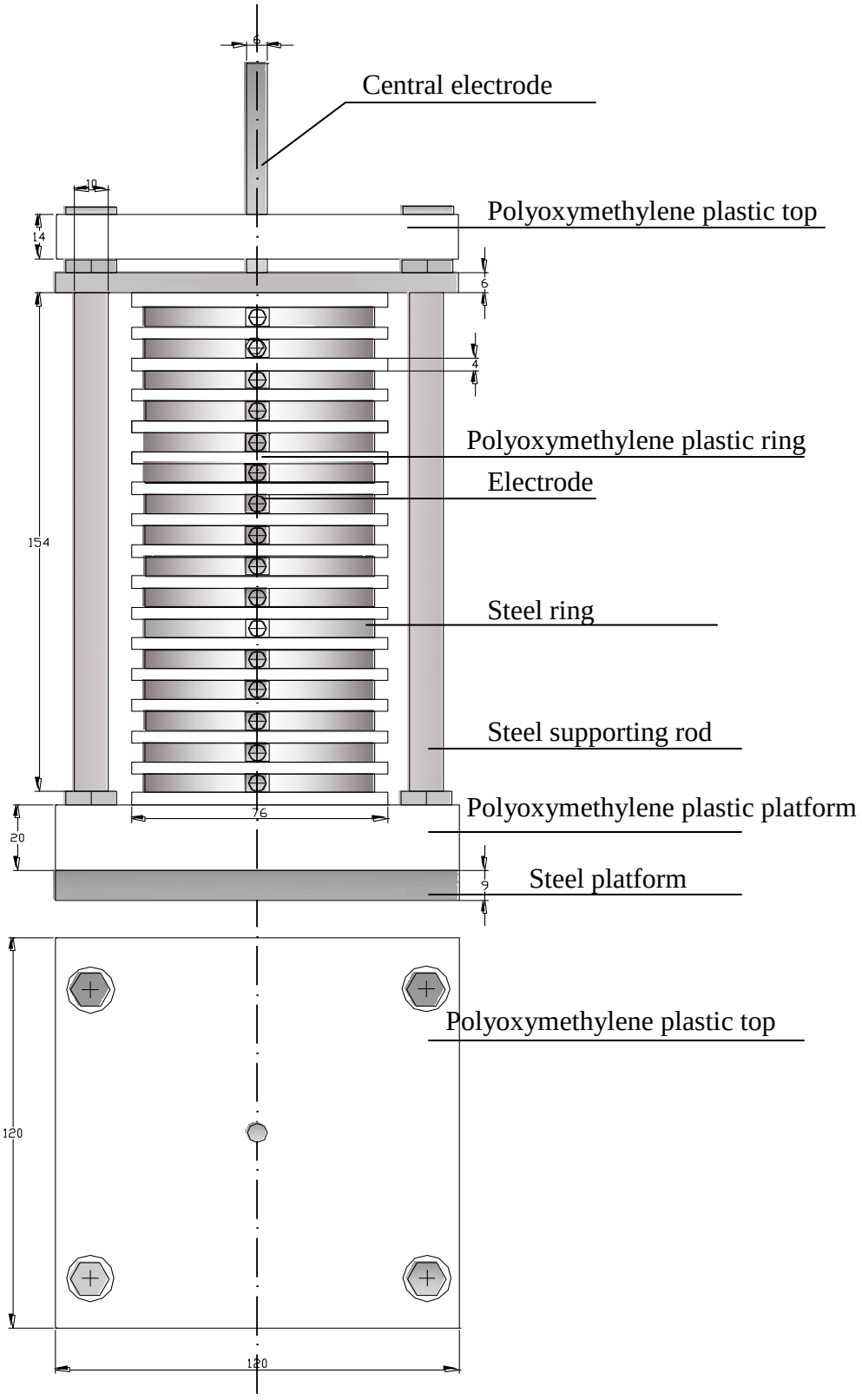

Figure 3.4. Design of the cell for electrical resistivity measurements. Dimensions given in millimeters.

3.4.2 Electrical properties of foam

Preliminary experiments were done in order to design the best electric circuit to measure accurately the changes in the aging foam at all height levels. From these measurements it was determined that the air content in the foam strongly increases the resistivity. From a literature review (Barigou *et al.*, 2001) and preliminary experiments I decided to use 1 kHz frequency alternating current. At this AC frequency, foam has a very small capacitance and the best way to describe foam from an electric circuit point of view is as a capacitor and resistor connected in parallel (Figure 3.5). Formulas 3.1, 3.2 and 3.3 describe the relationship between foam resistance and capacitance.

$$\frac{1}{R} + j' \omega C = \frac{1}{Z_i} \tag{3.1}$$

$$Y = \frac{1}{Z_i} = Z_i e^{j' \Phi} \tag{3.2}$$

$$\tan \Phi = \frac{\omega C}{1/R} \tag{3.3}$$

$$\omega = 2\pi f \tag{3.4}$$

$$\mathrm{R} = \frac{\sqrt{1+\tan^2 \phi}}{\mathrm{I}/V} \tag{3.5}$$

where: R - resistance; C - capacitance; Z_i - impedance; Y - admittance; j' - imaginary part; I - current; f - frequency of the alternating current; Φ - phase angle between the current and voltage, degrees; ω - angular frequency of alternating current, radians; V- voltage.

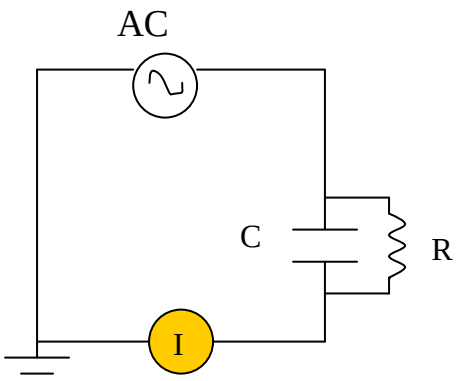

Figure 3.5. Electrical circuit diagram representing a foam.

3.4.3 Current meter-converter design

Direct measurements of the foam resistance are challenging and were not possible without measurement errors. From preliminary measurements it was determined that foam resistivity is relatively high and therefore measuring its resistivity using a voltmeter that also has a high resistance gives a big measurement error. For accurate foam aging measurements it was therefore necessary to design an electrical circuit which permits accurate measurements of the resistance of the foam. Therefore, instead of measuring the resistance directly the current was measured, and this was then converted into voltage. The principle diagram for one ring is shown in Figure 3.6. In total there are 15 sets like this, for each ring. The voltage applied to the central rod and the 15 rings has the same virtual ground, therefore the electric field lines going through the sample are straight. The measured current is proportional to the resistance of the foam. Therefore, after converting current to voltage (Figure 3.6, part B) and amplifying the signal 10 times (Figure 3.6, part C) we obtain the values for the electrical characteristics of the foam (including its resistance) as a result of measurements of the current flowing through the foam. In chapter 3.3.4 a description of how resistivity values of the foam were calculated by using the geometrical dimensions of the cylinder is provided.

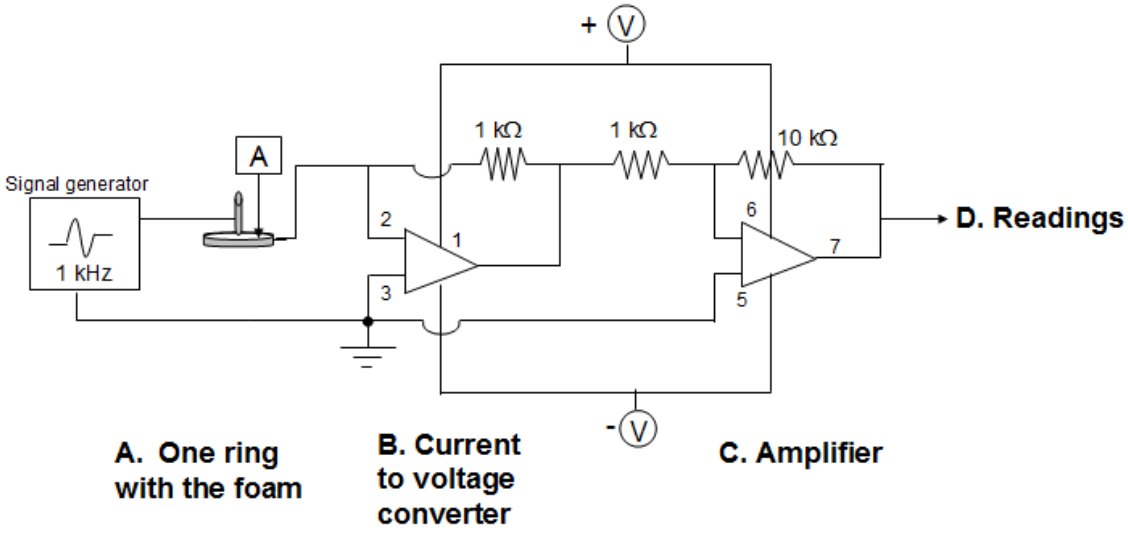

Figure 3.6. Electrical circuit scheme of current meter-converter for a single ring.

It is important to address the fact that the rings are not electrically isolated and as a result, the electric field lines of the top and bottom rings are not straight like the other ones. To solve this problem the measured resistance of the top and bottom rings was multiplied by numerical a constant (1.07). The value for this constant was determined experimentally from calibration measurements with salt solutions.

3.4.4 Electrical conductivity cell calibration

For calibration of the instrument two strong electrolytes were chosen: NaCl and KCl. The concentrations (for KCl, the concentration range was from 0.00745 g/L to 0.3725 g/L, and for NaCl salt the concentration was from 0.02 g/L to 0.5 g/L) were selected so as to have conductivities in the same range as foam conductivity. The salt solution conductivity values have been taken from *CRC Handbook of Chemistry and Physics* (Lide, 2005). The resistance of the

salt solution was calculated using equation (3.6) taking into account the cylindrical geometry of the cell:

$$R = \rho_R \int_{a_r}^{b_r} \frac{dr}{h(2\pi r)} = \frac{\rho_R}{2\pi h} ln \frac{b_r}{a_r} \tag{3.6}$$

where ρ_R – solution resistivity; b_r = 3.5 (cm) is radius of the cell and a_r = 0.32 (cm) is radius of the inner electrode; h = 0.9 (cm) is height of one ring.

Calibration results with KCl and NaCl salt solution are shown in Figure 3.7. The slopes show good agreement between measured and calculated salt solution conductivity.

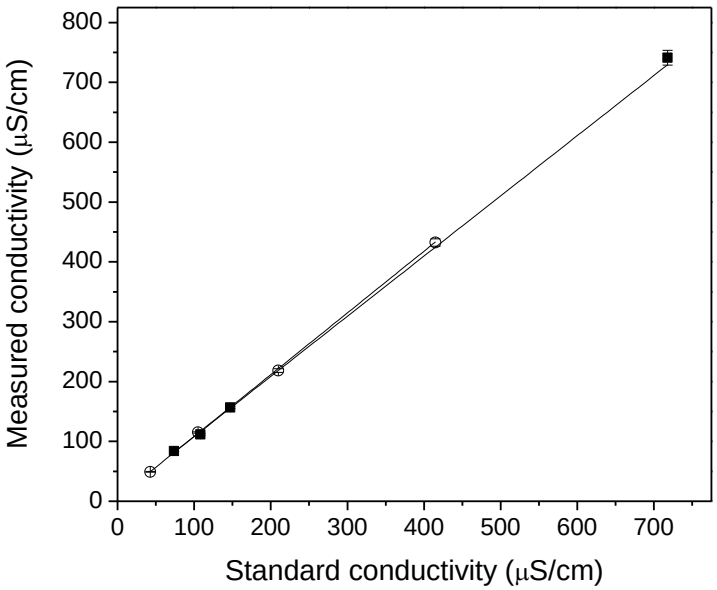

Figure 3.7. Measured and standard conductivity of KCl and NaCl solutions. Solid line represents Linear fit to measured conductivity. Symbols represent: ■ - measured conductivity of KCl, ▫ - measured conductivity of NaCl. Slope for KCl=1.006. Slope for NaCl=1.031.

3.5 Egg white and *Gillette* foam surface 2D digital image technique

A foam imaging technique was used to observe aging of foam samples. A sample holder was made using 1 mm thick microscope slides, in such a way that a 3 mm thickness layer of a

foam could be placed between the slides. During a typical experiment, as soon as the foam was made, it was placed on the bottom slide and covered with the top one. Both slides were firmly fixed together with tape in order to avoid any movement that could cause altering of foam structure. The imaging experiments with egg white and *Gillette* foams were done in quadruplicates. For *Gillette* foam experiments, the foam density was determined by spraying the foam into a known volume cylinder and weighing it. The details are given in section 3.2.

A **Carl Zeiss** microscope with compatible camera (**AxioCam HRm** 60N-C 1" 1,0x) was used to take pictures. Prior to each experiment, illumination from a polarized light source was set in the centre of the microscope eyepiece view. The white balance of the camera was set to 3200K. This particular white balance setting provides the best image reproduction of a sample that is in the microscope eyepiece. Exposure time varied depending on the sample. To ensure that the automatically measured distance was correct, a graticule was used. The measured foam sample view field was 890x667 μm (resolution 1388x1040 pixels). For foam sample bubble evolution observations, the camera was set to autofocus. The photo taking procedure was automated by using software **Axio Vision Release 4.6.3.**

For the analysis of changes in foam structure a free program **Image J 1.41o** was used. In Figure 3.8 a typical photo of the 600 s whipping time foam at 0 s aging time is shown.

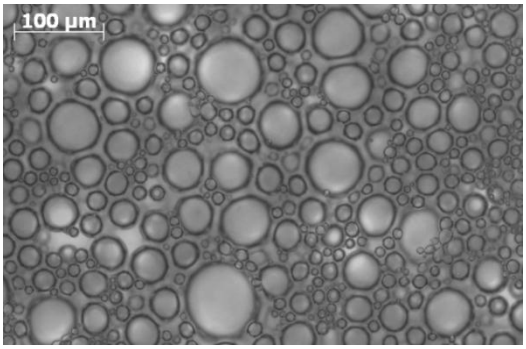

Figure 3.8 Foam (φ = 0.78) image at 0 s aging time.

Due to changing foam properties, the light transmitted through the foam sample caused photo areas to be somewhat unevenly illuminated. Therefore, an image processing procedure was developed by Spencer (2006) and followed in order to get accurate results on bubble sizes.

All photos were filtered using *Bandpass* filter. Afterwards, the threshold was adjusted using *Threshold* function, where the default value determined by the software was used. Tresholding in imaging processing is used for image segmentation. This step, *Threshold* adjustment was done for each individual image at the different aging times and for each experiment set. In addition, the *Threshold* function was used to convert photos from grey to 8-bit binary images. Afterwards, the images were inverted, using the *Invert* command.

After processing images, the functions *Area* and *Perimeter* were selected in *Analyze* function so that each bubble's area and perimeter would be the desired parameters to be calculated by Image J. In order to measure the bubble sizes accurately, the global scaling factor (154 pixels corresponds to 100 μm) to be set for all acquired images was needed. Using the function *Analyze particles* in the *Analyze* menu bar, the *particle size* was set to 8 μm^2. This is the minimum bubble size (area) that we allowed to be detected since we assumed that smaller bubbles than this value were most likely noise. By setting *circularity* from 0.15-1 the software filtered out features that are highly distorted and therefore unlikely to be real bubbles. The last setting to be mentioned is *show ellipse* - the software fitted an ellipse into each inner bubble area and calculated a corresponding value for each area and perimeter. These procedures allowed us to obtain the drawing d) in Figure 3.9. From there, the bubble radii were calculated from the perimeter data, assuming that the bubbles are circular.

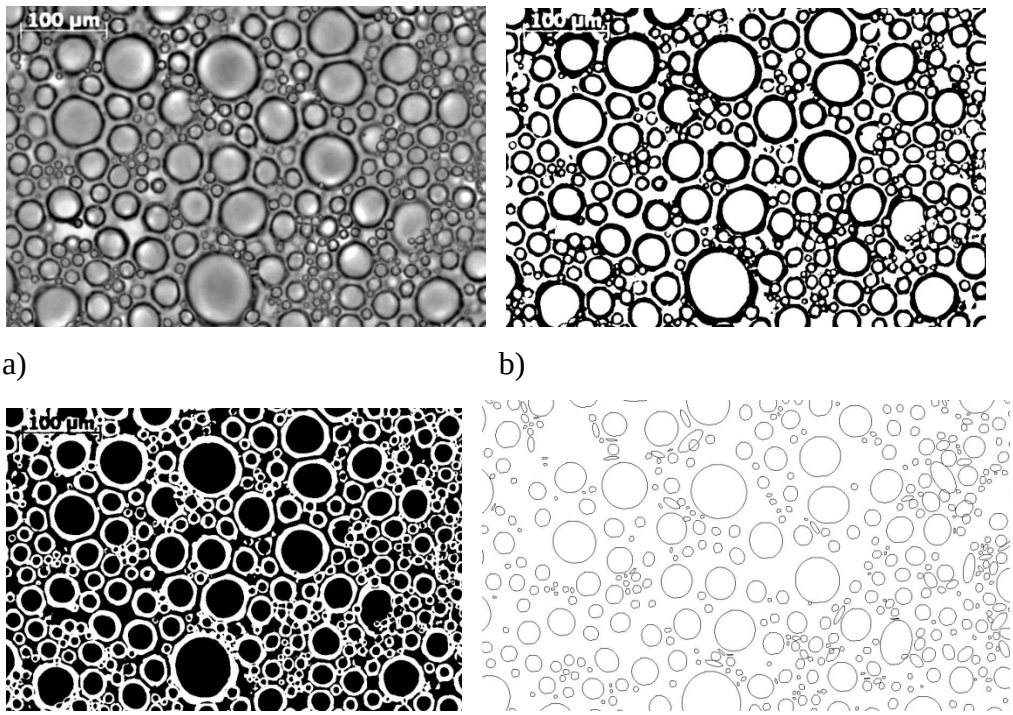

Figure 3.9. Photo processing steps for the image shown in Figure 3.8. a) After using *Bandpass* filter, b) After applying *Threshold* function, c) After applying *Invert* function, d) After selecting *Analyze particles* and choosing to show as a mask *ellipses*.

CHAPTER 4. IMAGE ANALYSIS

4.1 Introduction

The microscopy imaging of opaque foams is certainly challenging, but a feasible task if in a visible light transmission experiment the foam sample is relatively thin so that 2D foam images can be obtained. This technique allows image sequences to be obtained as the foam ages and results of the photo analysis give information on the bubble radii distributions. Besides quantitative information, from image sequences one can by eye observe the foam aging process and validate if bubble coalescence in the foam is occurring. In most food foams instability processes are intermixed - disproportionation is affected by the drainage process. From foam imaging it was observed that the mean bubble radius for fully disproportionating foams evolves as the square root of time (Weaire and Hutzeler, 1999). Thus the fits of $(t\text{-}t_i)^m$ where t_i is the initial aging time and m is the exponent, to the mean bubble radii versus aging time characterize the instability process that occurs in the foam. For wet, draining foams the exponent m is close to 1/3 (Durian *et al*., 1991).

Image analysis of aging egg white foam was conducted because it is of great relevance to ultrasound transmission results. The increase of bubble radii due to disproportionation in the aging foam, impacts to a big extent the attenuation of the transmitted ultrasonic signal (Mujica and Fauve, 2002). Overall bubble radii increase and the thickness of the lamella surrounding the bubbles increase as well. For image analysis the same void fraction (0.65 and 0.78) egg white foams as for the ultrasound experiments were chosen. The sample thicknesses in imaging and ultrasound experiments were similar: 3 mm and from 1mm to 2.5 mm respectively. Foams were prepared in the same manner, keeping the ambient temperature 22 ^oC for both type of experiments. Samples of foam images are displayed in Figure 4.1 (0.65 void fraction) and Figure 4.2 (0.78 void fraction).

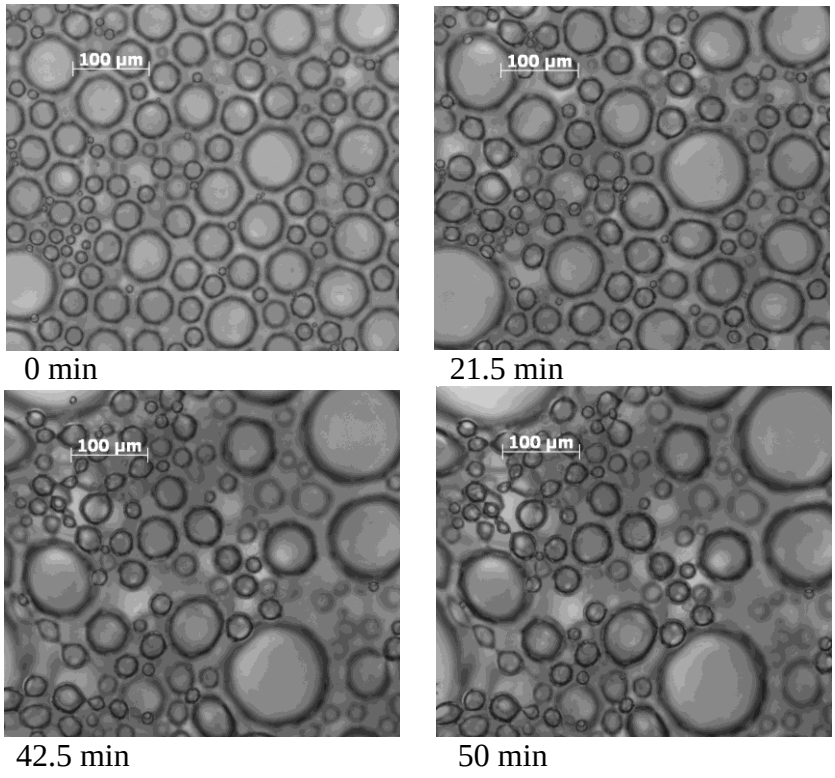

Figure 4.1. Images of aging egg white foam of 0.65 void fraction. Image dimensions 532 µm x 450 µm.

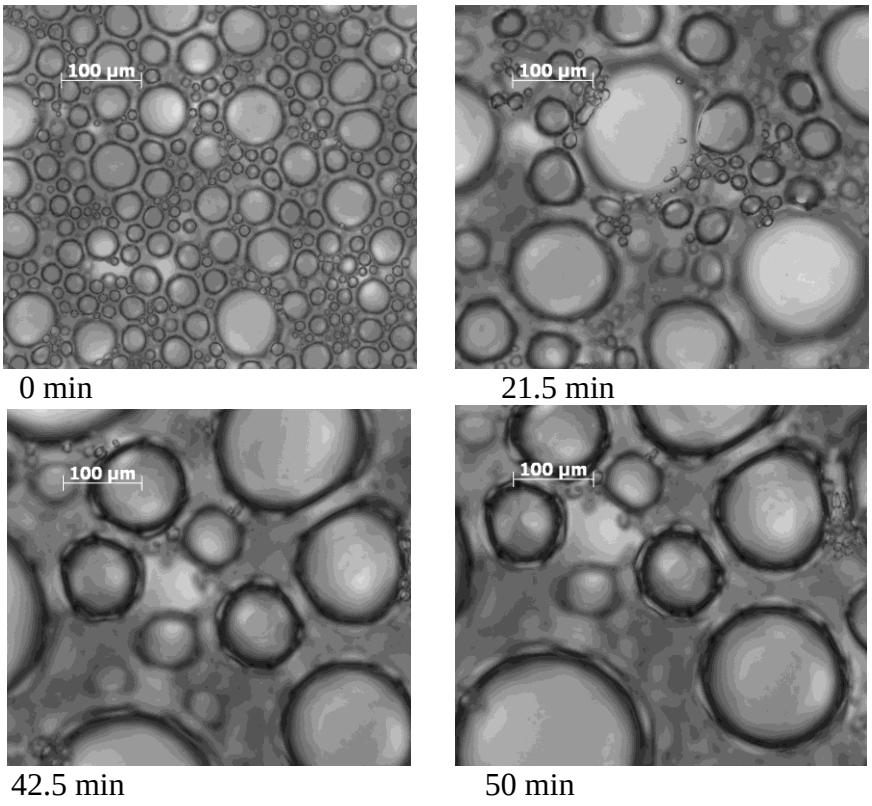

Figure 4.2. Images of aging egg white foam of 0.78 void fraction. Image dimensions 532 µm x 450 µm.

4.2 Results and discussion

From images of both void fraction foams, it is visible by eye that the aging process is mainly due to bubble size growth, but at different rates. Quantitative analysis was done using **Image J** free software, image analyser. The image analysis principles are described in "Materials and methods", chapter 3.4. Calculated bubble radii have been classified into bins of certain size, which varied depending on the sample. Bin size value was expressed in percent of the total bubble number, so that a frequency distribution of bubble radii could be obtained (Figures 4.3-4.8). Error bars represent standard deviation of four measurements. In Figure 4.6 the bubble radii distribution for the 0.78 void fraction foam is displayed, where the line represents an attempt to fit a two parameter log-normal distribution (Formula 2.7) by using **Origin 8** software.

$$f(r_j') = \frac{1}{\sigma_g r_j \sqrt{2\pi}} exp\left[-\frac{1}{2\sigma_g^2} ln^2\left(\frac{r_j}{\mu_r}\right)\right] \quad (2.7)$$

From Figure 4.3 and Figure 4.6 it is visible, that at 0 min aging time, the bubble size distribution is close to a log-normal distribution for both the 0.65 and 0.78 void fraction foams. However, as the foam ages, bubble size distributions become bimodal (Figure 4.4, 4.5, 4.7 and 4.8). An attempt was made to fit two log-normal functions manually to these size distributions at later aging times for the 0.78 void fraction foam (Figure 4.7). For application of physics theory to estimate ultrasound velocity and attenuation coefficient (chapter 6) the bubble size distributions versus frequency data were used, but not the bubble size distribution log-normal curve fit parameters. Since our data cannot be represented purely by log-normal distributions at all aging times, bubble size mean (μ_r) obtained from geometric mean (formula 2.9) or geometric mean (x_g) of the log-normal distribution were not used. Instead the arithmetic mean of the bubble size distribution was used.

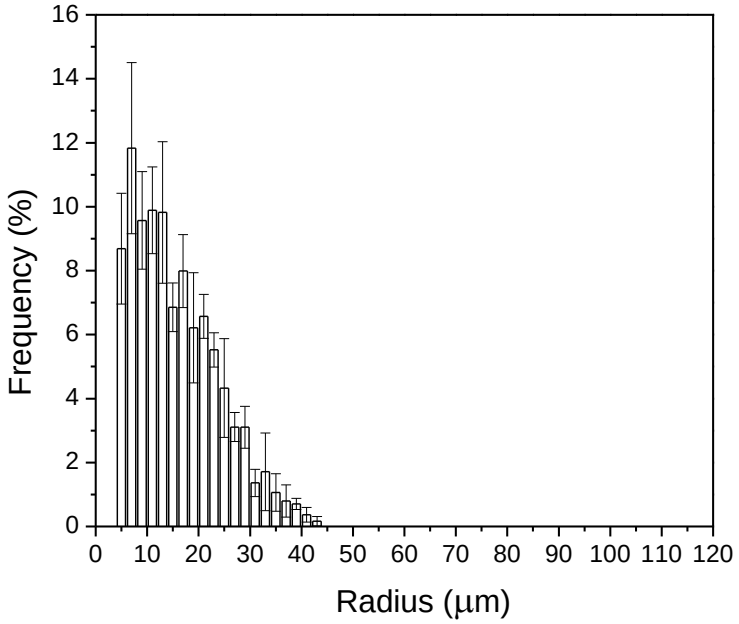

Figure 4.3. Bubble radii distribution in 0.65 void fraction egg white foam at 0 min of aging.

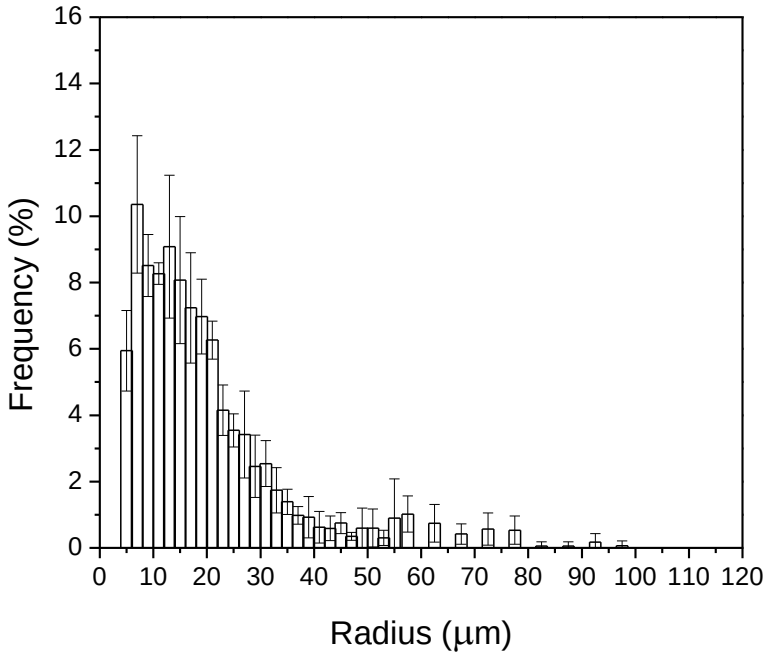

Figure 4.4. Bubble radii distribution in 0.65 void fraction egg white foam at 21 min of aging.

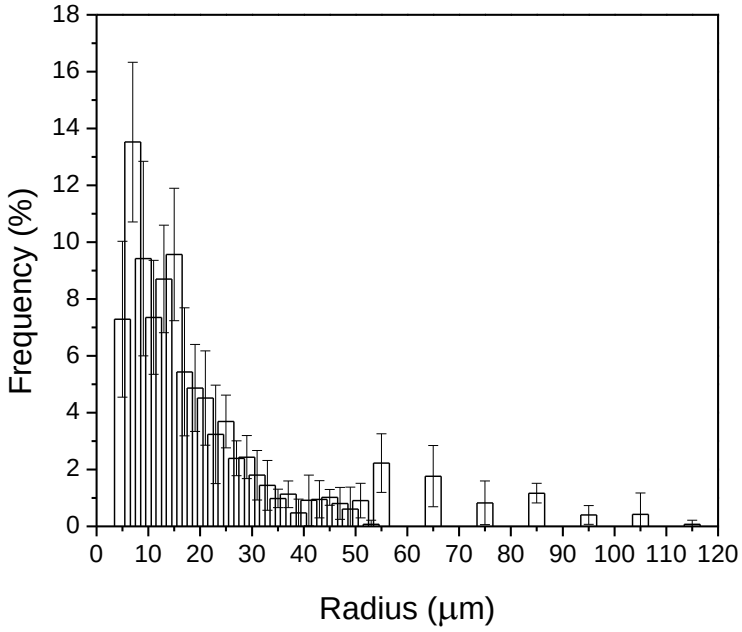

Figure 4.5. Bubble radii distribution in 0.65 void fraction egg white foam at 41.5 min of aging.

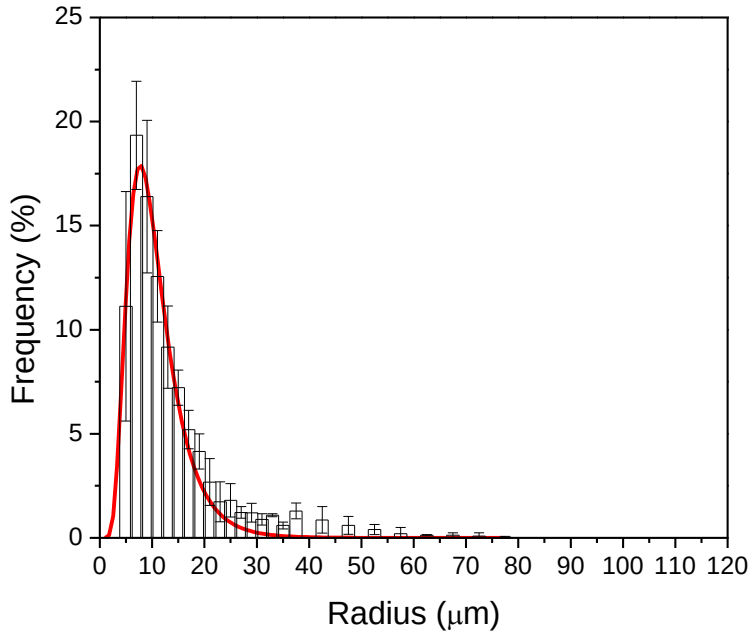

Figure 4.6. Bubble radii distribution in 0.78 void fraction egg white foam at 0 min of aging.

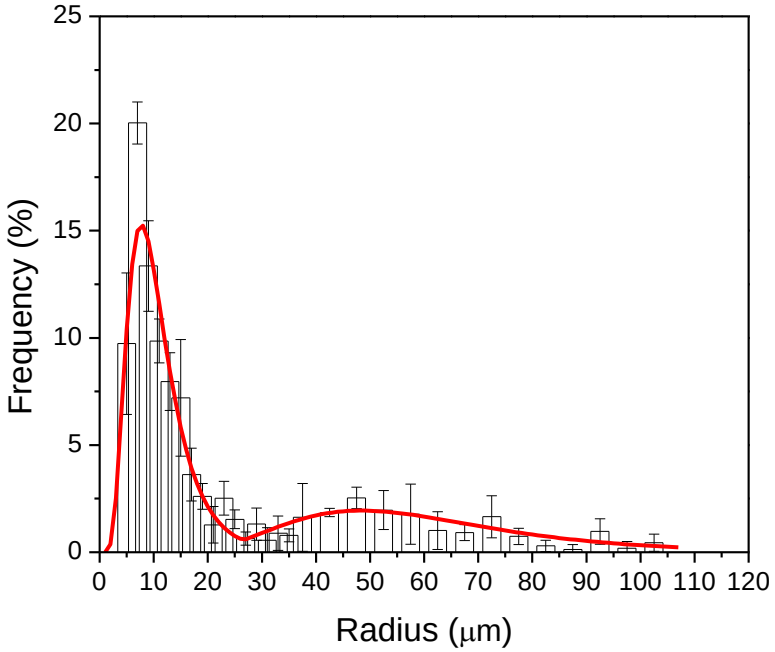

Figure 4.7. Bubble radii distribution in 0.78 void fraction egg white foam at 22 min of aging.

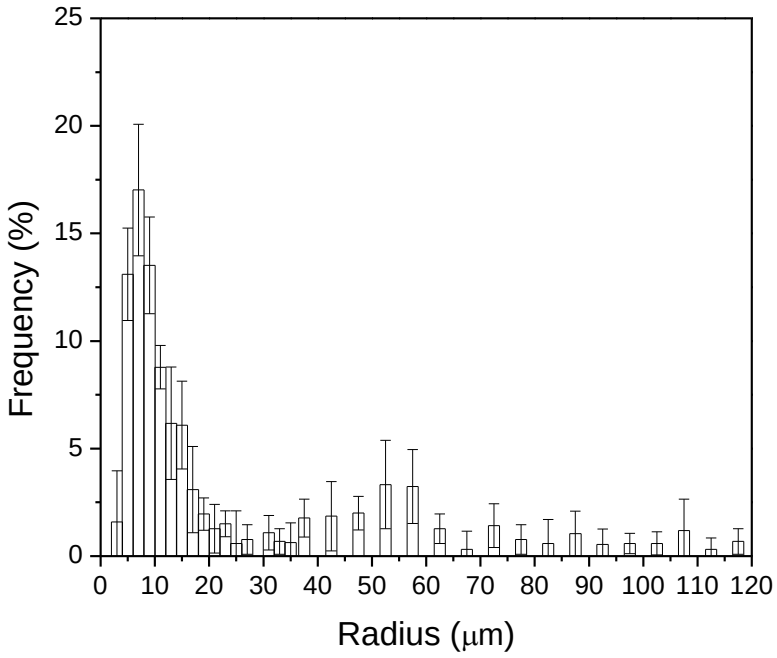

Figure 4.8. Bubble radii distribution in 0.78 void fraction egg white foam at 42 min of aging.

In order to understand the mechanisms of bubble size changes in egg white foams, image analysis was performed on *Gillette* foams. *Gillette* foam is a polyhedral and non-draining surfactant foam, whose samples are easy to reproduce. Therefore, it is reasonable to study disproportionation effects since coalescence and drainage effects are not observed (Durian *et al.*, 1991; Sessoms *et al*., 2010).

In Figures 4.9 and 4.10 images of aging *Gillette* foamy of two void fractions, 0.90 and 0.93, are represented. In Figures 4.11-4.22 bubble radius distributions for the two void fractions of *Gillette* foams are presented: 0.90 and 0.93 are shown as a function of aging time; here error bars represent standard deviations of three trials. From Figures 4.9 and 4.10 it is visible that Gillette foam consists of a majority of polyhedral bubbles. The drier (93 % of air) *Gillette* foam consists of almost similar sized small bubbles and as the foam ages, bubbles grow, but the bubble shape remains polyhedral. Lower air content (90%) *Gillette* foam consists of larger and smaller bubbles, whose shape during aging remains polyhedral also. From visual observations of aging *Gillette* foam we noticed relatively slow bubble movement and no coalescence effects.

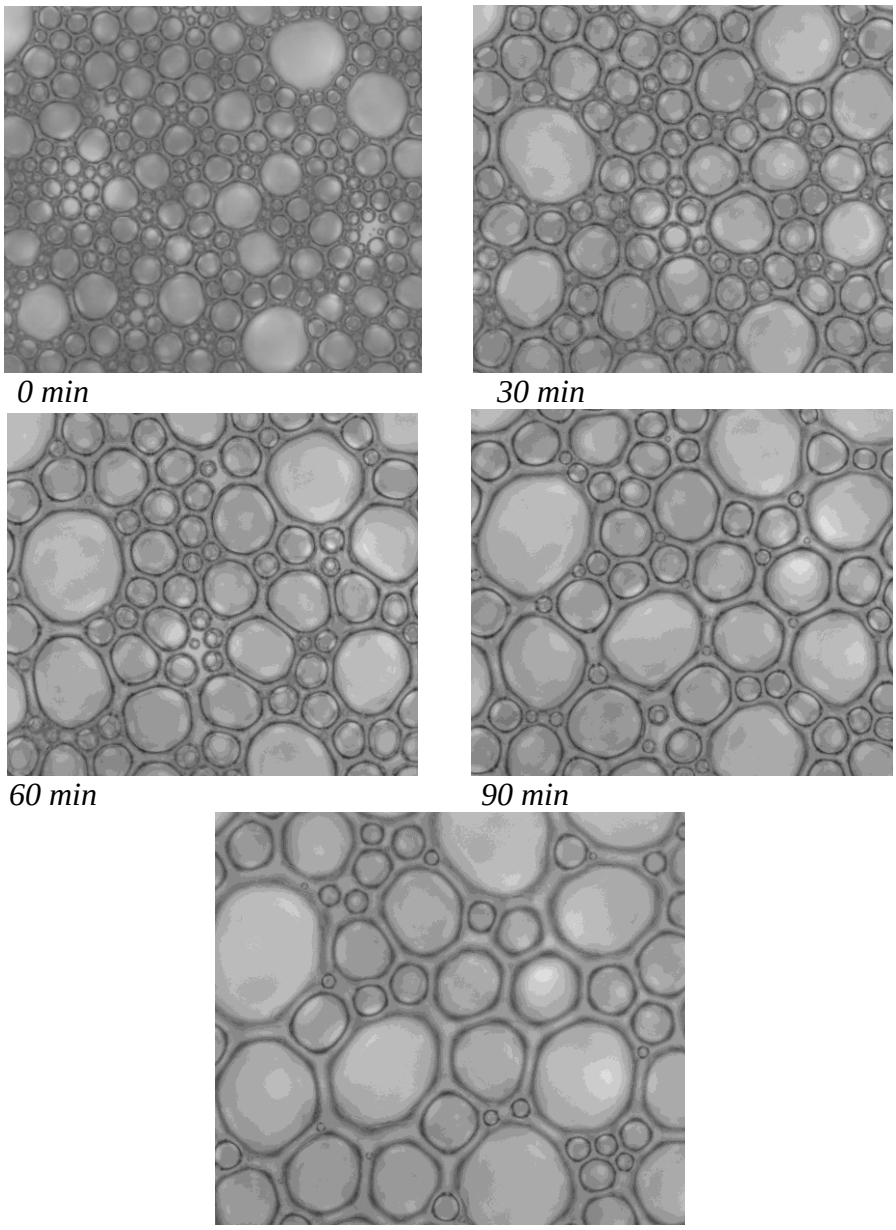

Figure 4.9. Photographs of aging *Gillette* foam of 0.90 void fraction (ρ = 0.084 g/cm^3). Image dimensions 532 μm x450 μm.

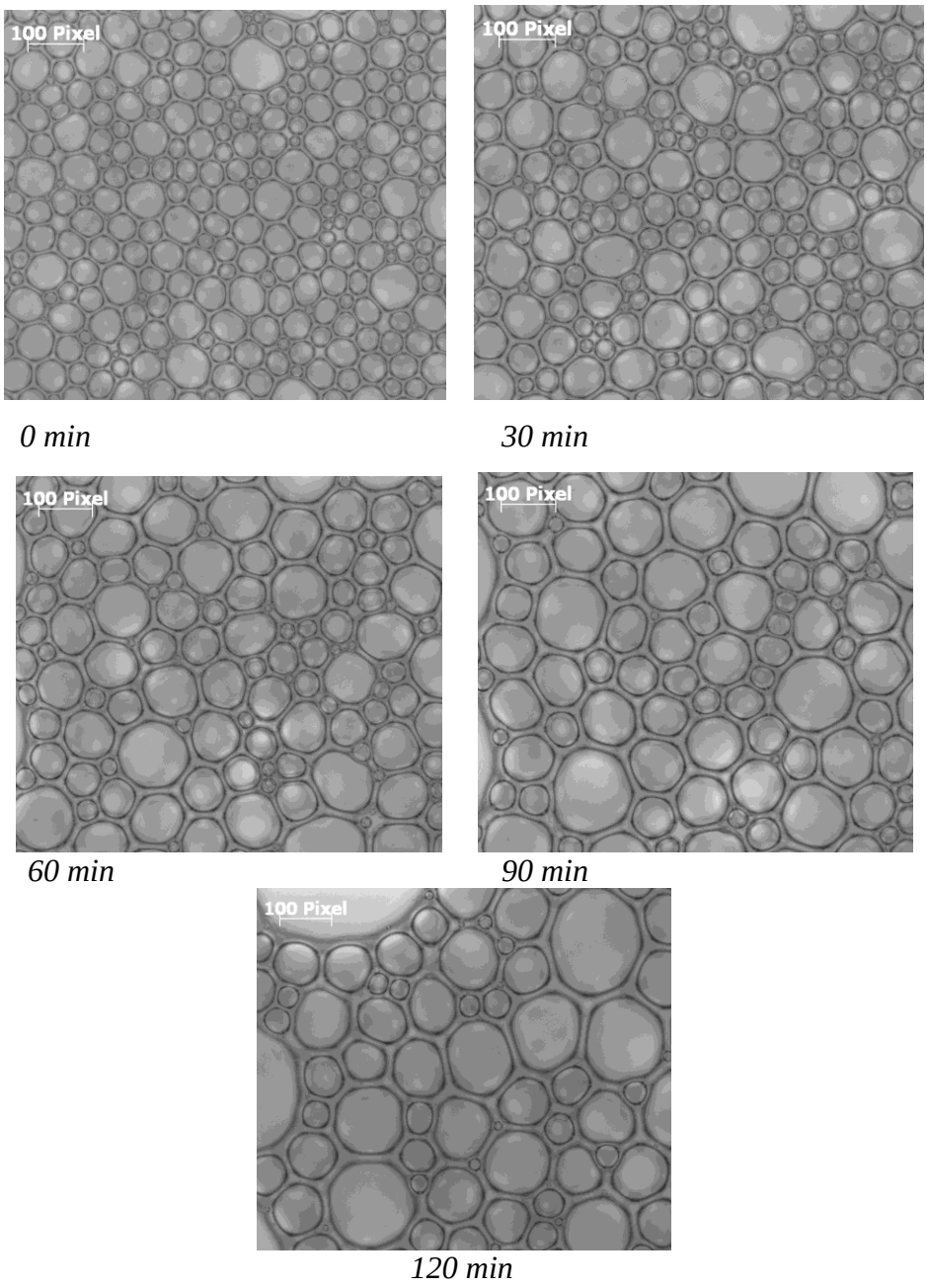

Figure 4.10. Photographs of aging *Gillette* foam of void fraction 0.93 (ρ = 0.064 g/cm^3). Image dimensions 532 μm x450 μm.

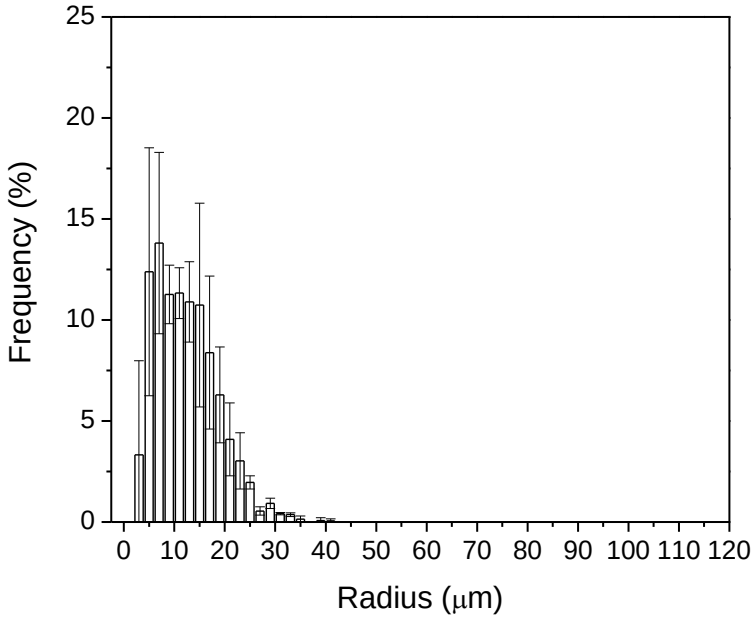

Figure 4.11. Bubble radii distribution in 0.064 g/cm^3 density *Gillette* foamy at 0 min of aging.

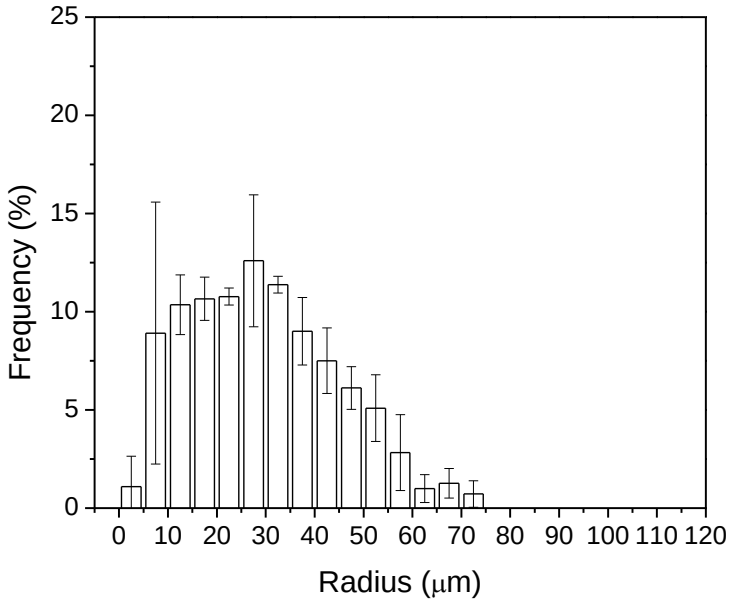

Figure 4.12. Bubble radii distribution in 0.064 g/cm^3 density *Gillette* foamy at 30 min of aging.

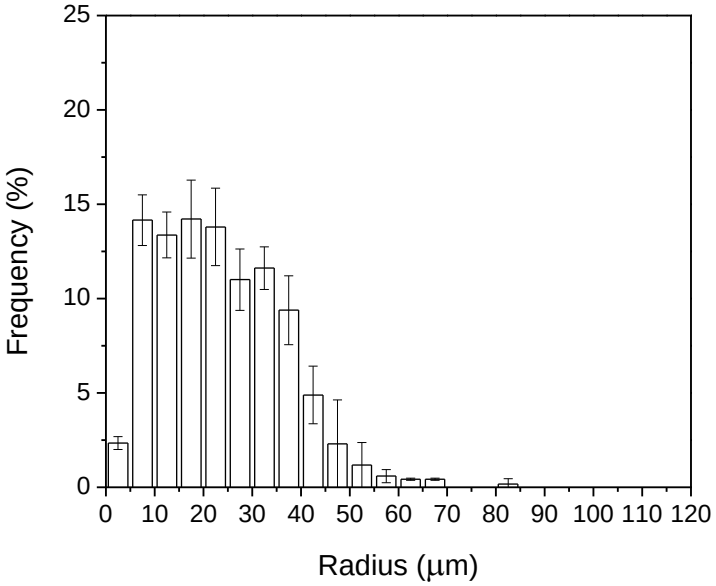

Figure 4.13. Bubble radii distribution in 0.064 g/cm^3 density *Gillette* foamy at 60 min of aging.

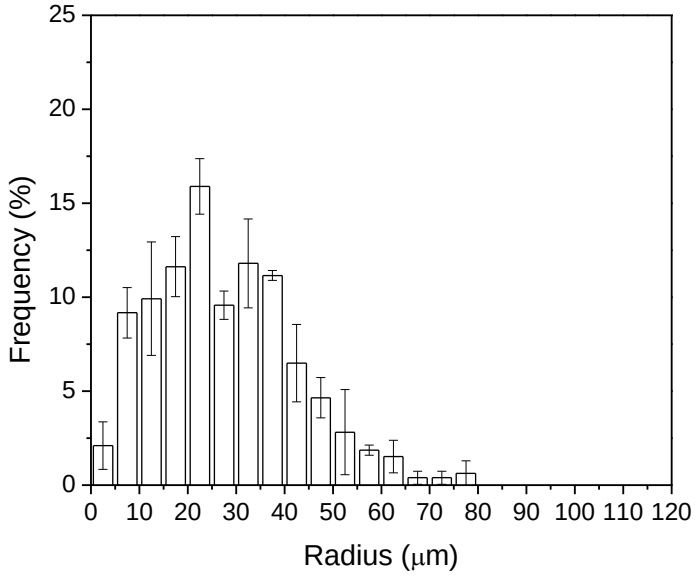

Figure 4.14. Bubble radii distribution in 0.064 g/cm^3 density *Gillette* foamy at 90 min of aging.

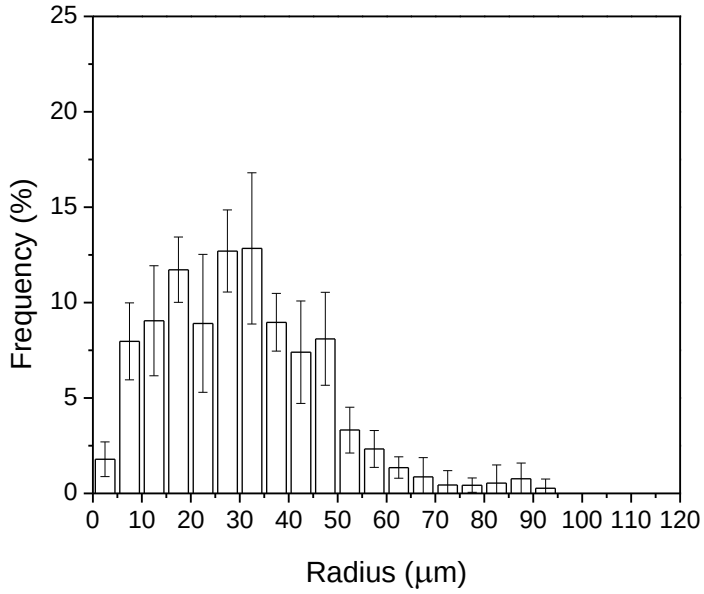

Figure 4.15. Bubble radii distribution in 0.064 g/cm^3 density *Gillette* foamy at 120 min of aging.

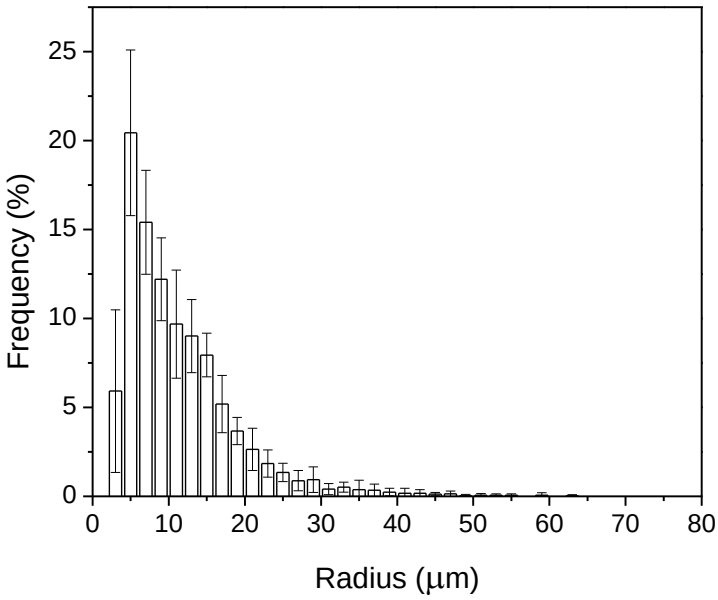

Figure 4.16. Bubble radii distribution in 0.084 g/cm^3 density *Gillette* foamy at 0 min of aging.

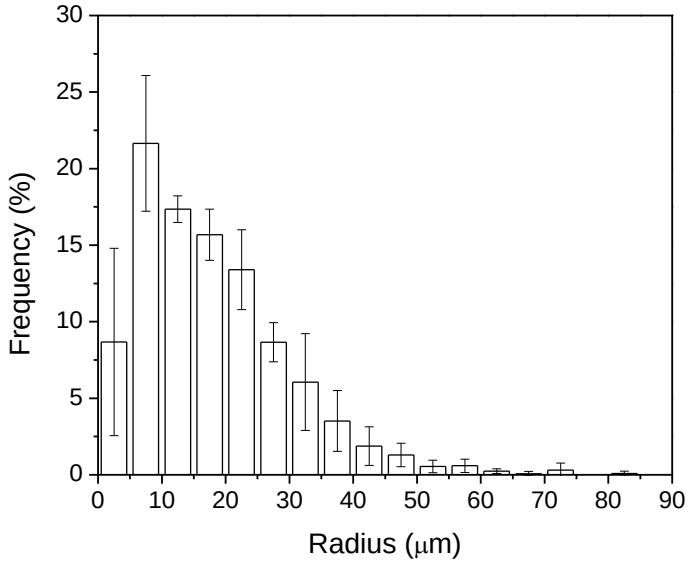

Figure 4.17. Bubble radii distribution in 0.084 g/cm^3 density *Gillette* foamy at 30 min of aging.

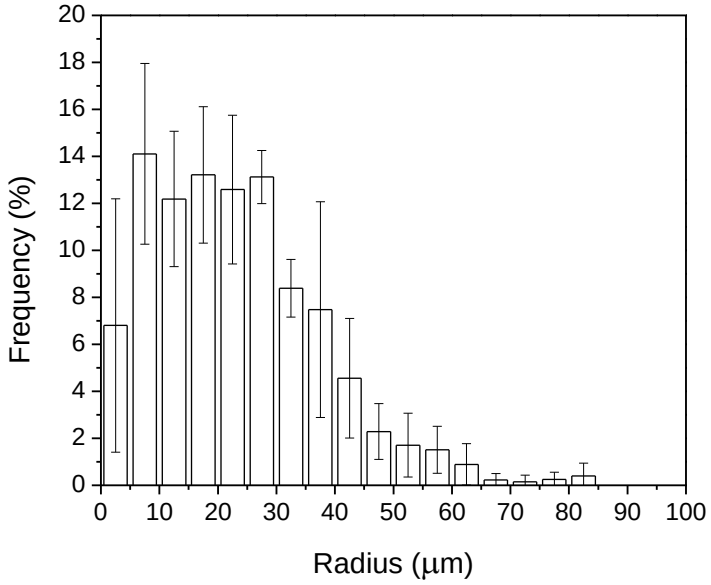

Figure 4.18. Bubble radii distribution in 0.084 g/cm^3 density *Gillette* foamy at 60 min of aging.

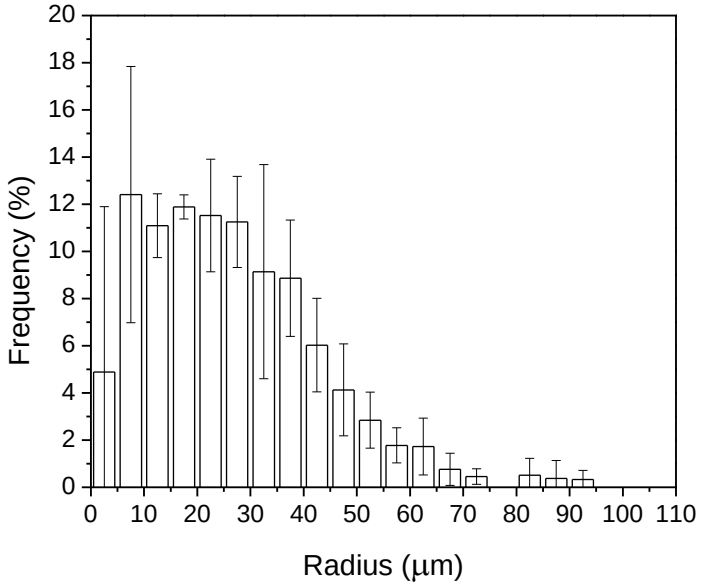

Figure 4.19. Bubble radii distribution in 0.084 g/cm^3 density *Gillette* foamy at 90 min of aging.

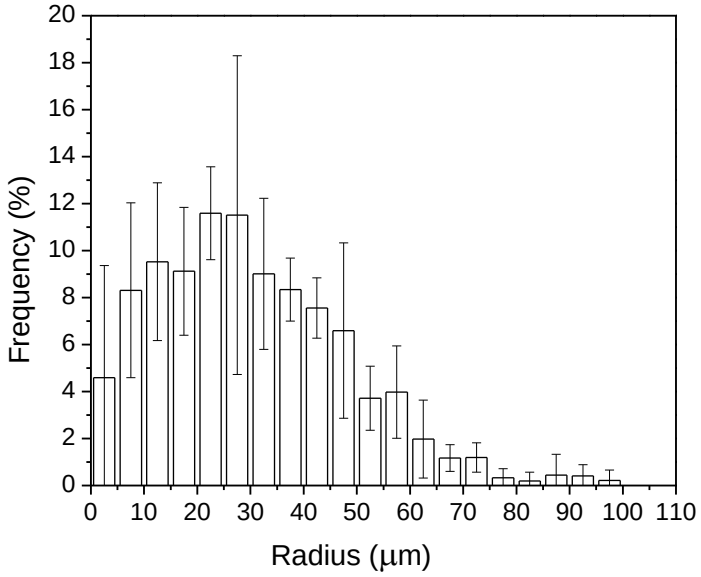

Figure 4.20. Bubble radii distribution in 0.084 g/cm^3 density *Gillette* foamy at 120 min of aging.

In Figure 4.21 and Figure 4.22 the average bubble radius of egg white and *Gillette* foams over aging time is represented. Literature on foam aging states that as a result of the disproportionation process, bubble radius grows in a simple manner, described by a power-law dependence. It is an indicator that a foam has reached scaling behaviour (Durian *et al.*, 1991; Weaire & Hutzler, 1999). Therefore, a power law fit was done to our measured bubble radius of egg white and *Gillette* foams versus aging time plot for all void fractions to validate which foam aging mechanism dominates. For very dry foams, where bubbles are polyhedral, like in a *Gillette* foam, the bubble radius grows as a power law, $t^{0.5}$. In wetter foams, where spherical bubbles exist, bubble radius grows as $t^{1/3}$ (Durian *et al.*, 1991).

Evolution of egg white foam bubble radius with aging time is slower than in a *Gillette* foam and the power law fit (Figure 4.22) shows that: $R \sim t^{0.34}$ for 78 % of air content egg white foam. From image analysis, Spencer (2006) found that in 81 % air content egg white foam, the geometrical mean radius at later aging time evolves as $t^{0.5}$. However at early aging time it was determined that there was a linear dependence of bubble radius with aging time. For the lower void fraction (0.65) egg white foam, the evolution of radius with aging time data was not fit to a power law function, indicating that in a wet foam bubble radius scaling as $t^{0.5}$ is not reached, since disproportionation is not the main bubble growth mechanism (Spencer, 2006). The power law fitting to our experimental values of bubble radius for *Gillette* foam shows scaling of R as $t^{0.4}$ and so it is somewhat in disagreement with theory for a polyhedral foam. However Durian *et al.* (1991) found a similar result: the radius of *Gillette* foam evolved as $t^{0.4}$.

In conclusion, visual inspection of the bubble radius distributions of two differently produced foams, *Gillette* by sparging and egg white by whipping, shows different bubble radius

evolution during foam aging. This difference can be attributed to different mechanisms, with disproportionation dominating in the aging of foams with higher void fractions.

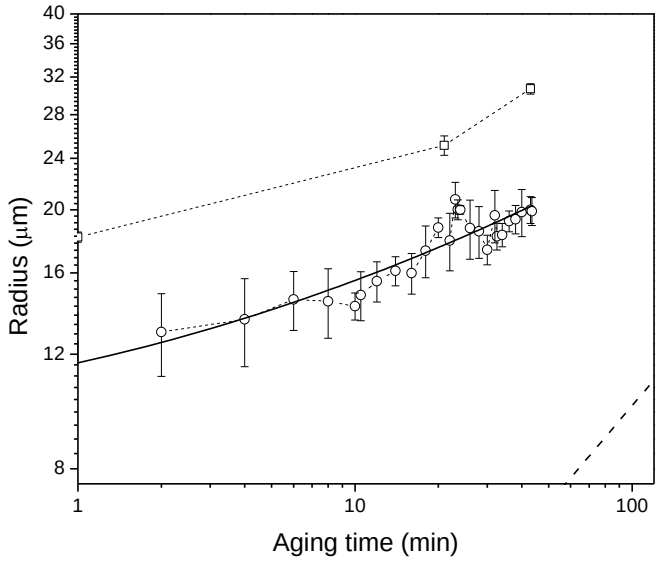

Figure 4.21. Average (arithmetic) bubble radius versus egg white foam aging time determined by image analysis. Symbols represents these two void fractions: −□− $\varphi = 0.68$, -○- $\varphi = 0.78$. The solid line represents a fitted power law expression to $\varphi = 0.78$ void fraction data points, which is $R = 8.3+3.3 \cdot t^{0.34}$ (t-aging time). Error bars represent standard deviation of 3 replicates. The broad dashed line represents a slope of 0.5.

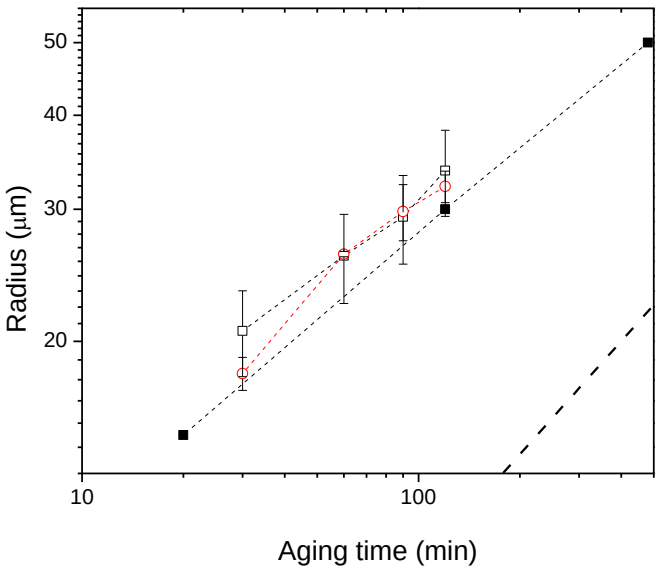

Figure 4.22. Average (arithmetic) bubble radius versus *Gillette* foam aging time determined by image analysis. Symbols represent these void fractions: −□− $\varphi = 0.90$, -○− $\varphi = 0.93$,−■− data from Durian *et al.* (1991). The broad dashed line represents a slope of 0.5, while our data and that of Durian *et al.* (1991) have a slope that is 0.4. Error bars represent standard deviation of 3 replicates.

4.3 Conclusions

The represented results from 2D optical imaging microscopy clearly show scaling behavior in aging egg white and *Gillette* foams. The evolution of the average bubble radius ($\langle r \rangle$) with aging time for egg white 0.78 void fraction foam shows that disproportionation is dominant but it is the only mechanism - the drainage is taking place as well. The bubble mean radius evolution of the comparatively wet 0.65 void fraction foam cannot be described by simple power law behaviour because foam aging is impacted considerably by liquid drainage. For *Gillette* high (0.90 and 0.93) void fraction foams bubble mean radius is proportional to aging time as $t^{0.4}$ and this indicates that disproportionation is the main aging process. Imaging results gives insights into foam aging mechanisms, and remain one of the most feasible though time consuming techniques in research on complex foam.

CHAPTER 5. ACQUISITION OF ULTRASONIC PARAMETERS IN HIGH VOID FRACTION FOAMS

Ultrasonic measurements with foams and extraction of sensible results was comparatively challenging due to several reasons: high signal absorption, complex impedance mismatch between the foam and transducer, and ringing of the ultrasonic transducer itself. In this work with high void fraction foams (φ = 0.65-0.93), 40 kHz narrow bandwidth transducers were used. Therefore, it was possible to extract information from the recorded signal waveform in the 20-40 kHz range. By trial and error the sample thickness through which the ultrasound signal can pass and could be recorded was determined. We were interested in foam aging studies and therefore we aimed to observe foam aging for as long as it was possible to obtain valuable data from ultrasound measurements. Very thin samples, such as those with thickness 0.5 mm, were avoided because with aging in this thin foam layer big bubbles appeared, so that there was the possibility of the ultrasound signal passing through the air directly from one transducer to another, instead of passing through the composite of bubbles and foam matrix. Egg white foam samples with thicknesses greater than 2.5 mm were not used due to high signal absorption. However, we were able to record transmitted signals through *Gillette* sensitive foam samples with the thicknesses as 1.5 mm, 3 mm and 5 mm.

Several difficulties were faced and dealt with in ultrasonic signal analysis. First of all, due to very different foam and transducer density and velocity, there was a large complex impedance mismatch that caused reflection of the signal and that resulted in an offset of the transit time and an offset in amplitude of the ultrasonic signal. The complex impedance mismatch problem is described in detail in Fan (2006). Some of the methods described by Fan

(2006) to correct complex impedance mismatch were used in this work too, and methods are briefly described.

Secondly, difficulty was faced then we tried to measure the signal going through the foam at later aging times. This difficulty arises from several mechanisms, discussed in detail below, that result in a noisy long tail in the signal and this problem was solved by manually truncating the end part of the signal for all recorded waveforms. These noisy long tails were larger relative to the main pulse at long aging times. Therefore, a truncation step was really important at longer aging times in order to study foam properties at all aging times.

In this work, accounting for the earlier mentioned difficulties in measuring ultrasonic signal going through the aging foam, two methods of sample measurement were used: a method where different sample thicknesses were used, and a method where one sample thickness was used, but measurements were acquired alongside a reference signal measurement. An example of a transmitted signal through the foam is given in Figure 5.1.

High complex impedance mismatch resulted in partial signal reflection from the foam contact area with the transducer, and as a result velocity and attenuation coefficient had an offset. In measurements with only one sample thickness, the offset could not be accounted for. Therefore, the different sample thickness method had an advantage over the one sample thickness and reference method, because no complex impedance mismatch correction was needed. However, if we wished to study foam aging processes, we used one sample thickness and needed to correct an offset in order to obtain reliable velocity and attenuation coefficient results (Fan, 2007).

The recorded signal (Figure 5.1) of all samples was first filtered with a bandwidth of 10 kHz using the **Gauss4** program. The **Gauss4** program was written in C by Michael Cowan. The

program first converts a time domain pulse into the frequency domain using a standard FFT algorithm. The complex FFT is multiplied by a Gaussian function centred at the frequency of interest, with a specified bandwidth. After taking the inverse FFT transform, the filtered bandwidth-limited pulse is obtained. An example of a waveform that was filtered using the **Gauss 4** program is shown in Figure 5.1. After filtering the signal, it was easier to identify the first minimum and first maximum of the transmitted signal (Figure 5.2). The **Gauss4** program was used to extract from the recorded ultrasonic signal that contains many frequencies, a waveform of selected frequency range. The transducer's central frequency, i.e., that of the reference signal, was determined to be 40 kHz, however, for foam samples the central frequency was determined to be 37 kHz. Therefore it was decided to analyse data at frequencies around the central frequency at 20 kHz, 25 kHz, 30 kHz, 37 kHz and 40 kHz using bandwidth of 10 kHz.

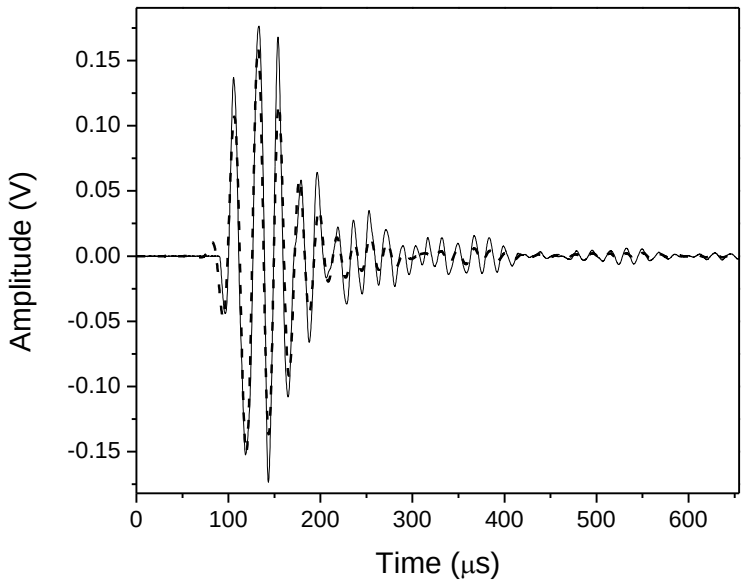

Figure 5.1. Amplitude versus transit time for a filtered reference signal (-----) and an unfiltered signal (line).

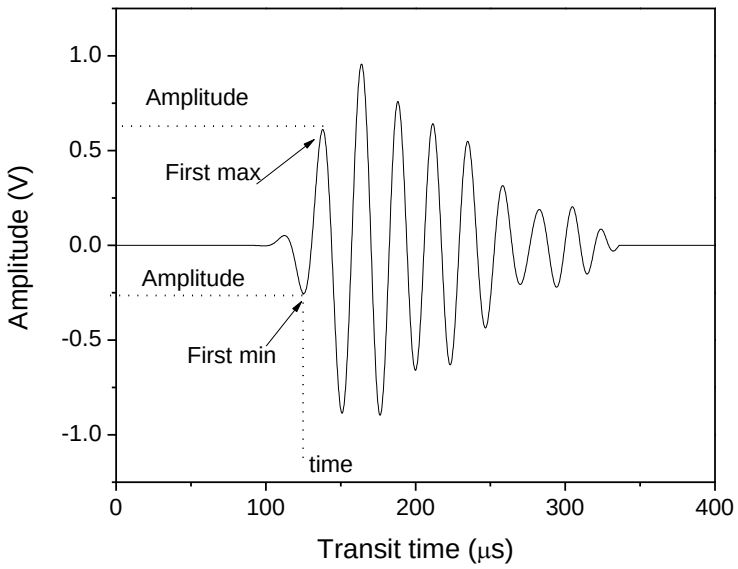

Figure 5.2. Signal transmitted through the 0.65 void fraction foam sample of 1mm thickness at 0 min of aging time. The central frequency and bandwidth were 30 kHz and 10 kHz.

Different sample thickness measurements at 0 min of aging allowed us to acquire the first minimum transit time and the first minimum amplitude as a function of thickness (Figure 5.3 and 5.4). The first minimum and first maximum method was used at the initial experimenting stage. By measuring the signal going through the foam at 0 min of aging time at different sample thicknesses we could determine the initial properties of the foam. Velocity (v) in the sample can be calculated from the first minimum by fitting a linear equation $t_{trans} = A_{off} + B \cdot L$ (t_{trans}- transit time, L-sample thickness, B-slope). So $v=1/B$, (m/s). The offset in transit time (coefficient A_{off} in the equation) can be found from a linear fit through the transit time data plotted versus thickness, Figure 5.3. The attenuation coefficient (α) can be calculated from an exponential decay fit ($A = A_1 e^{(-L/C_{con})}$, where A-amplitude, A_1 - pre-exponential factor, C_{con} is a decay constant, obtained using **Origin** software by fitting an exponential decay function to the data (Figure 5.4)), with the attenuation coefficient, α (mm^{-1}), being $\alpha=2/C_{con}$.

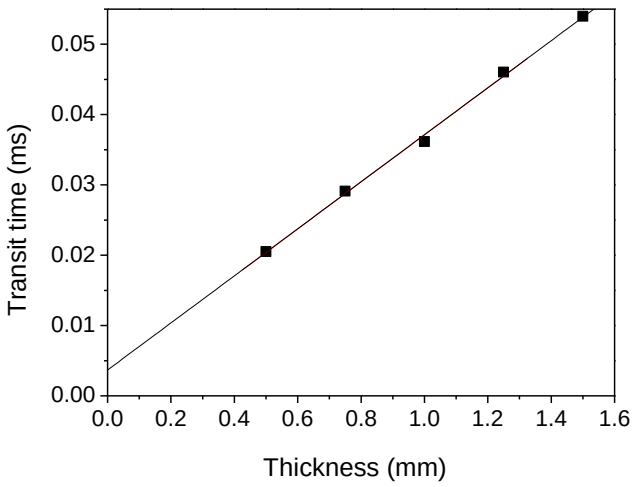

Figure 5.3 Transit time of first minimum as a function of foam sample thickness at 0 min of aging time.

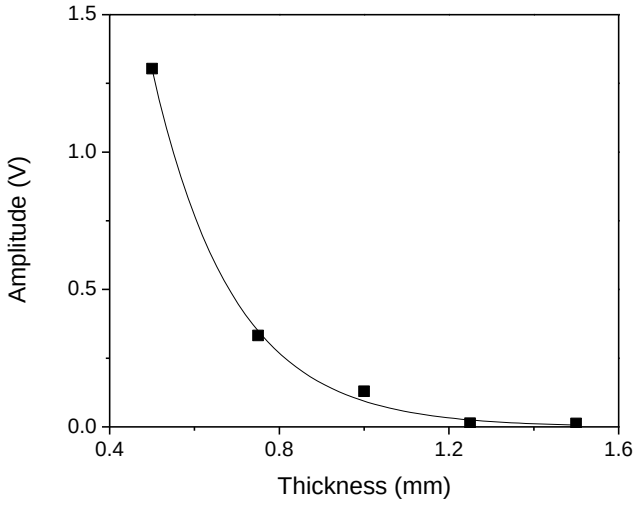

Figure 5.4 Amplitude of first maximum as a function of sample thickness at 0 min of aging time.

Due to changing foam properties with foam aging time, the first minimum and maximum of the signal waveform evolved as well, and became not very clear (Figure 5.5). Therefore the ability to measure the peak of the first minimum and first maximum in order to determine transit time and amplitude was not always feasible. For this reason, we decided to use all the information in the waveform by transforming the signal from the time domain into the frequency domain by using the **fftfull** algorithm, so that plots of phase and amplitude versus frequency are

obtained. In order to understand how phase and amplitude information relate to velocity and attenuation coefficient, a reference signal must be acquired with the foam measurements. For this reason, these frequency domain measurements are referred to as the reference method.

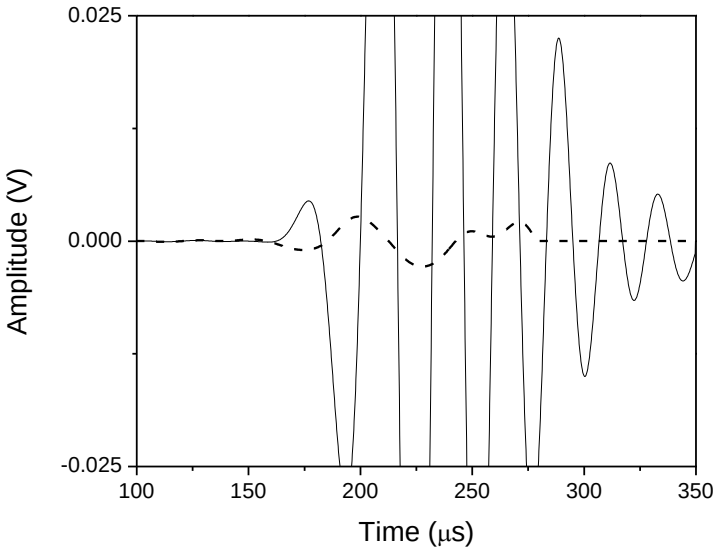

Figure 5.5. Waveform of the filtered signal of 0.65 void fraction foam, 2.5 mm thickness. Solid line represents signal at 0 min of aging, ----- represents signal after 43 min of aging.

The reference measurement method was used in all foam aging experiments in order to assess changing foam properties with time. A reference signal, as well as sample signals were first filtered using the **Gauss 4** program and truncated. For the longer aging times, the reduction in pulse amplitude meant that stray signal propagating along the plastic holder from one transducer to another distorted the received pulsed somewhat. In addition, at long aging time, foam drainage could alter the extent of coupling between the foam and the lower transducer compared to the upper transducer.

Truncation was done individually to every chosen waveform because the velocity in foam changes and the shape of the waveform also changes due to frequency-dependent attenuation increase that modifies the pulse bandwidth. As well, the complex impedance changes of the

sample with aging, so that coupling of the signal from one transducer to the other transducer changes too**.** At earlier aging times, the tail part of the signal is due to mainly transducer ringing. At later aging times, the main pulse becomes smaller due to increased attenuation and because of changes in the complex impedance, transducer and foam coupling is different and ringing can increase. Also at later aging times the tail part of the signal can be somewhat contaminated by spurious signal through the transducer holders. The truncation point (Figure 5.6) was chosen somewhat arbitrarily, leaving a similar number of wave oscillations and truncating the distorted waveform end using a truncation program script written in MATLAB. The truncation procedure eliminated from the signal waveform ringing of the transducer and the effects of the three previously mentioned mechanisms associated with changing foam properties and foam contact with transducer effects.

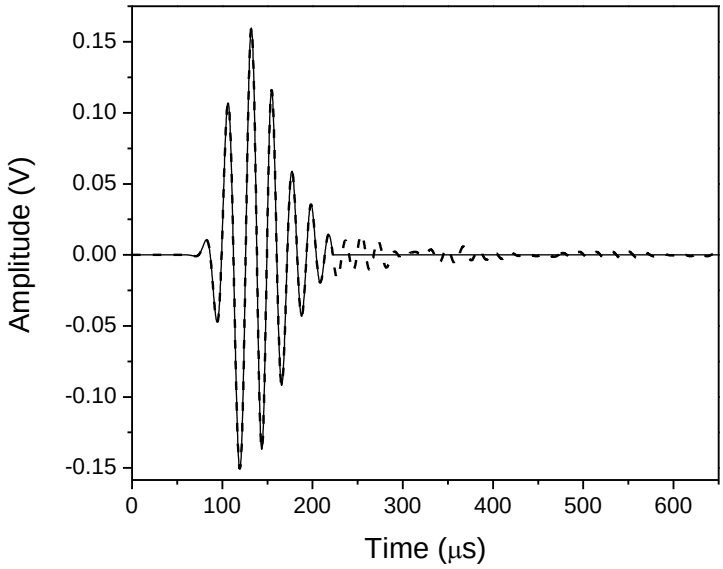

Figure 5.6 Filtered reference signal (-----) and truncated signal (line).

The filtered and truncated signals were converted into the frequency domain by using the Fast Fourier Transform (FFT) program **fftfull**. From this transformation we got phase (Figure 5.7) versus frequency and amplitude (Figure 5.8) versus frequency.

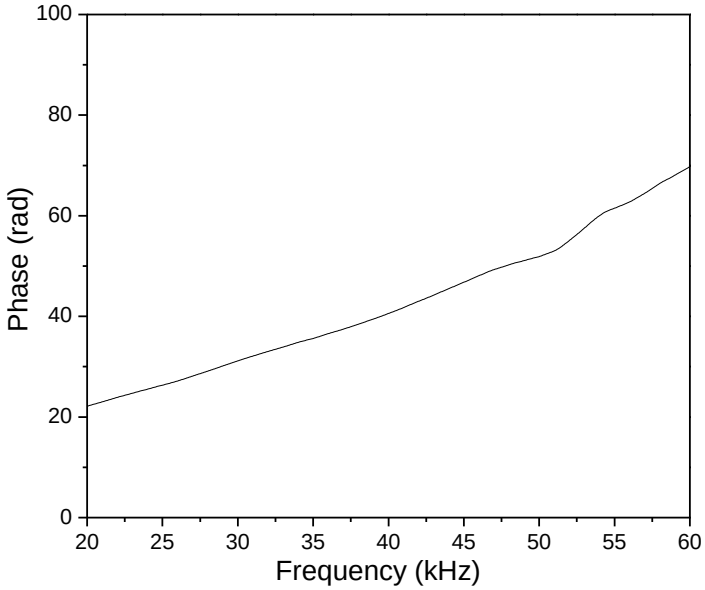

Figure 5.7. The phase as a function of frequency of the ultrasonic signal (0 min of aging, 0.65 void fraction egg white foam).

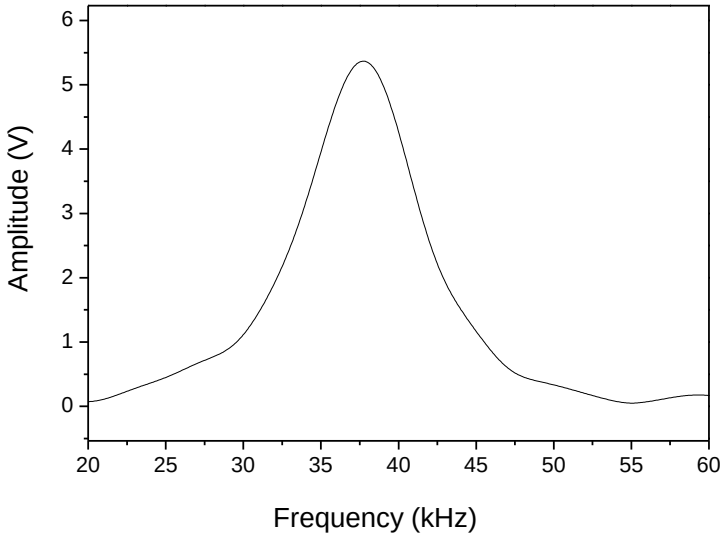

Figure 5.8. The amplitude as a function of frequency of the ultrasonic signal (0 min of aging, 0.65 void fraction egg white foam).

We determined phase velocity from the phase versus frequency dependence in the following way. Phase velocity was calculated using the formula (Fan, 2006):

$$v_p = \frac{2\pi f L}{\Delta\Phi} = \frac{L}{\Delta t} \tag{5.1}$$

where: f - frequency in Hz, L – sample thickness, $\Delta t = t_{sam} - t_{ref}$. According to Formula 5.2 and 5.3, from the phase information of the sample and reference signals time was calculated (Fan, 2006):

$$t_{sam} = \frac{\Phi_{sam}}{2\pi f} \tag{5.2}$$

$$t_{ref} = \frac{\Phi_{ref}}{2\pi f} \tag{5.3}$$

where: f - frequency in Hz; Φ_{sam}, Φ_{ref} – phase in radians obtained from sample and reference measurements; t_{sam}, t_{ref} - the transit time in seconds obtained from phase (Φ) for the sample and reference signal.

The acoustic signal going through the foam sample had an amplitude that was measured at 0 dB attenuation whereas the reference signal amplitude was measured at 80 dB, therefore we recalculated the amplitude of the foam sample to ΔdB = 80 dB attenuation using this general formula (Fan, 2006):

$$A = \frac{A_{sam}}{A_{ref}} 10^{-\Delta dB/20} \tag{5.4}$$

The attenuation coefficient $\alpha(t)$ at a time t for aging foam was calculated using this formula (Fan, 2006):

$$\alpha(t) = \frac{2}{L} ln\left(\frac{A_{sam}(t)}{A_{ref}}\right) \tag{5.5}$$

where $A_{sam}(t)$ is amplitude at aging time (t), and A_{ref} is reference amplitude, L - sample thickness (mm).

An offset problem caused by time dependent impedance mismatch existed in the reference method too and it caused discrepancies in phase velocity and attenuation coefficient. Therefore in order to estimate an offset in the attenuation coefficient, $\alpha(t)\cdot L$ was plotted versus sample thickness (L) for each selected frequency and each aging time. An example is shown in Figure 5.9. The fitted linear equation gives us the dependence: $\alpha(t)\cdot L = B\cdot L + a$, thus the offset in attenuation coefficient is a/L. A corrected attenuation was obtained by subtracting the offset from each measured $\alpha(t)$ value. An offset in phase velocity is calculated by plotting transit time t_{sam} obtained from phase (Formula 5.2) versus sample thickness. The intercept of the plotted linear equation gives the offset value.

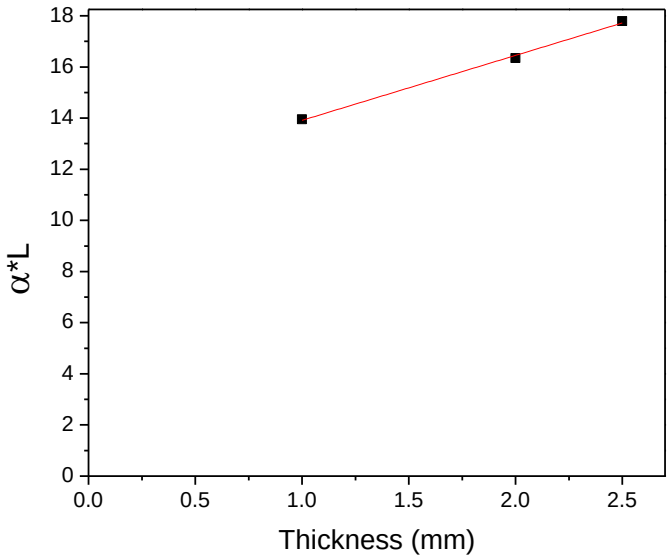

Figure 5.9 $\alpha\cdot L$ plotted versus thickness in order to estimate the offset in attenuation coefficient, at 37 kHz, at 6min of aging (0.65 void fraction egg white foam).

After correcting the offsets, the phase velocity and attenuation coefficient for different sample thicknesses was the same for a foam of given density and aging time, as can be seen for the example of an egg white foam at 20 kHz (Figures 5.10 and 5.11).

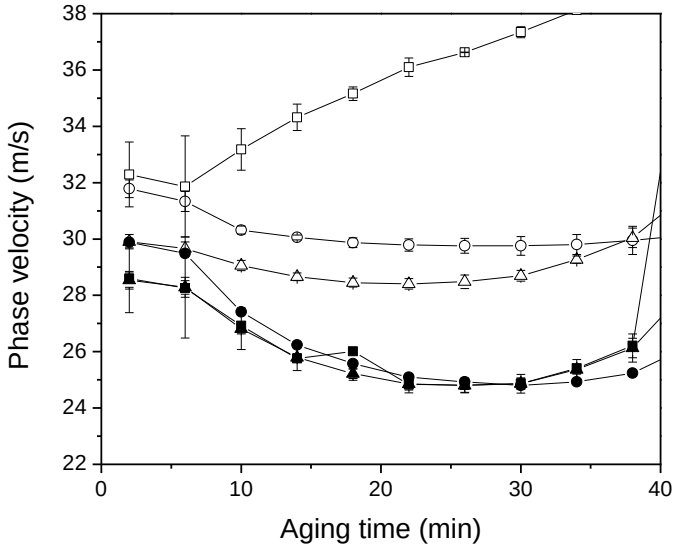

Figure 5.10. Phase velocity versus aging time for 0.78 void fraction foam at 20 kHz. Symbols represent uncorrected phase velocity for different thicknesses: -□- 1 mm, -○- 2 mm, -△- 2.5 mm; corrected phase velocity for different thicknesses: -■- 1 mm, -●- 2 mm, -▲- 2.5 mm.

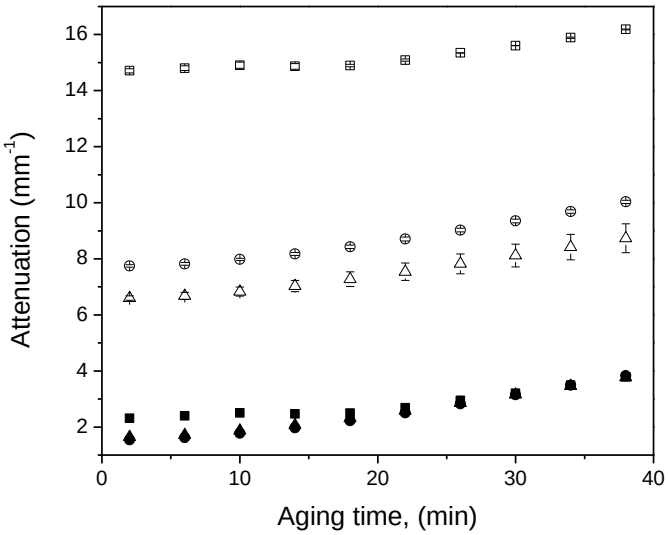

Figure 5.11. Attenuation coefficient versus aging time for 0.78 void fraction foam at 20 kHz for different thicknesses. Symbols represent uncorrected attenuation coefficient for different thicknesses: -□- 1 mm, -○- 2 mm, -△- 2.5 mm; corrected attenuation coefficient for different thicknesses: -■- 1 mm, -●- 2 mm, -▲- 2.5 mm.

CHAPTER 6. TIME-DEPENDENT ULTRASOUND MEASUREMENTS IN HIGH VOID FRACTION FOAMS

6.1 Experimental results and interpretation

Experimental data on two void fraction egg white foams was obtained at four frequencies: 20 kHz, 25 kHz, 30 kHz and 40 kHz. In Figures 6.1-6.4 phase velocity and attenuation coefficient results versus foam aging time are displayed. At 0 min aging time for the 0.65 void fraction foam, the phase velocity is around 26.5 m/s and does not vary significantly with aging time. For the 0.78 void fraction foam, phase velocity is roughly 28 m/s and is higher than for the drier foam at 0 min of aging time (Figure 6.2). The phase velocity of the higher void fraction foam reduces down to 26 m/s by 20 min of aging and further foam structure changes do not have an impact on phase velocity (Figure 6.2). The attenuation coefficient shows strong dependence on frequency and aging time for both foams (Figure 6.3 and 6.4).

In Figure 6.5 and Figure 6.6 is represented *Gillette* (Sensitive) foamy phase velocity and attenuation coefficient data for two void fractions: 0.93 and 0.90. It is clear that the two void fraction Gillette foamy samples are very similar; therefore the difference in phase velocity and attenuation coefficient magnitudes is very small. For the 0.90 and 0.93 void fraction *Gillette* foamy, phase velocity starting values are 52 m/s and 57 m/s and reduce to 38 m/s and 42 m/s after 120 min, respectively. Phase velocity is frequency independent at all aging times, but the attenuation coefficient for both void fractions *Gillette* foamy is strongly frequency dependent and sharply increases with aging time. Our measured phase velocity values are a little smaller than those that Mujica and Fauve (2002) have measured: at 5 kHz for 0.076 g/cm^3 density *Gillette* (Original) foam, the phase velocity at 0 min aging time was 65 m/s, while at the frequencies of 37 kHz, 63 kHz and 84 kHz a velocity of 50 m/s was observed. In our research only *Gillette*

Sensitive shaving foam was used, while Mujica and Fauve (2002) were using *Gillette* Original shaving foam, so acoustic differences due to composition differences might be expected (with the composition of *Gillette* Sensitive and *Gillette* being described in Chapter 3).

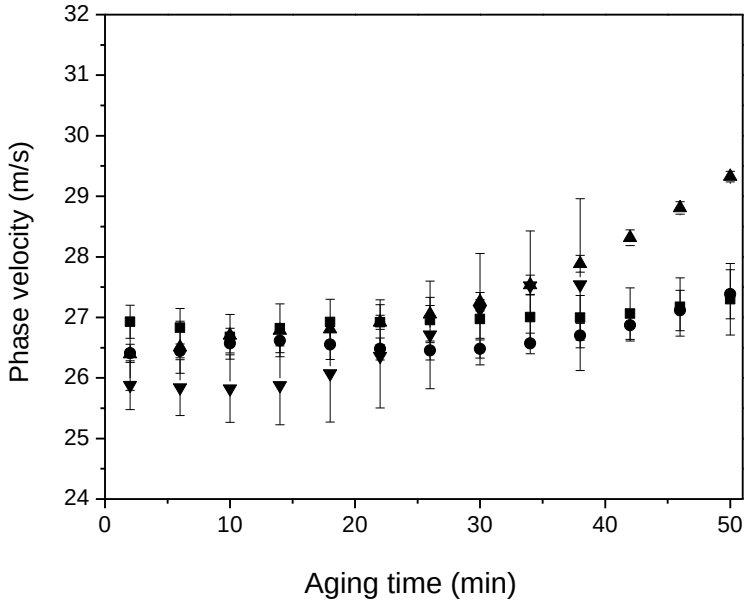

Figure 6.1. Phase velocity versus aging time of 0.65 void fraction egg white foam. The symbols represent these frequencies: ■ 20 kHz, ● 25 kHz, ▲ 30kHz, ▼ 40 kHz.

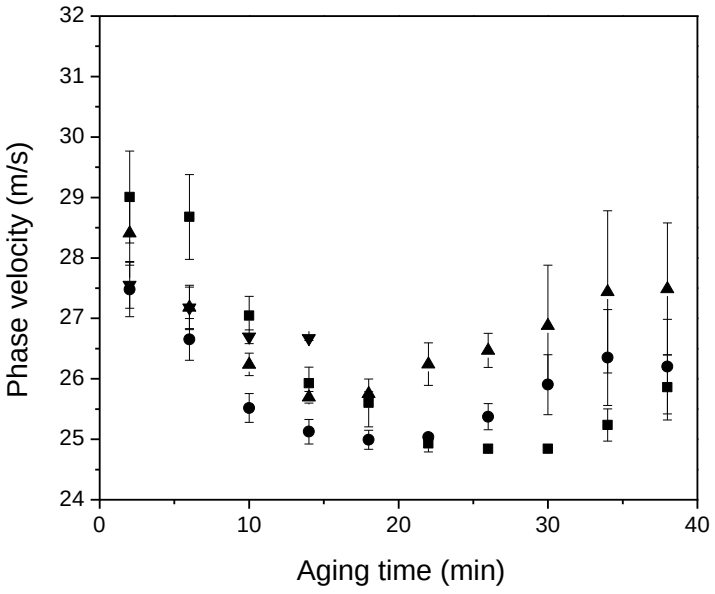

Figure 6.2. Phase velocity versus aging time of 0.78 void fraction egg white foam. The symbols represent these frequencies: ■ 20 kHz, ● 25 kHz, ▲ 30 kHz, ▼ 40 kHz.

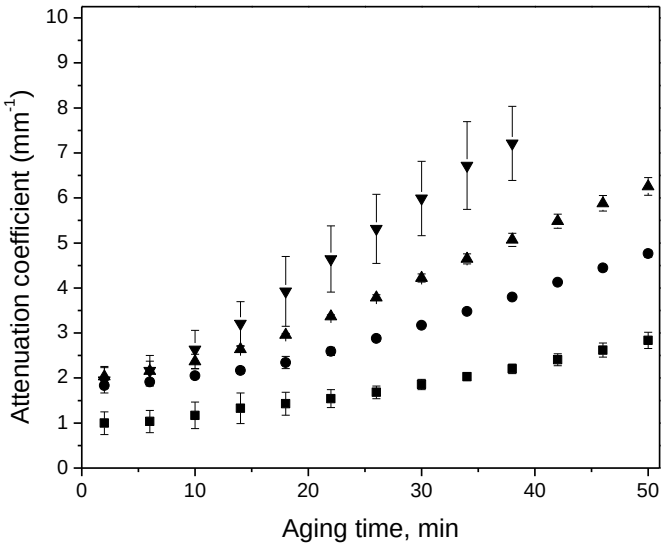

Figure 6.3. Attenuation versus aging time of 0.65 void fraction egg white foam. The symbols represent these frequencies: ■ 20 kHz, ● 25 kHz, ▲ 30 kHz, ▼ 40 kHz.

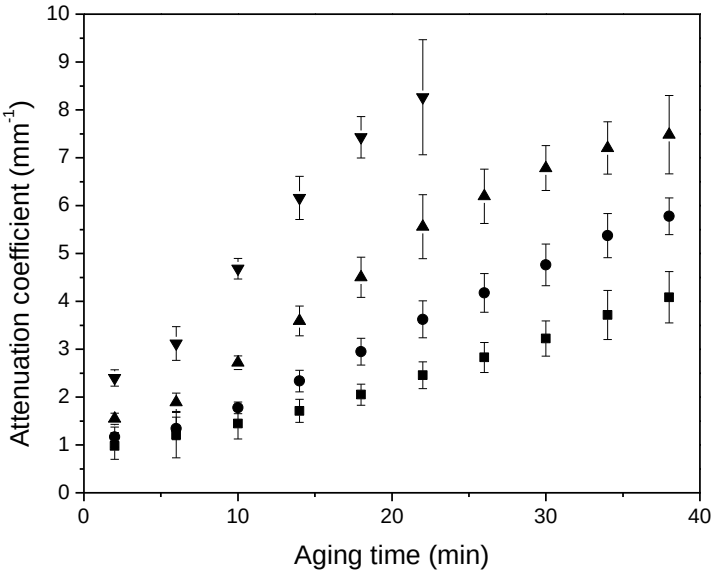

Figure 6.4. Attenuation versus aging time of 0.78 void fraction egg white foam. The symbols represent these frequencies: ■ 20kHz, ● 25 kHz, ▲ 30 kHz, ▼ 40 kHz.

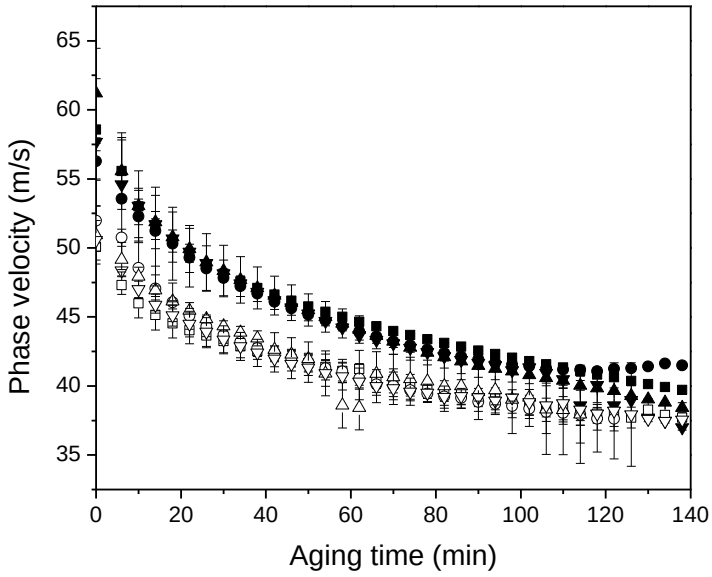

Figure 6.5. Phase velocity versus aging time for *Gillette* foamy. The closed symbols represent $\varphi = 0.93$ ($\rho = 0.064$ g/cm^3) *Gillette* foamy: ■ 25 kHz, ● 30 kHz, ▲ 37 kHz, ▼ 40 kHz. Open symbols represent $\varphi = 0.90$ ($\rho = 0.084$ g/cm^3) *Gillette* foamy: ▫ 25 kHz, ○ 30 kHz, △ 37 kHz, ▽ 40 kHz.

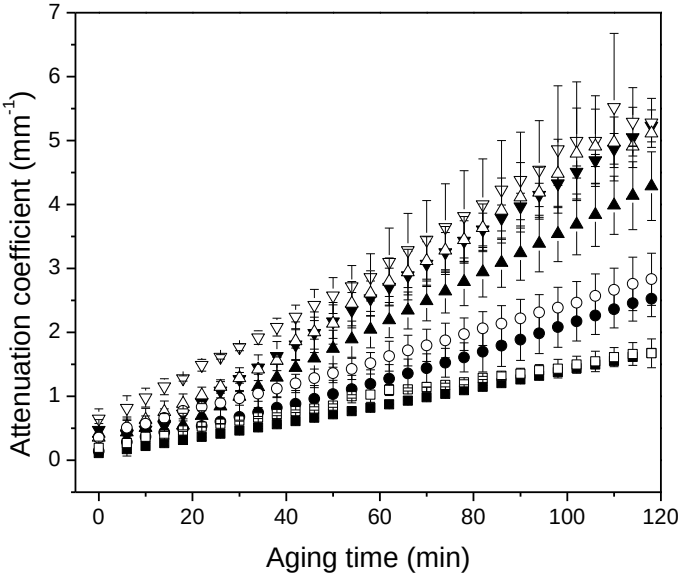

Figure 6.6. Attenuation versus aging time for *Gillette* foamy The closed symbols represent $\varphi = 0.93$; $\rho = 0.064$ g/cm^3 *Gillette* foamy: ■ 25 kHz, ● 30 kHz, ▲ 37 kHz, ▼ 40 kHz. Open symbols represent $\varphi = 0.90$; $\rho = 0.084$ g/cm^3 *Gillette* foamy: ▫ 25 kHz, ○ 30 kHz, △ 37 kHz, ▽ 40 kHz.

6.2 Interpretation of velocity results according to foam compressibility

To interpret our results, available theories will be used, based on the fundamental physics of wave propagation in materials. Sound propagation in a solid material is influenced by density and elastic modulus, which relates stress and strain in the material. Standard elasticity theory leads to the following relation for the longitudinal velocity of sound in a homogenous material (Povey, 1997):

$$v_L = \sqrt{\frac{\beta}{\rho}} \tag{6.1}$$

where β is the longitudinal modulus of the homogeneous material and ρ is the density. For homogenous liquids and gasses, as for example water or air, $\beta = \frac{1}{\chi}$, where χ is the compressibility of the material. For viscoelastic materials, the complex shear modulus (G) is a component of the longitudinal modulus and is frequency dependent, so that $\beta = \frac{1}{\chi} + \frac{4}{3}G$ and $G(\omega) = G'(\omega) + iG''(\omega)$.

The sound wave propagation in bubbly liquids also depends on the density (ρ_l) and adiabatic compressibility (χ_l) of the non-aerated liquid, as well as on the density and compressibility of the gas in the bubbles. The sound velocity can be expressed by Equation 6.1 but it will depend at low frequencies, on the mean density and mean compressibility of the two components, also called the effective density (ρ_{eff}) expressed by formula 6.2, and the effective compressibility (χ_{eff}) expressed by formula 6.3 (Wood, 1941). In a bubbly liquid or foam, the compressibility of a bulk liquid, like water, and air are very different: $\chi_{water}=3.5\cdot10^{-10}$ Pa and $\chi_{gas}=1\cdot10^{-5}$ Pa, respectively (Fine and Millero, 1973). As well, the density of gas and water are different too. Therefore changes in gas content of bubbly liquids and foams dramatically alter the effective density and compressibility, and therefore the velocity (Povey, 1997).

$$\rho_{eff} = (1 - \varphi) \cdot \rho_l + \varphi \cdot \rho_{gas} \tag{6.2}$$

$$\chi_{eff} = (1 - \varphi) \cdot \chi_{liq} + \varphi \cdot \chi_{gas} \tag{6.3}$$

Physicist Wood (1941) is credited with introducing this model for the effective density and compressibility, and hence explaining why the low frequency velocity of sound in bubbly liquids is so small. Therefore, further on in discussion, we will call the low frequency velocity of sound in bubbly liquids Wood's velocity (v_w):

$$v_w = \sqrt{\frac{1}{\rho_{eff} \cdot \chi_{eff}}} \tag{6.4}$$

In Figure 6.7, the Wood's velocity calculated from Formula 6.4 is presented as a function of void fraction. Also in the figure are the measured velocities for *Gillette* and egg white foams.

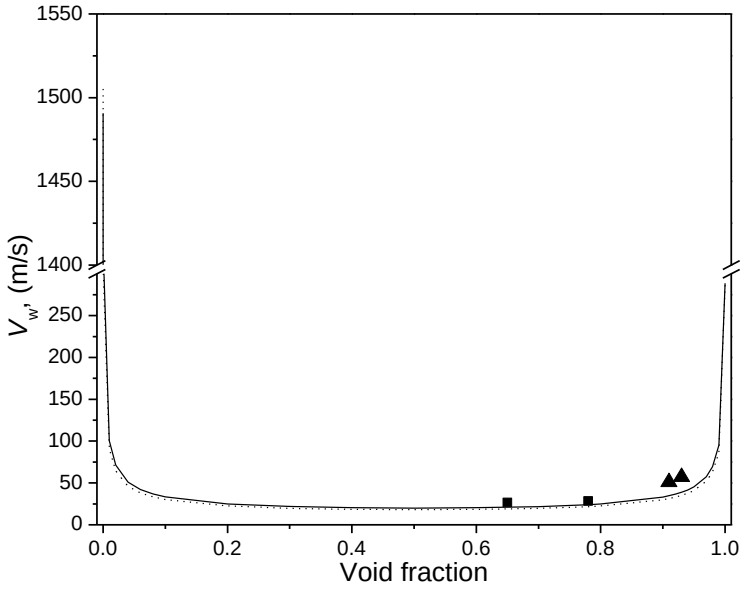

Figure 6.7. Simulated (according to Formula 6.4) Wood's velocity in egg white (·····) and Gillette (——) foam. Measured experimental values of egg white (at 37 kHz) (■) and *Gillette* (at 40 kHz) (▲) foams, where χ_{liq} = $3.5 \cdot 10^{-10}$ Pa, χ_{gas} = $1 \cdot 10^{-5}$Pa, ρ_{eggliq} = 1.226 g/cm^3, $\rho_{Gilletliq}$ = 1 g/cm^3. For the egg white foam of void fraction φ = 0.65, $v_{EggWood}$ = 18.9 m/s, and for φ = 0.78, $v_{EggWood}$ = 22 m/s. For *Gillette* foamy with φ = 0.90, $v_{GillWood}$ = 35 m/s and for φ = 0.93, $v_{GillWood}$ = 39 m/s.

As a starting point, we used Wood's model for interpretation of sound velocity in our foams. Sound velocity measured in egg white or *Gillette* foams is 26 m/s (φ = 0.65) and 52 m/s (φ = 0.90), respectively, and an average bubble size is around 14 μm for both foams. The wavelength for the 26 m/s and 56 m/s velocities at 40 kHz is 650 μm and 1400 μm, respectively. So we can consider that our experiments are conducted in the large wavelength regime where the waves sense the average properties of the medium, so that the effect of individual bubbles on sound wave propagation is not evident (Fan, 2007).

However, bubbly liquids and foams are very different materials in terms of mechanical properties, with the latter displaying solid-like characteristics (Cohen-Addad *et al*, 1998; Weaire and Hutzler, 1999; Murray and Ettelaie, 2004). Measured and calculated velocity values according to Wood's formula for egg white foam are 18.9 m/s (φ = 0.65) and 22 m/s (φ = 0.78), while measured phase velocities are 26.5 m/s and 28 m/s, respectively. For *Gillette* (Sensitive) foamy, Wood's velocities are 35 m/s (φ = 0.90) and 39 m/s (φ = 0.93), while we measure 52 m/s and 58 m/s, respectively. For both foams, the measured velocity is higher than that predicted by Wood`s velocity. In addition, with aging time, phase velocity for both foams moderately reduces. Mujica and Fauve (2002) showed that in *Gillette* (Original) foamy, the void fraction does not change over 2 hours of aging, so that there are no density changes and therefore Wood's model is not able to explain a change in foam velocity over aging time.

The Wood's approximation (equation 6.4) gives a simple estimate of the velocity of sound in foams, and shows why one would expect that the sound velocity in a foam is much less than the velocity of sound in either constituent material (liquid and air). However, there are many limitations to this simple effective medium approach, so that quantitative agreement with measured values of the sound velocity is not expected. Wood's model does not take into account

attenuation effects, and thus the influence of large attenuation on velocity, that can also lead to a frequency dependence, is not included (Povey, 1997). Therefore, sound dissipation associated with a large gas volume (Leighton, 1996), that causes high sound attenuation in foams, is absent. As well, Wood's equation for the velocity is valid only at low frequencies, and does not take into consideration the bubble size distribution in non-homogeneous materials such as foams; instead, the total gas volume in the mixture is the relevant parameter (Equations 6.2-6.4). These are two of the main disadvantages in the use of Wood's model for describing the velocity of sound in foams.

6.3 Interpretation of the results according to a second effective medium approach

We examined whether the approach of Mujica and Fauve (2002) would explain our experimental results for both foams. Mujica and Fauve (2002) based their analysis on an effective medium model, described in more detail in the next section, that considers the scattering of acoustic waves from bubbles in a liquid to determine the complex wave number *k* in the low gas volume fraction limit. It is important to mention that the resulting dispersion relation of the acoustic waves takes into account the bubble size distribution and encompasses a wave damping constant, which is a sum of viscous, thermal and radiation damping constants (Leighton, 1996). Mujica and Fauve (2002) examined contributions of each damping constant to the high attenuation in foams, and concluded that for air–water mixtures of 10 μm bubbles the thermal damping constant is dominant at 40 kHz. At low frequencies, if $\eta_v \to 0$ ($\eta_v = \frac{2r}{\sqrt{\frac{2D_{th}}{\omega}}}$, η_v – variable, D_{th} - gas thermal diffusivity, r - radius), then attenuation due to thermal damping, α_{th}, is given by:

$$\alpha_{th}\lambda \to \frac{4\pi\omega r^2}{3D_{th}} \tag{6.5}$$

and at high frequencies for $\eta_v \to \infty$

$$\alpha_{th}\lambda \to \frac{3\pi(\Upsilon-1)}{2}\sqrt{\frac{2D_{th}}{\omega r^2}} \tag{6.6}$$

where α_{th} is the thermal contribution to attenuation, λ - wave length, ω - angular frequency, D_g - gas thermal diffusivity, r - radius of the bubble, Υ is the ratio of specific heat capacities for air.

From experimental observations of $\alpha\lambda$ versus aging time, Mujica and Fauve (2002) observed that $\alpha\lambda$ increases with aging time and with frequency. After 20 min of foam aging, they found $\alpha\lambda$ evolution was linearly proportional to aging time *t*. Knowing that in this dry *Gillette* (Original) foam, disproportionation is the only process that makes bubbles grow, Mujica and Fauve (2002) compared $\alpha\lambda$ evolution with the parabolic growth law of the average bubble squared radius ($\langle r\rangle^2$) where both quantities have the same time scale, which is foam aging time. Since both $\alpha\lambda$ and $\langle r\rangle^2$ varied linearly with *t*, Mujica and Fauve (2002) concluded that $\alpha(t)\lambda(t) \propto \langle r(t)\rangle^2$. After suppressing the frequency dependence of $\alpha\lambda$, Mujica and Fauve (2002) obtained the result that $\alpha\lambda/f \propto \langle r\rangle^2$. Mujica and Fauve (2002) justified their conclusion that $\alpha\lambda/f$ is proportional to mean bubble radius squared ($\langle r\rangle^2$) at low frequencies, based on noting that thermal damping in the foam was expected to be dominant (equation 6.5) and other contributions at that low frequency range are small. We tried to apply this idea of scaling $\alpha\lambda/f$ and r^2 with aging time to our foams.

The attenuation coefficient and velocity data for the two foams shown in Figures 6.1 to 6.6 were used to calculate the parameter $\alpha\lambda/f$ for our egg white and *Gillette* foamy data. The ability to reduce the data by this procedure is shown in Figures 6.8 - 6.11. A comparison of the $\alpha\lambda/f$ parameter as a function of egg white foam aging time shown against the change in bubble

size, determined by image analysis, is shown in Figures 6.12 and 6.13. From these figures we found that the slopes of $\alpha\lambda/f$ and r^2 versus aging time vary as $11\cdot10^{-8}$ and $6\cdot10^{-8}$ for 0.78 and 0.65 void fraction foam, respectively. These results show that in the higher void fraction egg white foam, the bubble size changes almost two times faster than in the lower void fraction. In Figure 6.14 and Figure 6.15, $\alpha\lambda/f$ and bubble radius r^2 against aging time is displayed, averaged over all frequencies, for *Gillette* foamy. The slopes are similar for both *Gillette* foam void fractions (0.93 and 0.91) at a value of $1.5\cdot10^{-8}$. This leads to the conclusion that *Gillette* foams of very similar void fraction disproportionate at the same rate.

It can be seen that the evolution of $\alpha\lambda/f$, averaged over all frequencies (obtained from experiments), looks roughly like r^2 (Figure 6.12-6.15). The discrepancy between r^2 and $\alpha\lambda/f$ with time arises because maybe the image analysis doesn't catch all the big bubbles that have a big effect on ultrasound wave propagation. In image analysis the observed image area is comparatively small compared to the transducer surface area – that is one of the reasons.

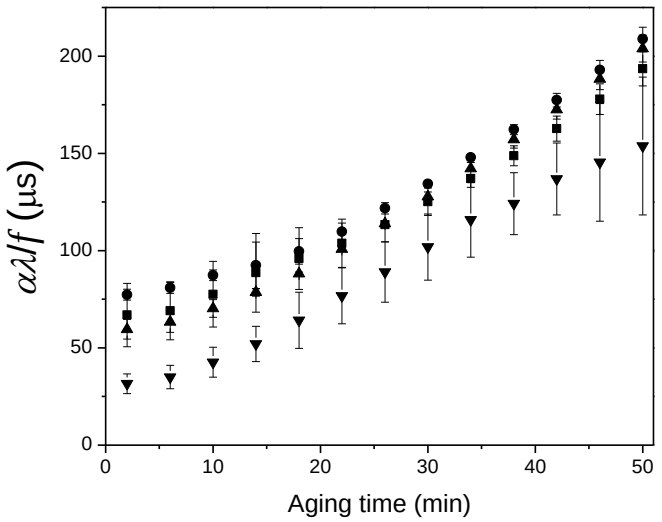

Figure 6.8. $\alpha\lambda/f$ versus aging time for 0.65 void fraction egg white foam. The symbols represents these frequencies: ■ 20kHz, ● 25 kHz, ▲ 30kHz, ▼ 40 kHz. Error bars represent standard deviation.

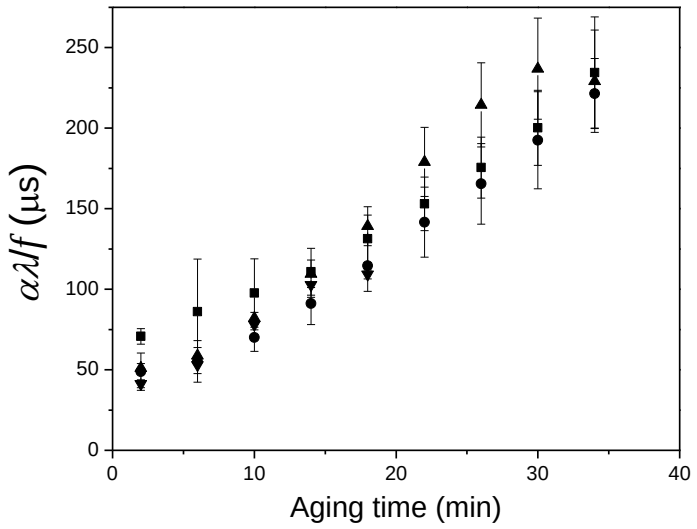

Figure 6.9. $\alpha\lambda/f$ versus aging time for 0.78 void fraction egg white foam. The symbols represents these frequencies: ■ 20kHz, ● 25 kHz, ▲ 30kHz, ▼ 40 kHz. Error bars represent standard deviation.

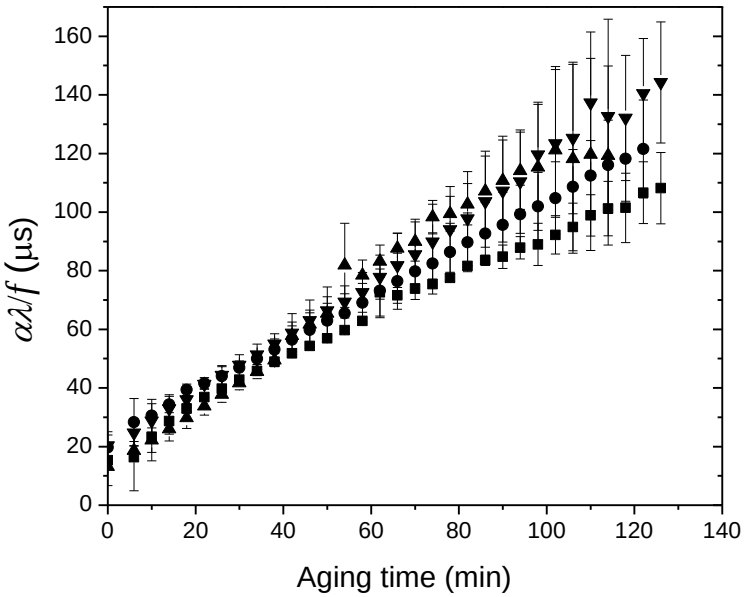

Figure 6.10. $\alpha\lambda/f$ versus aging time for *Gillette* foamy (φ = 0.90; ρ = 0.084 g/cm^3). The symbols represent: ■ 25 kHz, ● 30 kHz, ▲ 37 kHz, ▼ 40 kHz. Error bars represent standard deviation.

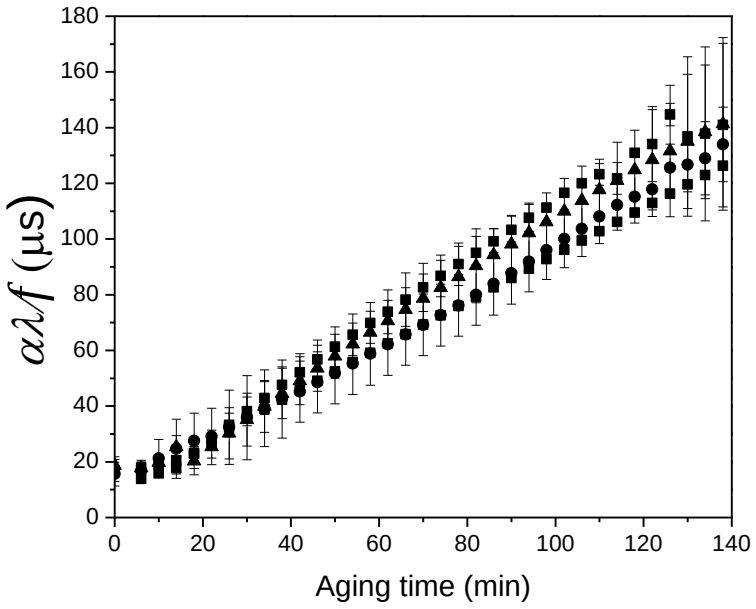

Figure 6.11. $\alpha\lambda/f$ versus aging time for *Gillette* foamy ($\varphi = 0.93$; $\rho = 0.064$ g/cm^3). The symbols represent: ■ 25 kHz, ● 30 kHz, ▲ 37 kHz, ▼ 40 kHz. Error bars represent standard deviation.

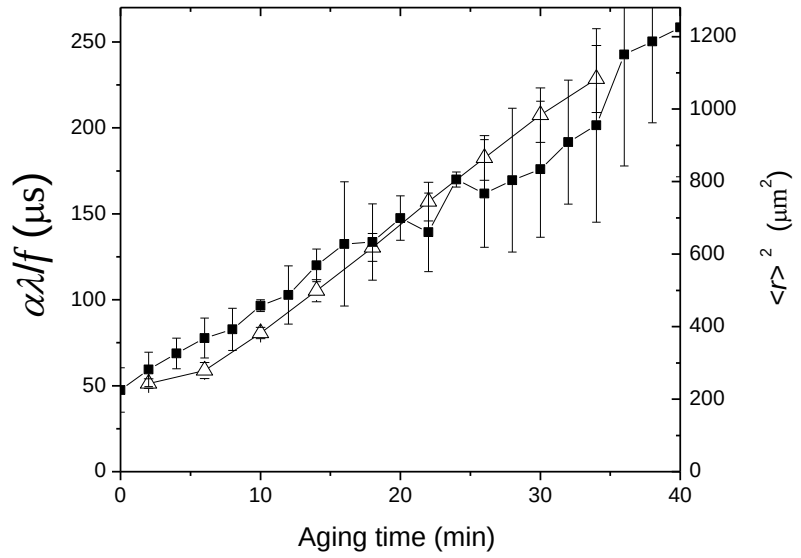

Figure 6.12. $\alpha\lambda/f$ (averaged $\alpha\lambda/f$ value of four frequencies: 20 kHz, 25 kHz, 30 kHz and 40 kHz) and r^2 (from image analysis) versus aging time for 0.78 void fraction egg white foam. Symbols represent: △ $\alpha\lambda/f$; ■ $\langle r\rangle^2$**.** Error bars represent standard deviation.

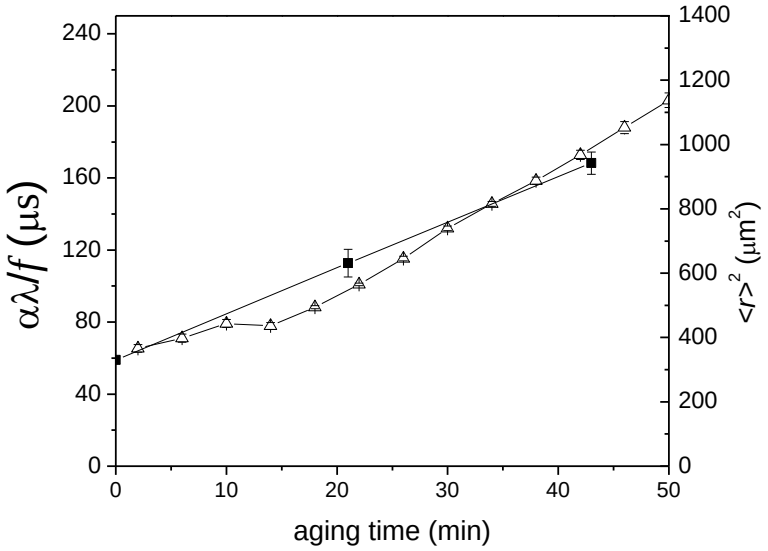

Figure 6.13. $\alpha\lambda/f$ (averaged $\alpha\lambda/f$ value of four frequencies: 20 kHz, 25 kHz, 30 kHz and 40 kHz) and r^2 (from image analysis) versus aging time for 0.65 void fraction egg white foam. Symbols represent: $\alpha\lambda/f$; $\langle r\rangle^2$. Error bars represent standard deviation.

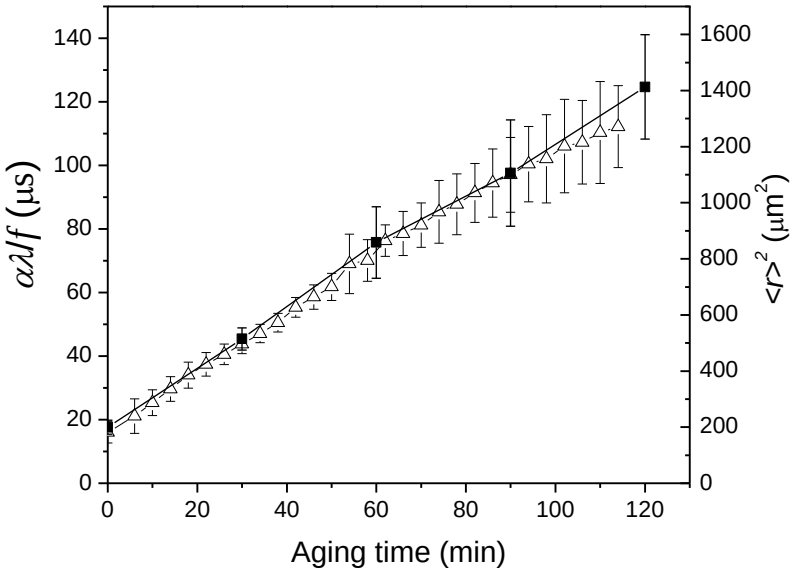

Figure 6.14. αλ/f (averaged $\alpha\lambda/f$ value of four frequencies: 25 kHz, 30 kHz, 37 kHz and 40 kHz) and r^2 (from image analysis) versus aging time for void fraction *Gillette* foam ($\varphi = 0.90$; $\rho = 0.084$ g/cm^3). Symbols represent: $\alpha\lambda/f$; $\langle r\rangle^2$. Error bars represent standard deviation.

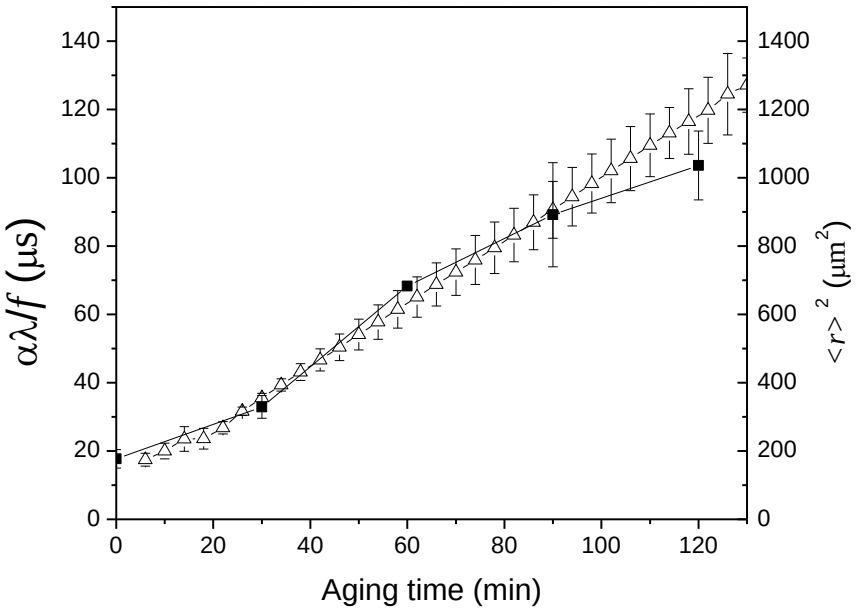

Figure 6.15. $\alpha\lambda/f$ ((averaged $\alpha\lambda/f$ value of four frequencies: 25 kHz, 30 kHz, 37 kHz and 40 kHz) and r^2 (from image analysis) versus aging time for void fraction *Gillette* foam ($\varphi = 0.93$; $\rho = 0.064$ g/cm^3). Symbols represent: $\alpha\lambda/f$; $\langle r\rangle^2$. Error bars represent standard deviation.

To pursue further the validation of the idea that $\alpha\lambda/f$ is proportional to r^2, we looked at which damping constant (δ) is dominant for egg white foams. Mujica and Fauve (2002) had proposed the idea that the thermal damping contribution is dominant. I reanalyzed their data to determine if this was also true for egg white liquid. The total damping constant is dimensionless, and is the sum of thermal (δ^{ther}), radiation (δ^{rad}) and viscous (δ^{visc}) damping constants. Explicit details of the parameters affecting each damping constant, and the determination of these parameters, will be given in chapter 6.4. However, results show that egg white foams are distinctly different from those produced by *Gillette*.

The results (Figure 6.16) show that in the case of water, thermal damping is dominant, as noted by Mujica and Fauve (2002). However, in the case of egg white liquid, viscous damping is

the biggest contributor (Figure 6.17) with a total damping constant that is substantially greater. At 40 kHz for water (for r = 10 μm) we have calculated that δ^{ther} = 1.26, δ^{rad} = 0.00168 and δ^{visc} = 0.159. In the case of egg white liquid medium with the same bubble radius, δ^{ther} = 1.01, δ^{rad} = 0.00168 and δ^{visc} = 4.4 at 40 kHz. We see that the viscous damping constant for egg white liquid is 30 times higher than that of water. Our calculated δ^{visc} for water is significantly different to the value reported by Mujica and Fauve (2002). Mujica and Fauve (2002) gives δ^{visc} = 0.0024 for water. The main difference for water and egg white liquid is viscosity; although it is behaving in a Newtonian fashion, egg white liquid is significantly more viscous than water.

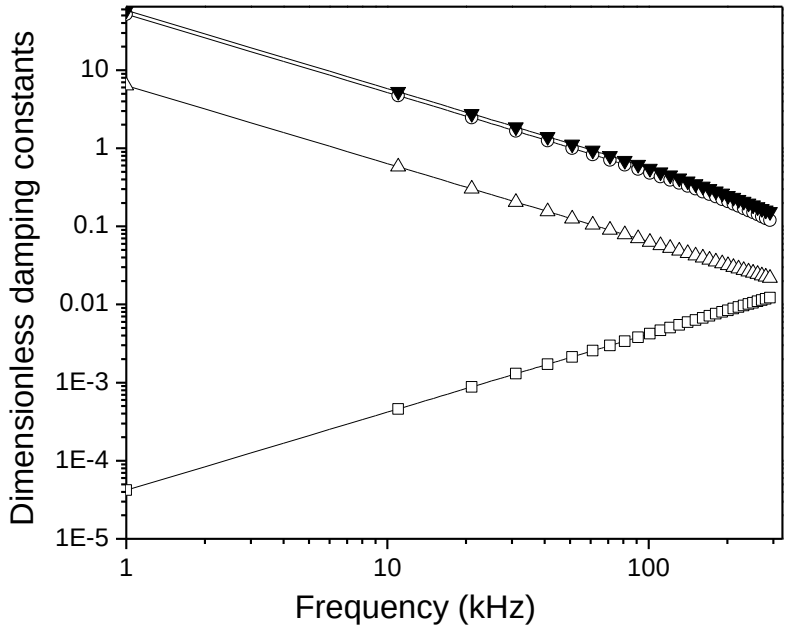

Figure 6.16. Damping constant contributions for 10 μm radii bubble distribution (σ_{st} = 0.1) if the matrix is water liquid. The symbols represent: —□— radiation, —○— thermal, —△— viscous, -▼- total damping.

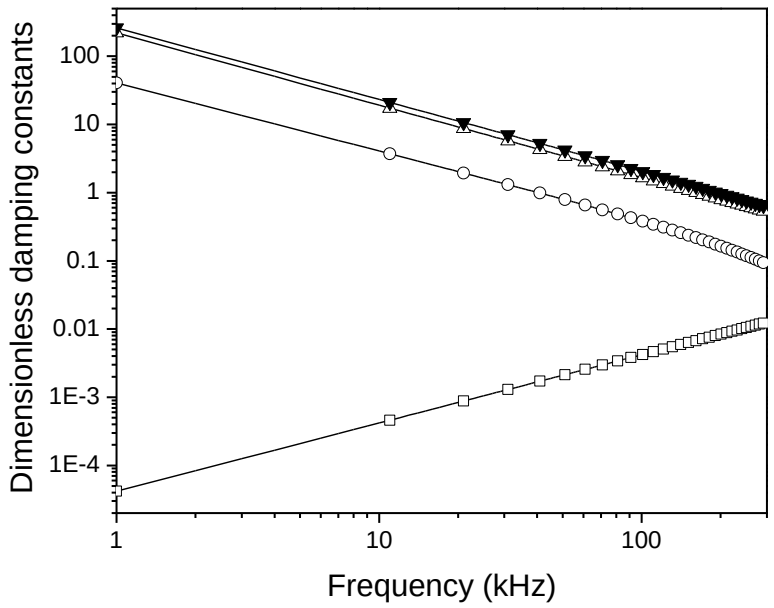

Figure 6.17. Damping constant (δ) contributions for 10 μm radii bubble distribution (σ_g = 0.1) if the matrix is egg white liquid. The symbols represent: —□— radiation, —○— thermal, —△— viscous, -▼- total damping.

The fact that the viscous losses dominate over thermal losses in egg white foams indicates that the thermal loss mechanism (equ. 6.5) invoked by Mujica and Fauve (2002) cannot explain the relation between $\alpha\lambda$ and $\langle r \rangle^2$ suggested by Figs. 6.12 and 6.13. To seek a more complete understanding of this relationship, we consider in the next section the model of the interaction of acoustic waves with bubbles in a liquid or weakly elastic medium, examining its predictions in more detail and proposing a possible extension of the model to make it more suitable for describing the acoustic properties of foams.

6.4 Application of Foldy model to interpret the results for high void fraction foams

6.4.1 The Foldy model

The Foldy model, which is based on multiple scattering theory, has been used to describe ultrasound wave propagation in viscoelastic bubbly liquid media. For bubbly media, it was generalized to include the effects of viscosity, radiative and thermal damping by Prosperetti (1977). The Foldy model is good for bubbly liquids (Leroy *et al*., 2008); however by modifying this model and looking at lower than resonance frequencies, it is more reasonable to apply this model in order to predict the properties of highly aerated systems (Leroy, 2009). With such a model, we would expect better qualitative and quantitative agreement between measured results and theoretical predictions.

Foam consists of many gas bubbles, and waves are scattered from the many air-water interfaces. The scattered wave vector can be written as (Leroy *et al.*, 2008):

$$k_{eff}^2 = k^2 + \int 4\pi n(r) dr f(\omega, r) \tag{6.7}$$

$$k^2 = k_0^2 = \omega^2 \chi_l \rho_l \tag{6.8}$$

$$n(r) = \frac{n_{tot}}{\sqrt{2\pi}\sigma_g r_j} exp\left(- \frac{\left(ln\frac{r_j}{\mu_r} \right)^2}{2\sigma_g^2} \right) \tag{6.9}$$

Here k_{eff} is the effective wave vector, $f(\omega, r)$ - scattering function at angular frequency ω for a bubble of radius r, $n(r)$ – the bubble size distribution in the foam, ρ_l – liquid density, χ_l – effective compressibility, n_{tot} – total number of bubbles per unit volume, σ_g - the logarithmic standard deviation, μ_r – bubble mean size of the log-normal distribution. For a fresh foam sample, the bubble size distribution is considered to be log-normal (Spencer, 2006). The scattering function is described by Formula 6.10:

$$f(\omega, r) = \frac{r}{(\omega_0/\omega)^2 - 1 + i(\delta^{ther} + \delta^{vis} + \delta^{rad})} \tag{6.10}$$

So the scattering function at a given angular frequency (ω) depends on the δ^{ther}, δ^{vis} and δ^{rad} – thermal, viscous and radiative damping constants, and the resonance frequency (ω_0) of a bubble of a given size, *r*. The resonance frequency and the damping constants are given by:

$$\omega_0^2 = \frac{3\mathrm{Re}(\kappa)(\mathrm{P_a}+2\gamma/\mathrm{r})+4\mathrm{G}'}{\rho_l \mathrm{r}^2} - \frac{2\gamma}{\rho r^3} \tag{6.11}$$

$$\delta^{\mathrm{rad}} = rk_0; \qquad \delta^{\mathrm{ther}} = \frac{3\,Im(\kappa)P_a}{\rho_l r^2\omega^2}; \qquad \delta^{\mathrm{vis}} = \frac{4G''}{\rho_l \mathrm{r}^2\omega^2}; \tag{6.12}$$

where κ is the complex polytropic index, γ - surface tension, P_a– atmospheric pressure (10^5Pa), $k_0 = \omega/v_0$ – the wave vector in the matrix, v_0 – sound velocity in the matrix (Strybulevych *et al*., 2007; Leroy *et al*., 2008), D_{th} (the thermal diffusivity of air)=$2\cdot10^{-5}$ m^2/s. The complex polytropic index is defined as:

$$\kappa(\omega, r) = \frac{\Upsilon}{1+3(\Upsilon-1)i\frac{D_{th}}{\omega r^2}ß} \tag{6.13}$$

where Υ is the ratio of specific heat capacities for air, D_{th} is the thermal diffusivity of air, and the parameter ß is defined as:

$$ß = 1 - \sqrt{i}\, r\sqrt{\frac{\omega}{D_{th}}}coth\left(\sqrt{i}\, r\sqrt{\frac{\omega}{D_{th}}}\right) \tag{6.14}$$

From these parameters a phase velocity and an attenuation coefficient can be predicted for the bubbly medium based on the real and imaginary parts of the effective wave vector.

$$v_{ph} = \frac{\omega}{\Re e(\boldsymbol{k}_{eff})} \tag{6.15}$$

$$\alpha = 2\Im m(\boldsymbol{k}_{eff}) \tag{6.16}$$

The model described by Leroy *et al.* (2008) for bubbly gels was modified, as proposed by Valentin Leroy (2009), because in the gels they studied their void fraction was from 0.15 % to 5% but the void fraction of our foams was in the range of 65 % to 93 %. The Foldy model at low void fraction considers a bubbly liquid density to be the same as the matrix (or liquid) density (ρ_l), but for a high void fraction foam, the density is an effective density (ρ_{eff}) that is very

different from that of the egg white liquid or *Gillette* liquid. In the standard Foldy model an effective compressibility is accounted for (Formula 6.7), but not an effective density. At frequencies much lower than the resonance frequency, the Foldy model becomes comparable to Wood's; $v_w = \sqrt{\chi_{eff}/\rho_{eff}}$, only at low bubble concentrations (Mujica and Fauve, 2002). For our foams with void fraction ranging from 65-93 % and with an average bubble size of 14 μm, ω_0 is in the range of 300 to 400 kHz. Therefore keeping in mind this equivalency of Wood's model and the low frequency limit of Foldy`s model, the phase velocity and the attenuation coefficient obtained from the standard Foldy`s model for large void fraction was corrected by using a correction factor b_c, which incorporates the effective density. This corrected model we will call Foldy 1 model, and the corrected phase velocity (v_{cor}) and attenuation coefficient (α_{cor}) are given by:

$$b_c = \sqrt{\frac{\varphi\rho_g + (1-\varphi)\rho_l}{\rho_l}} \tag{6.17}$$

$$v_{cor} = v_p / b_c \tag{6.18}$$

$$\alpha_{cor} = \alpha / b_c \tag{6.19}$$

We also used another Foldy model correction mechanism which seems more self consistent. Instead of using the matrix density (ρ_l), which is that of egg white liquid and *Gillette* liquid, an effective density (ρ_{eff}) of material was used throughout. This correction affects the resonance frequency (ω_0) also. Futher on, the results of both Foldy models, referred to as Foldy 1 and Foldy 2, will be presented. The Foldy model for a bubbly liquid takes into account the matrix parameters: density, the complex shear modulus, the phase velocity and the surface tension. Bubble size distribution was obtained by taking images of foam samples with a digital

microscope. From processed images the bubble size distribution during foam aging was measured.

6.4.2 Data acquisition for the Foldy model

6.4.2.1 Properties of egg white foam matrix

The surface tension value of egg white liquid was taken from the literature (Vadehra and Nath, 1973; Ma *et al,* 1986). The density of the egg white foam matrix was determined experimentally (Chapter 3). Velocity of sound in egg white liquid and sugar mixture, and in *Gillette* liquid was measured using 2.25 MHz frequency transducers.

Frequency dependent expressions of the storage (G') and loss (G'') moduli of the egg white and *Gillette* liquid were obtained by performing two measurements using oscillatory rheology (0.01-100 Hz frequency) and shear wave reflection (500 kHz frequency) techniques in liquid egg white and sugar mixtures with no air.

The complex shear modulus G is expressed through the parameters G' and G'', Formula 2.14:

$$G(\omega) = G'(\omega) + iG''(\omega)$$

For the ultrasonic shear wave determinations, G' and G'' can be evaluated through the shear phase velocity (v_s) and attenuation coefficient (α) (Fan, 2007):

$$G' = \rho v_s^2 \left[\frac{1-\left(\frac{\alpha v_s}{2\omega}\right)^2}{\left[1+\left(\frac{\alpha v_s}{2\omega}\right)^2\right]^2} \right] \tag{6.20}$$

$$G'' = \frac{2\rho v_s^2 \left(\frac{\alpha v_s}{2\omega}\right)}{\left[1+\left(\frac{\alpha v_s}{2\omega}\right)^2\right]^2} \tag{6.21}$$

In Figure 6.20 G' and G'' versus frequency (Hz) are displayed, with the results obtained from both oscillatory rheology and ultrasound measurements. The shear phase velocity (v_s) and

attenuation coefficient (α) at 500 kHz were: v_s = 8 m/s and α = 300 mm^{-1}. The shear modulus is frequency dependent. The following expression was obtained from these results and was used to estimate the shear storage (G') and loss (G'') modulus at intervening frequencies:

$$G' = 0.027(f/1\text{ Hz})^{1.10}\text{ Pa} \tag{6.22}$$

$$G'' = 0.407(f/1\text{ Hz})^{0.94}\text{ Pa} \tag{6.23}$$

where f is expressed in Hz.

The real part for the shear modulus is 3.98 kPa at 50 kHz, so the matrix elasticity is small compared to the imaginary part (10.6 kPa). The imaginary part provides a viscosity of $\eta = 33 \cdot 10^{-3}$ Pa.s (33 times the viscosity of water) at a frequency of 50 kHz. The viscosity of liquid egg white mixture changes the damping mechanism for sound compared to aqueous solutions. The details of the effect of thermal and viscous damping losses to total damping will be discussed later.

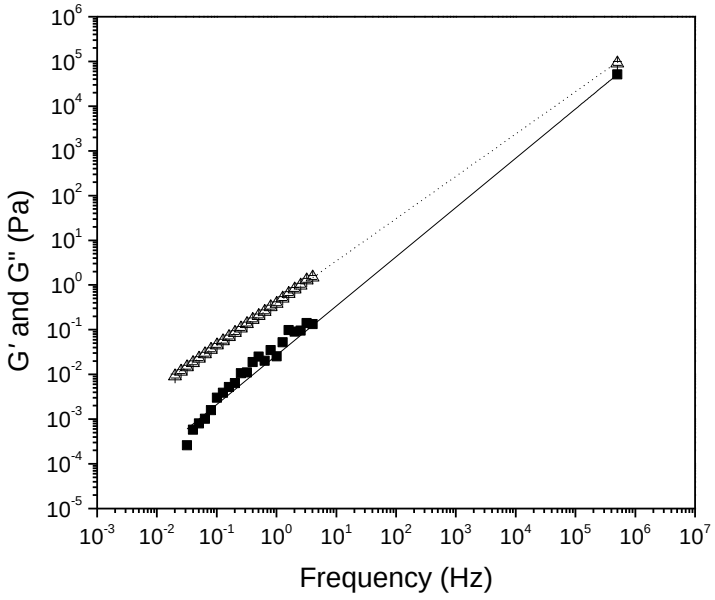

Figure 6.18. G' (■) and G'' (△) of egg white versus frequency. Linear fit of G' (——) and G'' (·····) through data obtained from rheological and ultrasound measurements.

A summary of matrix properties for egg white sugar mixtures is given in Table 6.1.

Table 6.1. Liquid egg white and sugar foam matrix* parameters

Density	ρ_l	1226 kg/m^3
Shear storage modulus	G'	$0.027(f/1\text{ Hz})^{1.10}$ Pa
Shear loss modulus	G''	$0.407(f/1\text{ Hz})^{0.94}$ Pa
Velocity of sound in liquid egg white and sugar mixture	v	1530 m/s
Surface tension	σ	50 mJ/m^2

*foam matrix here means that egg white and sugar was blended together but no air was mixed in. The void fraction is 0.

6.4.2.2 Properties of Gillette foam matrix

In order to determine *Gillette* liquid matrix properties, the *Gillette* foam was sprayed out in a large (one litre) container and left for several weeks. The liquid started appearing as a result of drainage in the *Gillette* foam. Density was measured as for egg white liquid, and velocity at 2.25 MHz. Liquid surface tension was taken from literature (Rouyer *et al*., 2005) for the value of SDS surface tension value, because SDS is the major surfactant responsible for creating and keeping this synthetic foam stable. The following expression estimates the shear storage (G') and loss (G'') modulus of *Gillette* foam matrix at intervening frequencies:

$$G' = 0.2637(f/1\text{ Hz})^{1.0022}\text{ Pa} \tag{6.24}$$

$$G'' = 0.013(f/1\text{ Hz})^{1.162}\text{ Pa} \tag{6.25}$$

Gillette foam matrix parameters are given in Table 6.2. For comparison of rheological parameters of *Gillette* (Sensitive), egg white liquid with sucrose and water, G' and G''versus frequency is given in one figure (Figure 6.19).

Table 6.2. *Gillette* (Sensitive) foam matrix* (without air) parameters

Density of liquid *Gillette*	ρ_l	1000 kg/m^3
Shear storage modulus	G'	$0.2637(f/1\text{ Hz})^{1.0022}$Pa
Shear loss modulus	G''	$0.013(f/1\text{ Hz})^{1.162}$ Pa
Velocity of sound in liquid *Gillette*	v	1500 m/s
Surface tension	σ	32 mJ/m^2

*foam matrix here means *Gillette* liquid. The void fraction is 0.

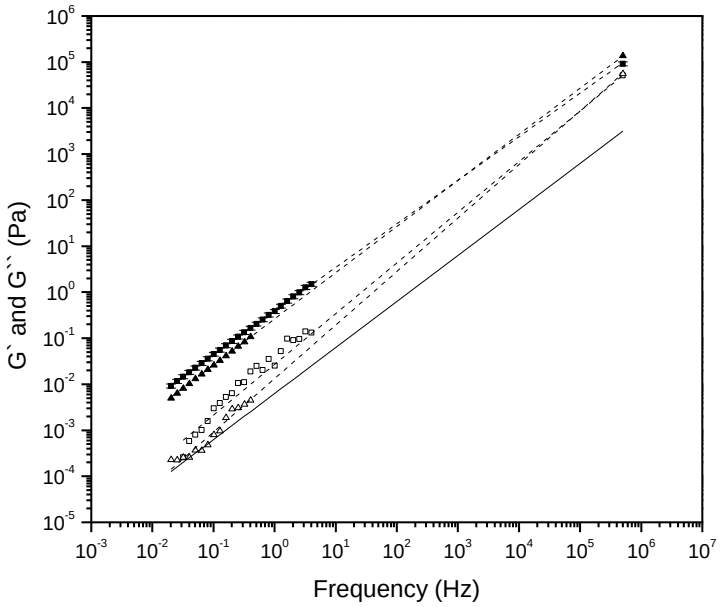

Figure 6.19. *G′* (■) and *G″* (▫) of egg white liquid versus frequency. *G′* (▲) and *G″* (△) of *Gillette* liquid versus frequency. (Linear fit of *G′* and *G″* (- - - -) through the egg white and *Gillette* liquid data obtained from rheological and ultrasound measurements). Solid line represents *G″*of water.

6.4.2.3 Bubble properties

The Foldy model requires the total number (n_{tot}) of bubbles per unit volume and it is given as a separate factor from the bubble size distribution. In order to determine the total volume of the bubbles in the foam sample, we used bubble size distributions obtained from image analysis data. We can calculate the total number of bubbles (n_{tot}) (Spencer, 2006; Fan, 2007; Strybulevych *et al*., 2007):

$$n_{tot} = \frac{3\varphi}{4\pi r^3 exp\left(\frac{9\sigma_g^2}{2}\right)} \tag{6.26}$$

$$\sigma_g = \frac{1}{n'_{total}} \sum_{j=1}^{k'_0} \left[\left(lnr_j \right)^2 \cdot n_j \right] - \left[\frac{1}{n'_{total}} \sum_{j=1}^{k'_0} lnr_j \cdot n_j \right]^2 \tag{6.27}$$

where σ_g are the standard deviations of the log-normal distribution, *r*- bubble mean radius, n'_{total} - total number of observed bubbles, k_0'- the number of classes (bins), n_j - number of individual bubble in size class (bin) *j*.

6.4.3 Comparison of Foldy model predictions with experiment

In Figures 6.20-6.27 the phase velocity and attenuation coefficient results for two void fraction egg white and two *Gillette* foams are presented. As well, predictions of the Foldy 1 and Foldy 2 models are shown as empty symbols and filled symbols, respectively. Both Foldy models predict the same order of magnitude of the phase velocity and attenuation coefficient. For egg white foams, the Foldy 1 model shows a decrease of phase velocity at lower frequencies in comparison with Foldy 2. Foldy 1 model shows an increase in attenuation at lower frequencies in comparison with Foldy 2 for both void fraction egg white foams.

Wood's approximation considers that only void fraction is responsible for the magnitude of the velocity seen in the foams. However, in our foams we see changes in velocity and attenuation coefficient. The possible effect that influences phase velocity and attenuation coefficient is resonance (Leighton, 1996; Leroy *et al*., 2008). At a frequency close to the bubble resonance, velocity decreases and attenuation increases sharply. As a result of changes in bubble size with foam aging time, the bubble sizes that are in our foams might fall into the resonance effect range. To examine this possibility, we pursued this idea further.

The resonance frequency changes, depending on the properties of the matrix and on the size of the bubble (Leighton, 1996). For a single bubble of 14 μm, a bubble resonance effect ($\omega_M = 1/r\sqrt{(3\gamma P_0)/\rho_l}$ (Povey, 1997)) would be at a frequency (f_r) of 232 kHz in water and 210 kHz in the egg white sucrose medium. The wavelength at resonance is much larger than bubble size: $\lambda_r = v_l / f_r$ (v_l - sound velocity in the liquid), in water λ_r = 6.4 mm, in egg white

media λ_r = 7.14 mm. However, in foam, in calculating the resonance frequency, the effective density (ρ_{eff}) (see formula 6.2) instead of liquid density (ρ_l) should be considered. Therefore, in egg white foam (φ = 0.65), with an average bubble radius of 14 μm, the resonance frequency is 360 kHz. The Foldy 1 model shows a resonance effect occurring at lower frequencies at the very early aging times, but we should not expect it to happen for our egg white foam bubble sizes. Therefore the Foldy 2 model is more realistic even though we don't see quantitative agreement with the experimental results.

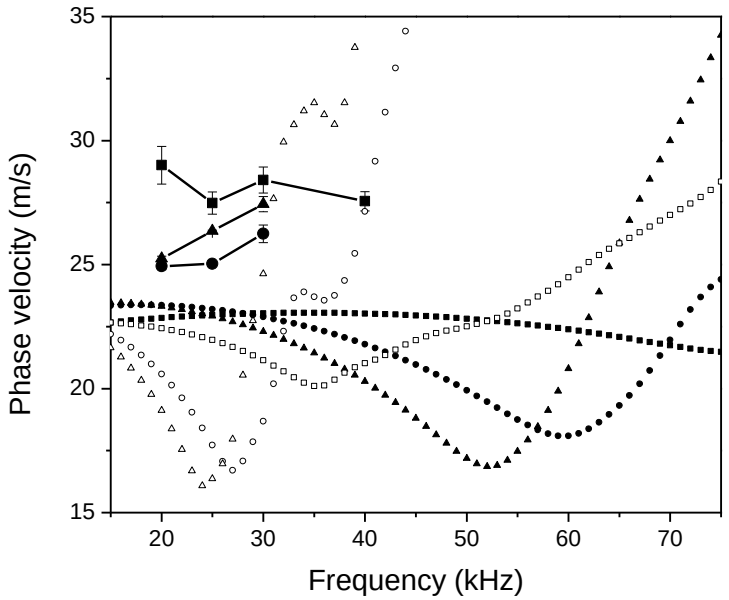

Figure 6.20. Experimental results and prediction of modified Foldy's models for phase velocity in the 0.78 void fraction egg white foam. Three aging times, for experimental data: —■— 0 min, —●— 22 min, —▲— 34 min; Foldy 1 model prediction: ▫ 0 min, ○ 22 min, △ 34 min; Foldy 2 model: ■ 0 min, ● 22 min, ▲ 34 min. For comparison v_w = 22 m/s.

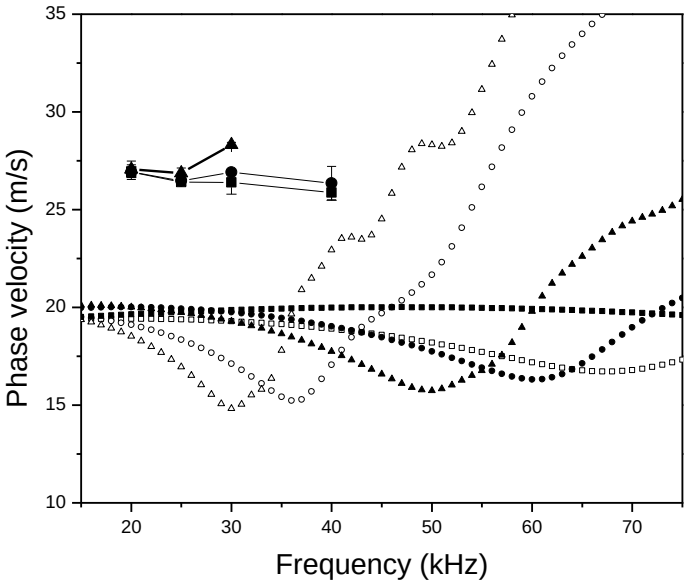

Figure 6.21. Experimental results and prediction of modified Foldy's models for phase velocity in the 0.65 void fraction egg white foam. Three aging times, for experimental data: —■— 0 min, —●—: 22 min, —▲— 42 min; Foldy 1 model prediction: ▫ 0 min, ○ 22 min, △ 42 min; Foldy 2 model: ■ 0 min, ● 22 min, ▲ 42 min. For comparison v_w = 18 m/s.

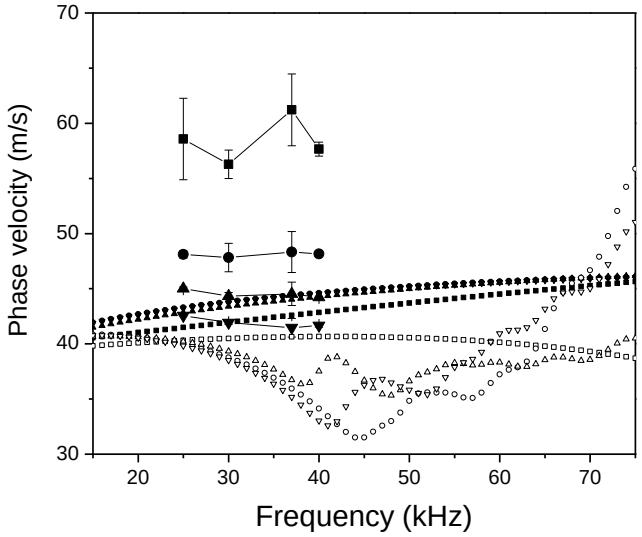

Figure 6.22 Experimental results and prediction of modified Foldy's models for phase velocity in the lower density *Gillette* foam (φ = 0.93; ρ = 0.064 g/cm^3). Four aging times: —■— 0 min, —●—: 30 min, —▲— 60 min, —▼— 90 min. Foldy 1 model prediction: ▫ 0 min, ○ 30 min, △ 60 min, ▽ 90 min; Foldy 2 model: ■ 0 min, ● 30 min, ▲ 60 min, ▼ 90 min. $v_{GillWood}$ = 39 m/s.

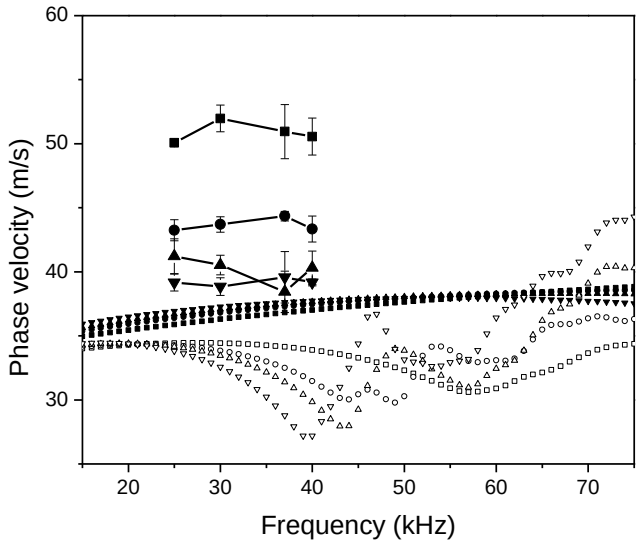

Figure 6.23. Experimental results and prediction of modified Foldy's model for phase velocity in the higher density *Gillette* foam (φ = 0.90; ρ = 0.084 g/cm^3). Four aging times: —■— 0 min, —●—: 30 min, —▲— 60 min, —▼— 90 min. Foldy 1 model prediction: ▫ 0 min, ○ 30 min, △ 60 min, ▽ 90 min; Foldy 2 model: ▪ 0 min, ● 30 min, ▲60 min, ▼ 90 min. $v_{GillWood}$ = 35 m/s.

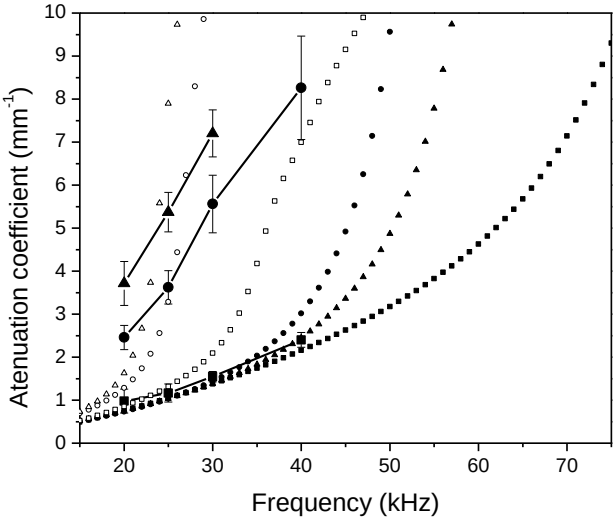

Figure 6.24. Results and prediction of modified Foldy's models for attenuation coefficient in the 0.78 void fraction egg white foam. Three aging times, for experimental data: —■— 0 min, —●—: 22 min, —▲— 34 min; Foldy 1 model prediction: ▫ 0 min, ○ 22 min, △ 34 min; Foldy 2 model: ▪ 0 min, ● 22 min, ▲ 34 min.

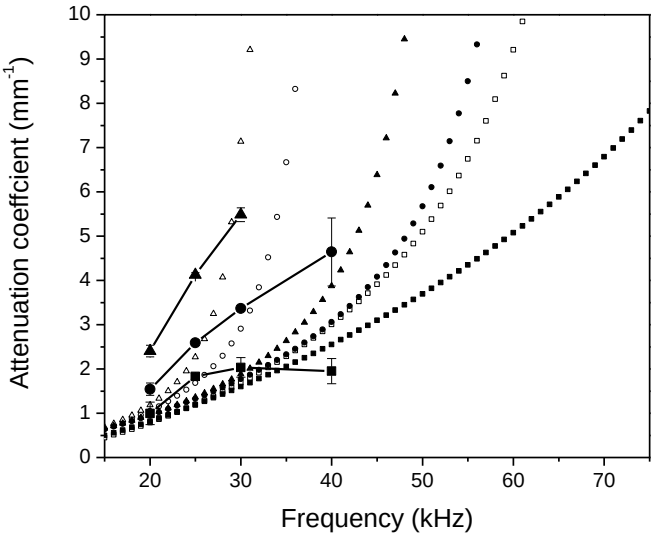

Figure 6.25. Results and prediction of modified Foldy's models for attenuation coefficient in the 0.65 void fraction egg white foam. Three aging times, for experimental data: —■— 0 min, —●—: 22 min, —▲— 42 min; Foldy 1 model prediction: ▫ 0 min, ○ 22 min, △ 42 min; Foldy 2 model ■ 0 min, ● 22 min, ▲ 42 min.

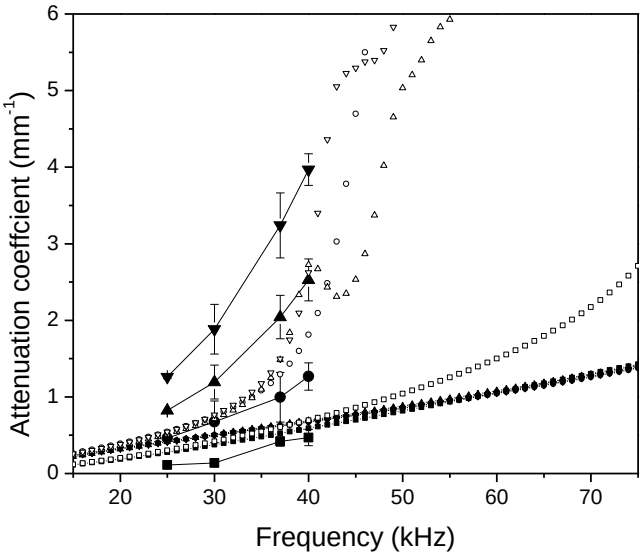

Figure 6.26. Results and prediction of modified Foldy's models for attenuation coefficient in the (φ = 0.93; ρ = 0.064 g/cm^3) *Gillette* foam. Four aging times: —■— 0 min, —●—: 30 min, —▲— 60 min, -▼- 90 min. Foldy 1 model prediction: ▫ 0 min, ○ 30 min, △ 60 min, ▽ 90 min; Foldy 2 model: ■ 0 min, ● 30 min, ▲ 60 min, ▼ 90 min.

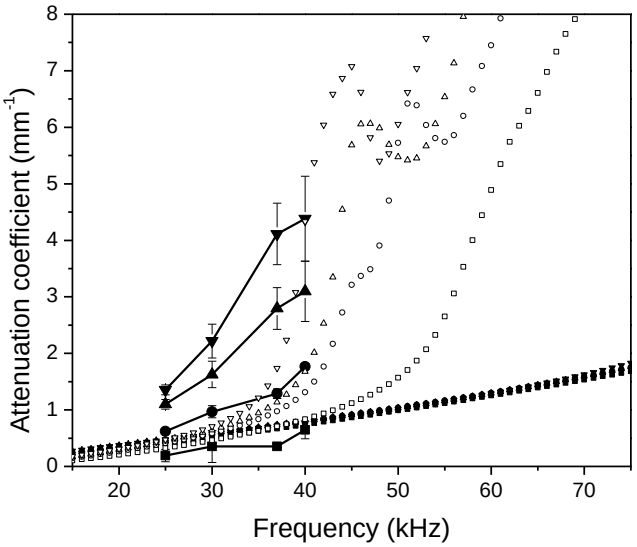

Figure 6.27. Results and prediction of modified Foldy's models for attenuation coefficient in the (φ = 0.90; ρ = 0.084 g/cm^3) *Gillette* foam. Four aging times: 0min, 30min, 60 min, 90 min. Foldy 1 model prediction: 0min, 30min, 60min, 90 min; Foldy 2 model: - 0min, 30min, 60min, 90min.

6.5 Interpretation of $\alpha\lambda/f$

Mujica and Fauve (2002) suggested that $\alpha\lambda/f$ is proportional to mean bubble radius squared ($\langle r\rangle^2$) at low frequencies based on the assumption that thermal damping in the foam is dominant and that other contributions at that low frequency range are small. We investigated this idea to determine if it is valid for our egg white foams.

The velocity and attenuation data of Figures 6.20 to 6.27 were used to calculate $\alpha\lambda/f$ as a function of aging time at different frequencies (Figure 6.28-6.31). For egg white foams, neither Foldy model really agrees with an $\alpha\lambda/f$ increase consistently for all frequencies. As for example, 0.78 void fraction egg white foam (Figure 6.28) for the lower frequencies, 20 kHz and 25 kHz, the $\alpha\lambda/f$ increase with aging time is under predicted, while for the higher frequency (30 kHz), the $\alpha\lambda/f$ increase is over predicted. The Foldy 1 model predicts resonance at lower frequencies. As a

result, when the foam ages and bubble size increases, $\alpha\lambda/f$ increases, a result better predicted by the Foldy 1 model.

For both void fraction *Gillette* foams, an increase of $\alpha\lambda/f$ with aging time is under predicted for the Foldy 1 and Foldy 2 models, except the values of $\alpha\lambda/f$ agree with the model at 0 min of aging. Since initial *Gillette* foamy bubble size is a little smaller than the egg white foam, any resonance effects that are seen as an altering of velocity and attenuation profiles would be expected at higher frequencies than in egg white foams. As we can see from image analysis data (Figure 4.7) increases in bubble size at later aging times will decrease bubble resonance frequency. For example, in egg white 0.78 void fraction foam, the average bubble size increases to 26 μm at 22 min of aging time. The resonance in the egg white foam of 0.78 void fraction would be expected at 250 kHz frequency and for the 0.65 void fraction foam with 26 μm bubble size, the resonance would be at 200 kHz. However, at this 22 minutes aging time there are some big bubbles (100 μm) in the egg white foam, and for these large bubbles the resonance frequency is 50 kHz and 62.5 kHz, respectively, for the 0.65 and 0.78 void fraction foams. In the foam, bubbles are not isolated, they are separated by only thin lamellae, and the resonance of one bubble is affected by its neighbours (Page, 2010). As a result, the resonance effect in real foam would be averaged over a range of frequencies due to bubbles of different sizes resonating at different frequencies. The effective resonance frequency is likely shifted. In Foldy`s model the bubbles in the foam are considered isolated, not coupled. At the range of frequencies that we are examining, the bubbles in water will likely resonate, but our medium is not water. It is a very viscous medium and if the bubble tries to resonate, where it is surrounded by many other bubbles, the resonance effect is smaller (Leroy, 2009; Page, 2010).

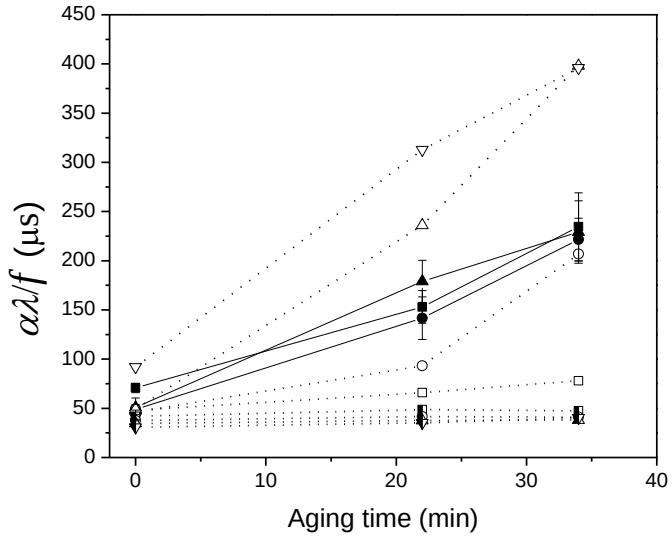

Figure 6.28. Foldy's prediction and experimental result of $\alpha\lambda/f$ versus frequency for 0.78 void fraction egg white foam. Three aging times, for experimental data: 20 kHz, 25 kHz, 30 kHz, 40 kHz (only for 0min); Foldy 1 model prediction: 20 kHz, 25 kHz, 30 kHz, 40 kHz; Foldy 2 model 20 kHz, 25 kHz, 30 kHz, 40 kHz. Error bars represent standard deviation.

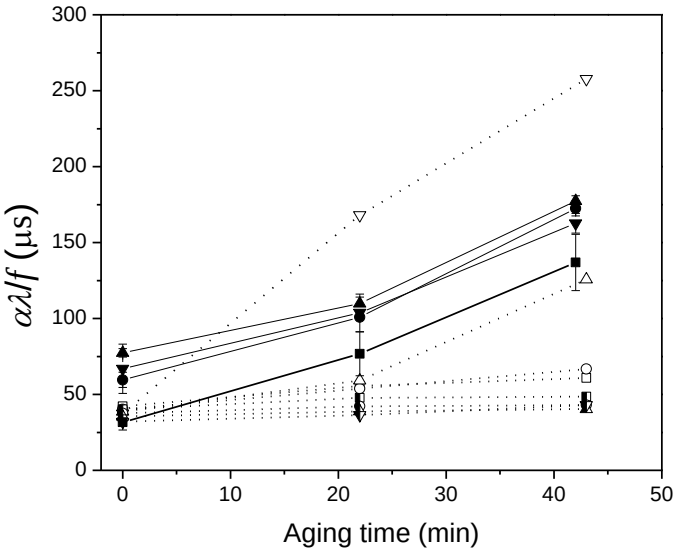

Figure 6.29. Foldy's prediction and experimental result of $\alpha\lambda/f$ versus frequency for 0.65 void fraction egg white foam. Three aging times, for experimental data: 20 kHz, 25 kHz, 30 kHz, 40 kHz (only for 0 min); Foldy 1 model prediction: 20 kHz, 25 kHz, 30 kHz, 40 kHz; Foldy 2 model 20 kHz, 25 kHz, 30 kHz, - 40 kHz. Error bars represent standard deviation.

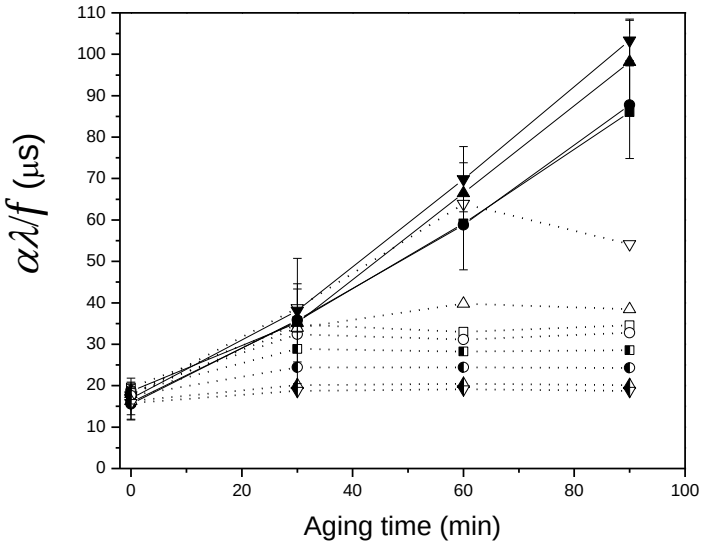

Figure 6.30. Foldy's prediction and experimental result of $\alpha\lambda/f$ versus frequency for 0.93 void fraction *Gillette* foam. Four aging times, for experimental data: —■— 25 kHz, —●— 30 kHz, —▲— 37 kHz, —▼— 40 kHz; Foldy 1 model prediction: ···▫··· 25 kHz, ···○··· 30 kHz, ···△··· 37 kHz, ···▽··· 40 kHz; Foldy 2 model ···◧··· 25 kHz, ···◐··· 30 kHz, ···◭··· 37 kHz, ···▼··· 40 kHz. Error bars represent standard deviation.

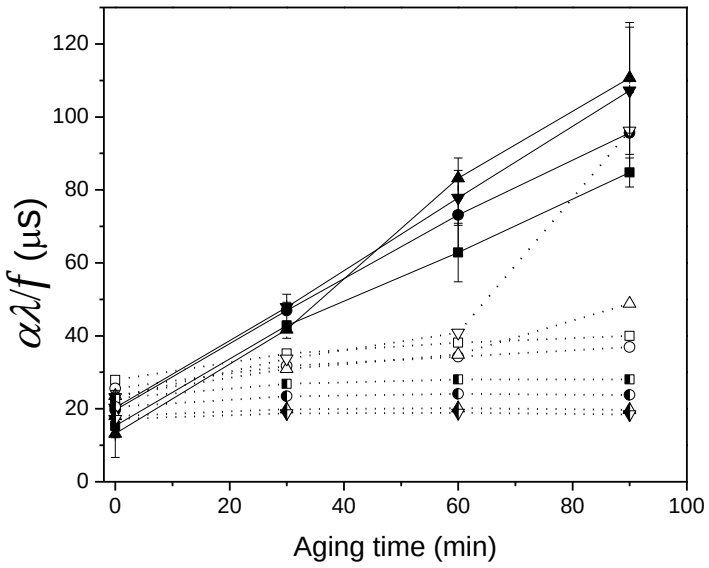

Figure 6.31. Foldy's prediction and experimental result of $\alpha\lambda/f$ versus frequency for 0.90 void fraction *Gillette* foam. Four aging times, for experimental data: —■— 25 kHz, —●— 30 kHz, —▲— 37 kHz, —▼— 40 kHz; Foldy 1 model prediction: ···▫··· 25 kHz, ···○··· 30 kHz, ···△··· 37 kHz, ···▽··· 40 kHz; Foldy 2 model ···◧··· 25 kHz, ···◐··· 30 kHz, ···◭··· 37 kHz, ···▼··· 40 kHz. Error bars represent standard deviation.

6.5.1 Comparison of Foldy model to theoretical monodispersed and polydispersed egg white foams

To understand what is contributing to changes in ultrasonic signals with foam aging time, we challenged the Foldy 1 model to see if $\alpha\lambda/f$ scales with the bubble mean radius squared (r^2). To do this, an ideal monodisperse distribution of bubbles was simulated and modelled at the very low frequencies starting at 1 kHz. The foam bubble radii distributions (Figure 6.32) were created manually, where bubble mean radius (μ_r) was in the 5 to 50 μm range. Also a very narrow bubble size distribution width (in other words log standard deviation, σ_g was maintained, ranging from 0.05 to 0.1 and keeping the area under the curve constant (100), so that we would have almost monodisperse bubble size distributions.

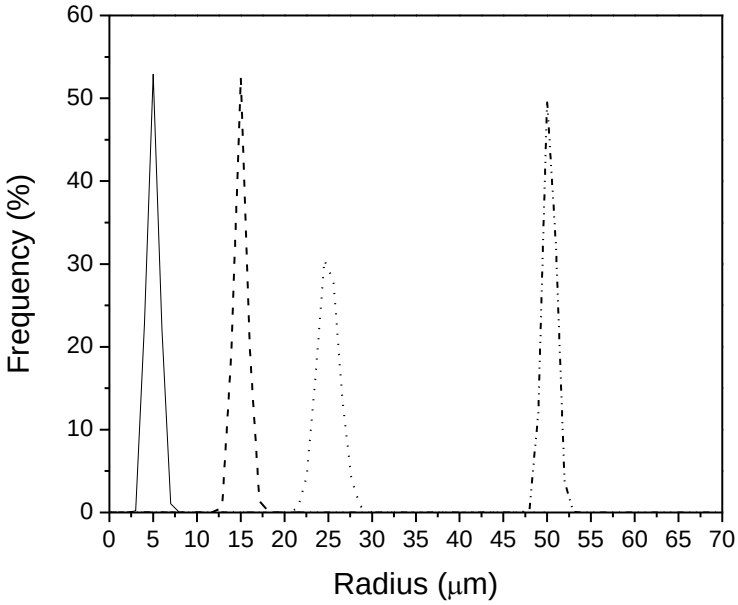

Figure 6.32. Theoretical monodispersed bubble distribution where the symbols represent radius (μ_r), and the standard deviation or width (σ_{st}) of the bubble distribution are: —— μ_r = 5 μm, σ_{st} = 0.15; - - - · μ_r =15 μm, σ_{st} = 0.05; ····· μ_r = 25 μm, σ_{st} = 0.05; -·-·- μ_r = 50 μm, σ_{st} = 0.015.

In Figure 6.33, $\alpha\lambda/f$ versus frequency is displayed for different bubble sizes in the simulated media of egg white liquid and water. A clear dependence on frequency is only evident for 50 μm

bubbles. To make the dependence on bubble size more evident, the data from this figure were plotted on a log-log scale as $\alpha\lambda/f$ versus r^2 (Figures 6.34 and 6.35) starting from the very lowest frequency of 1 kHz and going up to 50 kHz, the frequency at which our experiments were performed. According to Mujica and Fauve (2002), $\alpha\lambda/f$ dependence on the radius squared should look linear for power law behaviour, if plotted on a double logarithmic plot. However, the Foldy 1 model predicts that such a dependence on radius does not occur at any frequency for the range of bubble sizes and frequencies considered, although the predictions for bubbles in water are fairly close at the lowest frequency of 1 kHz (Figure 6.34). For higher frequencies, the departures of $\alpha\lambda/f$ from r^2 behaviour become increasingly pronounced (the drawn solid line in Figure 6.34 and the dashed line in Figure 6.35 represent the power law behaviour), with the values of $\alpha\lambda/f$ deviating the most from power law scaling for the largest bubble size of 50 μm. As a result of increasing the bubble size, the frequencies investigated were closer to resonance, so that the regime in which thermal damping can cause r^2 behaviour was no longer accessible. This requires not only that thermal damping dominates over other attenuation mechanisms but also that the total attenuation is not too large. Mujica and Fauve (2002), after calculating values of the damping constants, stated that scattering contributions are low for the frequencies smaller than the resonance frequency and viscous contributions are negligible, so that only thermal mechanisms dominate for the low frequencies. However, our calculated values of viscous and radiative damping contributions are higher than the ones Mujica and Fauve (2002) reported. So that means for bubbles in an egg white liquid matrix there is more than one contribution to $\alpha\lambda/f$, not just the one supposed to depend on r^2.

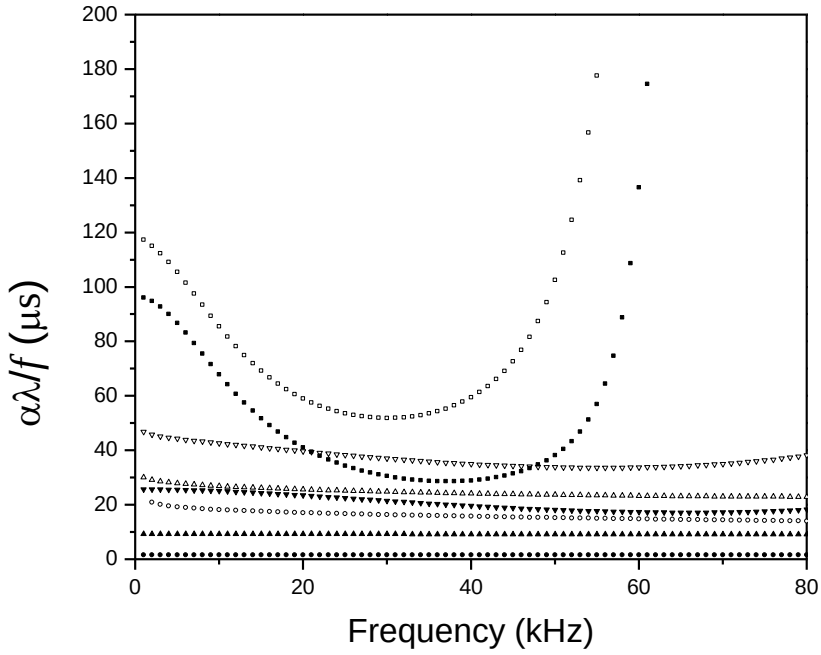

Figure 6.33. Foldy 1 prediction of $\alpha\lambda/f$ versus frequency for an almost monodisperse distribution of bubbles in egg white and water media. Symbols for water media: • μ_r = 5 μm, ▲ μ_r = 15 μm, ▼ μ_r = 25 μm, ■ μ_r = 50 μm; for egg white media: ○ μ_r = 5 μm, △ μ_r =15 μm, ▽ μ_r = 25 μm, □ μ_r = 50 μm.

Earlier, in section 6.3, we examined the acoustic damping mechanisms to ascertain which damping constant is dominant. The scattering contribution is very weak at very low frequency and increases with frequency, compared to thermal and viscous damping constant contributions in both water and egg white liquid (Figure 6.16 and 6.17). The viscous damping constant is dominant for egg white liquid and not insignificant in water in the range up to 200 kHz frequencies. As discussed previously, for an egg white liquid, viscous losses are higher, and this appears to lead to an offset in the egg white case as $\alpha\lambda/f$ scales with r^2: the $\alpha\lambda/f$ value for the 5 μm bubble size is 18 μs while for water media and the same bubble size $\alpha\lambda/f$ is 1.5μs (Figures 6.34 - 6.35). In Figure 6.35, this apparent offset is illustrated by the solid curve, which shows that it is possible to fit the predictions at the lowest frequency by an empirical relation given by a

constant plus an r^2 contribution. However, in this case where viscous losses dominate, the relationship between $\alpha\lambda/f$ and bubble radius is more complicated than a simple power law, and one should be cautious in using this empirical relation as a basis for interpreting experimental data. In Figure 6.34, where water is the continuous medium, we see r^2 scaling at low frequencies, because the viscosity of water is very low in comparison with egg white liquid; however $\alpha\lambda/f$ does not scale this way with radius for the higher frequencies. Thus, at the higher frequencies, the Foldy 1 model does not predict r^2 behaviour even when thermal losses dominate, reflecting the fact that at high frequencies, δ^{ther} is no longer proportional to r^2 (see equation (6.12)), the $\delta << 1$ condition needed for the attenuation to be proportional to δ is no longer satisfied.

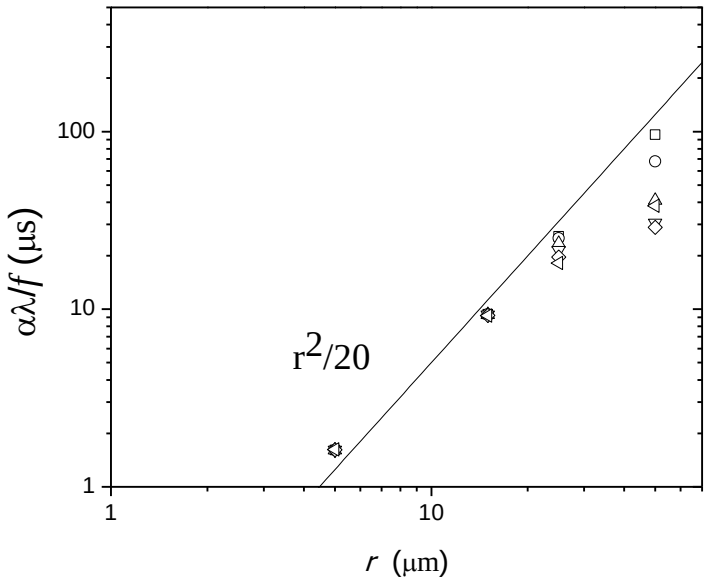

Figure 6.34. Simulation of $\alpha\lambda/f$ versus r for water media based on Foldy 1 model. The symbols represent: ··□··· 1 kHz, ··○·· 10 kHz, ··△·· 20 kHz, ···▽·· 30 kHz, ··◇·· 40 kHz, ··◁·· 50 kHz. Solid line represents fit $\alpha\lambda/f=r^2/20$.

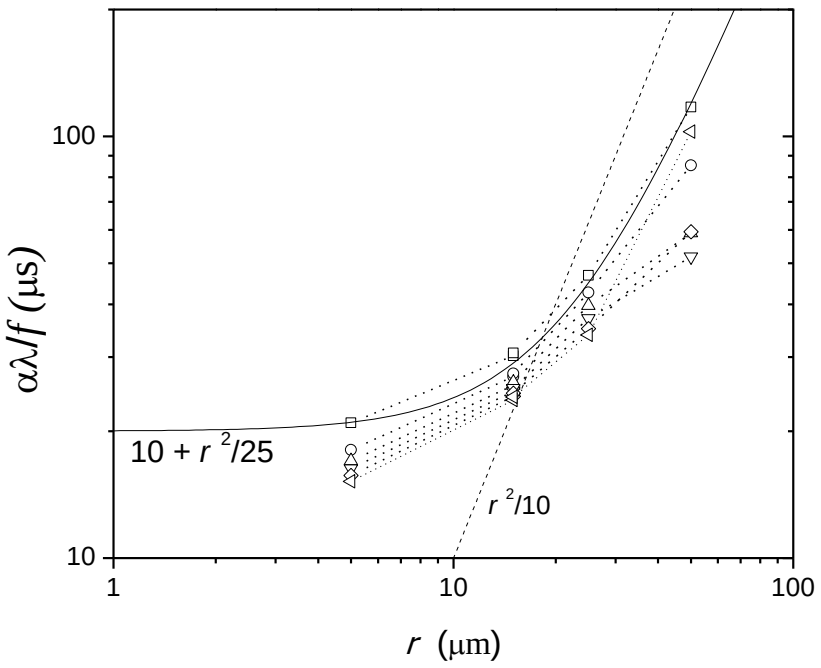

Figure 6.35. Simulation of $\alpha\lambda/f$ versus r for egg white media based on Foldy 1. The symbols represent: ··□··· 1 kHz, ··○·· 10 kHz, ··△·· 20 kHz, ···▽·· 30 kHz, ··◇·· 40 kHz, ··◁·· 50 kHz. Solid line represents fit $\alpha\lambda/f$=10+r^2/20, dashed line represents fit $\alpha\lambda/f$=r^2/10.

Lastly we plotted average experimental values of $\alpha\lambda/f$ versus r for egg white and *Gillette* foams (Figure 6.36), as we did for the theoretical bubble size distributions for egg white and water media (Figures 6.34-6.35). For *Gillette* foam, $\alpha\lambda/f$ is proportional to r^2 (within error bars) and there is no offset. If we recall from chapter 4, *Gillette* foam radius scales as $t^{0.4}$, because disproportionation is the main process in this high void fraction foam. In this case, we see almost linear scaling of $\alpha\lambda/f$ with r^2 for both void fraction *Gillette* foams. For egg white foam of 0.78 void fraction, $\alpha\lambda/f$ appears to increase with radius more rapidly than r^2 with the best power-law fit to the data giving $\alpha\lambda/f \propto r^{2.75}$. Image analysis for this foam shows that $r \sim t^{0.34}$. For 0.65 void fraction egg white foam, the data are not well fitted by a simple power law, with the best fit yielding $\alpha\lambda/f \propto r^{1.9}$ (with a reduced chi-squared of 9). Better fits to the data can be obtained by including a constant offset (Figure 6.37), yielding $\alpha\lambda/f$ = 30.7+0.00016·$r^{4.1}$, (χ^2_{red}=

0.49) for φ = 0.78 and $\alpha\lambda/f$ = 54.6+2.32·10^{-5}·$r^{4.5}$ (χ^2_{red}= 0.89) for φ = 0.65. Although the simulations in Fig. 6.35 suggest a mechanism (large viscous damping) by which such an offset can occur, the large exponent of 4 is not expected. This different behaviour may be attributed to two possible mechanisms: the larger contribution of viscous damping to the attenuation and the fact that disproportionation is not the only foam aging mechanism in these lower void fraction foams. For instance, departures from simple power law behaviour appear greater in the lower void fraction foam where drainage effects would be expected to be more significant.

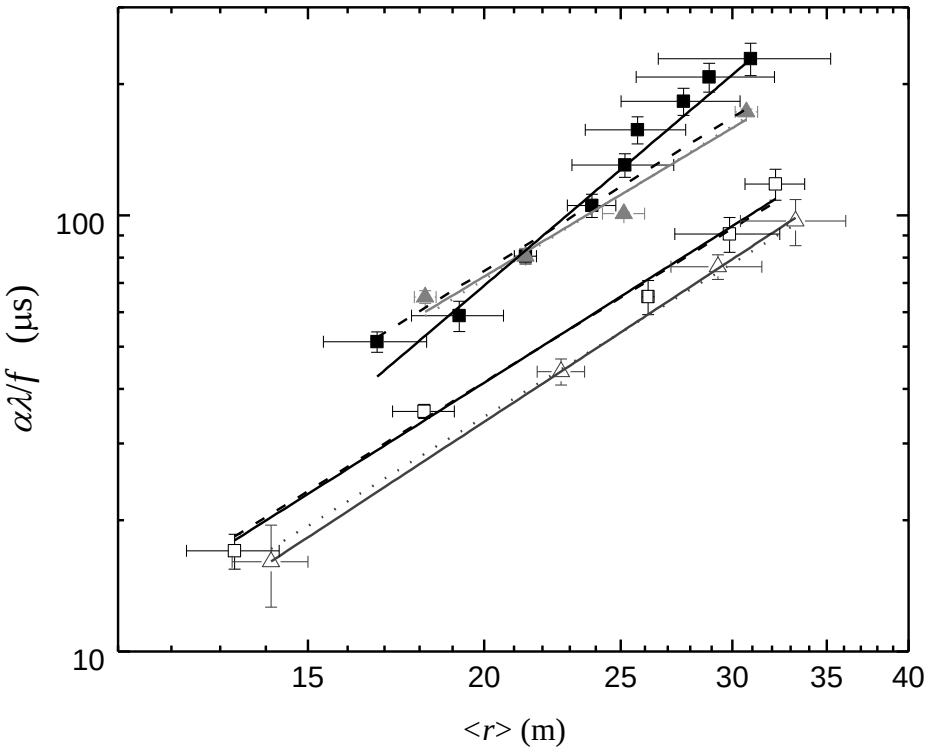

Figure 6.36. $\alpha\lambda/f$ (averaged over four frequencies) versus $\langle r \rangle$ (mean radius) for egg white and *Gillette* foams. The symbols represent: ▫ *Gillette* foam with 0.93 void fraction, solid line represents best power law fit, $\alpha\lambda/f = 0.09 \cdot r^{2.04}$; ($\chi^2_{red}$= 0.87, R–Squared = 0.98), dashed line (- - -) represents forced r^2 power law fit, $\alpha\lambda/f = 0.104 \cdot r^2$, ($\chi^2_{red}$= 0.68, R–Squared = 0.98).

△ *Gillette* with 0.90 void fraction, solid grey line represents best power law, $\alpha\lambda/f = 0.059 \cdot r^{2.12}$, ($\chi^2_{red}$= 0.013, R-Squared = 0.999); Dotted grey line (·····) represents forced r^2 power law fit $\alpha\lambda/f = 0.086 \cdot r^2$, ($\chi^2_{red}$= 0.078, R–Squared = 0.99).

■ egg white foam with 0.78 void fraction, solid line represents best power law fit, $\alpha\lambda/f = 0.018 \cdot r^{2.75}$; ($\chi^2_{red}$= 0.91, R–Squared is 0.94), black dashed line represents r^2 forced fit $\alpha\lambda/f = 0.19 \cdot r^2$, ($\chi^2_{red}$= 2.17, R-Squared = 0.88).

▲ egg white foam with 0.65 void fraction, solid grey line represents simple power law fit, $\alpha\lambda/f = 0.22 \cdot r^{1.94}$, ($\chi^2_{red}$= 9.1, R–Squared = 0.95), dashed grey line represents forced to r^2 fit, $\alpha\lambda/f = 0.18 \cdot r^2$, ($\chi^2_{red}$= 6.22, R –Squared = 0.96).

Error bars represent standard deviation.

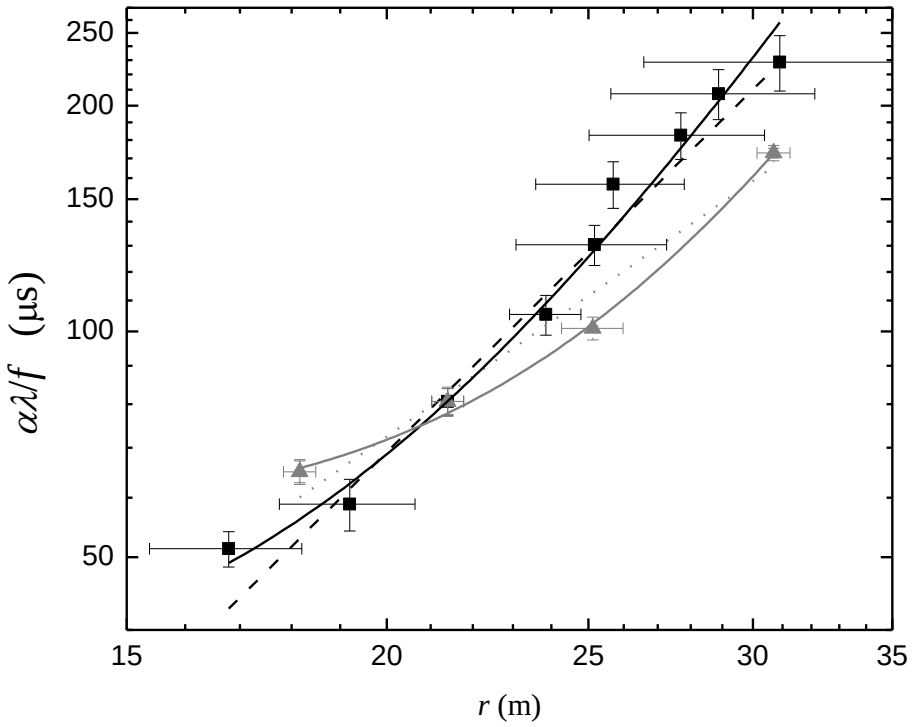

Figure 6.37. $\alpha\lambda/f$ versus $\langle r \rangle$ (mean radius) for egg white foams, replotted to show fits to a power law with a constant offset (solid lines). The symbols represent:

■ egg white foam with 0.78 void fraction: solid line represents the best fit to a power law plus a constant, $\alpha\lambda/f = 30.7+0.00016 \cdot r^{4.1}$, ($\chi^2_{red}$= 0.49, R–Squared = 0.97). The dashed line represents the best fit to a simple power law (no offset) from Figure 7.38.

▲ egg white foam with 0.65 void fraction, solid grey line represents best fit to a power law plus a constant, $\alpha\lambda/f = 54.6+2.32\cdot10^{-5} \cdot r^{4.5}$. ($\chi^2_{red}$= 0.89, R–Squared is 0.99). The dotted line is the fit to a simple power law (no offset) from Figure 7.38.

Error bars represent standard deviation.

It should also be noted that the relatively large uncertainties in the measurements of $\langle r \rangle$ at long times, due to the limited field of view of the images, means that we cannot rule out completely a possible $\langle r \rangle^2$ dependence for $\alpha\lambda/f$ in the egg white foams, at least for the higher volume fraction egg white foam at the earlier aging times. The dashed and dotted lines for the egg white foams in Fig. 6.36 show forced fits of the data for $\alpha\lambda/f$ to such an $\langle r \rangle^2$ dependence, with a reduced chi-squared of 2.2 and 6.2 for the $\varphi = 0.78$ and $\varphi = 0.65$ foams, respectively; thus this forced r^2 fit does not represent the observed dependence on r very well for the entire range of aging times. However, for the $\varphi = 0.78$ foam, fitting the data for just the lowest 4 values of $\langle r \rangle$ to an unrestricted power law (corresponding to the early times before the apparently anomalous dip in $\langle r \rangle^2$ versus t in Fig. 6.12 occurs), gives $\alpha\lambda/f \propto \langle r \rangle^{2.1}$ with a chi-squared of 1, suggesting that the early time evolution of the foam may be more similar to the high void fraction Gillette foams. Thus, even though Figs. 6.36 and 6.37 clearly show that $\alpha\lambda/f$ tracks the evolution of bubble sizes in these foams, the exact relation between $\alpha\lambda/f$ and $\langle r \rangle$ for egg white foams has yet to be determined definitively. A better method of image analysis would be needed to determine this relationship empirically – an advance that could enable the average bubble radius to be measured from $\alpha\lambda/f$.

Let us come back to the experimental results and the predictions of Foldy's models for the two egg white foams that are represented in Figures 6.28-6.29. In the Foldy 1 model, we see an increase of $\alpha\lambda/f$ with aging time and also we start seeing changes in $\alpha\lambda/f$ that could be associated with resonance effects. However, in our modeled Foldy 1 and Foldy 2 results we do not see the same rise in $\alpha\lambda/f$ with aging time as we see in the measured results. Also we know that power law scaling of $\alpha\lambda/f$ with r^2 is not predicted by the Foldy 1 model, largely because of the high viscosity contribution to the attenuation in the model. This simple behaviour is also not

seen in the experimental results, although the variation of the experimental data for $\alpha\lambda/f$ is closer to an r^2 dependence. Although the Foldy 1 model predicts a rise in $\alpha\lambda/f$ with aging time at the higher frequencies, an effect seen in the measured data at all frequencies, this rise is likely due to the approach to bubble resonance in the model (Leroy, 2008; Page, 2010), but the resonances of single bubbles in a uniform medium are likely to be quite different to possible resonances of the foam cells; for this reason, the modified Foldy models would not be expected to work close to bubble resonance, consistent with the discrepancies seen between $\alpha\lambda/f$ obtained from the Foldy 1 model and our experimental data.

As was mentioned before, the Foldy 1 model predicts resonance at lower frequencies than the Foldy 2 model. However, the Foldy 2 modelling of $\alpha\lambda/f$ agrees less well with the measured results for both foams, as it predicts much smaller values, and does not exhibit even the observed trend with aging time. The Foldy model in general describes sound wave propagation in bubbly liquids, but structurally, bubbly liquids and foams are different. Therefore, even with the new effective medium approximations made in the modified Foldy models, which attempt to account for the reduced density of the medium surrounding each bubble, it would appear that these modifications are not sufficient to account for the behaviour of high concentration bubbly media such as foams. Thin films in foams are somewhat elastic and can propagate shear waves; in the original formulations of Foldy's model, this physical aspect of the foam was not included (Kann and Kislitsyn, 2003; Mujica and Fauve, 2002), although in our formulation, the effect of the average shear modulus on the bubble resonance frequency was included (see equation 6.11). Thus, it is not so much the effects of finite shear for foams that is the reason for failure of the Foldy models to account for our experimental data, but the different structure of the bubbles in foam that leads to different behaviour.

6.6 Conclusion

In high void fraction foams, ultrasound attenuation is very high and thermal dissipation is not the only contribution determining high sound absorption in the foams. For both foams, egg white and Gillette, high void fraction and matrix viscosity is responsible for high sound attenuation. Both Foldy 1 and Foldy 2 models predict values of the phase velocity and attenuation coefficient in the same magnitude range as the experimental data at zero aging time; however these models do not account for the experimental observations of bubble size evolution with aging time. The experimental data for $\alpha\lambda/f$ as a function of r^2, measured during aging of the foams, show clearly that both foams, egg white and *Gillette,* with different void fractions, evolve at different rates. Further model development is necessary in order to account for effects of bubble lamellas on sound propagation (Kann and Kislitsyn, 2003; Mujica and Fauve, 2002).

CHAPTER 7. EGG WHITE FOAM RESISTIVITY RESULTS AND DISCUSSION

7.1 Introduction

Ultrasonic studies revealed that foams have an unstable nature, and their aging processes can be complicated. Food foams are rarely very dry, like synthetic *Gillette* foams, where oneinstability process, such as disproportionation, is the main aging mechanism. In food foams, aging mechanism very often impact each other, for instance disproportionation can be accelerated by drainage effects (Campbell, 2008; Saint-Jalmes, 2006; Spencer, 2006). In previuos experiments on egg white foam rheology (Spencer, 2006) and my imaging results in chapter 4 it is apparent that egg white foams tend to drain, and at void fractions as low as 0.65, the drainage process dominates. Therefore, there is a need to study the liquid drainage process, parameters affecting drainage, and look for appropriate models in order to understand fully the evolution in structure and properties of these type of food foams. Even though egg white foams have high resistivity due to their high void fraction, they will conduct electric current and therefore an electrical resistivity technique was employed to follow liquid drainage.

7.1 Egg white foam resistivity measurement results

Egg white foam stability was evaluated by measuring the electrical resistance at different foam heights, thereby investigating the free drainage of liquid in the foam. All foam samples of four void fractions (0.60, 0.65, 0.78 and 0.81) were 9 cm in height and remained at this height throughout all 600 min aging time. Resistivity values were obtained at 9 equally spaced (0.01 m) locations. To quantitatively evaluate the resistance changes, 3 foam height locations were chosen. In this chapter, foam height will be referred as the bottom (H = 0.005 m), middle (H = 0.035 m) or top (H = 0.075 m) part of the foam. Other measurements of the evolution of

resistance changes with aging time are interpolated in a sequence, according to foam height (*H*: 0.015 m; 0.025 m; 0.045 m; 0.055 m; 0.065 m).

The resistivity change with aging time for four different void fraction foams is displayed in figure 7.1. Since all measured resistance values depend on apparatus dimensions (Figure 3.4), the use of Formula 3.6 allows foam resistivity (ρ_R) to be determined using the formula: $\rho_R = 0.0236 \cdot \mathrm{R}$. In Figure 7.1 b) the early time resistivity evolution with aging time for 4 void fraction foams at 3 foam column heights is shown.

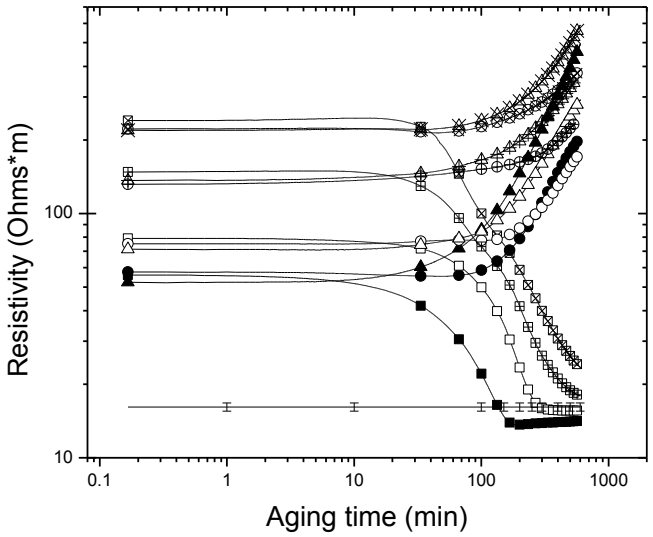

a)

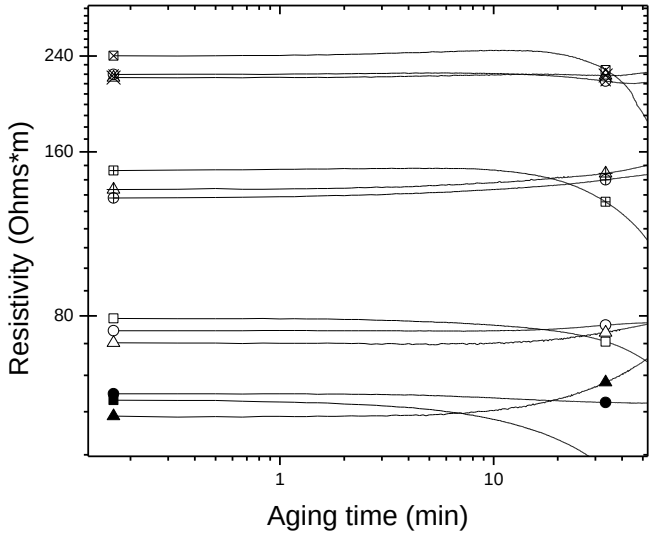

b)

Figure 7.1. Resistivity versus aging time for foams of 4 void fractions (φ) at different foam heights (H): φ = 0.60: H = 0.005 m (■), H = 0.035 m (●), H = 0.075 m (▲); φ = 0.65: H = 0.005 m (□), H = 0.035 m (○), H = 0.075 m (△); φ = 0.78: H = 0.005 m (⊞), H = 0.035 m (⊕), H = 0.075 m (⊞); φ = 0.81: H = 0.005 m (⊠), H = 0.035 m (⊛), H = 0.075 m (✳). In Figure 4.1 a), the horizontal line of low resistivity represents the resistivity value of the egg white and sugar mixture without air. Figure 4.1 b) is the magnified early foam aging stage results that are displayed in Figure 4.1 a). The standard deviation of expemeriments performed in duplicates varied between 0.4 to 5 Ohms*m for all aging times and all foam heights. Error bars are smaller than the symbols.

Egg white foam stability varies depending on the void fraction (Figure 7.1 a) with the first changes in foam resistivity occuring at the bottom part of the foam. The wettest foam (φ = 0.60) is the most unstable foam, therefore changes in resistivity occur after 1 min. For other foams, we see changes in resistivity at the bottom of the foam at the void fraction of 0.65 in 3 min, of 0.78 in 10 min and of 0.81 in 20 min, respectively. This time is needed for egg white foams to overcome capillary forces in foam films and Plateau borders (Saint-Jalmes, 2006), after which liquid starts to flow downwards through the foam. Not surprisingly, for the wettest foam it takes almost no time to see liquid drainage, since the liquid fraction of this foam is higher than the critical liquid fraction ε_c = 0.36 (random close packing of non-deformed spheres) for almost monodisperse surfactant or protein foams (Britan *et al*., 2009). Britan *et al.* (2009) stated that when the liquid fraction in the foam reaches the critical volume fraction of ε_c = 0.36 bubbles are spherical and the foam cannot hold any additional liquid, so that the drained liquid accumulates underneath the foam (Saint-Jalmes, 2006; Britan *et al*., 2009). For the wettest foam, after 150 min of aging the resistivity value of the foam bottom layer reaches approximately that measured in the egg white liquid and sugar mixture containing no air, which is ρ_R = 16.15 Ohms·m. In fact, for the lowest void fraction (0.60) foam, the resistivity reaches a minimum value of 13.9 Ohms·m after 150 min, and for foam of φ = 0.65, the resistivity drops to 15.6 Ohms·m after 450 min. of aging. It is evident from the low resistivity values that egg white liquid starts fully accumulating at the foam bottom and at longer aging times the measured resistivity is that of an egg white liquid and sugar mixture. For both higher void fraction (φ = 0.78 and φ = 0.81) foams, the resistivity of drained out liquid is higher than the initial egg white liquid and sugar mixture with no air. In addition, for foams of 0.78 and 0.81 void fraction, the resistivity at the foam bottom is decreasing for all 600 min of aging time and reaches

17.9 Ohms·m and 23.5 Ohms·m, respectively. Different measured resistivity values of the drained out egg white liquid reflect changes in the egg white liquid and sugar mixture: egg white protein quality is altered, and, in addition, protein composition might have been changed (MacDonnell *et al.,* 1955; Cunningham, 1976; Halling, 1981). In this research I have not conducted any experiments to identify how these proteins change , since there is available literature in this research area. From published results on egg white drainage experiments, it is clear that the drained out liquid protein composition is different from unwhipped egg white (MacDonnell *et al.,* 1955; Cunningham, 1976; Halling, 1981). In addition, Bazine *et al*. (2005) reported that the electrical conductivity of liquid bio-products such as milk is due to the presence of minerals and charged species - proteins. To measure the protein contribution to electric current is not simple, particularly in such complex food systems as milk or egg whites, especially when changes in pH change protein charge and other system factors (Bazine *et al*., 2005).

The resistivity values of the middle (H = 0.035 m) and top (H = 0.075 m) foam parts increase continuously for all void fraction foams with the foam resistance values of the top layer increasing at a higher rate. The differentiation in resistivity values with foam height and void fraction indicates that the drainage processes occur at different rates at different foam heights. The liquid at the top part of the foam can only flow down, while in the middle part of the foam the liquid will be moving down from the upper layers, as well as liquid flowing out from this part down to the bottom of the foam. The increase in resistivity at the foam top layer reflects the reduction of liquid in the foam layer, essentially the foam is drying out, because no drained liquid flows into this region. Overall, comparing the four void fraction foams, the higher the amount of air that is whipped into the foam, the higher the foam resistivity at a given height that is measured at all aging times.

7.2 Egg white foam conductivity and liquid fraction results

From foam resistivity (ρ_r) values the foam relative conductivity (σ_r), which is inversely proportional to foam resistivity, was calculated. In addition, by measuring foam density and using Formula 7.3 and 7.4 liquid fractions (ε) at different foam heights (H) were determined. Thus plots of relative conductivity against liquid fraction can be determined.

In Figure 7.2 measured relative conductivity (σ_r) values of the foam at different liquid fractions (0.19, 0.22, 0.35 and 0.4) at 0 min of aging is presented. Conductivity was measured at all heights of the foam and values plotted in Figure 7.2 are the average of 8 rings. At this time, no drainage will have occurred. As well, in Figure 7.2 the calculated theoretical conductivity value over the full liquid fraction range, from 0 to 1, is shown.

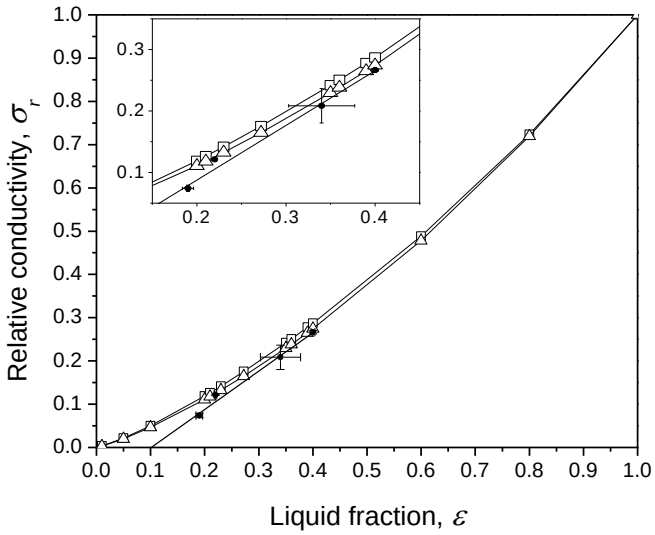

Figure 7.2. Theoretical and measured (●) relative conductivity versus liquid fraction. There is linear dependence between ε and σ up till ε = 0.6. Symbols represent: theoretical relative conductivity (equation 2.84) (-▫-), theoretical relative conductivity with tortuosity model (equation 2.85) (-△-). Linear fit (represents the line through experimental points in the figure) resulting in this ε and σ_r relationship: $\sigma_r = \varepsilon \cdot 0.8894 - 0.09028$. Error bars represent standard deviation of 3 replications of ε and σ_r (In Figure 7.2 some error bars are smaller than the symbol).

From the inset of Figure 7.2 it is visible that the measured foam conductivity values deviate at the lower void fraction range from the calculated ones based on the empirical Formula 2.84. Including a tortuosity element in relation 2.78 does not have a big impact on the conductivity values over all the liquid fraction range. It is known that systems rich in proteins are capable of binding water or ions into their structure (Zayas, 1997), even though egg white proteins, among all the proteins, are classified as poor water binders (Kneifel *et al.,* 1991). From Figure 7.2 it is visible that, as the liquid fraction in the foam decreases, egg white foam conductivity deviates from Formula 2.84 and measured liquid fraction in the foam is smaller than the calculated values. One of the possible explanations is that, as the bubbles are formed in the foam, protein polar polypeptide chains interact with water molecules at the air-water surface (Zayas, 1997). As water is being held in the foam structure, ion and charged species mobility are limited to some extent (Zayas, 1997). A second possible explanation why measured and calculated results are different comes from the work of Datye and Lemlich (1983). Datye and Lemlich (1983) in their experiments on the same void fraction of monodispersed foams but different bubble sizes found that measured conductivity is lower for the foam with small bubbles than for the foam with larger bubbles. In addition, different conductivity values were measured for these two different size monodispersed foams along all the liquid fraction range that was studied: from 0.01 to 0.05. This can be explained by taking into account the classical Laplace relationship 2.22. Keeping the same liquid fraction of the foam and decreasing bubble radius, triangular Plateau border cross section dimensions do not decrease proportionally, due to the increased suction pressure in the Plateau border. The increased suction pressure draws more liquid into the Plateau borders, therefore the conductivity in the lamellae increases (Datye and Lemlich, 1973).

7.3 Estimation of liquid fraction in aging egg white foams from resistivity measurements

By measuring resistivity of the foam at different heights and using equation 2.84 it is possible to estimate the liquid fraction change in the aging foam. Due to differences in the mechanisms relating the liquid fraction and the conductivity of surfactant foam and egg white protein foams, it was necessary to establish a correction for Formula 2.84. Hence, an attempt was made to fit the linear equation through the experimental conductivity values at the lower liquid fraction range. This allowed me to empirically evaluate the liquid fraction changes in the foams during the aging process. This is particularly necessary for higher void fraction foams where bigger deviation at zero seconds of aging time was evident. The possible reasons of this fact were explained in the previous section. Therefore, to ensure accurate estimation of liquid fraction change in the aging foam, relative conductivity values versus liquid fraction was plotted and a linear equation: $\sigma_r = \varepsilon \cdot 0.8894 - 0.09028$, was fitted. The latter equation was used to obtain liquid fraction (ε) as it changed during foam aging and plots of $\varepsilon/\varepsilon_o$ versus aging time for different foam heights were constructed (Figures 7.3-7.8, in section 7.4).

7.4 Egg white foam liquid fraction changes during aging

In Figures 7.3-7.8 the results of relative liquid fraction changes due to aging in 4 void fraction foams are presented. The liquid fraction is normalized by ε_0, defined as the liquid fraction at 0 min of aging as the foam is just poured into the measurement cylinder. Slopes (ψ) (in equation 2.31: $\varepsilon(z) = t^{\psi}$) of the $\varepsilon/\varepsilon_0$ curves against aging time were taken at two foam heights (0.035 m and 0.075 m) for 3 aging time periods: 150 to 250 min, 250 to 500 min and 500 to 600 min. Depending on the foam height and void fraction, the ψ exponent varied from -0.55 to -0.37 for the wettest foam (φ = 0.60) and from -0.1 to -0.23 for the driest foam (φ =

0.81). Depending on the foam height and aging time, the calculated exponent ψ from equation 2.31 varies from $3.5 \cdot 10^{-4}$ to $1.9 \cdot 10^{-4}$ for the middle (0.035 m) and top (0.075 m) parts respectively of the foam at 0 min of aging. For the same foam heights at 600 min of aging, the ψ exponent varies from -0.07 to -0.04. The slope ψ varies with aging time and with foam height: for the wettest foam the slopes are the highest, while drier foam exhibits the slowest drainage (ψ is the smallest). A small exponent ψ confirms that egg white foams fall into the immobile drainage regime (Equation 2.36: for $\chi<1$ $\varepsilon \sim t^{-2/3}$ and for $\chi>1$ $\varepsilon \sim t^{-1}$), which agrees with drainage results for β-lactoglobulin foams (Rullier *et al.*, 2008; Rullier *et al.*, 2009), where ψ = -0.5.

Looking at the $\varepsilon/\varepsilon_o$ slope (ψ) change for the same height (0.075 m) locations for the wettest foam (φ = 0.60) we see that drainage is fastest at the beginning (150 min to 250 min period) and slows gradually. The exponent ψ is reducing from -0.53 to -0.37 (Figure 7.8). However, $\varepsilon/\varepsilon_o$ slope change for the middle (0.035 m) location of the same foam shows an increase in liquid flow during the second (250 min till 500 min) drainage period, and in the third, the last (500 min to 600 min) liquid flow decreases again (Figure 7.7 and Figure 7.8). For the driest foam (φ = 0.81) $\varepsilon/\varepsilon_o$ slope (ψ) increases with aging time for all heights: from -0.1 to -0.17 at H = 0.035 m and from -0.14 to -0.23 at H = 0.075 m respectively.

From these results we see that changes in relative liquid fraction in all egg white foams at these void fractions are relatively very slow. This can be explained by the fact that drainage was not the dominant process at these void fractions. From Spencer's (2006) work on the rheological behaviour of aging egg white foams it is clear that foams are subject to rapid disproportionation rather than drainage at higher void fractions. Spencer (2006) determined that for wet egg white foams, the void fraction was required to be as low as φ < 0.45 in order to exhibit changes due

more to drainage than to coarsening. In addition, drainage rates were observed to be significantly smaller for protein foams and higher for surfactant foams (Maurdev *et al.*, 2006). This is especially the case when proteins are used as a foaming agent: the proteins unfold during whipping and their hydrophilic portions reside in the Plateau borders, so that the resistance to liquid flow within the Plateau borders is increased (Maurdev *et al.*, 2006).

In our resistivity studies on foam aging, simultaneous image analysis experiments on the same egg white foams were not conducted. Therefore, we can not directly measure the coarsening effect on foam drainage. Saint-Jalmes and Langevin (2002) in their studies show that coarsening and drainage coupling depends on the gas used and the bubble size. Strong coarsening eventually impacts drainage rates in the foam, since due to coarsening, the thickness of the lamellae increases and the Plateau borders widen, therefore accelerating liquid flow. Thicker lamellae in turn slow down gas diffusion through the films (Hilgenfeldt *et al*., 2001; Saint-Jalmes *et al*., 2000; Saint-Jalmes and Langevin, 2002).

We have attempted to calculate the velocity (v_d) of freely draining liquid at 0 min of aging time by using equation 2.40 for egg white foams of void fractions 0.65 and 0.78. Respectively the liquid flow velocities are: $2.5 \cdot 10^{-9}$ m/s and $8.12 \cdot 10^{-10}$ m/s. The velocities are very small if compared with the liquid flow velocity for surfactant foam (φ = 0.99) containing hydrophilic particles, with an average bubble size of 40 μm (Britan *et al*., 2009), which is in the range of 10^{-6} m/s to 10^{-8} m/s.

Small liquid flow velocity of egg white liquid can be explained by the protein aggregate formation during whipping process. It is known that thermal and mechanical protein treatment changes protein conformational structure, therefore albumin (the major foaming protein) is denatured through forming a coagulated network and surface active insoluble particles, or so

called aggregates with very little water holding capacity (Nakamura and Sato, 1964; Du *et al*., 2002b; Lau and Dickinson, 2004; Croguennec *et al*., 2007; Raikos *et al*., 2007; Schmitt *et al*., 2007; Rullier *et al*., 2008; Rullier *et al*., 2009; Dickinson, 2010). These protein aggregates can reach the size of a few hundred nanometers and can reduce foaminess. However, the presence of these aggregates increases foam stability (Davis and Foegeding, 2004; Rullier *et al.*, 2008). If the particles are able to adsorb at the air-liquid interface, they enhance the viscoelasticity of the films. Foam structure stabilization due to formed aggregates can be explained by the weak-gel like network formation between the foam bubbles (Rullier *et al*., 2008). On another hand, if there are large particles, purposely added or formed during the foam making process, then particles may get stuck in foam structure elements like lamellae and Plateau borders and act like a cork, thus potentially reducing the drainage rate. As is reported for both casein and β-lactoglobulin foams (Saint-Jalmes *et al*., 2005; Rullier *et al*., 2008), particles (aggregates) cause percolations, and as a consequence this rigidifies the foam films and prevents liquid flow. By limiting flow, further thinning of the lamellae to their critical thickness, where the film ruptures, is prevented. Two hypotheses of foam stabilization, either by adsorption at the interface and gel-like network formation or by cork effect, depend on the aggregate concentration and size. The small amount of large aggregates will cause a cork effect and drainage rate reduction (Rullier *et al.*, 2008). Notably, gel-like structure formation or cork effect occurs in any foam made from high molecular weight protein or a compound that forms particles during the foaming process (Rullier *et al.*, 2008). Similarly, egg white protein ovalbumin is sensitive to mechanical overbeating, therefore aggregates (dense solid particles) in foam during the whipping process are formed through the physical and chemical bonding. Through different types of denaturation under certain conditions (pH, ionic strength, protein concentration), albumin may form aggregates as

thin strands or solid particles (Du *et al*., 2002b; Croguenneca *et al*., 2007). As egg white liquid is a mixture of positively and negatively charged proteins, the interaction between oppositely charged ovalbumin and lysozyme proteins may occur causing aggregate formation (Wierenga *et al.,* 2010). Solid foam structure formation, from liquid to soft solid is accelerated because of these formed aggregates (Zayas, 1997).

From these experiments we see that foam structure is stable if it consists of smaller bubbles and higher void fraction. This limits the possibility of strong drainage effects occurring in the well-whipped high void fraction foam. However, using a simple relation for liquid fraction and electrical conductivity becomes challenging when protein foams are being tested. Changes in total ion and charged particle amount as the liquid fraction of the foam increases introduces a measurement error in estimating the liquid fraction change over aging time. However, considering the possible mechanisms causing deviation in Formula 2.84 when protein foams are being tested and applying the corrected equation ($\sigma_r=\varepsilon\cdot0.8894-0.09028$) instead of Formula 2.84, a corrected estimated relative liquid fraction during egg white foam aging can be determined.

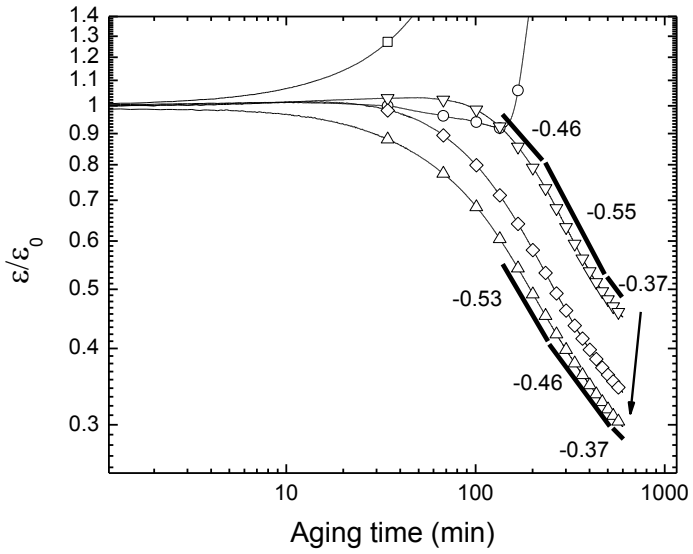

Figure 7.3. Foam (φ=0.60) normalized liquid fraction ($\varepsilon/\varepsilon_o$) versus aging time at different foam heights (H). An arrow indicates an increase of the foam height (H) from the bottom to the top. Symbols represent these foams heights: H = 0.05 m (□), H = 0.015 m (○), H = 0.035 m (▽), H = 0.065 m (◇), H = 0.075 m (△).

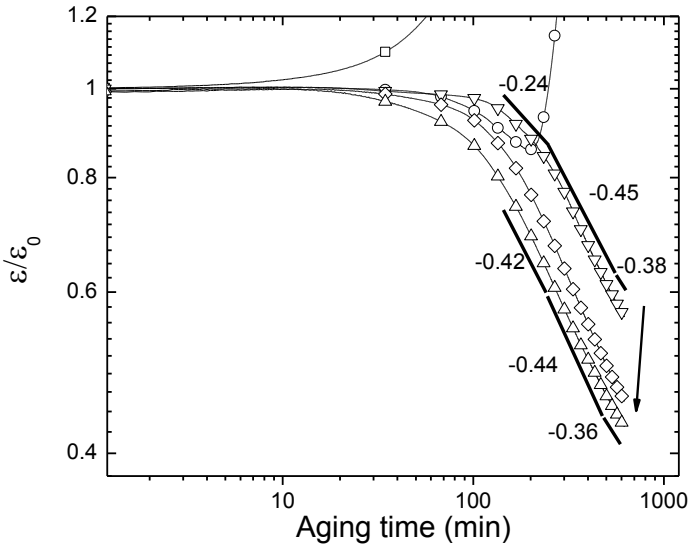

Figure 7.4. Foam (φ = 0.65) normalized liquid fraction ($\varepsilon/\varepsilon_o$) versus aging time at different foam heights (H). An arrow indicates increase of the foam height from the bottom to the top. Symbols represent these foams heights: H = 0.05 m (□), H = 0.015 m (○), H = 0.035 m (▽), H = 0.065 m (◇), H = 0.075 m (△).

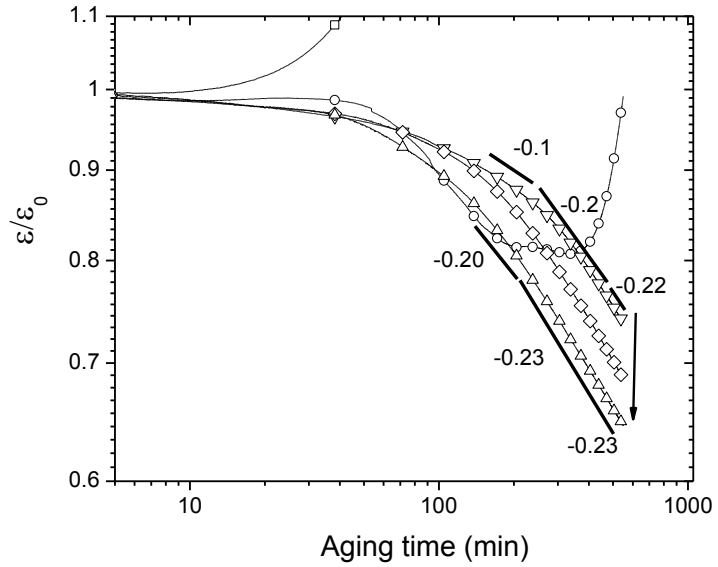

Figure 7.5. Foam (φ = 0.78) normalized liquid fraction ($\varepsilon/\varepsilon_o$) versus aging time at different foam heights (H). An arrow indicates increase of the foam height from the bottom to the top. Symbols represent these foams heights: H = 0.05 m (□), H = 0.015 m (○), H = 0.035 m (▽), H = 0.065 m (◇), H = 0.075 m (△).

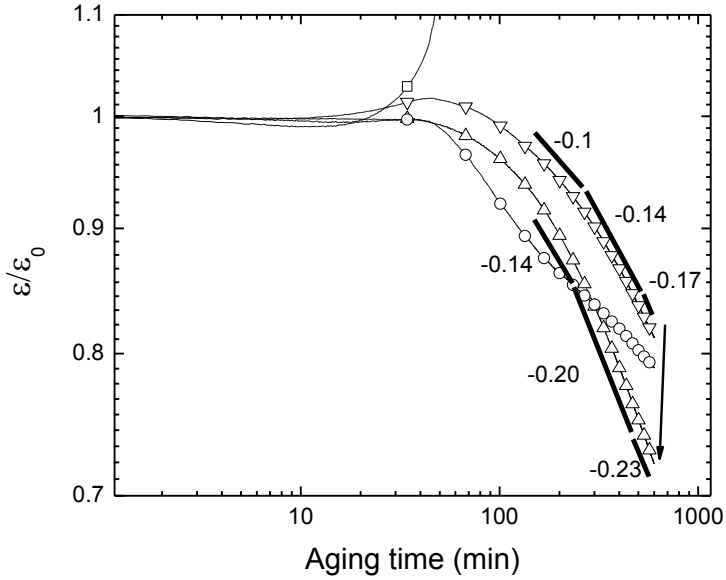

Figure 7.6. Foam (φ = 0.81) normalized liquid fraction ($\varepsilon/\varepsilon_o$) versus aging time at different foam heights (H). An arrow indicates increase of the foam height from the bottom to the top. Symbols represent these foams heights: H = 0.05 m (□), H = 0.015 m (○), H = 0.035 m (▽), H = 0.075 m (△).

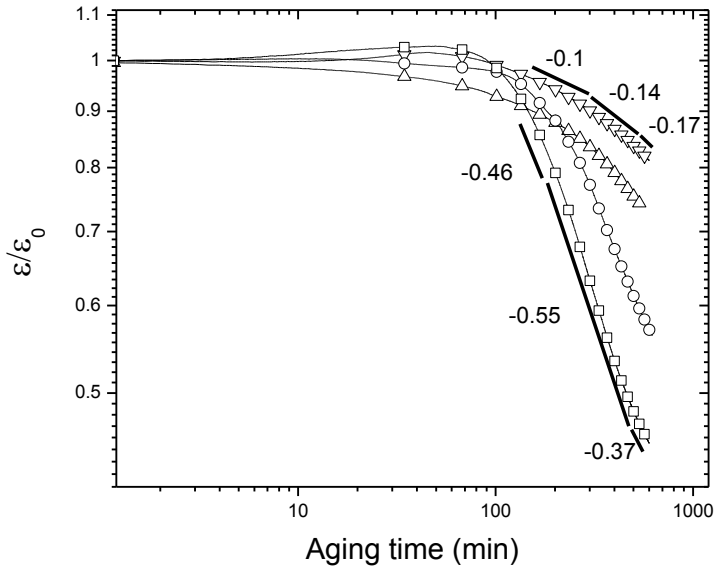

Figure 7.7. Foam normalized liquid fraction ($\varepsilon/\varepsilon_o$) versus aging time at a foam heights of H = 0.035 m. Symbols represent different void fractions (φ): 0.60(□), 0.65(◇), 0.78(△), 0.81(▽).

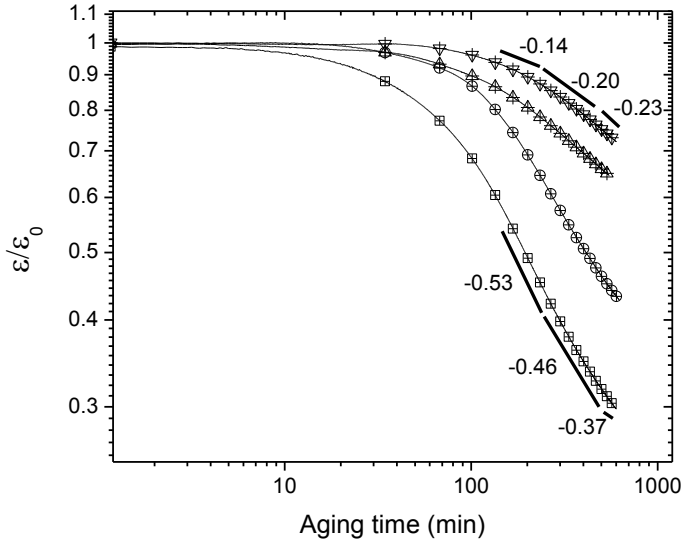

Figure 7.8. Foam normalized liquid fraction ($\varepsilon/\varepsilon_o$) versus aging time at a foam heights of H = 0.075 m. Symbols represent different void fractions (φ): 0.60(⊟), 0.65(⊕), 0.78(⊞), 0.81(⊞).

7.5 Immobility of egg white foams

Drainage experiments on egg white foam are evaluated from two perspectives: how fast foams drain, and employing drainage theory for boundary conditions, how the foam drains. Qualitatively and quantitatively foam drainage is analysed from mobile and immobile regime views.

Drainage is much slower for all void fraction (from 0.60 till 0.81) egg white foams as compared to other protein foams, such as WPI, casein or α, β-lactoglobulin with aggregates (Rullier *et al*., 2008; Nicorescu *et al*., 2009). In the foam the liquid fraction change over time conforms to a power law with an exponent ψ. In comparison with published results, the exponent ψ for β-lactoglobulin foam (φ = 0.74) with 90% of aggregates is the same as for the wettest egg white foam (φ = 0.60): -0.5 (Rullier *et al*., 2008). However, in these egg-white foams, this is the highest exponent ψ value, since for the highest void fraction foam (φ = 0.81), the drainage rate is even slower and the exponent ψ is even lower: -0.1.

An attempt was made to evaluate which parameters influence the exponent ψ and determine if egg white foams fall into the mobile or immobile surfaces drainage regime. The exponent ψ is a function of void fraction, bubble size distribution, geometry elements (Plateau border L_P), nature of the surfactant, viscosity, interfacial properties (shear viscosity) and K_x (permeability constant). Therefore, from my experimental results we can evaluate qualitatively the influence of void fraction and bubble size distribution on the exponent ψ. The parameter χ and the dimensionless parameter *M,* which take into account the surface shear and bulk viscosities, the average bubble size and the void fraction, quantitatively estimate the type of drainage regime in which the egg white foams may be classified (Saint-Jalmes and Langevin, 2002).

Free drainage experiments are easier to perform, but more difficult to analyse, because of the disproportionation occurring at the same time (Saint-Jalmes and Langevin, 2002; Feitosa and Durian, 2008; Goyon *et al*., 2010). Bubble size distribution evolution with time varies from foam to foam, depending on the void fraction and this has an impact on drainage rate. Therefore, as the liquid drains out of the foam, bubble size along the foam column evolves unevenly: at the top - as the lamellae are getting thinner the bubbles will grow faster, obtaining polyhedral shape, while at the bottom, as the foam is getting wetter, bubbles will be more spherical, therefore lamellae are thicker and one would expect disproportionation to be slower (Britan *et al*., 2009). Bubble size changes along the foam height will have an effect on the exponent ψ. As an example, for all void fraction foams the exponent ψ is higher for the top part of the foam, rather than for the bottom. That could be related to disproportionation occurring at different rates at different foam heights as the foam ages. For the 0.60 void fraction foam, where the bubbles are large and round, the exponent ψ is the highest for all the foams and is decreasing from -0.46 to -0.37 for the bottom (H = 0.035 m) and from -0.53 to -0.37 for the top (H = 0.075 m), respectively. The decrease of the exponent ψ indicates slowing down in liquid fraction change over all foam heights for this particular void fraction (0.60) foam. On another hand, for the highest void fraction (0.81) foam, the exponent ψ starts increasing from -0.1 to -0.17 for the bottom (H = 0.035 m) and from -0.14 to -0.23 for the top (H = 0.75 m) layer. This indicates that in the driest egg white foam, through these aging times (150 to 600 min) drainage only accelerates. For the driest foam the bubbles are small and disproportionation occurs rather than liquid drainage. The larger the bubbles get, the more the exponent ψ increases over aging time, indicating that bubble lamellae are getting thicker and this results in faster liquid fraction change over all foam heights.

Parameter χ was found for our egg white foams in the range of $1.53 \cdot 10^{-5}$ to $7.34 \cdot 10^{-6}$ at 0 min of aging for 0.6 and 0.81 void fraction foam, respectively. At very long aging times, 600 min, the parameter χ was higher: in the range of $8.4 \cdot 10^{-4}$ to $4 \cdot 10^{-4}$, for 0.6 and 0.81 void fraction foam, respectively. This leads to agreement with Saint-Jalmes and Langevin (2002) research results for protein foams: as $\chi < 1$ the drainage regime is immobile and remains so for the entire aging time for all egg foam heights, for all void fractions of egg white foam and aging times. It is shown in the literature that with the bulk viscosity (η) higher than 10 times that of water for surfactant foams, the drainage regime remains immobile (Saint-Jalmes and Langevin, 2002). In our case, egg white liquid bulk viscosity is 33 times higher than water. The dimensionless number *M*, which describes the balance between surface dissipation effects and bulk viscosity dissipation, is 0.012 for egg white foams (where $M = (\eta r_P)/\eta_s, \eta$ = 0.065 g/(cm·s), for proteins surface shear viscosity η_s = 0.02 g/(cm·s) (Saint-Jalmes and Langevin, 2002), $r_P \sim D\varepsilon^{1/2}$). Protein has a higher surface shear viscosity than that of surfactant ($\eta_s = 3.6 \cdot 10^{-5}$g/s), as well as a higher bulk viscosity than surfactant (η = 0.01 g/(cm·s)), which results in a rigid Plateau border surface (Koehler *et al*., 2002; Saint-Jalmes and Langevin, 2002). As was mentioned before, $M < 1$ predicts Poiseuille like flow and our results for 40 μm bubble radius foams are in agreement with the findings of Saint-Jalmes and Langevin (2002) for protein foams.

7.6 Conclusion

The presented results show that protein foam drainage is complex and distinct from surfactant foam liquid drainage. In contrast to low molecular weight surfactants, from which the synthetic foams are made, proteins are charged species, and during foam formation the available amount of ions that conduct electric current changes, while in surfactant foams the amount of

charged species does not change. Using a corrected relative conductivity relation, it was shown that in the void fraction range of 0.60 to 0.81, liquid drainage in the egg white foams is very slow. Applying the generalized liquid drainage model and boundary conditions at the Plateau borders, it was confirmed that similarly to other protein foams, egg white foams fall into the immobile regime category. To slow down the liquid drainage in the egg white foam besides changing the surface rheology, bubble size or void fraction, it is also necessary to increase the bulk viscosity.

CHAPTER 8. GENERAL DISCUSSION

In this thesis, four techniques were used to understand complex behaviour of aging food and non-food foams. The fragile nature of the foam requires delicate approach, i.e. non-invasive methods, in order to observe degrading structure and obtain meaningful results for foam aging process evaluation. An attempt was made to develop methodology and utilise an ultrasound technique to study high void fraction egg white foam and also commercial synthetic *Gillette* (Sensitive) foam, which is a good representative of dry polyhedral foam. Egg white foam is relatively "simple" to make. However, as all food products, it is more complex and complicated to investigate; therefore we used *Gillette* foamy as a model foam for interpreting the ultrasonic results.

The main purpose of this research was to investigate two foam instability mechanisms, drainage and disproportionation, by using macroscopic and microscopic techniques. To follow free drainage in the egg white foams, an electrical conductivity method was employed and a macro scale experimental set up was built. Measurements gave good/accurate results on egg white foams in the range of 60% to 81% of air content and we were able to evaluate quantitatively liquid drainage at different heights in a standing column of the egg white foam. In order to monitor the aging process in egg white and *Gillette* foams as a result of disproportionation, an ultrasound technique was used and, as a complementary technique, imaging was also employed. Image analysis provides a good insight on the disproportionation process, as well as on the coalescence effect, which potentially could occur in egg white foams. However, there were no signs of coalescence just visually observing aging foams and inspecting images.

The free egg white foam drainage experiment design was based on a realistic angel food cake making process: the experimental container height is the same as the pan height for an angel

food cake. Drainage experiments were not conducted on *Gillette* foams. The results from electrical resistivity experiments were used in the determination of liquid fraction change during the foam aging process. By using a corrected relation between relative conductivity and liquid fraction of Formula 2.83 and 2.84 the liquid fraction change due to drainage was estimated. The correction was established experimentally, specifically for our egg white protein foams, because egg white proteins are altered through the whipping process (Davis and Foegeding, 2004; Rullier *et al*., 2008). The experiment results show that the wettest, 0.60 void fraction egg white foam was the most unstable, where changes in liquid fraction were seen within minutes of foam aging. The driest, 0.81 void fraction egg white foam, showed stability for the first 20 minutes of aging.

To interpret mechanisms associated with the drainage process in egg white foams, a generalized free drainage model and two different boundary conditions at the Plateau borders (mobile or immobile) was used. This model helped to understand what factors affected the foam instability. Our results showed that all void fraction egg white foams, for all aging times, fall into the immobile regime (Saint-Jalmes and Langevin, 2002) where the flow in the channels is Poiseuille-like. This observation is in agreement with results found in the literature on protein foam drainage (Saint-Jalmes and Langevin, 2002). In our egg white foam case, the most important factors determining that our foams fell into the immobile regime was high liquid viscosity and foam bubble size. By applying the generalized free drainage equation we were able to evaluate the velocity of free liquid flow in egg white foams, and this was observed to be relatively slow.

Image analysis on egg white and *Gillette* foams provides bubble size distributions necessary for ultrasound experiment analysis and application of the effective medium model. As well, we investigated the disproportionation process quantitatively in these foams. In aging

foams, the bubble radius growth due to disproportionation is described by a power law function. From our experiments we found that *Gillette* (93 % of air) bubble radius grows as $t^{0.4}$, while in egg white foam (78 % of air): $r \sim t^{0.34}$, whereas t corresponds to aging time. These results show that *Gillette* and egg white foam bubble radii evolve at a different rate. While in egg white foam of 0.65 void fraction, drainage is still the dominant aging mechanism, but other mechanisms likely contribute to the bubble growth and it was difficult to fit a power law function to our experimental data.

There is a lack of research work done on high void foams using ultrasound techniques. Despite the technical difficulties, I have been able to obtain meaningful results and this research makes a contribution to overall knowledge and understanding. We interpreted our results from ultrasound measurements on aging egg white and *Gillette* foams by applying Wood's model for aerated liquids and an effective medium model based on Foldy's original multiple scattering theory (Strybulevych *et al*., 2007; Leroy *et al*., 2008).

Since our foam bubble size is much smaller than the propagating wavelength at 0 min of aging, we started our interpretation of the experimental results with Wood's approximation. However, Wood's approximation does not take into account attenuation, as well as the shear elasticity associated with the Plateau borders, and Wood's original model only holds for non-dispersive media at very low frequencies. As well, bubbles grow due to disproportionation, and we expected resonance effects to influence the observed behaviour in the frequency range in which we are doing our measurements.

The results obtained from the low frequency ultrasound measurements were interpreted by using an effective medium model, in which Foldy's model, originally developed and applied to low void (< 0.1 %) fraction bubbly liquid systems, was modified to approximate the behaviour

expected at high void fractions. The argument for applying the modified Foldy's models in our case is the potential for describing wave propagation in high void fraction foam at low frequencies (20 kHz to 40 kHz), capitalizing on the ability of Foldy's model to account for the bubble resonance effect and rheological medium properties. Due to disproportionation, the largest bubble sizes increase to the sizes that satisfy conditions for bubble resonance to occur in egg white and *Gillette* liquids. In this thesis progress has been made in extending the Foldy model to a form that is more applicable to very high air fractions, such as in *Gillette* foams (93 % gas), by incorporating two different reasonable corrections to the original Foldy model. Predicted and measured values for phase velocity and attenuation are the same order of magnitude, but Foldy 1 model over predicts the effects of resonance for all void fraction foams. The difficulty of using the Foldy model faced in this study and by many other scientists, is the inability to take into account the bubble interactions or coupling as the resonance occurs.

The idea, initially suggested by other researchers (Mujica and Fauve, 2002), that the quantity $\alpha\lambda/f$ is proportional to $\langle r\rangle^2$, which is based on the Foldy-Prosperetti model for bubbles in a liquid, was applied to our results for both foams. From the slopes of $\alpha\lambda/f$ versus aging time, we can conclude that egg white foams and *Gillette* foams disproportionate at different rates. As well, we re-examined the statement made by Mujica and Fauve (2002) that $\alpha\lambda/f \propto \langle r\rangle^2$ is valid for water and egg white foams because of the dominance of thermal dissipation. We found a discrepancy in Mujica and Fauve (2002) calculation of the damping constant values, and therefore we examined whether or not the Foldy 1 model predicts that $\alpha\lambda/f$ is proportional to $\langle r\rangle^2$ in the 20 kHz to 40 kHz frequency range for bubble sizes from 5 to 50 μm. As a result, we found that the model predicts that $\alpha\lambda/f$ increases with $\langle r\rangle$, but that the increase is close to $\langle r\rangle^2$ scaling *only* for the smallest bubble size in water. From our experiments, we found different behaviour:

for *Gillette* foams $\alpha\lambda/f$ is proportional to $\langle r \rangle^2$ over the entire range of bubble sizes that evolve during aging, and that for egg white foams the scaling behaviour appears more complicated. As we mentioned earlier, in aging egg white foam (78 % of air), bubble mean radius does not scale as $t^{0.5}$ but rather as $t^{0.34}$, suggesting that the bubble size growth during aging is determined not only by disproportionation but is influenced by additional mechanisms. While the modified Foldy models serve as a useful starting point for interpreting the acoustic properties of foams, they do not fully predict the changes in velocity and attenuation seen during aging in our ultrasonic experiments, so that further theoretical work is needed.

Several difficulties are faced in integrating results obtained from using all techniques, ultrasound, electrical resistivity and imaging. For example, drainage experiments were conducted longer than disproportionation experiments. This is due to the difficulty in transmitting ultrasonic signal through the foam sample at longer aging times. However, reliable and meaningful results for the first 50 minutes of aging for foams with void fractions of 0.65 and 0.78 were obtained using all three techniques. Over this range of aging times, the slow drainage process that was observed in the resistivity experiments for 0.78 void fraction egg white foams leads to a conclusion that disproportionation is the dominant aging mechanism for the sample thicknesses that were used in the ultrasound experiments. However, the $t^{.34}$ time dependence of bubble growth seen in the image analysis suggests that liquid drainage does have some impact on the disproportionation process itself. For the 0.65 void fraction egg white foam, the disproportionation process was impacted more by drainage. By contrast to these results for the influence of drainage on disproportionation, we were not able to assess the impact that bubble disproportionation is likely to have on the liquid drainage process, as this would have required

the ability to image the bubble distributions inside the resistivity cell – something that was not feasible with the current cell geometry.

One step aside in this research was to investigate how instability processes, such as liquid drainage in the foam, could potentially affect cake structure setting during the baking process. Even though addition of flour in the foam slows down the drainage in the system, minor changes in the available water content affects the thermal setting temperature of the ingredients responsible for forming a strong cake texture. The thermal transition temperatures of angel food cake ingredients and their combinations in the presence of different amounts of water were examined by using a DSC technique. By using this technique, results on the thermal setting temperatures of angel food cake batter and its individual components confirmed that moisture content in a batter with a high sugar content is an important factor in order to obtain a good quality baked product. For all components (starch and egg white proteins) that are important in setting cake structure, increasing the amount of sugar in the system leads to higher thermal transition temperatures. We were able to detect thermal transition temperatures of two egg white proteins (conalbumin and ovalbumin) that are very important in setting the cake structure. Thermal transition temperatures of these proteins were determined in different amounts of an egg white liquid and sugar mixture. In a complete angel cake batter mixture, if liquid drainage is not occurring, thermal transitions of egg white proteins and wheat starch occur at the same temperature, which is around 92^{o}C.

CHAPTER 9. CONTRIBUTIONS TO KNOWLEDGE AND SUGGESTIONS FOR FUTURE WORK

This thesis is a comprehensive investigation of food and non-food foams structure as affected by two major time dependent instability mechanisms: liquid drainage and disproportionation. A novel technique in foam research area was used - low frequency (40 kHz) ultrasound to probe the changes occurring in egg white and *Gillette* foams. The data were interpreted by using a modified Foldy multiple scattering effective medium model, which was extended so that it would to be applicable to characterize relatively wet egg white foams (0.65 to 0.78 void fraction) and dry *Gillette* foams (0.90 and 0.93 void fraction) foams. As a support technique for the ultrasound research, microscopy imaging was used to obtain the quantitative information on bubble radius changes as the foam aged. To characterize liquid drainage in egg white foams only (excluding *Gillette* foam) electrical resisitivity measurements were used and the data was analyzed by applying a generalized free drainage model using two different boundary conditions. The main contributions to knowledge are as follows:

9.1 Bubble size evolution in aging egg white and *Gillette* foams

The goal of this study was to obtain accurate bubble size distributions in both types of aging foams. Characterizing those obtained bubble size distributions in aging foams by a two parameter lognormal distribution was challenging due to emergence of a second peak. For this reason the arithmetic mean of bubble size as a function of aging time was chosen. For the dry *Gillette* foams, bubble mean radius was proportional to aging time as $t^{0.4}$ indicating that disporpotionation is the dominant aging process. The bubble mean radius in the egg white foam (0.78 void fraction) bubble mean radius evolved slower, as $t^{0.34}$, leading to thesuggestion that

disproportionation is affected by liquid drainage. The wet, 0.65 void fraction, foam bubble radius evolved slower due to strong drainage effects, and therefore it was not possible to obtain a good fit which would describe bubble radius evolution in terms of aging time. Imaging analysis on its own provided an insight into instability mechanisms occurring in the foam.

9.2 Liquid drainage in egg white foams

This study provides a technique able to monitor the liquid flow in protein foams by measuring electrical resistivity. Liquid drainage in aging foam was determined by using the full void fraction range covering experimentally established relationships between relative conductivity and liquid fraction. Specifically for egg white foams the relation between liquid fraction and relative conductivity was determined. Due to differences between surfactants and proteins, it was necessary to make a correction to the derived equation of Feitosa *et al*. (2005), because as protein foams iare being whipped, the amount of charged species that are participating in carrying electrical current changes. Application of a physical generalized drainage model allowed analysis in detail of the parameters affecting the drainage process in complex food foams. Overall, a generalized free liquid drainage model was able to define the necessary conditions in order to stabilize food foam structure.

9.3 Low intensity (40kHz) ultrasound study on high void fraction foam aging process

This study provides the methodology and technique to measure changes in the ultrasonic parameters as a foam ages. Low intensity studies especially were useful for foam aging studies as ultrasound senses the bubble size changes in the foam. Since the bubble size distribution and void fraction affects the quality of aerated products, this information on the bubble radii changes with aging time is very important. It was observed that the ultrasonic parameter (phase velocity

and attenuation product) after a particular aging time, $\alpha\lambda/f$, becomes proportional to $\langle r\rangle^2$ for high void fraction disproportionating foams, such as *Gillette*. Even though similar behaviour was observed for the driest (0.78 void fraction) egg white foam, more complex behaviour that could not be described by $\alpha\lambda/f$ being proportional to $\langle r\rangle^2$ was observed for the wetter 0.65 foam, where disproportionation is affected by the drainage process at later aging times. A corrected scattering effective medium model, originated from Foldy (1945), was used to understand and delineate the mechanisms of sound wave propagation and foam properties (bubble size distribution and and matrix properties) that causes $\alpha\lambda/f$ scaling with $\langle r\rangle^2$ in a linear fashion. The original effective medium model was corrected in a way that it would applicable to foams with not only very low but also high bubble concentrations. Even though the Foldy effective medium model prediction results on foam aging were satisfactory, they lead to the understanding that the aging process in high void fraction food foams aging process is more complex and requires a more enhanced physical model to describe wave propagation in these foams.

A deeper insight on foam aging and stability can be obtained by extending this work and performing several suggested studies:

1) Food foams usually fall into intermediate void fraction or even wet foam regime, where two instability mechanisms (disproportionation and drainage) are competing and impacting each other. Therefore conducting electrical resistivity (evaluation of liquid fraction change within the different heights of the foam) and imaging (bubble size distribution change) experiments simultaneously would give a better quantitative stability evaluation of such foams. Also this would help to understand how disproportionation process affects liquid drainage in food foams with different void fractions.

2) Use different foam producing method instead of whipping, i.e. use aerosol aeration. Foams produced by using aerosol aeration method have much smaller bubble sizes than any other foam produced by whipping or mixing action (Martin *et al.*, 2002; Gittings and Durian, 2008). As a result of a different than whipping foam making method, the bubble size distribution of the foam would be different and therefore foam stability would be affected as well.
3) Low – frequency ultrasound potentially could be used also in foam drainage experiments, where the pairs of transducers would be located alongside the vertical column filled with the foam. However, comparatively small sample thickness has to be kept in order to have enough ultrasonic signal going through the sample.
4) Angel food cake batter is made as the flour is mixed into the egg white foam and it is a final product before it enters the oven. Therefore it is worth investigating the stability of the batter as the temperature rises up to 60 ^{o}C, by using ultrasonic technique, because we would expect to increase instability events due to reduced viscosity. Batter mixtures made from different void fraction egg white foams would provide full scope of occurring instability events.
5) Information how effects of delay of putting angel cake food batter in the oven as a result of disproportionation and liquid drainage can be obtained by using DSC experiments and determining thermal transition temperatures. Different void fraction batters would be made, poured into the baking pans and kept at room temperature. Small samples of the batter would be taken from different heights at the pans by using a syringe. We would expect to see changes in thermal transition temperatures as the batter ages at room temperature. The same experiments can be performed at higher than room temperatures,

because as the temperature rises, batter viscosity decreases, therefore allowing drainage to accelerate. Preliminary work was done on determination of thermal trasition temperatures that are important in cake structure setting. Separate angel food cake ingredient (flour, sugar egg white liquid and water) combinations in different ratios were used in this experiment. The literature, review results are presented in the Appendix of this thesis.

REFERENCES

Achwal, S.K. and Stepanek, J.B. (1975). Alternative method of determining hold-up in gas-liquid systems. *Chemical Engineering Science*, 30(11), 1443-1444.

Ahn, D.U., Kim, S.M. and Shu, H. (1997). Effect of egg size and strain and age of hens on the solids content of chicken eggs. *Poultry Science*, 76(6), 914-919.

Agnihotri, A. and Lemlich, R. (1981). Electrical conductivity and the distribution of liquid in polyhedral foam. *Journal of Colloid and Interfaces Science*, 84, 42-46.

Alleoni, A.C.C. (2006). Albumen protein and functional properties of gelation and foaming. *Scientia Agricola*, 63(3), 291-298.

Allen, K.E., Dickinson, E. and Murray, B. (2006). Acidified sodium caseinate emulsion foams containing liquid fat: A comparison with whipped cream. *LWT - Food Science and Technology*, 39, 225–234.

Arboleya, J.C., Olabarrieta, I., Luis-Aduriz, A., Lasa, D., Vergara, J., Sanmartín, E. and Iturriaga L. (2008). From the chef's mind to the dish: how scientific approaches facilitate the creative process. *Food Biophysics*, 3, 261–268.

Axelos, M.A.V. and Bouè, F. (2003). Foams as viewed by small-angle neutron scattering, *Langmuir*, *19*, 6598-6604.

Baete, S.H., De Deene, Y., Masschaele, B., and De Neve, W. (2008). Microstructural analysis of foam by use of NMR R-2 dispersion. *Journal of Magnetic Resonance*, 193(2), 286-296.

Bagotsky, V.S. (2006). *Fundamentals of Electrochemistry*, (2^{nd} ed.), (pg. 722). John Wiley & Sons, Inc.

Baldwin, C.A., Sederman, A.J., Mantle, M.D. and Gladden, L.F. (1996). Determination and characterization of the structure of a pore space from 3D volume images. *Journal of Colloid and Interface Science*, 181(1), 79-92.

Balerin, C., Aymard, P., Ducept, F., Vaslin, S. and Cuvelier. G. (2007). Effect of formulation and processing factors on the properties of liquid food foams. *Journal of Food Engineering*, 78, 802–809.

Bamforth, C.W. (2004). The relative significance of physics and chemistry for beer foam excellence: Theory and practice. *Journal of the Institute of Brewing*, 110(4), 259–266.

Banik, I. and Sain, M. (2008). Water blown soy polyol based polyurethane foams of different rigidities. *Journal of Reinforced Plastics and Composites*, 27, 357-373.

Barham, P., Skibsted, L.H., Bredie, W.L.P., Frost, M.B., Moller, P., R., Snitkjaer, P. and Mortensen, L.M. (2010). Molecular gastronomy: a new emerging scientific discipline. *Chemical Reviews,* 110(4), 2313-2365.

Barigou, M., Deshpande, N. S. and Wiggers, F. N. (2001). An enhanced electrical resistance technique for foam drainage measurement. *Colloids and Surfaces A: Physicochemical and Engineering Aspects*, 189(1-3), 237-246.

Barik, T.K. and Roy, A. (2009). Statistical distribution of bubble size in wet foam. *Chemical Engineering Science*, 64, 2039-2043.

Bazine. L., Castaigne, R. and Pouliot, Y. (2005). Relative contribution of proteins to conductivity changes in skim milk during chemical acidification. *Applied Engineering in Agriculture,* 21(3), 455-464.

Bawendi, S.A. (2005). *Physical Chemistry*, (4^{th} ed.), (pg. 960), John Wiley & Sons, Inc.

Bellido, G.G. (2007). Creation, Growth and Stability of Aerated Structures in Chemically Leavened Wheat Flour Dough Systems and Relationships to Mechanical Properties Assessed with Low-Intensity Ultrasound. *PhD Thesis*, University of Manitoba, Canada.

Bennett, M.A., West, R.M., Luke, S.P. and Williams, R.A. (2002).The investigation of bubble column and foam processes using electrical capacitance tomography. *Minerals Engineering*, 15(4), 225-234.

Bennion, E.B. and Bamford, G.S.T. (1973). *The Technology of Cake making*, (pg.390). Leonard Hill Publishers, Bucks.

Bezelgues, J.B., Serieye, S., Crosset-Perrotin, L. and Leser, M.E. (2008). Interfacial and foaming properties of some food grade low molecular weight surfactants, *Colloids and Surfaces A: Physicochemical Engineering Aspects,* 331, 56–62.

Bhakta, A. and Ruckenstein, E. (1997). Decay of standing foams: drainage, coalescence and collapse, *Advances in Colloid and Interface Science*, 70, 1-124.

Bisperink, C.G.J., Ronteltap, A.D. and Prins, A. (1992). Bubble-size distributions in foams. *Advances in Colloid and Interface Sciences*, 38, 13-32.

Bleaney, B.I. and Bleaney, B. (1976). *Electricity and Magnetism*, (pg. 762). Oxford University Press., 3rd edition.

Bos, M. A. and Van Vliet, T. (2001). Interfacial rheological properties of adsorbed protein layers and surfactants: a review. *Advances in Colloid and Interface Science*. 91, 437-471.

Bos, M.A., Dunnewind, B. and Ton van Vliet. (2003). Foams and surface rheological properties of β-casein, gliadin and glycinin, *Colloids and Surfaces B: Biointerfaces*, 31, 95-105.

Britan, M., Liverts, Ben-Dora, G., Koehler, S.A. and Bennani, N. (2009). The effect of fine particles on the drainage and coarsening of foam, *Colloids and Surfaces A: Physicochemical Engineering Aspects,* 344, 15–23.

Burgett, C., Klivans, E. and Pappas, L. S. (2003). *Essentials of Baking*, (pg. 319). Oxmoor House, Menlo Park, CA.

Caillet, A., Cogne, C., Andrieu, J., Laurent, P. and Rivoire A. (2003), Characterization ofice cream structure by direct optical microscopy. Influence of freezing parameters, *Lebensmittel-Wissenschaft und-Technologie*, 36, 743–749.

Campbell, G. M. (2008). A history of aerated foods. In book *Bubbles in Food 2: Novelty, Health and Luxury*, Ed. Campbell, G. M., Scanlon, M. G. and Pyle, D. L., (pg. 1-22). St. Paul, MN, AACC International.

Campbell, G.M. and Mougeot, E. (1999). Creation and characterisation of aerated food products, *Trends in Food Science and Technology*, 10(9), 283-296.

Carrier, V. and Colin, A. (2003). Coalescence in draining foams. *Langmuir*, 19 (11), 4535-4538.

Cents, A. H. G., Brilman, D. W. F., Versteeg, G. F., Wijnstra, P. J. and Regtien, P. P. L. (2004). Measuring bubble, drop and particle sizes in multiphase systems with ultrasound. *American Institute of Chemical Engineers Journal*, 50(11), 2750- 2762.

Chang, Y. and Hartel, R.W. (2002). Measurement of air cell distributions in dairy foams. *International Dairy Journal*, 12 (5), 463–472.

Chavez-Montesi, E., Choplin, L. and Schaer, Eric. (2006). Rhelogical characterization of wet food foams. *Journal of Texture Studies*, 38, 236–252.

Cheng, H.C. and Lemlich, R. (1983). Errors in the measurement of bubble size distribution in foam. *Industrial and Engineering Chemistry Fundamentals, 22,* 105-109.

Cilliers, J.J.L. and Sadr-Kazemi, N. (1999). Image analysis of food foams, In *Bubbles in Food*., Ed by Campbell, G.M., Webb C., Pandiella S.S. and NiVanjan K., Egan press, St Paul, USA, (pg. 245-251).

Cobus, L. A. E. B., Ross, K. A., Scanlon, M.G. and Page, J. H. (2007). Comparison of ultrasonic velocities in dispersive and nondispersive food materials. *Journal of Agricultural and Food Chemistry, 55,* 8889–8895.

Cohen-Addad, S., Hoballah, H. and Höhler, R. (1998). Viscoelastic response of a coarsening foam. *Physical Review E*, 57(6), 6897-6902.

Coke, M., Wilde, P.J., Russell, E.J. and Clark, D.C. (1990). The influence of surface-composition and molecular diffusion on the stability of foams formed from protein surfactant mixtures. *Journal of Colloid and Interface Science,* 138(2), 489-504.

Coughlin, M.F., Ingenito, E.P. and Stamenovic, D. (1996). Static shear modulus of gas-liquid foam determined by the punch indentation test. *Journal of Colloid and Interface Science,* 181(2), 661-666.

Cox, A.R., Aldred, D.L. and Russell, A.B. (2009). Exceptional stability of food foams using class II hydrophobin HFBII. *Food Hydrocolloids,* 23(2), 366-376.

Croguennec, T., Renault, A., Beaufils, S., Dubois, J.J. and Pezennec, S. (2007). Interfacial properties of heat-treated ovalbumin. *Journal of Colloid and Interface Science,* 315(2), 627-636.

Cunningham, F.E. (1976). Properties of egg white foam drainage. *Poultry Science*, 55(2), 738-743.

Damodaran, S. (2005). Protein Stabilization of Emulsions and Foams. *Journal of Food Science,* 70(3), R54-R66.

Datye, A.K. and Lemlich, R. (1983). Liquid distribution and electrical-conductivity in foam. *International Journal of Multiphase Flow*, 9(6), 627-636.

Davis, J.P. and Foegeding, E.A. (2004). Foaming and interfacial properties of polymerized whey protein isolate, *Journal of Food Science,* 69, C404–C410.

Davis, J.P., Foegeding, E.A. and Hansen, F.K. (2004). Electrostatic effects on the yield stress of whey protein isolate foams. *Colloids and Surfaces Biointerfaces*, 34(1), 13-23.

Dickinson, E. (2010). Food emulsions and foams: Stabilization by particles. *Current Opinion in Colloid and Interface Science*, 15(1-2), 40-49.

Donovan, J.W. (1977). Study of baking process by differential scanning calorimetry. *Journal of the Science of Food and Agriculture,* 28(6), 571-578.

Donovan, J.W. and Mapes, C.J. (1976). Differential scanning calorimetric study of conversion of ovalbumin to s-ovalbumin in eggs. *Journal of the Science of Food and Agriculture,* 27(2), 197-204.

Donovan, J.W., Mapes, C.J., Davis, J.G. and Garibaldi, J.A. (1975). Differential scanning calorimetric study of stability of egg-white to heat denaturation. *Journal of the Science of Food and Agriculture*, 26(1), 73-83.

Du, L., Prokop, A. and Tanner, R.D. (2002a). Effect of bubble size on foam fractionation of ovalbumin. *Applied Biochemistry and Biotechnology,* 98–100, 1075-1091.

Du, L., Prokop A. and Tanner, R.D. (2002b). Effect of denaturation by preheating on the foam fractionation behavior of ovalbumin, *Journal of Colloid and Interface Science* 248, 487–492.

Durian, D.A., Weitz, D., Pine J. and Source, D. J. (1991a). Multiple light-scattering probes of foam structure and dynamics. *Science*, New Series, 252(5006), 686-688.

Durian, D.J., Weitz, D.A. and Pine, D.J. (1991b). Scaling behaviour in shaving cream, *Physical Review A*, 44(12), 7902-7905.

De Vries, A. J. (1972): Morphology, coalescence and size distribution of foam bubbles. In Lemlich, R. (Ed.): *Adsorptive Bubble Separation Techniques* (pg. 9-31). New York: Academic Press.

Eisner, M.D.,Wildmoser, H. and Windhab, E.J. (2005). Air cell microstructuring in a high viscous ice cream matrix. *Colloids and Surfaces A: Physicochemical and Engineering Aspects*, 263 (1–3), 390.

Eisner, M.D., Jeelani, S.A.K., Bernhard, L. and Windhab, E.J. (2007). Stability of foams containing proteins, fat particles and nonionic surfactants. *Chemical Engineering Science*, 62, 1974 – 1987.

Eliasson, A.C. and Hegg, P.O. (1980). Thermal-stability of wheat gluten. *Cereal Chemistry*, 57(6), 436-437.

Eliasson, A. and Larsson, C. (1993).Cereals in breadmaking. Marcel Dekker, Inc, New York.

Elmehdi, H.M. (2001). An Ultrasonic Investigation of the Effect of Voids on the Mechanical properties of Bread Dough and the Role of Gas Cells in Determination the Cellular Structure of Freeze-Dried Breadcrumb. *PhD Thesis*, University of Manitoba, Canada.

Elmehdi, H.M., Page, J.H. and Scanlon, M.G. (2003). Monitoring dough fermentation using acoustic waves. *Transactions of the American Institute of Chemical Engineers*. Part C, 81, 217-223.

Fairley. P., McClements, D.J. and Povey, M.J.W. (1991). Ultrasonic characterization of aerated foodstuffs. *Ultrasonics International 91 - conference proceedings*, 79-82.

Fan, Y. (2007). Ultrasonic inspection methods for food-products Using Ultrasound to Investigate Relaxation and Resonance Phenomena in Wheat Flour Dough. *Master Thesis*, University of Manitoba, Canada.

Feitosa, K., Halt, O.L., Kamien, R. D. and Durian, D. J. (2006). Bubble kinetics in a steady-state column of aqueous foam. *Europhysics Letters*, 76 (4), 683–689.

Feitosa, K. and Durian, D.J. (2008). Gas and liquid transport in steady-state aqueous foam. *The European Physical Journal E*, 26, 309–316.

Feitosa, K., Marze, S., Saint-Jalmes, A. and Durian, D. J. (2005). Electrical conductivity of dispersions: from dry foams to dilute suspensions. *Journal of Physics: Condensed Matter*, 17, 6301–6305.

Ferreira, M., Hofer, C. and Raemy, A. (1997). A calorimetric study of egg white proteins, *Journal of Thermal Analysis*, 48, 683-690.

Fine, R.A. and Millero, F. J. (1973). Compressibility of water as a function of temperature and pressure. *Journal of Chemical Physics* 59 (10):5529-5536.

Foegeding, E. A., Luck, P.J. and Davis, J.P. (2006). Factors determining the physical properties of protein foams. *Food Hydrocolloids*, 20, 284–292.

Foldy, L. L. (1945). The multiple scattering of waves. *Physics Review*, 67, 107–119.

Ganan-Calvo, M., Fernandez, J.M. and Oliver, M.A. (2004). Coarsening of monodisperse wet microfoams. *Applied Physics Letters*, 84(24), 14-20.

Gandolfo, F. G. and Rosano, H. L. (1997). Interbubble gas diffusion and the stability of foams, *Current Opinion in Colloid and Interface Science*, 194, 31–36.

Gaonach, H., Lovejoy, S., Stix, J. and Scherzter, D. (1996). A scaling growth model for bubbles in basaltic lava flows. *Earth and Planetary Science Letters*, 139(3-4), 395-409.

Garrett, P.R. and Gratton, P.L. (1995). Dynamic surface tensions, foam and the transition from micellar solution to lamellar phase dispersion. *Colloids and Surfaces A*, 103, 127–145.

Georgieva, D., Schmitt, V., Leal-Calderon, F. and Langevin, D. (2009). On the possible role of surface elasticity in emulsion stability. ***Langmuir*****,** 25 (10), 5565-5573.

German, J.B. and Phillips, L. (1994). Protein interactions in foams: protein-gas phase interactions. In Hettiarachchy, N.S. and Ziegler, G. R. (Eds.), *Protein Functionality in Food Systems*, (pp. 181-209). New York: Marcel Dekker Inc.

Ghiasi, K., Hoseney, R.C. and Varriano-Marston, E. (1983). Effects of flour components and dough ingredients on starch gelatinization. *Cereal Chemistry*, 60(1), 58-61.

Gittings, S. and Durian, D. J. (2008). Statistics of bubble rearrangement dynamics in a coarsening foam, *Physical Review E* 78, (066313) 1-8.

Goldfarb, I., Schreiber, I. and Vafina, F. (1992) Heat transfer effect on sound propagation in foam. *The Journal of the Acoustical Society of America*, 92 (5), 2756-2770.

Goldfarb, I., Orenbakh, Z., Shreiber, I. and Vafina, F. (1997). Sound and weak shock wave propagation in gas-liquid foams. *Shock Waves*, 7, 77–88.

Goyon, J., Bertrand, F., Pitois, O. and Ovarlez, G. (2010). Shear induced drainage in foamy yield-stress fluids. *Physical Review Letters*, 104(12) Nr:128301.

Gonatas, C.P., Leigh, J.S., Yodh, A.G., Glazier, J.A. and Prause, B. (1995). Magnetic-resonance images of coarsening inside a foam. *Physical Review Letters*, 75(3), 573-576.

Gopal, D. and Durian, D. J. (2003). Relaxing in foam. *Physical Review Letters*, 91(18), 188303:1-4.

Halling, P.J, (1981). Protein-stabilized foams and emulsions, *CRC Critical Reviews in Food Science and Nutrition*, 15(2), 155-203.

Hammershøj, M., Prins, A. and Qvist, K.B. (1999). Influence of pH on surface properties of aqueous egg albumen solutions in relation to foaming behaviour *Journal of the Science of Food and Agriculture*, 79, 859-868.

Harwalkar, V.R. and Ma, C.Y. (1987). Study of thermal-properties of oat globulin by differential scanning calorimetry. *Journal of Food Science*, 52(2), 394-398.

Heller, J.P. and Kuntamukkula, M.S. (1987). Critical review of the foam rheology literature. *Industrial & Engineering Chemistry Research*, 26 (2), 318-325.

Henyey, F.S. (1999). Corrections to Foldy's effective medium theory for propagation in bubble clouds and other collections of very small scatterers, *The Journal of the Acoustical Society of America*, 105(4), 2149- 2154.

Hilgenfeldt, S., Koehler, S.A. and Stone, H.A. (2001). Dynamics of coarsening foams: accelerated and self-limiting drainage. *Physical Review Letters*, 86 (20), 4704-4710.

Höhler, R. and Cohen-Addad, S. (2005). Rheology of liquid foam, *Journal of Physics: Condensed Matter*, 17(41), 1041-1069**.**

Hoseney, R.C., Zeleznak, K. and Lai C.S. (1986). Wheat gluten - a glassy polymer. *Cereal Chemistry*, 63(3), 285-286.

Hoseney, R.C. (1998). Principles of cereal science and technology. (2nd Ed.), (pg. 327).St. Paul, MN: American Association of Cereal Chemist, INC.

Hutzler, S. and Weaire, D. (2000). Foam coarsening under forced drainage. *Philosophical Magazine Letters*, 80(6), 419-425.

Hutzler, S., Verbist, G., Waeire D. and Van der Steen, J.A. (1995). Measurement of foam density profiles using AC capacitance. *Europhysics Letters*, 31 (8), 497-502.

Ibeh, C.C. and Bubacz, M. (2008). Current trends in nanocomposite foams. *Journal of Cellular Plastics*, 44, 493-515.

Jang, W., Nikolov, A., Wasan, D. T., Chen K. and Campbell B. (2005). Prediction of the bubble size distribution during aeration of food products, *Industrial and Engineering Chemistry Research*, 44, 1296-1308.

Johnson, T.M. and Zabik, M. E. (1981a). Egg albumen proteins interactions in an angel food cake system, *Journal of Food Science*, (46), 1231- 1236.

Johnson, T.M. and Zabik, M. E. (1981b). Ultrastructural examination of egg albumen protein foams, *Journal of Food Science*, 46(4), 1237-1240.

Johnson, J.M., Davis, E.A. and Gordon, J. (1990). Interaction of starch and sugar water measured by electron spin resonance and differential scanning calorimetry. *Cereal Chemistry*, 67(3):286-291.

Joseph, D.D. (1997). Questions in fluid mechanics: Understanding foams and foaming. *Journal of Fluids Engineering-transactions of the ASME*, 119(3), 497-498.

Jurine S, Cox S, and Graner, F. (2005). Dry three-dimensional bubbles: growth-rate, scaling state and correlations. *Colloids and Surfaces a Physicochemical and Engineering Aspects*, 263(1-3), 18-26.

Kamat, V.B., Lawrence, G.A., Hart , C.J., and Yoell, R. (1973). Contribution of egg-yolk lipoproteins to cake structure, *Journal of the Science of Food and Agriculture*, 24(1) 77-88.

Kaminski, M. (1956). Globulins in the chicken egg whites. *Nature*, 178, 981-982.

Kann, K. B.and Kislitsyn, A. A. (2003). A film model of sound propagation in gas–liquid foams: 1. The sound velocity, *Colloid Journal*, 65(1), 26-30.

Karapantsios, T.D. and Papara, M. (2008). On the design of electrical conductance probes for foam drainage applications. Assessment of ring electrodes performance and bubble size effects on measurements. *Colloids and Surfaces A: Physicochemical and Engineering Aspects*, 323, 139-148.

Kinsella, J.E. and Whitehead, D.M. (1987). Film, foaming and emulsifying properties of food proteins: Effects of modification. In *Proteins at Interfaces: Physicochemical and Biochemical Studies* (629-646 pg.) ACS Symposium Series, American Chemical Society. Washington, DC.

Kneifel, W., Paquin, P., Abert, T. and Richard, J.P. (1991). Water-holding capacity of proteins with special regard to milk-proteins and methodological aspects - a review. *Journal of Dairy Science*, 74(7), 2027-2041.

Koehler, S. A., Stone, H. A., Brenner, M. P. and Eggers, J. (1998). Dynamics of foam drainage. *Physical review E*, 58(2), 2097-2106.

Koehler, S.A., Hilgenfeldt S. and Stone, H.A. (2000). A generalized view of foam drainage: experiment and theory. *Langmuir*, 16 (15), 6327-6341.

Koehler, S.A., Hilgenfeldt, S. and Stone, H.A. (2004a). Foam drainage on the microscale I. Modeling flow through single Plateau borders, *Journal of Colloid and Interface Science*, 276, 420–438.

Koehler, S.A., Hilgenfeldt, S., Weeks, E.R. and Stone, H.A. (2004b). Foam drainage on the microscale II. Imaging flow through single Plateau borders, *Journal of Colloid and Interface Science*, 276, 439–449.

Koehler, S. A., Stone, H. A., Brenner, M. P. and Eggers, J. (1998). Dynamics of foam drainage. *Physical Review E*, 58(2), 2097-2106.

Kokini, J. and van Aken, G. (2006). Discussion session on food emulsions and foams. *Food Hydrocolloids*, 20, 438–445.

Kralova, I. and Sjöblom, J. (2009). Surfactants used in food industry: A Review. *Journal of Dispersion Science and Technology*, 30, 1363–1383.

Kulmyrzaev, A., Cancelliere, C. and McClements, D.J. (2001). Characterization of aerated foods using ultrasonic reflectance spectroscopy, *Journal of Food Engineering*, 46, 235-241.

Lambert, J., Cantat, I., Delannay, R., Renault, A., Graner, F., Glazier, J.A., Veretennikov, I. and Cloetens, P. (2005). Extraction of relevant physical parameters from 3D images of foams obtained by X-ray tomography. *Colloids and Surfaces a Physicochemical and Engineering Aspects*, 263(1-3), 295-302.

Langevin, D. (2009). Complexation of oppositely charged polyelectrolytes and surfactants in aqueous solutions. A review. *Advances in Colloid and Interface Science*, 147–148, 170–177.

Lau, K. and Dickinson, E. (2004). Structural and rheological properties of aerated high sugar systems containing egg albumen. *Journal of Food Science*, 69(5), 232-239.

Lau, K. and Dickinson, E. (2005). Instability and structural change in an aerated system containing egg albumen and invert sugar, *Food Hydrocolloids*, 19, 111–121.

Leighton, T.G. (1996). *The acoustic bubble*, (pg. 613). Academic Press, London.

Lemlich, R. (1978a). Prediction of changes in bubble size distribution due to interbubble gas diffusion in foam. *Industrial and Engineering Chemistry Fundamentals*, 17(2), 89-93.

Lemlich, R., (1978b). Theory for limiting conductivity of polyhedral foam at low density, *Journal of Colloid and Interfaces Science*, 64, 107-111.

León, A., Rosell, C.M., and Barber, C.B. (2003). A differential scanning calorimetry study of wheat proteins. *European Food Research and Technology*, 217, 13–16.

Leonard, R.A. and Lemlich, R. (1965). A study of interstitial liquid flow in foam. Theoretical model and application to foam fractionation. *AICHE Journal***,** 11(1), 18-25.

Leroy, V. (2009). Personal communication.

Leroy, V., Strybulevych, A., Page, J.H. and Scanlon, M.G. (2008). Sound velocity and attenuation in bubbly gels measured by transmission experiments. *Journal of Acoustical Society of America*, 123 (4), 1931-1940.

Leroy, V., Piture, K.M, Scanlon, M.G. and Page, J.H. (2010). The complex shear modulus of dough over a wide frequency range. *Journal of Non-Newtonian Fliud Mechanics*, 165, 475-478.

Li-Chan, E.C.Y., Powrie W.D. and Nakai, S. (1995). The chemistry of eggs and egg products. In *Egg science and technology*, 4th edition. Edited by William J. Stadelman, Owen J. Cotterill, (pg. 105-177).

Lide, D. R. (2005). *CRC Handbook of Chemistry and Physics*, 86th edition. Edited by David R. Lide. CRC Press, 2616 pg.

Liu, J., Xu, G., Liu, J.; Xin, X., Luan, Y. J. (2005). Properties of foam formed from BSA/Tween-20, *Journal of Dispersion Science and Technology*, 26, 559-564.

Lostie, M**.,** Peczalski, R**.,** Andrieu, J. and Laurent, M. (2002). Study of sponge cake batter baking process. Part I: Experimental data, *Journal of Food Engineering*, 51(2), 131-137

Ma, C.Y., Poste, L.M. and Holme, J. (1986). Effects of chemical modification on the physiochemical and cake-baking properties of egg white. *Canadian Institute of Food Science and Technology Journal*, 19: 17-22.

MacDonell, L.R., Feeney, R.E. and Hanson, H.L. (1955). The functional properties of egg white proteins. *Food Technology*, 9(2), 49-53.

Magdassi, S., Vinetsky, Y. and Relkin, P. (1996). Formation and structural heat-stability of beta-lactoglobulin/surfactant complexes. *Colloids and Surfaces B: Biointerfaces*, 6, 353-362.

Magrabi, S.A., Dlugogorski, B.Z. and Jameson, G.J. (1999). Bubble size distribution and coarsening of aqueous foams. *Chemical Engineering Science*, 54, 4007-4022.

Magrabi, S. A., Dlugogorski, B. Z and Jameson, G. J. (2001). Free drainage in aqueous foams: model and experimental study, *American Institute of Chemical Engineers Journal*, 47(2), 314-327.

Mann, K. (2007). The chicken egg white proteome. *Proteomics*, 7(19), 3558-3568.

Marquez, M., Ganan-Calvo, M., Fernandez , J. M. and Marquez Oliver A. (2004). Coarsening of monodisperse wet microfoams. *Applied Physics Letters*, 84(24), 4989 – 4991.

Martin, A.H., Grolle, K., Bos, M.A., Martien, A., Cohen, S. and van Vliet, T. (2002). Network forming properties of various proteins adsorbed at the air/water interface in relation to foam stability. *Journal of Colloid and Interface Science*, 254, 175–183.

Marze, S.P.L., Saint-Jalmes, A. and Langevin, D. (2005). Protein and surfactant foams: linear rheology and dilatancy effect. *Colloids and Surfaces A: Physicochemical Engineering Aspects*, 263, 121–128.

Marze, S. Guillermic, R. M. and Saint-Jalmes, A. (2009). Oscillatory rheology of aqueous foams: surfactant, liquid fraction, experimental protocol and aging effects. *Soft Matter*, 5, 1937–1946.

Mason, T.G., Bibette, J. and Weitz, D.A. (1996). Yielding and flow of monodispersed emulsions. *Journal of Colloid and Interface Science*, 179(2), 439-448.

Maurdev, G., Saint-Jalmes, A. and Langevin, D. (2006). Bubble motion measurements during foam drainage and coarsening. *Journal of Colloid and Interface Science,* 300, 735–743.

May, K., Jeelani, S.A.K., Panoussopoulos, K. and Hartland, S. (1996). Foam head and stability of beer foams. *Chemical and Biochemical Engineering Quarterly,* 10 (3), 107–112.

McClements, D.J. (1995). Advances in the application of ultrasound in food analysis and processing. *Food Science and Technology*, 6(9), 293-299.

McClements, D.J. and Fairley, P. (1991). Ultrasonic pulse echo reflectometer. *Ultrasonics***,** 29(1), 58-62**.**

Mine Y. (2002). Recent advances in egg protein functionality in the food system. *World's Poultry Science Journal*, 58(1), 31-39.

Minnaert, M. (1933). On musical air-bubbles and the sound of running water. *Philosophical Magazine*, 16, 235–248.

Mita, T., Ishida, E. and Matsumoto, H. (1978). Physicochemical studies on wheat-protein foams. 2. Relationship between bubble-size and stability of foams prepared with gluten and gluten components, *Journal of Colloid and Interface Science*, 64(1), 143-153.

Mizukoshi, M. (1983). Model studies of cake baking. IV. Foam drainage in cake batter. *Cereal Chemistry*, 60(5):399-402.

Mizukoshi, M., Maeda, H. and Amano, H. (1980). Model studies of cake baking. 2. Expansion and heat set of cake batter during baking. *Cereal Chemistry*, 57(5):352-355.

Monin, D., Espert, A. and Colin, A. (2000). A new analysis of foam coalescence: from isolated films to three-dimensional foams, *Langmuir, 16,* 3873-3883.

Monnereau, C. and Vignes-Adler, M. (1998). Dynamics of 3D real foam coarsening. *Physical Review Letters,* 80(23), 5228-5231.

Monnereau, C., Prunet-Foch, B. and Vignes-Adler, M. (2001). Topology of slightly polydisperse real foams. *Physical Review E,* 63(6), 061402 (1-10).

Morris, R.M. and Morris, A. (1965). Measurement of interfacial areas of foams and froths by a radiographic technique. *Chemistry and Industry*, 46, 1902-1906.

Mortimer, G.R. (2008). *Physical chemistry*, 3rd edition, (pg. 1395). Elsevier Applied Sciences, London and New York.

Murray, B.S. (2007). Stabilization of bubbles and foams. *Current Opinion in Colloid and Interface Science*, 12(4-5), 232-241.

Murray, B.S. and Ettelaie, R. (2004). Foam stability: proteins and nanoparticles. *Current Opinion in Colloid and Interface Science,* 9, 314–320.

Mujica, N. and Fauve, S. (2002). Sound velocity and absorption in a coarsening foam, *Physical Review E,* 66, (021404) 1-14.

Nakamura, R. (1963). Studies on the foaming properties of the chicken egg white. Part VI. Spread monolayer of the protein fraction of the chicken egg white, *Agricultural and Biological Chemistry*, 27(6), 427-432.

Nakamura, R., (1964). Studies on the foaming properties of the chicken egg white. Part VII. On the foaminess of the denatured ovalbumin, *Agricultural and Biological Chemistry*, 28(6), 403-407.

Nakamura, R. and Sato, Y. (1964). Studies on the foaming properties of the chicken egg white. Part IX. On the coagulated proteins under various whipping conditions (The mechanism of foaminess (1), *Agricultural and Biological Chemistry*, 28(8), 524-529.

Narchi, I., Vial, C. and Djelveh, G. (2008). Effect of matrix elasticity on the continuous foaming of food models. *Applied Biochemical Biotechnology*, 151, 105–121.

Nicorescu, I., Riaublanc, A., Loisel, C., Vial, C., Djelveh, G., Cuvelier, G. and Legrand J. (2009). Impact of protein self-assemblages on foam properties, *Food Research International*, 42, 1434–1445.

Page. J. (2010). Personal communication.

Page, J.H., Schriemer, H.P., Jones, I.P, Sheng, P. and Weitz, D.A. (1997). Classical wave propagation in strongly scattering media. *Physica A*, 241, 64 71.

Patino, J. M. R., Delgado, M. D. N. and Fernfindez, J. A. L. (1995). Stability and mechanical strength of aqueous foams containing food proteins, *Colloids and Surfaces, A: Physicochemical and Engineering Aspects*, 99, 65-78.

Patino, J. M. R., Sánchez, C. C. and Niño, M. R. R. (2008). Implications of interfacial characteristics of food foaming agents in foam formulations, *Advances in Colloid and Interface Science*, 140, 95–113.

Pernell, C.W., Foegeding, E.A. and Daubert, C.R. (2000). Measurement of the yield stress of protein foams by vane rheometry. *Journal of Food Science*, 65(1), 110-114.

Phelan, R., Weaire, D., Peters, E.A.J. F. and Verbistz, G. (1996). The conductivity of a foam, *Journal of Physics: Condensed Matter*, 8, L475–L482.

Poole, S., Wee, S.I. and Fry, J.E. (1987). Effects of basic proteins on the denaturation and heat-gelation of acidic proteins. *Food Hydrocolloids*, 1(4), 301-316.

Povey, M. J. W. (1989). Ultrasonics in food engineering, Part II: Applications, *Journal of Food Engineering*, 9, l-20.

Povey, M.J.W. (1997). *Utrasonic techniques for fluids characterization*, (pg. 214). Academic Press, San Diego, CA.

Povey, M. J. W. and McClements, D. J. (1989). Ultrasonics in Food Engineering. Part I: Introduction and Experimental Methods, *Journal of Food Engineering*, 8, 217-245.

Prause, B.A., Glazier, J.A., Gravina, S.J. and Montemagno, C.D. (1995). 3-dimensional magnetic-resonance-imaging of a liquid foam. *Journal of Physics: Condensed Matter*, 7(40), L511-L516.

Princen, H.M. (1985). Rheology of foams and highly concentrate emulsions, II. Experimental study of the yield stress and wall effects for concentrated oil in water emulsions. *Journal of Colloid and Interface Science*, 105: 150-171.

Princen, H.M. (2001) The structure, mechanics, and rheology of concentrated emulsions and fluid foams. In Sjöblom, J. (Eds.). *Encyclopedic handbook of emulsion technology*. (243-278pg.). CRC Press, 1th Edition.

Princen, H.M. and Kiss, A.D. (1986). Rheology of foams and highly concentrated emulsions. III. Static shear modulus. *Journal of Colloid and Interface Science*, 112: 427-437.

Prins, A. (2006). Surface forces' role in the foaming behaviour of liquids. In *Encyclopedia of surface and colloid science*. Volume 2. Edited by Somasundaran P. pages (5926-5949).

Prins, A. (1988). Principles of foam stability. In: E. Dickinson and G. Stainsby, Editors, *Advances in food fmulsions and foams*, (pg. 91–123).Elsevier Applied Science, London.

Procter and Gamble. (2011) http://www.pg.com/productsafety/msds/beauty_care/Gillette_Consumer_Products/Gillette_Foamy_Sensitive_Skin_(98683124).pdf

Prosperetti, A. (1977). Thermal effects and damping mechanisms in the forced radial oscillations of gas bubbles in liquids, *The Journal of the Acoustical Society of America* **,** 61, 17–27.

Proussevitch, A.A., Sahagian, D. L. and Tsentalovich, E.P. (2007). Statistical analysis of bubble and crystal size distributions: Formulations and procedures. *Journal of Volcanology and Geothermal Research*, 164, 95–111.

Pugh, R.J. (1996). Foaming, foam films, antifoaming and defoaming. *Advances in Colloid Interface Science*, 64, 67-142.

Pugh, R.J. (2005). Experimental techniques for studying the structure of foams and froths. *Advances in Colloid and Interface Science*, 114 – 115, 239 – 251.

Pyler E. J., (1988). *Baking science and technology*, Volume II, (pg. 1392). Sosland Publishing company, Kansas, Merriam.

Raikos, V., Campbell, L. and Euston, S. R. (2007). Effects of sucrose and sodium chloride on foaming properties of egg white proteins. *Food Research International*, 40, 347–355.

Rami-Shojaei, S., Vachier, C. and Schmitt, C. (2009). Automatic analysis of 2D foam sequences: Application to the characterization of aqueous proteins foams stability. *Image and Vision Computing*, 27, 609–622.

Rouyer, F., Cohen-Addad, S. and Höhler, R. (2005). Is the yield stress of aqueous foam a well-defined quantity? *Colloids and Surfaces A: Physicochemistry Engineering Aspects*, 263, 111–116.

Rullier, B., Novales, B. and Axelos, M. A.V. (2008). Effect of protein aggregates on foaming properties of β-lactoglobulin, *Colloids and Surfaces A: Physicochemical Engineering Aspects*, 330, 96–102.

Rullier, B., Axelos, M.A.V., Langevin, D. and Novales, B. (2009). beta-Lactoglobulin aggregates in foam films: Correlation between foam films and foaming properties. *Journal of Colloid and Interface Science*, 336(2), 750-755.

Rusell, P.L. (1987). Gelatinisation of starches different amylase/amylopectin content. A study by differential scanning calorimetry. *Journal of cereal science*, 6, 133-145.

Saggin, R. and Coupland, J.N. (2001), Non-contact ultrasonic measurements in food materials, *Food Research International*, 34, 865–870.

Sahi, S.S. and Alava, J.M. (2003). Functionality of emulsifiers in sponge cake production. *Journal of the Science of Food and Agriculture*, 83(14), 1419-1429.

Saint-Jalmes, A. (2006). Physical chemistry in foam drainage and coarsening, *Soft Matter*, 2(10), 836-849.

Saint-Jalmes, A. and Durian, D.J. (1999). Vanishing elasticity for wet foams: Equivalence with emulsions and role of polydispersity, *Journal of Rheology*, 43(6), 1411-1422.

Saint-Jalmes, A. and Langevin, D. (2002). Time evolution of aqueous foams: drainage and coarsening, *Journal of Physics: Condensed Matter*, 14: 9397-9412.

Saint-Jalmes, Peugeot M. L., Ferraz, H. and Langevin, D. (2005). Differences between protein and surfactant foams: Microscopic properties, stability and coarsening. *Colloids and Surfaces A: Physicochemical Engineering Aspects* 263, 219–225.

Saint-Jalmes, A., Vera, M.U., and Durian, D.J. (2000). Free drainage of aqueous foams: Container shape effects on capillarity and vertical gradients, *Europhysics Letters*, 50(5), 695-701.

Samari, S. (1994). Ultrasonic inspection methods for food-products. *Food Science and Technology-Lebensmittel-Wissenschaft und Technologie*, 27(3), 210-213.

Schmitt, C., Bovay, C., Rouvet, M., Shojaei-Rami, S. and Kolodziejczyk, E. (2007). Whey protein soluble aggregates from heating with NaCl: physicochemical, interfacial, and foaming properties, *Langmuir*, 23, 4155–4166.

Schofield, J.D., Bottomley, R.C., Timms, M.F. and Booth, M.R. (1983). The effect of heat on wheat gluten and the involvement of sulfhydryl-disulfide interchange reactions. *Journal of Cereal Science*, 1(4), 241-253.

Schramm, L.L. (2005). *Emulsions, foams, and suspensions: fundamentals and applications*, (pg. 448). Wiley - VCH, Weinheim, Germany.

Sessoms, D. A., Bissig, H., Duri, A., Cipelletti, L. and Trappe, V. (2010). Unexpected spatial distribution of bubble rearrangements in coarsening foams, *Soft Matter*, 6, 3030–3037.

Shrestsha, L.K., Acharya, D.P., Sharma, S.C., Aramaki, K., Asaoka, H., Ihara, K., Tsunehiro, T. and Kunieda, H. (2006) Aqueous foam stabilized by dispersed surfactant solid lamellar liquid crystalline phase, *Journal of Colloid and Interface Science*, 301, 274–281.

Silberman, E. (1957). Sound velocity and attenuation in bubbly mixtures measured in standing wave tubes. *Journal of the Acoustical Society of America*, 29, 925-935.

Silbey, R.J., Alberty, R.A. and Bawendi, M.G. (2004). *Physical Chemistry.* 4th Edition, (pg 960), Wiley.

Spencer, J.E. (2006). Examining the time-dependent changes in the bubble structure of whole egg and egg white foams and batters using small strain shear oscillatory rheology, large strain shear flow rheology and image analysis techniques. *Thesis*. University of Manitoba, Canada.

Spies, R.D. and Hoseney, R.C. (1982). Effect of sugars on starch gelatinization. *Cereal chemistry*, 59(2), 128-131.

Stevens, L. (1991). Mini Review: Egg white proteins. *Comparative Biochemistry and Physiolgy*, 100B(1),11-9.

Stevenson, P., Mantleb, M. D. and Hicksa, J. M. (2007). NMRI studies of the free drainage of egg white and meringue mixture froths. *Food Hydrocolloids*, 21, 221–229.

Strybulevych, A., Leroy, V., Scanlon, M. G. and Page, J. H. (2007). Characterizing a model food gel containing bubbles and solid inclusions using ultrasound. *Soft Matter*, 3, 1388–1394.

Squeo, E.A. and Quadrini, F.(2010). Shape memory epoxy foams by solid-state foaming, *Smart Materials and Structures,* 19(10): 105002.

Thomas, P.D., Darton, R.C. and Whalley, P.B. (1998). Resolving the structure of cellular foams by the use of optical tomography. *Industrial and Engineering Chemistry Research*, 37(3), 710-717.

Thomas, G. L., De Almeida, R. M. C. and Graner, F. (2006). Coarsening of three-dimensional grains in crystals, or bubbles in dry foams, tends towards a universal, statistically scale-invariant regime, *Physical Review E*, 74, 021407.

Vadehra, D.V. and Nath, K.R. (1973). Eggs as a source of protein. *CRC Critical Reviews in Food Technology*, 4: 193-309.

Van der Net, A. Blondel, L., Saugey, A. and Drenckhan, W. (2007). Simulating and interpretating images of foams with computational ray-tracing techniques, *Colloids and Surfaces A: Physicochemical* Engineering Aspects, 309, 159–176.

Vera, M.U. and Durian, D. J. (2002). Enhanced Drainage and Coarsening in Aqueous Foams. *Physical Review Letters.* 88 (8), 88304-88308.

Von der Schulenburg, D.A.G., Paterson-Beedle, M., Macaskie, L.E., Gladden, L. F. and Johns, M.L. (2007). Flow through an evolving porous media-compressed foam. *Journal of Materials Science*, 42(16), 6541-6548.

Verbist, G., Weaire, D. and Kraynik, A. M. (1996). The foam drainage equation. *Journal of Physics: Condensed Matter*, 8, 3715–3731.
Walstra, P. (2003). *Physical chemistry of foods*, (pg. 807), Marcel Dekker Inc.

Wang, M. and Cilliers, J.J. (1999). Detecting non-uniform foam density using electrical resistance tomography. *Chemical Engineering Science*, 54(5), 707-712.

Weaire, D. (2008). The rheology of foam. *Current Opinion in Colloid & Interface Science,* 13, 171–176.

Weaire, D. and Hutzler, S. (1999). *The Physics of Foams*, (pg. 264), New York: Oxford University Press.

Weaire, D., Finlay, S. and Verbst, G. (1995). Measurements of foam drainage using AC conductivity, *Journal of Physics: Condensed Matter,* 7, L217-L222**.**

Weissberg, H.L. (1963). Effective diffusion coefficient in porous media, *Journal of applied physics*, 34(9), 2636-2639.

Wierenga, P.A., van Norél, L. and Basheva, E.S. (2010). Reconsidering the importance of interfacial properties in foam stability, *Colloids and Surfaces A: Physicochemical Engineering Aspects,* 344, 72–78.

Wilde, P.J. (1996). Foam measurement by the microconductivity technique: An assessment of its sensitivity to interfacial and environmental factors, *Journal of Colloid and Interfaces Science.* 178,733-739.

Wilde, P., Mackie, A., Husband, F., Gunning, P. and Morris, V. (2004). Proteins and emulsifiers at liquid interfaces. Advances in Colloid and Interface Science, 108–109, 63–71.

Wilson, P. S. (2005). Low-frequency dispersion in bubbly liquids. *Acoustics Research Letters Online* 6, (3), 188-194.

Wootton, M., Nguyen, T.H. and Hoang, L.P.T. (1981). A study of the denaturation of egg-white proteins during freezing using differential scanning calorimetry. *Journal of Food Science*, 46(5), 1336-1338.

Wright, D.J. and Hemmant, J.W. (1987). Foaming properties of protein solutions: comparison large-scale Whipping and conductimetric methods, *Journal of the Science of Food and Agriculture.* 41:361-371**.**

Wu, N., Dai, J.L. and Micale, F.J. (1999). Dynamic surface tension measurement with a dynamic Wilhelmy plate technique. *Journal of Colloid and Interface Science*, 215(2), 258-269**.**

Wu, C., Wang, Z.Y., Zhi, Z.Z., Jiang, T.Y., Zhang, J.H. and Wang, S.L. (2011). Development of biodegradable porous starch foam for improving oral delivery of poorly water soluble drugs. *International Journal of Pharmaceutics,* 403(1-2):162-169.

Yianatos, J.B., Laplante, A.R. and Finch, J.A. (1985). Estimation of local holdup in the bubbling and froth zones of a gas-liquid column. C*hemical Engineering Science,* 40(10), 1965-1968.

Yu, L. and Christie, G., (2001). Measurement of starch thermal transition using differential scanning calorimetry, *Carbohydrate Polymers,* 46, 179–184.

Zhang, Y.Z., Jiang, T.Y., Zhang, Q.A. and Wang, S.L. (2010) Inclusion of telmisartan in mesocellular foam nanoparticles: Drug loading and release property. *European Journal of Pharmaceutics and Biopharmaceutics,* 76(1):17-23.

Zayas, J., F., (1997) *Functionality of Proteins in Food,* (p. 206-304).Springer, Berlin.

Zhu, H.M. and Damodaran, S. (1994). Proteose peptones and physical factors affect foaming properties of whey-protein isolate. *Journal of Food Science*, 59(3), 554-560.

APPENDIX

A. DSC STUDY ON ANGEL FOOD CAKE BATTER AND ITS COMPONENTS

A.1. Introduction

Due to liquid drainage, the change of available liquid for denaturation and gelatinization of cake batter components (proteins and starch) will change the thermal transition temperature during baking. Thermal transition temperature is important because it affects the batter viscosity and the rate at which the air bubbles expand (Mizukoshi *et al.*, 1980; Pyler, 1988; Lostie *et al*., 2002), therefore affecting the optimal product volume that can be reached. In addition, at the thermal transition temperature in the batter, disproportionation and liquid drainage are stopped. As a result of high sugar amount and lack of moisture, the thermal transition temperature where drainage and disproportionation are stopped is elevated, and more so in regions where significant drainage has occurred. Thus a solid cake structure is not formed and therefore, the cake collapses. Therefore, the objective is to investigate the effect of sugar on the thermal transition temperatures of cake batter components (flour, egg white and sugar).

A.2 Literature review

A.2.1 DSC basic principles

Differential scanning calorimetry (DSC) is very often used to study the phase transitions of food compounds (gelatinisation, denaturation, crystallization) and enthalpy changes of the foods. In general, DSC measures the energy absorbed or released by the sample during continuous heating, cooling or under isothermal conditions and is determined from the peak size in the thermogram. Usually the sample thermal effects are measured with relevance to a

reference material: either water if the sample has moisture or an empty pan. The amount of sample used for a DSC test is relatively small: 4-60 mg, however the amount of sample and water content are related to the peak size of the thermal events (León *et al*., 1997).

DSC is very well suited to studying the baking process, as by selecting the appropriate temperature increase rate, the thermal processes occurring during baking can be simulated (Donovan, 1977). Baking is a final, very important processing stage in the creation of a stable foam structure, therefore control of thermal transition temperatures of structure-setting compounds is extremely important in order to obtain a good quality product. In particular, in the angel cake making process it is important to attain egg white protein denaturation and starch gelatinization temperatures, bearing in mind that these occur in the presence of a high amount of sugar in the system (Hoseney, 1998; Pyler, 1988).

A.2.1.1 Endotherms of wheat flour

The main components of wheat flour are proteins and starch, whose functional properties during baking are setting of the product structure (Eliasson and Hegg, 1980). In bread dough making, an important wheat protein is gluten, which is insoluble and is composed of gliadin and glutenin proteins. Soft wheat flour and strong wheat flour have different protein and starch ratios. A general rule in cake making is that soft wheat flour is preferred, where the gluten protein amount is small (Eliasson and Hegg, 1980; Pyler, 1988; Hoseney, 1998).

In DSC experiments of wheat flour doughs, proteins and starch compete for the available water in the system and observed peaks usually belong to starch gelatinization rather than to protein denaturation. Water is transferred from proteins to starch as the temperature rises and in addition, starch gelatinization temperatures are altered in the presence of proteins in the sample (Donovan, 1977; Eliasson and Hegg, 1980; León *et al*., 2003). The distinction if the peak is due

to protein or starch thermal transition can be made by estimating the enthalpy of the peaks, keeping in mind that water content affects the peak area. Studies on wheat proteins are feasible if they are isolated from starch (León *et al*., 2003).

A.2.1. 2 Endothems of wheat flour starch

Wheat starch thermal effects during the bread or cake baking process are one of the major effects that influence product structure. Starch gelatinization can be described as a sequence of conformational changes and thermal events occurring within the starch and water mixture (Donovan, 1977). In cold water, starch granules are insoluble, however as the mixture is heated, starch hydrates and the volume of the granule increases. A conformational change of starch due to the hydration process of the granule causes big heat uptake and this endothermic effect can be detected by DSC techniques. Ultimately, the starch granule breaks down and starch macromolecules uptake free water (Donovan, 1977; Rusell, 1987). The starch gelatinization process is partially reversible – the starch retrogradation process leads to an ordered structure, as for example, during bread staling (León *et al.*, 1997). Additional compounds and a lack of water elevate the starch gelatinization temperature in dough and therefore not all starch undergoes thermal changes. In a wheat flour sample (moisture content 11.8%), two thermal transition peaks are at 52.0 ^{o}C and 70.1 ^{o}C (León *et al*., 1997; Eliasson and Hegg, 1980), while starch gelatinization in a dough sample begins at 62.9 ^{o}C and finishes at 78.6 ^{o}C (León *et al*., 1997).

A.2.1.3 Endotherms of wheat proteins

The thermal denaturation properties of wheat proteins, like gluten, are important in the bread baking process, since proteins participate in the formed gluten network thermal setting and therefore proteins impact the final baked product structure texture (Donovan, 1977; Eliasson and

Hegg, 1980; Schofield *et al*., 1983). In the cake baking case, wheat protein is unwelcome and therefore the baked cake structure setting is controlled by starch gelatinization.

By using the thermal calorimetry technique, endothermic peaks of wheat flour proteins (gluten: glutenin and gliadin) were not really easily detectable. Different opinions are presented to explain the absence of wheat protein endothermic peaks (Eliasson and Larsson, 1993; León *et al*., 2003). Wheat proteins have no ordered structure or they are thermally very stable, or protein thermal peaks occur, but the total endothermic effect is zero (Eliasson and Larsson, 1993).

Studies done by León *et al*. (2003) on wheat proteins explained the peak disappearance in the thermogram as due to the lack of moisture in the system. León *et al.* (2003) observed at 4% moisture content for gliadin an endothermic peak at 58 ^{o}C; glutenin showed two peaks: 64.3 ^{o}C and 84.2 ^{o}C. Albumins and globulins (4% of moisture content) showed an endothermic peak in the temperature range of 50-55 ^{o}C (León *et al*., 2003). Harwalkar and Ma (1987) detected two small endothermic peaks of isolated wheat globulins at 84 ^{o}C and 96 ^{o}C. The different results of globulin endothermic peaks obtained by León *et al*. (2003) and Harwalkar and Ma (1987) can be explained by different moisture content in the sample. Wheat protein endothermic peaks are measurable if the moisture content in the sample is between 4-63%. (León *et al.*, 2003).

In previous studies (Hoseney *et al*., 1986) it was shown that gluten is an amorphous random polymer, whose glass transition temperature (T_g) depends on the moisture content, as for example, dry gluten T_g occurs at 160 ^{o}C and gluten T_g occurs at room temperature above 13 % moisture content (Hoseney *et al*., 1986). Gluten can be characterised as a glassy material at low temperatures and low moisture content, and at high temperatures and high moisture content it behaves as a rubbery material. Overall, the measured enthalpies of gluten denaturation are very

small, suggesting that during baking protein doesn't have much influence on the final structure setting process (Eliasson and Hegg, 1980).

A.2.1.4 Egg white protein endotherms

Though egg white consists of many proteins (Table 2.1), the recorded endotherms show three peaks at 65 ^{o}C, 74 ^{o}C and 84 ^{o}C attributable to thermal transitions of conalbumin, lysozyme and ovalbumin at pH 7, where the peak of lysozyme is relatively small (Donovan *et al*., 1975). Other egg white proteins are not detected in endotherms due to the wide ovalbumin denaturation peak, because egg white consists of 60% ovalbumin. An increase of heating rate (2-10^{o}C/min) shifts peaks to higher temperatures as the heating rate directly influences the protein denaturation rate (Donovan *et al*., 1975). A change of pH slightly shifts the denaturation temperatures of some proteins as well (Donovan *et al*., 1975).

An interesting DSC study done on ovalbumin and s-ovalbumin is very much related to the angel food cake making process (Donovan and Mapes, 1976). Due to improper egg white storage or even aging, part of the ovalbumin is converted to s-ovalbumin, which is more heat stable. The denaturation temperature of ovalbumin and s-ovalbumin are respectively 84.5 ^{o}C and 92.5 ^{o}C. DSC thermograms of egg whites stored for 2 weeks at temperatures of 22 and 37 ^{o}C showed that 2 weeks is enough to produce heat stable s-ovalbumin and therefore in the thermogram a third middle peak at 88.5 ^{o}C appears. As Donovan and Mapes (1976) suggest, the third peak appearance at 88.5 ^{o}C could be an intermediate state between ovalbumin and s-ovalbumin.

A.2.1.5 Sugar effect on starch and protein endotherms

In general, the presence of sugar increases the endothermic transition temperature in mixtures of water and proteins and water and starch. Addition of 10 % sugar to egg white shifts

the denaturation temperature by 2 degrees, though the enthalpy doesn't change (Donovan *et al*., 1975). The sugar proportion that is used in the angel cake making process raises egg white denaturation temperatures by 13 ^{o}C, while starch gelatinization temperature is elevated by up to 30 ^{o}C (Donovan, 1977). Therefore in cakes with a sugar amount of 55-60 %, starch gelatinization occurs around 92 ^{o}C (Spies and Hoseney, 1982). The sugar molecule binds some of the water molecules and therefore reduces the amount of free water in the system. Monosaccharides and disaccharides are capable of binding water to different degrees (Spies and Hoseney, 1982). A second reason for higher gelatinization temperatures is sugar interaction with the amorphous parts of starch and as a result the formed complex is more heat stable (Spies and Hoseney, 1982). The bigger the sugar molecule, the bigger the number of starch chains that can be stabilized.

The presence of previously discussed heat stable s-ovalbumin in the angel food cake batter at high sugar ratios elevates the thermal transition temperature by 3 ^{o}C. Overall, all angel food cake batter components shows a peak around 95 ^{0}C, therefore there is a danger that using aged egg whites the actual thermal transition temperatures will be higher than could be reached inside the cake during baking (Donovan *et al*., 1975).

Ghiasi *et al.* (1983) performed experiments on high sugar ratio wheat flour-sugar and wheat starch-sugar systems with the same 60 % water amount and found that thermograms were very similar, indicating that gluten endothermic peaks are not visible. Sugar can bind more water from room temperature up to 40 ^{o}C, but sugar loses this ability at higher temperatures (Donovan, 1979; Ghiasi *et al*., 1983).

A.3 Materials and methods

DSC experiments were performed using a **Micro DSC III** model instrument manufactured by **SETARAM** (Caluire, France). Experiments were performed in the 20-100 ^{o}C

temperature range with a 1 ^{o}C/min temperature increase rate. Prior to experimental work, in order to assure that the machine is calibrated well, 3 samples of crystal naphthalene were tested as a standard. It was noticed that it was necessary to keep the sample inside the machine for 1 hour in order to reach temperature equilibrium and therefore increase accuracy of the results. The maximum sample amount that would fit into the stainless steel DSC pan was 0.85 ml. Samples were prepared by blending small amount (3-8 g) of ingredients (ratio is given in Table 3.1) and water. From a literature review, it was determined that optimal amount of sample that should be placed in the DSC pan can vary from 20 mg to 30 mg (Yu and Christie, 2001). After the material was added into a pan, the pan was sealed. The pan was reweighed to precisely determine the amount of material analyzed. From this weight, we were able to calculate the amount of water that is needed to add as a reference into the second pan. In our case all the samples contained moisture; therefore distilled water was used as a reference.

The gelatinization temperature of soft wheat flour (Soft White Spring, flour protein content of 9.1%), and the denaturation temperature of egg white protein, with and without sugar, was measured by detecting endothermic peaks in the thermogram. As well, the thermal effects of sugar in soft wheat flour and egg white protein mixtures of different ratios were investigated. The experiment list is given in Table A.3.1. The ratios of ingredients were selected with the purpose of mimicking typical angel food cake recipes. In experiment runs where egg whites are not being used, an adequate amount of water is used to replace the moisture contained in the egg whites using a solids content of 11 % (Ahn *et al*., 1997).

Table A.3.1. List of experiments used for DSC analyses. Experiments were done in three replicates.

Component	Ratio (w.b.)
Flour:water	1:3
Flour:sugar:water	1:1:1
Flour:sugar:water	1:1:2
Flour:sugar:water	1:1:3
Flour:sugar:water	1:1:6
Flour:sugar:water	1:1:0.89
Sugar:egg white	1:1
Sugar:egg white	1:0.5
Egg white	1
Egg white:flour	83:26
Egg white:flour:sugar	83:26:83 (angel food cake recipe ratio)

A.4 Results and discussion

One of the goals of my thesis research had been to apply non-invasive ultrasound techniques as a tool to detect changes in egg white foam and angel food cake batter structure at a room temperature and during the baking process. In order to investigate the complex baking process of angel food cake, as a support technique we chose to use the DSC technique, where we can simulate temperatures to which ingredients will be subject to the baking process (Donovan *et al.*, 1975). As a meringue mass, which is well whipped egg white with sugar foam, or a batter is placed into the oven for baking, the temperature of the mass starts rising, and the viscosity of the mixture is reduced and instability events such as drainage and disproportionation are commencing. Mizukoshi (1983) reports that during the early baking stage, the apparent viscosity of cake batter decreases and reaches a minimum at 60 ^{0}C and liquid drainage increases linearly

between 40 ^{0}C and 55 ^{0}C. The available amount of water determines the temperature of thermal transitions of proteins and starch in the aerated mixture (Donovan and Mapes, 1976; Donovan *et al.*, 1975). In the presence of sugar, the available water amount is reduced for protein denaturation and starch gelatinization and therefore cake structure setting temperature is shifted to higher value. In order to see the impact of sugar on protein and starch we have investigated the thermal transitions of angel food cake ingredients with different amounts of water. This was either done alone or by combining two or three ingredients, keeping the ratios the same as those in the angel food recipe.

In Figure A.4.1 the effect of sugar on egg white liquid protein denaturation temperatures is shown. As the sugar ratio increases, the egg white protein denaturation peaks are shifted to higher temperatures, a result consistent with that reported in literature (Donovan *et al*., 1975; Donovan and Mapes, 1976). In our DSC experiments on egg white liquid and sugar mixture we see two peaks which are due to conalbumin and ovalbumin thermal transitions. As the sugar ratio increases conalbumin denaturation temperature shifts from 65 ^{0}C to 76 ^{0}C, and the ovalbumin denaturation peak shifts from 78 ^{0}C to 90 ^{0}C. Donovan *et al.* (1975) reported similar denaturation temperature values: 65 ^{0}C for conalbumin and 84 ^{0}C for ovalbumin, respectively, with no sugar added. Therefore conalbumin is the most-heat sensitive protein in egg white. In our DSC experiment on egg white liquid other protein denaturation peaks were not detected because as the literature states (Donovan *et al*., 1975; Ferreira *et al.*, 1997), the ovalbumin thermal transition peak covers or coincides with that of other proteins, like globulins and ovomucoid (Ferreira *et al*., 1997). Purified ovomucin doesn't show thermal transition peak because it exists in random coil form, therefore doesn't contribute to thermogram area (Donovan *et al*., 1975). Denaturation of ovalbumin in general is very important as it contributes to the structure setting of the cake,

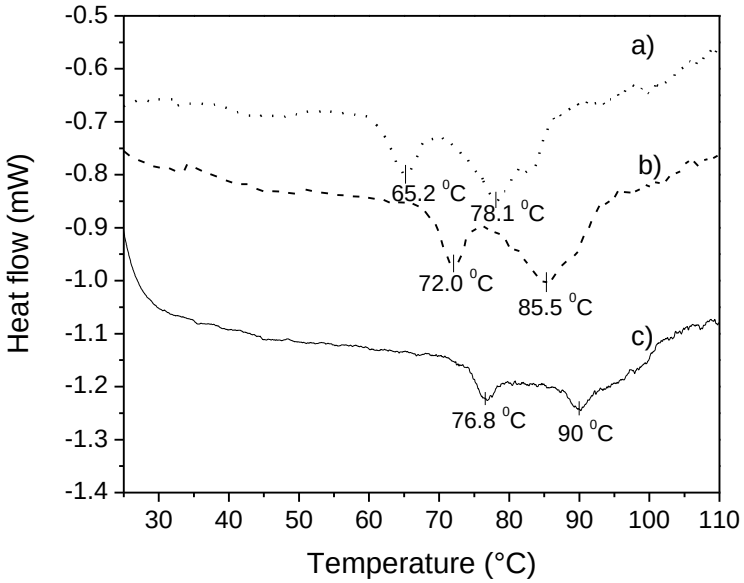

Figure A.4.1 Effect of sugar on denaturation of egg white proteins. Thermal effects of sugar and egg white liquid were prepared in these proportions (w.b.): a) 0:1, b) 0.5:1, c) 1:1.

otherwise most likely the cake collapses (Johnson and Zabik, 1981a). In our case as the sugar amount increases in egg white liquid mixture, denaturation temperatures of conalbumin and ovalbumin increases linearly (Figure A.4.2).

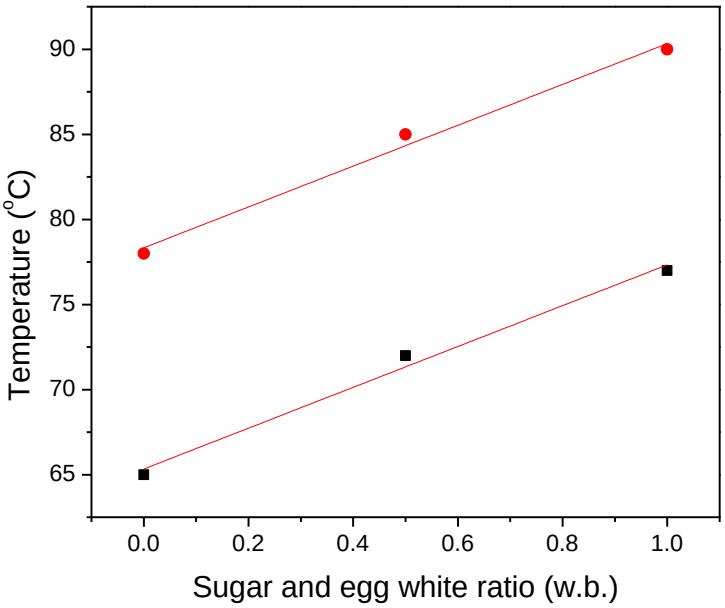

Figure A.4.2 Denaturation temperatures of egg white proteins over different sugar ratio in egg white liquid (w.b.). Symbols represent: ■ is conalbumin, ● is ovalbumin.

In Figure A.4.3 the thermal effect of sugar increase in water-soft wheat flour mixtures is shown. The proportion of added sugar in the mixture is equal to the amount that is in angel food cake. We see the expected tendency of sugar being able to shift the thermal transition peak of starch gelatinization to higher temperatures as the amount of sugar increases. The thermal transition of wheat flour-water and sugar mixture that is present in an angel food cake recipe is seen as one peak at a temperature of 92 ^{o}C. In Figure A.4.3 a) the thermogram of soft wheat flour and water mixture with no sugar added shows a first starch gelatinization temperature at 61 ^{o}C and a wider peak around 100 ^{o}C, which is due to denaturation soft wheat flour proteins (Donovan, *et al*., 1975). The major water absorbing component in angel food cake recipe is starch in the flour and the water source is egg white liquid. However in the presence of a high amount of sugar, water is no longer available for starch gelatinization at the lower 61 ^{o}C temperature, and full cake structure setting process occurs at the higher temperature of 93.3 ^{o}C.

Due to changes in the available water in sugar and egg white mixtures, it is evident that higher temperatures are needed in order for biopolymers in the mixture to undergo conformational changes. This fact is important in the meringue making process, since baking temperature is kept at 100 ^{o}C (Pyler, 1988). In egg white and sugar mixture DSC experiments, we were not able to reduce the water content in the mixture, since we worked with fresh egg whites not egg white powder, therefore we increased the sugar amount. However, in the literature it is mentioned that the effect of decreasing water amount or increasing sugar amount is not the same, at least for starch, water and sugar mixtures (Johnson *et al.*, 1990). The observed increase of starch gelatinization temperature in soft wheat flour, sugar and water mixture is in agreement with other author's findings (Donovan *et al.*, 1975) and is due to lowered water activity and interaction of sugar with starch chains (Spies and Hoseney, 1982).

In Figure A.4.4 a) the thermal effect of egg white and soft wheat flour mixtures that are present in angel food cake ratios is presented. First peak at 65.2 ^{o}C is a joint peak due to starch gelatinization process and conalbumin denaturation, which occurs at a slightly higher temperature due to a lack of available water in the egg white and wheat flour mixture. The second peak is attributable to egg white protein ovalbumin denaturation at a temperature of 77 ^{o}C.

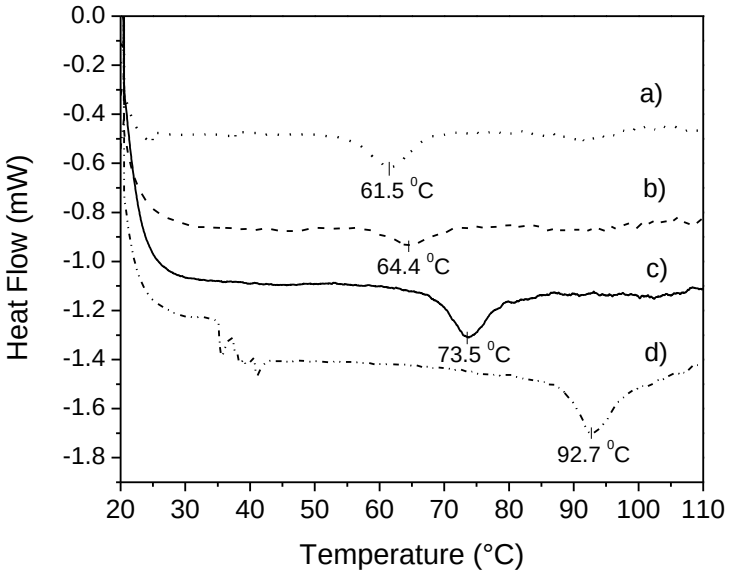

Figure A.4.3. Effect of sugar on denaturation of soft wheat flour components. Flour, water and sugar mixture was prepared in these proportions (w.b.) a) 1:3:0, b) 1:6:1, c) 1:2:1, d) 1:0.89:1.

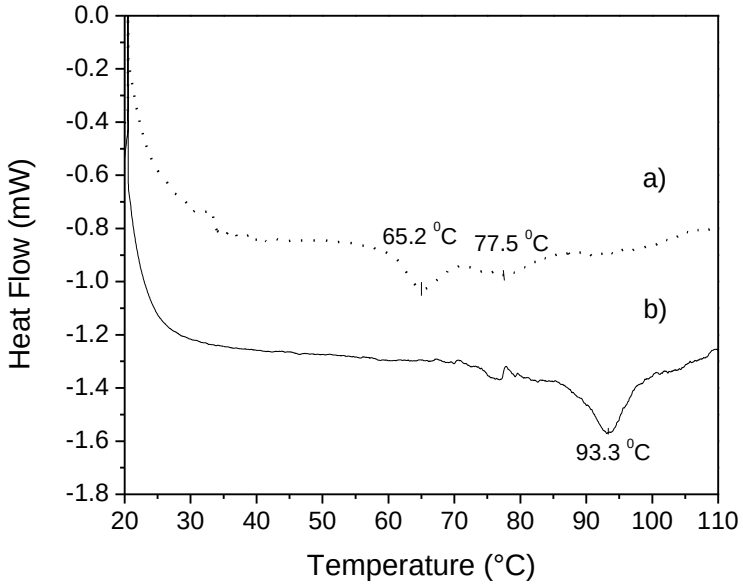

Figure A.4.4. Thermogram of a) egg white and flour mixture in a ratio of (w.b) 0.83:0.26, b) angel food cake batter, sugar, egg white and flour in a ratio (w.b): 0.83:0.83:0.26.

A.5 General difficulties encountered

The DSC instrument is useful in studying thermal transitions occurring during baking process, because partially is possible to simulate the temperature rise in a sample as in a real baking situation. However, our DSC instrument has limitations in heating rate: the maximum heating rate is 1.2 ^{o}C/min, while in a baking simulation 5 ^{o}C/min is preferable (Donovan, *et al*., 1975). The sample size and heating rate impacts the enthalpy at which thermal transitions occurs (Donovan *et al.,* 1975). We were not concerned about the enthalpy, because we were interested only in the thermal transition temperatures and all experiments were conducted at a constant 1.2 ^{o}C/min rate. As well, in DSC experiments the mixtures were not aerated, as they would be in a real cake batter.

A.6 Conclusions

The thermal transition temperatures of angel food cake ingredients and their combinations in the presence of different amounts of water were examined by using a DSC technique. By using this technique, results on the thermal setting temperatures of angel food cake batter and its individual components confirmed that moisture content in a batter with a high sugar content is an important factor in order to obtain a good quality baked product. For all components (starch and egg white proteins) that are important in setting cake structure, increasing the amount of sugar in the system leads to higher thermal transition temperatures. We were able to detect thermal transition temperatures of two egg white proteins (conalbumin and ovalbumin) that are very important in setting the cake structure. Thermal transition temperatures of these proteins were determined in different amounts of an egg white liquid and sugar mixture. In a complete angel cake batter mixture, if liquid drainage is not occurring, thermal transitions of egg white proteins and wheat starch occur at the same temperature, which is around 92^{o}C.